Acknowledgments.

I wish to thank Professor B.Bleaney for extending the facilities of his department to an errant chemist, and Dr W.P.Wolf for introducing me to many of the physical properties of the garnets.

I am very grateful to Dr G.Garton for his willing, helpful and friendly supervision of the work.

It has been a great pleasure to collaborate with Mr D.Ryan, and Drs M.J.M.Leask, A.F.G.Wyatt and M.T.Hutchings whose wide interests and intelligent conversation helped to speed many long hours spent in the mechanics of experimentation.

I am indebted to Mr R.Sutton, Dr J.R.Chadwick, Mr R.Shore, Mr S.Itzcovitz, Mr E.S.Albone, Mr D.A.Hukin and Dr R.C.Rau for supplying samples, or assisting with experiments.

I wish to thank the Clarendon technical staff, but particularly the hydrogen and helium men, and Miss S.Newbery and Mrs J.Wiggins, who helped to make my time in the department a happy one.

I wish to express my gratitude to the U.S.Air Force Cambridge Research Centre for sponsoring the research through its European Office, and for giving me a maintenance grant throughout the period of the work.

Finally, I wish to thank my parents, my fiancée, and my friends for their interest, encouragement and patience.

INDEX.

Chapter 1. Introduction.

1.1 ... 1.6

Chapter 2. The furnace and control equipment.

2.1 Introduction 2.2

2.2 The furnace 2.4

2.4 The control equipment 2.7

Chapter 3. The preparation of garnets.

3.1 Introduction 3.2

3.2 Melt composition 3.6

3.6 Size of melt and cooling rate 3.7

Detailed experimental technique

3.7 (i) Introduction 3.8

3.8 (ii) Crucible protection 3.9

3.9 (iii) Crucible packing 3.10

3.10 (iv) Crucible cooling

(v) Separation of crystals 3.11

3.11 (vi) Discussion of results 3.12

3.12 Crystal quality and characteristics 3.14

3.14 Special problems 3.16

3.16 List of garnets produced as single crystals 3.17

3.18 Polycrystalline garnets. Introduction 3.20

3.20 Experimental method 3.23

3.23 Discussion

3.24 The Verneuil flame fusion technique 3.28

Chapter 4. The paramagnetic susceptibility apparatus.

4.1	Introduction	4.2
4.2	The Hartshorn Bridge Circuit	4.4
4.4	The mutual inductance coils	4.6
4.6	General description of the cryostat	4.8
4.9	The specimen containers	4.10
4.10	Gas-handling, and experimental procedure	4.11
4.11	Calibration of the apparatus	4.13
4.13	The magnetic properties of the calibration standard	4.14

Chapter 5. The paramagnetic susceptibilities of rare earth garnets.

5.1	Introduction	5.2
5.2	Comparison of results with resonance g-values	5.4
5.4	YbAlG and YbGaG	5.6
5.6	GdAlG and GdGaG	5.7
5.7	NdGaG	5.8
5.8	ErAlG	
5.9	ErGaG and DyAlG	
5.10	DyGaG and the 'Non-Kramers' ions - introduction	5.11
5.11	PrGaG and TmAlG, TmGaG	5.12
5.12	TbAlG and TbGaG	5.13
5.13	HoAlG and HoGaG. Conclusions	5.14

Chapter 6. The susceptibility of dysprosium aluminium garnet.

6.1 Introduction and Historical Introduction 6.4

6.5 Fe-doped powder samples of DAG 6.6

6.7 Cr- and Y-doped samples of DAG

Anomalous a.c. susceptibility of pure DAG powder 6.7

6.8 Ballistic measurements on pure DAG powder 6.10

6.10 Ballistic measurements on single crystals and specific heat sample 6.11

6.11 Susceptibility of a spherical DAG crystal 6.12

6.12 Discussion 6.16

6.16 Conclusions 6.17

Chapter 7. The specific heat of DAG.

7.1 Introduction

Description of apparatus 74

7.5 Experimental procedure 7.6

7.6 Corrections to the data 7.9

7.9 Discussion of results 7.13

7.13 Conclusions

Chapter 8. Magnetic transitions in DAG.

8.1 Introduction

Description of the apparatus 8.3

8.3 Preparation of the DAG sample 8.4

8.4 Orientation of sample 8.5

8.5 The experiments 8.6

8.6 Discussion 8.8

8.9 Conclusions.

Chapter 9. The oxides of europium.

9.1	Introduction	9.4
9.4	Eu_2O_3	9.5
9.5	EuO	9.7
9.7	'Ortho I'	9.8
9.8	Results and discussion	9.13
9.13	'Eu_3O_4'	9.15
9.15	Conclusions	9.17
9.17	Postscript	

Chapter 10. The paramagnetic susceptibilities of various materials.

10.1	A)Terbium tetrafluoride and gadolinium iodide	10.3
10.3	B)The rare earth oxyfluorides	
	Introduction	10.5
10.5	GdOF	10.6
10.6	DyOF	10.7
10.7	ErOF and NdOF	10.8
10.8	C)The rare earth-transition metal nitrates	
10.10	Experimental	10.11
10.11	Results and discussion	10.13

List of references.

Chapter 1.

Introduction.

Natural garnet crystals are widely distributed in igneous rocks, and good single crystals have long been prized as semi-precious stones. They are mentioned, for instance, in the biblical book of Exodus as one of the twelve stones which represented the twelve Tribes of Israel on the breastplate worn by the Priests.

They have the general composition $(Ca,Mg)_3Al_2(SiO_4)_3$, but often contain Fe^{II}, Fe^{III}, Mn^{II}, Cr^{III} or Ti^{IV} as well. Another mineral, cryolithionite $Na_3Al_2(LiF_4)_3$, also crystallises in the garnet structure, suggesting that a wide variety of compounds with the same general formula might exist with garnet structure, assuming that overall charge neutrality were possible, and elements appropriate to the various lattice site sizes and co-ordination were present. Thus, for instance, Yoder and Keith (1951) replaced equal mole amounts of Mn^{II} and Si^{IV} by Y^{III} and Al^{III} respectively in $Mn_3Al_2(SiO_4)_3$ to make a series of mixed garnets. They also prepared the end-member of this series, $Y_3Al_2(AlO_4)_3$, now known as yttrium aluminium garnet (YAlG).

Independently of this work, and of each other, Bertaut and Forrat (1956) and Geller and Gilleo (1957) discovered that the apparently anomalous magnetic properties of some mixed oxide systems could be explained by the presence in them of a phase with garnet structure, $Y_3Fe_2(FeO_4)_3$, yttrium iron garnet (YIG). The same authors also discovered the series of rare earth iron, aluminium and gallium garnets.

Various authors soon demonstrated that the garnets are capable of a bewildering array of substitutions (see, for instance, Geller,1960). Besides yttrium,the rare earths and the ions found in natural garnets, Ca,Sr,Ba,Zn,Ni, Sn,Ge,Sc,In can all be introduced into the garnets, either partially or completely occupying one or more of the cation lattice sites.

A number of these compounds have interesting magnetic properties, particularly the rare earth and yttrium iron garnets, which are ferrimagnetic.

Wolf (1961) has listed the properties desirable in a group of ferrimagnetic compounds suitable for detailed physical research:

(i) Strong antiferromagnetic coupling between neighbouring inequivalent magnetic ions.

(ii) Well-defined, regular and preferably simple crystal structure.

(iii) One-to-one relationship between the different crystal sites and types of constituent ions.

(iv) Unique valency for each type of ion present, with accurate control of valency in the method of preparation.

(v) A simple method for growing large and perfect single crystals.

(vi) A wide range of compositions possible for the same structure in order to vary the magnetic properties.

Of the known types of ferrimagnetic compounds, the garnets come closest to fulfilling these requirements. Although their structure is well-defined and regular, it is rather complicated, and the detailed positions of the oxygen ions in the unit cell are defined by structure parameters which must be determined separately for each compound. The only iron garnet likely to present valency troubles is terbium iron garnet which might contain a certain percentage of Tb^{IV} and Fe^{II}. The major problem was (v).

The rare earth iron and gallium garnets are incongruently melting, and can only be crystallised from the melt (by Stockbarger or Verneuil techniques, for instance) by means of elaborate seeding procedures and careful adjustment of conditions. Even then, the crystals obtained are of doubtful stoichiometry and poor quality (Rudness and Kebler, 1960).

Remeika (1956) had discovered that single crystals of some ferrites can be grown from solution in molten lead oxide. Nielsen and Dearborn (1958) extended this work to the production of single crystal yttrium and rare earth iron garnets. They investigated the phase relationships of the system $PbO-Fe_2O_3-Y_2O_3$ and showed that the process is not simply deposition from solution, since other phases (Fe_2O_3, $PbFe_{12}O_{19}$) are precipitated in addition to the garnet. The magnetoplumbite is in fact the primary phase.

Nielsen (1960) found that bigger and better crystals are obtained from a mixture of lead oxide and lead fluoride as flux. It is perhaps symptomatic of the present state of understanding of crystal growth from the flux that Nielsen's reasons for adding PbF_2 to the melt were partly founded on an inaccurate published phase diagram which indicated that there is no compound formed between PbO and PbF_2! Some part of the improvement seems to result from the greatly reduced viscosity of the oxide-fluoride flux, but owing to the complication of the system, no full phase investigation has been made.

There is no obvious reason why this flux in particular should be so effective, but no other flux which has been tried for growing ferrites, garnets or other refractory oxide crystals seems to be as good, though large crystals of aluminium oxide can be obtained from PbF_2 melts. Amongst other flux materials which have been tried are Bi_2O_3, NaF, NaB_4O_7, Na_2CO_3, KCl, $Pb(BO_2)_2$ and various mixtures, for instance, NaF plus NaB_4O_7.

Thus, the garnets come very close to being 'ideal' ferrimagnetic materials according to Wolf's criteria. As a result, the garnets have been the subject of a very substantial volume of research in a number of countries, and already find commercial applications in microwave technology. Many physical measurements are discussed in Wolf, 1961, and also in the proceedings of most recent Conferences on Low

Temperature Physics, Magnetic Materials and Magnetism. The ferrimagnetism of the rare earth iron garnets results from the combined effect of the three cation sublattices, two of iron ions and one of rare earth ions, in which the two iron sublattices align antiparallel to each other (the situation in YIG) while the rare earth sublattice aligns parallel with one of the iron sublattices.

In a sense, the current work may be regarded as a section of a long-term international programme of research into the magnetic properties of the garnets. Our part has been to investigate the behaviour of the rare earth sublattice, and for the sake of simplicity, our measurements have been made in garnets not complicated by the iron sublattices, namely in the garnets containing diamagnetic aluminium and gallium. This thesis is largely concerned with the preparation of good single crystals of most of the possible rare earth aluminium and gallium garnets, and the measurement of their paramagnetic susceptibilities at low temperatures. One of these garnets, dysprosium aluminium garnet proved to be very interesting in its own right, and has been the subject of specific heat and magnetic moment measurements, as well as detailed and exhaustive susceptibility studies. Where appropriate, we have prepared and measured polycrystalline garnet samples.

All of these measurements are bulk measurements, and the behaviour of individual ions and groups of ions must also be

studied for a better understanding of the bulk properties. Therefore, we have also prepared crystals of diamagnetic yttrium and lutecium gallium and aluminium garnets doped with the rare earth ions in which electron spin resonance can be observed, and these have been measured by closely associated workers. In addition, some specific heat measurements have been made on polycrystalline garnet samples (Bailey, unpublished), and crystals have been supplied to workers in the U.S.A. for optical spectroscopy and x-ray structural work. The bearing of the work on understanding of the properties of the garnets is discussed in Wolf and Bozorth (1961), Wolf and Van Vleck (1960), Wolf (1959), Wolf (1960), Ball et al. (1961).

Besides the main work on the garnets, the paramagnetic susceptibilities of a number of other compounds at low temperatures have been measured. Using the apparatus to be described in Chapter 4, these measurements can be made quickly and fairly accurately, and in appropriate cases, can yield useful information on such diverse topics as identification of chemical species, analysis of substances for chemical purity, determination of the strength of the interactions of magnetic ions in crystals, and survey of the properties of a family of compounds in order to select interesting materials for further studies. These measurements occupy the final two chapters.

Chapter 2.

The Furnace and Control Equipment.

Introduction.

High quality crystals from solution are normally obtained by slow deposition of material upon suitable seeds. The slightly super-saturated solution from which deposition occurs is obtained in one of a number of ways. Crystals are frequently obtained from qqueous solution by slow evaporation of the solvent, and also by slow cooling of a solution whose solubility falls with decrease in temperature. A variant of this latter method makes use of a temperature gradient within the system, so that one part of the system contains a store of the material to be crystallised, and is maintained at a slightly higher temperature than the part of the system containing the seed crystal. The solvent circulates from the warmer part, and becomes slightly super-saturated in the cooler part, causing the crystal to grow.

The technique for growing garnets from the flux can be regarded essentially as the method of cooling a solution slowly, even though the phase relationships involved are much more complicated than simple deposition from solution. The actual situation is further complicated by inevitable evaporation of the solvent during crystallisation, and in our experimental arrangement, by a temperature gradient within the system.

Because of the technical difficulties of introducing seeds at the elevated temperatures involved, it is necessary to rely on spontaneous generation of seed crystals in the solution as the temperature is lowered. If the size of crystals ultimately obtained is to be reasonably large, then their number must be relatively small, that is, the solution must not be allowed to polynucleate through a high degree of supersaturation. Thus, a high order of temperature stability is mandatory, and the furnace control equipment must be of high quality.

The furnaces, on the other hand, must be expendable. It is inevitable that considerable amounts of lead oxide and lead fluoride volatilise during long experiments at temperatures comparable with their boiling points. These vapours can also be expected to condense to highly corrosive liquids on the cooler parts of the furnace. The heating elements must either be relatively resistant to the corrosive atmosphere of volatilised lead compounds, or must alternatively be completely isolated from it. In the event of total crucible failure, which is by no means unknown, it is essential that the furnace can be quickly, cheaply and easily rebuilt if undue delays are to be avoided.

The Furnace.

The furnace was constructed of M.I.23 insulating bricks, manufactured by Morgan Refractories Limited. These bricks contain a high percentage of alumina and will stand temperatures

of up to 1550°C. They are porous in texture and friable; hence they are very easily worked with simple tools. Holes can be drilled very easily by hand with copper or brass tubes of appropriate diameter.

A block diagram of the furnace is reproduced as Figure 2.1. The detailed design is such as to reduce working the bricks to a minimum. The eight transverse heating elements span the furnace through holes drilled in the walls ½" below the roof. The thermocouple sheath is introduced from the back of the furnace, and is located very slightly below the elements. Two bricks serve as the door of the furnace, and the whole construction is lined outside with sheet aluminium, and held together with a 'Dexion' framework. The working space inside the furnace measures 9" by 6" by 4". No cement is used in the construction, since it is much easier to replace single flux-damaged bricks when no cement is involved. Any spaces around the element admission holes or the door are backed with asbestos or silica wool.

The elements chosen are Morgan 'Crusilite' silicon carbide elements, which have a maximum working temperature of about 1500°C. They are used in sets of eight, wired to give two parallel series of four elements. By this method, if one element breaks in the later stages of an experiment, the remaining set of four is sufficient to provide the necessary power to maintain the furnace temperature. Power is supplied through the control equipment (see below) from a 50B 'Variac' with a maximum power rating of 7½kw. The resistance of the

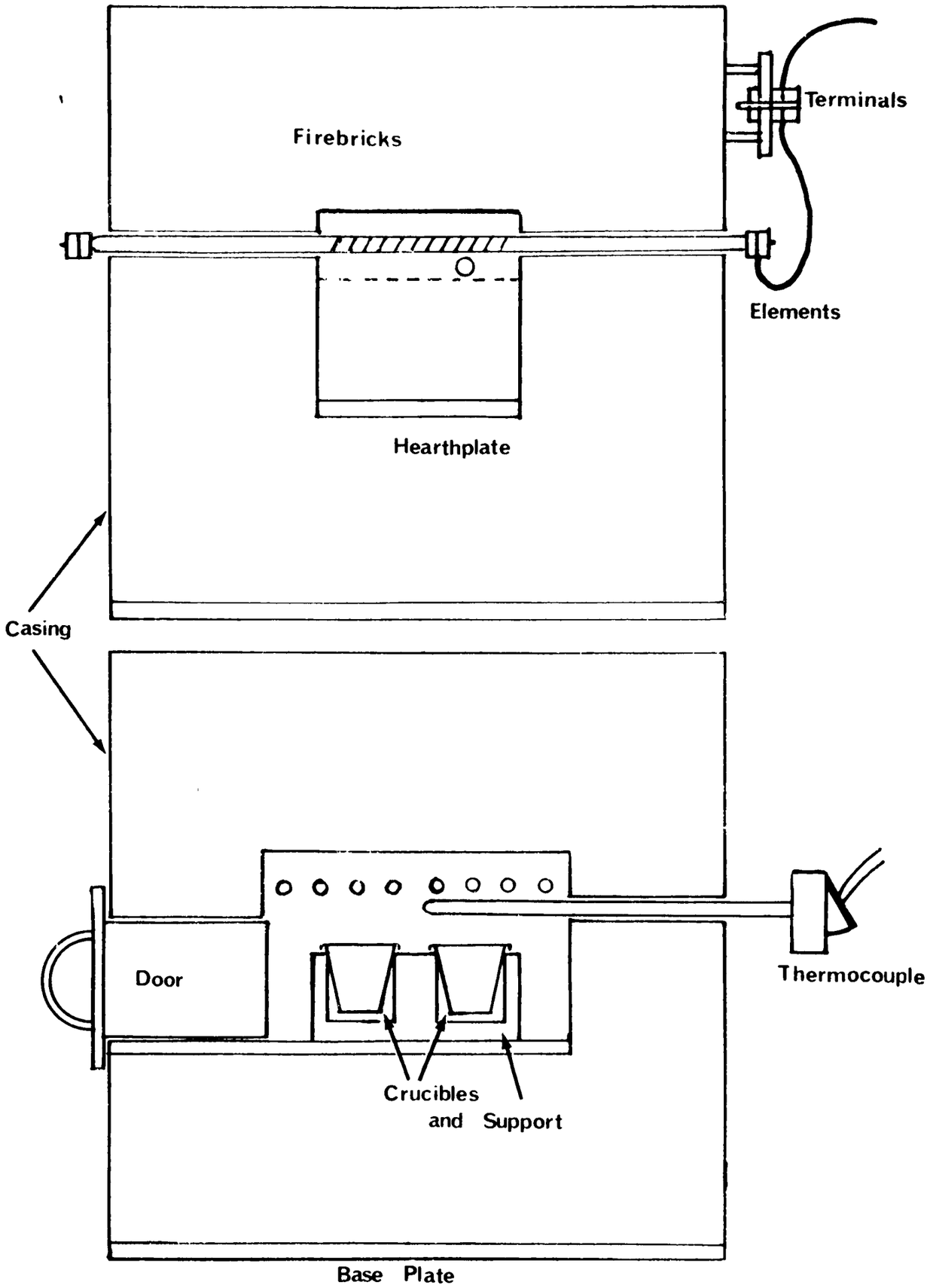
Terminals
Firebricks
Elements
Hearthplate
Casing
Thermocouple
Door
Crucibles
and Support
Base Plate

Figure 2.1

elements increases by as much as a factor of four with age, so that it must be possible to vary the voltage quite considerably over a period of months to maintain the power.

The alumina sheath which holds the thermocouple is placed as close to the elements as possible to decrease the response time of the control equipment and minimise the danger of 'hunting'.

It is inevitable that a furnace of this design should have a vertical temperature gradient, but far from being detrimental to good crystal growth, it is actually advantageous, since it causes nucleation to take place at the bottom of the crucibles, which are somewhat cooler. If there were no temperature gradient, nucleation would tend to take place as a result of evaporation of the solvent at the surface, and experience shows that crystals growing at the surface are of inferior quality. It is also probable that the temperature gradient reduces the total number of nuclei. Since the garnets are less dense than the flux, any nuclei which are not attached to the sides or bottom of the crucible tend to float to the surface of the melt and re-dissolve at the higher temperature.

The Control Equipment.

The control equipment chosen was a 'West Instruments Gardsman' stepless programme temperature controller. This contains no electronic devices apart from one photo-electric cell, ensuring reliability of operation, and has sufficient

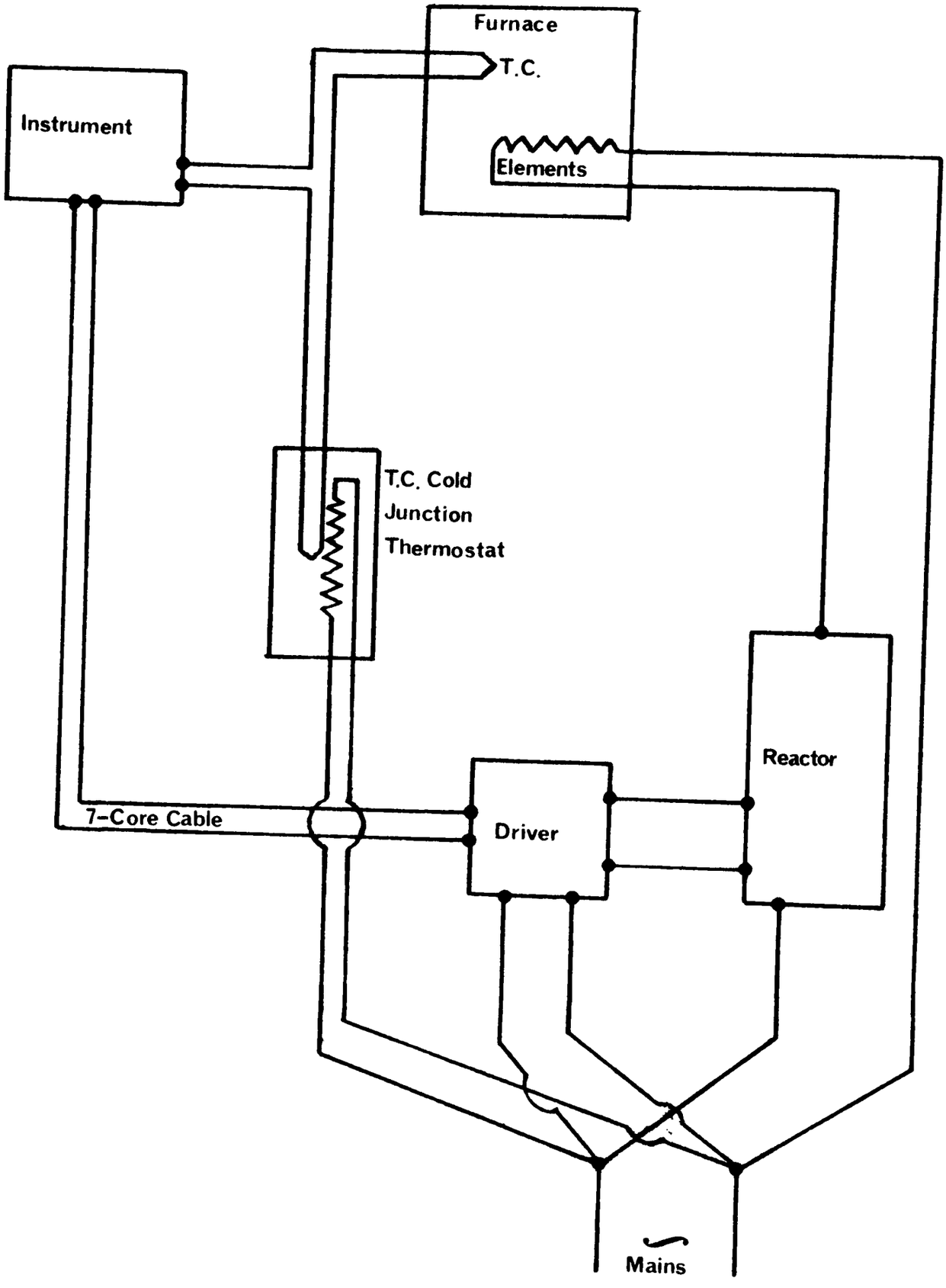
Furnace
T.C.
Instrument
Elements
T.C. Cold
Junction
Thermostat
Reactor
7-Core Cable
Driver
Mains

Figure 2.2

adjustment of power output to overcome the considerable variations in mains voltage during the course of a cooling run. A block diagram of this equipment is reproduced as Figure 2.2.

The equipment comprises three main units, the instrument, the driver and the reactor.

In the instrument unit (Figure 2.3a) the output from the furnace thermocouple is registered on an indicating millivoltmeter calibrated in degrees Centigrade. The cold junction of the thermocouple is in an electrically heated thermostatic bath, maintained at about 40°C. A setting arm carrying a setting pointer (I) is positioned on the temperature scale either manually or by the motion of the programme cam. Located on this arm are a small light source (L) and a photo-cell (P) arranged so that the beam from the light source falls on the sensitive surface of the cell. As the temperature approaches the desired level, an opaque flag (F) carried on the milli-voltmeter pointer arm interrupts the light beam, and the current flowing in the photo-cell circuit falls.

The instrument also contains (Figure 2.3b) a synchronous slow speed electric motor and gear train causing the programme cam to revolve, and a primary magnetic amplifier for the photo-cell current. The programme cam consists of an aluminium disc graduated on one side in even divisions of time whose absolute magnitude depends on the gear train. The cam is fixed to a mount (M) which also incorporates a small

Figure 2.3

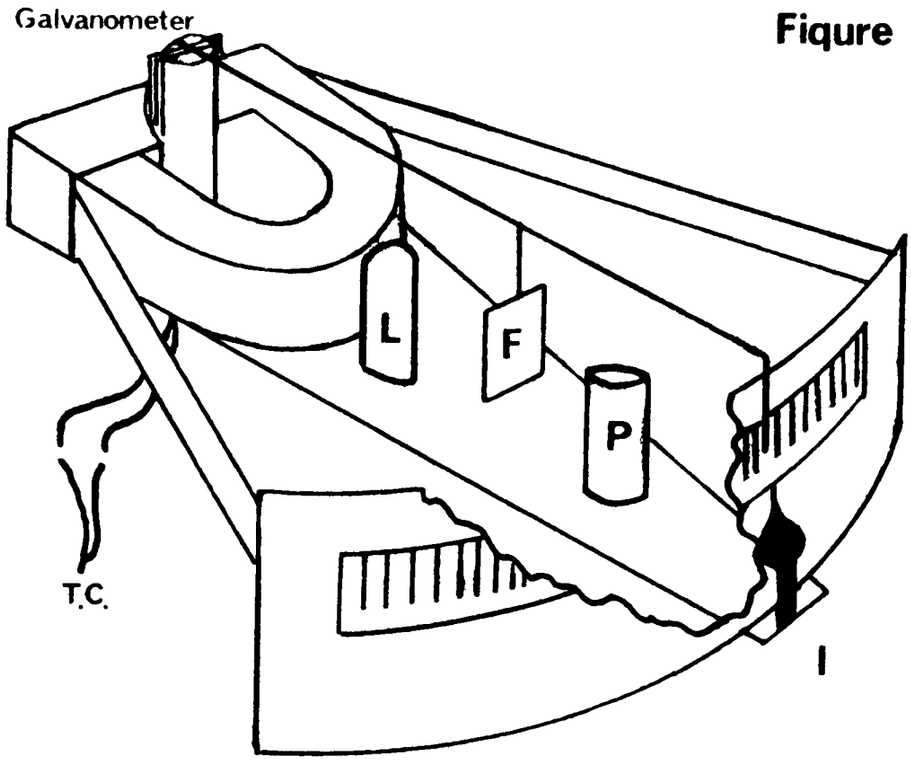

(A)

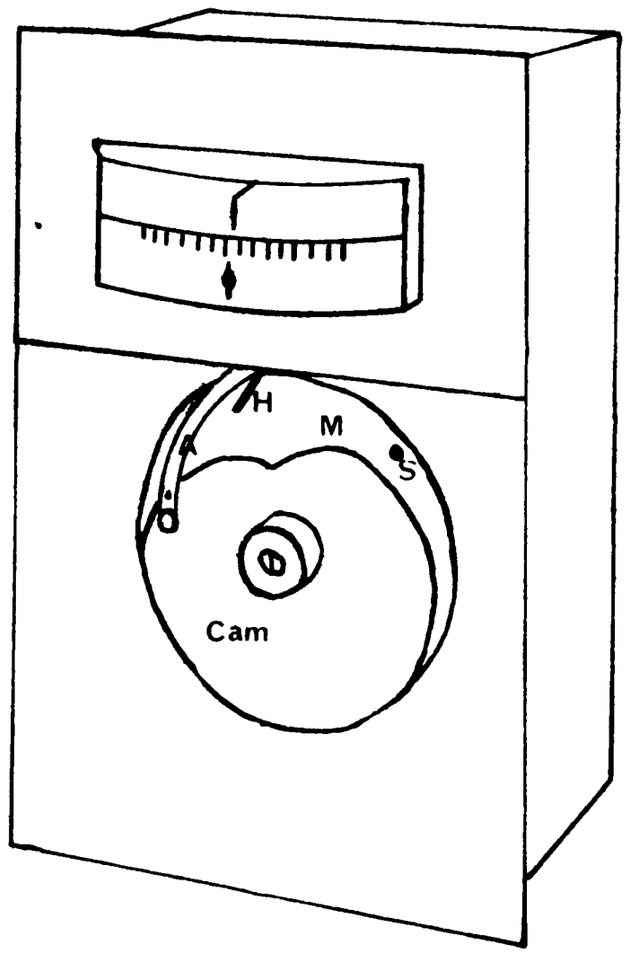

(B)

side-arm (S) arranged to actuate a micro-switch and stop the slow speed motor at the appropriate point in the cooling cycle. The cam can be cut to any shape to give any desired cooling programme. The shape of the cam is followed by a tracking arm (A) and the temperature range of the programme is varied by means of a setting control (H).

The amplified photo-cell current is fed to the driver unit. This contains an indicator which shows the percentage of power being supplied to the heating elements, and adjustments for the percentage of maximum and minimum power outputs to be applied to the heating elements if the temperature is too low or too high respectively. These controls give better temperature stability, since by limiting the variation of power which the control equipment can make, it is possible to reduce overshooting and 'hunting'. The optimum settings are derived empirically by trial and error, The unit also contains further stages of magnetic amplification, and supplies a D.C. current to the control windings of the reactor unit.

This unit is a saturable core reactor , wired in series with the furnace heating elements. The power supplied to them is governed by the current in the reactor control windings, which in turn is directly proportional to the current flowing in the photo-cell. Thus, as the flag in the instrument unit gradually intercepts the light source, the power supplied to the furnace falls. The reactor takes its power directly from the mains through the Variac.

The power input to the elements is therefore proportional only to the difference between the actual and desired furnace temperatures, and variations in heat loss from the furnace, and in mains voltage, are automatically compensated. Short term temperature fluctuations measured at a crucible with a probe thermocouple and potentiometer were undetectable in the range 1000-1500°C, and long-term stability was of a high order. The equipment has given trouble-free service throughout the period of the current work.

Chapter 3.

The Preparation of Garnets.

Introduction.

Although the rare earth gallium and iron garnets are incongruently melting substances, the aluminium garnets melt congruently, though at temperatures in the range 1700-1800°C, and there is no reason in principle why they should not be prepared as single crystals by the flame fusion technique, or one of the other methods for obtaining crystals from the melt. Indeed, Carson and White (1960) and Wickersheim and White (1960) mention in passing that they prepared crystals large enough for electron spin resonance and optical absorption spectroscopy of yttrium aluminium garnet doped with ytterbium by the Verneuil process, but they report no details.

Although Rudness and Kebler (1960) have made single crystals of yttrium iron garnet by the Verneuil process, it is not such a convenient method as the lead oxide, or lead oxide-lead fluoride flux technique developed by Nielsen and Dearborn (1958) and Nielsen (1960). We have shown that this method can be extended to the growth of yttrium aluminium garnets too, so that in general, an adaptation of Nielsen's technique has been the basis of production of all our garnet single crystals, whether gallium, iron or aluminium.

However, we have investigated the possibility of growing one ~~yttrium~~ aluminium garnet by the Verneuil technique.

The preparation of large, good quality single crystals depends mainly upon three factors: (a) composition of the melt; (b) a sufficiently large melt; (c) a sufficiently slow and even cooling rate. The paramagnetic susceptibility and resonance measurements, for which these crystals were primarily grown, do no demand very large crystals, a few millimeters in diameter being a perfectly adequate size. Thus, in general, we have compromised with respect to factors (b) and (c) since, especially in the early stages of the work, yield and size of crystals was less important than promptness in supplying specimens for the physical measurements. For the same reason, we have only carried out a limited number of experiments on melt composition.

Melt Composition.

Following Nielsen and Dearborn (1958), the earliest attempts to produce garnet crystals were made using melts with the following compositions: -

PbO	72.7 mole%
Ga_2O_3	26.0 mole%
M_2O_3	1.3 mole% where $M = Y_2O_3$ 99%, Dy_2O_3 1%

and

PbO	52.5 mole%
Fe_2O_3	44.0 mole%
Y_2O_3	3.5 mole%

Both of these melts were tried in 200 g batches. They were heated to 1250°C for 12 hours to allow the rare earth and other oxides to dissolve in the molten litharge, heated to 1325°C and cooled at a rate of 6°C per hour to 900°C.

After rapid cooling to room temperature, the melt containing gallium was found to have produced a multitude of pale violet, approximately spherical transparent crystals, which appeared to have the correct crystal habit for garnet, but were too small (less than ½mm diameter) to be useful. The crucible containing iron was half full of shiny black plates, up to a centimetre in diameter, and hexagonal in shape. These were readily attracted by a bar magnet, and were crystals of the magnetoplumbite phase ($PbFe_{12}O_{19}$) stated by Nielsen to be primary product from the melt. There were also many small garnet crystals which were easily separated from the magnetoplumbite mechanically, owing to the great differences in crystal habit. These garnets had grown in the elongated shape typical of a fast rate of cooling, Nielsen and Dearborn, 1958, indicating that the cooling rate was probably too fast for the gallium garnets too.

At this stage of the work, Dr J.W.Nielsen kindly communicated the results of his work before publication, Nielsen(1960) on an improved melt composition which includes lead fluoride as well as lead oxide. His recommended compositions are: -

PbO	39.4 mole%
PbF_2	40.8 mole%
Ga_2O_3	14.8 mole%
R_2O_3	5.8 mole% where R = rare earth or Y

and

PbO	30 mole%
PbF_2	40 mole%
Fe_2O_3	20 mole%
R_2O_3	10 mole%

In general, we have found that both of these melts give good results. The composition for producing gallium garnets works well for all rare earths from europium to lutecium inclusive, and also for yttrium. Many attempts to prepare samarium and praseodymium gallium garnets were unsuccessful. The compositions of the melts were altered in various ways, relatively more gallium oxide and/or rare earth oxide being added, but without success. Unlike the aluminium melts which tended to yield perovskites rather than garnets in some cases, these melts produced no appreciably sized crystals at all. All the products formed were soluble in acids which would dissolve the body of the melt. Possibly the rare earths formed oxyfluorides, which are normally only obtained microcrystalline from lead fluxes(Albone,1963). The oxyfluorides of the lighter rare earths and particularly of praseodymium are soluble in dilute acids (Albone,1963). Similarly, crystals of neodymium gallium garnets were only once obtained, and were of very low crystal quality, with badly formed faces and

mary inclusions of flux.

Our experience of the iron garnet melt has been less exhaustive, but the results were satisfactory in every experiment.

We discovered that molar proportions similar to those recommended by Nielsen for gallium garnets (see above) give reasonable yields of aluminium garnets when aluminium oxide is substituted for gallium oxide. The yields are generally very much lower than those for the corresponding gallium garnets, and we tried various experiments to try to improve the yield. The melt composition was altered in various ways, cooling was commenced 75°C higher than for the gallium compounds, all without effecting substantial improvement.

Lefever et al. (1961) published a melt composition which they claim gives larger and better quality aluminium garnets: -

PbO	41.5 mole%
PbF_2	48.1 mole%
Al_2O_3	7.0 mole%
R_2O_3	3.4 mole%

We have tried this melt composition a number of times, but in our experience, and under the temperature gradients and cooling rates pertaining in our equipment, it is less satisfactory than the modified 'Nielsen' melt we normally use.

During recent months, we have been attempting to grow large single crystals of rare earth oxyfluorides from a lead oxide-lead fluoride flux. Only very small crystals were

obtained, and in one experiment we added some aluminium oxide to the melt, hoping that garnets would crystallise first, removing some of the nucleation particles and resulting in larger oxyfluoride crystals. The final composition of this melt was: -

PbO	30.5 mole%
PbF_2	41.5 mole%
Al_2O_3	16.5 mole%
Y_2O_3	11.5 mole%

The oxyfluoride crystals obtained were no better than usual, but some large, very good quality garnets were produced. We have not thoroughly investigated this melt composition, but we have shown that it yields good crystals of yttrium and dysprosium aluminium garnets which are substantially larger than any aluminium garnet crystals made with any previous flux composition.

Size of Melt and Cooling Rate.

Throughout these experiments, charges of between 160 and 500 g have been employed, contained in 50 or 100 ml capacity platinum crucibles. The lower limit was found to be the minimum charge which could be relied upon to give several perfect crystals of a few millimetres diameter for resonance work. In the case of the more expensive rare earths such as lutecium, europium and terbium, economic factors had to be considered, since about £50 worth of oxide was involved in each charge. The largest melts were only used

when especially large single crystals were wanted, as for instance in the production of a large crystal of dysprosium aluminium garnet to be made into a sphere for susceptibility and magnetic moment experiments.

We found that 2-3°C per hour was the maximum cooling rate capable of giving sufficiently large crystals. Other authors (Nielsen,1960;Harrison,1959) recommend rates of 1 or even ¼°C per hour, but if such a low rate is to be worthwhile, the design of the furnace must be more elaborate, otherwise random temperature fluctuations are likely grossly to exceed the desired temperature fall. In addition, such a slow cooling run takes a month rather than a week, and either much larger furnaces, or four times as many furnaces would be needed to produce garnets at the same rate, not allowing for the greater time wasted as a result of power cuts, crucible failure and other accidents.

Detailed Experimental Technique.

(i) Introduction.

Boakes (1959) in this laboratory made a number of attempts to prepare garnets by the flux method of Nielsen and Dearborn (1958) but in every case except one, he experienced trouble with the platinum crucibles. Sometimes, these were obviously suffering from some form of chemical attack, resulting in large holes with jagged edges. Sometimes at the end of a run, the crucibles were quite empty, though apparently unharmed

and not porous to water. He checked that the contents of the crucible had not escaped by evaporation or capillary rise by filling a crucible, and welding on a lid. This crucible also was empty at the end of the run.

(ii) Crucible Protection.

This situation was unsatisfactory from all points of view, since no crystals were being produced in spite of the expenditure in time and materials. We concluded that there were two likely mechanisms for the attack on the platinum. (A) Platinum is very soft at high temperatures, and the considerable hydrostatic pressure of the molten lead compounds must subject the crucibles to severe mechanical strain. This could result either in large holes produced by stretching, or in re-crystallisation of the platinum with concentration of impurities at grain boundaries, followed by attack on these impurities by the flux. (B) Rare earth oxides are sometimes prepared from the oxalates, lead fluoride is sometimes prepared by precipitation from the acetate, and even 'Analar' grade reagents sometimes contain filter-paper fibres, wood splints, hairs etc. Any, or all of these could be responsible for introducing carbonaceous material into the melt. If the melt were then heated quickly, some metallic lead might be produced by reduction, falling to the bottom of the crucible where it would form a low-melting alloy with platinum.

In order to eliminate these possibilities, we adopted the following procedure. The charges are packed into the crucibles, and then heated for a period at about 460°C. At this temperature, the reaction

$$3\ PbO + \tfrac{1}{2}O_2 \rightleftharpoons Pb_3O_4$$

takes place, and when the crucible is heated further, an atmosphere of oxygen is provided inside it which oxidises any foreign reducing agents which might be present. Atmospheric oxygen is sufficient to maintain oxidising conditions after this.

The crucibles are set in high temperature cement or alumina powder in cavities drilled in refractory bricks (see Figure 2.1) thus providing adequate mechanical support. In addition, more robust crucibles with twice normal wall thickness (i.e. 0.30 mm instead of 0.15 mm) are used. As well as providing mechanical support, the firebricks facilitate manipulation of the crucibles and lessen the chance of their falling over in the furnace, help to protect the furnace fabric in the event of crucible failure, and stabilise the temperature of the flux by providing a large thermal capacity.

(iii)Crucible Packing.

The powders for the melt are weighed out in the correct proportions into a clean glass bottle, and mixed thoroughly by shaking. They are then poured a little at a time into a crucible and firmly compacted with an aluminium rod or glass stopper. The crucible is then closed



Figure 3.1

with a tightly fitting lid and embedded in cement or alumina powder, and heated to about 460°C. The temperature is then raised to about 1250°C for between 4 and 12 hours, according to the size of melt involved. The volume of the melt falls by about half upon melting, so that when very big charges are wanted, the crucibles are removed from the furnace at this stage and re-packed with powder, the whole process being repeated until all the charge is accommodated.

(iv) Crucible Cooling.

After the soaking period at the maximum temperature, the cooling cycle is commenced, and the melt cooled from 1250°C to about 950°C at 2-3°C per hour. The cooling rate is in fact slightly slower at the start of the run, speeding up somewhat after nucleation has taken place. The recently discovered melt composition for aluminium garnets is cooled to about 850°C.

At the lower end of the cooling cycle, the crucibles are removed from the furnace and allowed to cool naturally to room temperature.

(v) Separation of Crystals.

The lead matrix may be dissolved in hot nitric or acetic acids, or a mixture of the two, but generally, crystals are removed from the matrix mechanically and cleaned by boiling with 50% nitric acid. The contents of the crucibles are readily dislodged by tapping the bottom of the crucible sharply with a hammer. Only on rare occasions

are garnet crystals damaged by this method, and its two advantages, namely speed of extracting the garnets and the possibility of re-using the flux after replacement of PbF_2 lost by evaporation and garnet constituents by crystallisation far outweigh this minor trouble. The distinctive crystal habit of the garnet makes separation very simple. This is apparent from Figure 3.1 which is a photograph of horizontal and vertical sections through a garnet flux.

Discussion of Results.

The yields of really good crystals are very low. In the case of gallium garnets, about 40 g from a 475 g charge were obtained. Individual crystals up to about 5 g were grown, but the larger crystals were almost invariably twinned, or included some of the flux, or were otherwise defective. The best crystals normally grew from the sides or bottom of the platinum crucibles, and very occasionally in the body of the flux. Those growing at the surface, presumably by evaporation of the flux, were usually of very poor quality, and often multiple. The yields of useful crystals from small charges were proportionately even lower, since their surface area/ volume ratio is higher, resulting in relatively less useful crystallisation.

The yields of rare earth-aluminium garnets from the melt adapted from Nielsen's composition were even lower, about 13 g from a 475 g charge, the largest crystals being on average at least five times smaller than in the case of the gallium runs. The new melt composition still gives a

relatively low weight yield, but the size of individual crystals is greatly increased. Perfect single crystals of more than 0.7 g have been obtained from melts of 450 g.

Crystal Quality and Characteristics.

Gallium garnets are usually coloured in addition to the inherent colours of the constituent ions. For instance, yttrium gallium garnets have been obtained coloured pink, mauve, brown, yellow, green, grey as well as almost colourless. Sometimes, crystals from different parts of the same charge have displayed very different colours (mauve and yellow, for example). We have not been able to find an explanation for these colours. Spectroscopic analysis for likely transition metal impurities failed to reveal any substantial difference between differently coloured samples. A batch of yttrium gallium garnet crystals grown from the highest purity materials available displayed colours as strong as those obtained from standard materials, even though an examination of their paramagnetic resonance spectrum by Dr M.T.Hutchings revealed significantly lower iron and transition metal impurities than in the ordinary garnets.

The aluminium garnets on the other hand are almost invariably of excellent crystal quality and colour, and apart from a very slight yellowish tint in a few crystals, no 'rogue' colours have been found. Attempts to remove the colours from the gallium garnets by annealing in air, and heating in vacuum were unsuccessful, nor was it possible to induce colours in the aluminium garnets by bombardment with

relatively low weight yield, but the size of individual crystals is greatly increased. Perfect single crystals of more than 0.7 g have been obtained from melts of 450 g.

Crystal Quality and Characteristics.

Gallium garnets are usually coloured in addition to the inherent colours of the constituent ions. For instance, yttrium gallium garnets have been obtained coloured pink, mauve, brown, yellow, green, grey as well as almost colourless. Sometimes, crystals from different parts of the same charge have displayed very different colours (mavue and yellow, for example). We have not been able to find an explanation for these colours. Spectroscopic analysis for likely transition metal impurities failed to reveal any substantial difference between differently coloured samples. A batch of yttrium gallium garnet crystals grown from the highest purity materials available displayed colours as strong as those obtained from standard materials, even though an examination of their paramagnetic resonance spectrum by Dr M.T.Hutchings revealed significantly lower iron and transition metal impurities than in the ordinary garnets.

The aluminium garnets on the other hand are almost invariably of excellent crystal quality and colour, and apart from a very slight yellowish tint in a few crystals, no 'rogue' colours have been found. Attempts to remove the colours from the gallium garnets by annealing in air, and heating in vacuum were unsuccessful, nor was it possible to induce colours in the aluminium garnets by bombardment with

in the body of the melt, or from the sides or bottom of the crucibles had almost exclusively {211} faces, with occasional small {110} faces, while those on the surface were never found with {110} faces, in agreement with the observations of Nielsen and Dearborn (1958). The aluminium garnets on the other hand grow with mostly {110} faces, and very occasional {211} . These facts prove very useful in orienting garnet crystals for paramagnetic resonance experiments, since the measurements are made with the crystals oriented along a [110] axis.

Special Problems in Garnet Growth.

We have already mentioned attempts to produce samarium and praseodymium gallium garnet crystals. We also made several attempts, with various melt compositions, to make europium aluminium garnet, whose existence is neither reported, nor denied in the literature, but with no success. In every instance, we obtained crystals of $EuAlO_3$.

Initial attempts to grow gadolinium aluminium garnet using the modified Nielsen composition also produced the aluminate, $GdAlO_3$. In an attempt to favour formation of the garnet (which contains more aluminium relative to gadolinium than the aluminate), we increased the aluminium oxide content of a melt by 20% by weight. After crystallisation, we found a few excellent crystals of the garnet amongst the mass of aluminate crystals.

We also attempted to grow yttrium aluminium garnet doped with Ce^{III} by adding CeO_2 to a normal flux, in the hope that if there were an equilibrium

$$2\ CeO_2 \rightleftharpoons Ce_2O_3 + \tfrac{1}{2}O_2$$

at the elevated temperatures of crystal growth, any trivalent cerium would be incorporated in the crystals as they grew. There were no lines in the paramagnetic spectrum of these crystals which could be attributed to Ce^{III}, however.

Although the crystals produced were generally of a satisfactory standard of purity, there were always very many small unexplained lines in the paramagnetic resonance spectrum. These were probably largely caused by traces of Fe^{III} which has a very complicated spectrum in the garnet. If these lines could be eliminated, the garnets would be very suitable compounds in which to study the effects of nearest neighbour interactions between rare earth ions in dilute samples, which give rise to very weak absorption lines. We therefore attempted to produce ultra pure garnets with a view to investigating these interactions. We obtained very high purity PbO, PbF_2, Y_2O_3 and Ga_2O_3 (all at least 99.999% pure) and also some high purity platinum crucibles and lids (total impurities less than 10 p.p.m.). The resulting crystals of yttrium gallium garnet were substantially more pure than the ordinary products, but although the intensities of the impurity lines were very much reduced, their numbers remained much the same, and it was not judged worthwhile to pursue the project further. The flux technique, with the necessary long

crystallisation time and large weights of materials involved in producing small amounts of crystal, is not a suitable one for the very highest purity work.

The following garnets have been grown, at least once, as single crystals by the flux-melt method. GaG means 'gallium garnet', AlG means 'aluminium garnet', IG means 'iron garnet'.

Pure Rare Earth Gallium,Aluminium and Iron Garnets.

NdGaG	EuGaG	GdGaG	TbGaG	DyGaG	HoGaG	ErGaG	TmGaG	YbGaG	YGaG
		GdAlG	TbAlG	DyAlG	HoAlG	ErAlG	TmAlG	YbAlG	YAlG
						ErIG			YIG

'Doped' Yttrium or Lutecium Gallium and Aluminium Garnets.

0.1% Nd in YAlG

1.0% Nd in YAlG,YGaG,LuAlG,LuGaG

1.0% Sm in YAlG,YGaG

5.0% Tb in YGaG

0.1% Dy in YAlG,YGaG,LuGaG

0.3% Dy in YAlG

0.5% Dy in YAlG

1.0% Dy in YAlG,YGaG,LuAlG

5.0% Dy in YAlG

5.0% Ho in YAlG

0.05% Er in LuAlG

0.1% Er in YAlG,YGaG,LuGaG

1.0% Er in YAlG, YGaG, LuAlG, EuGaG, TmAlG, YIG

1.0% Yb in YAlG, YGaG, LuAlG, LuGaG, EuGaG, DyAlG, TmAlG, TmGaG.

5.0% Yb in TbAlG

0.05% Fe (80% isotope 57) in YGaG

0.1% Fe (80% isotope 57) in YGaG

0.1% Fe in TmAlG

1.0% Fe in YbAlG

1.0% Cr in YAlG.

Polycrystalline Garnets.

Introduction.

Single crystals of garnets are necessary for measurements of anisotropic physical properties (magnetic moment, paramagnetic resonance etc), and even for isotropic properties such as susceptibility, they have the advantage that there is no uncertainty concerning stoichiometry. This is not true of mixed garnets, however. If, for instance, a DAG (dysprosium aluminium garnet) specimen containing accurately 1% of Fe is needed, suitable single crystals cannot be made. Even if exactly 1% of Fe is added to the flux, it is almost certain that Fe will be preferentially deposited in the crystals, or remain in the flux with respect to the aluminium. Thus, the concentration in the crystal will be unknown, and may also vary from one part of the crystal to another, as the relative concentration of Fe in the melt changed during crystal growth. We have demonstrated this effect by measuring the paramagnetic susceptibilities of two different samples of nominally 1% Dy in YGaG from the same melt, and finding that the Dy concentration differed by about 5%. The garnets are not easy materials to analyse chemically, so that it is better to prepare samples in some other way in which the concentrations can be accurately controlled.

Polycrystalline samples are the obvious answer to this problem. In addition, specific heat measurements generally

need larger samples than can be made conveniently from a flux, and again, polycrystalline material is suitable. In this case, there is a further requirement, namely that the sample should be a high density non-porous sample which conducts heat well, so that it rapidly attains thermal equilibrium, and does not absorb excessive amounts of helium gas under the experimental conditions of specific heat measurements (see Chapter 7).

Wolf and Rodrigue (1957) have developed a method of preparing polycrystalline rare earth iron garnets by co-precipitation of the hydroxides, followed by heat processing.

Roberts (1960) attempted to prepare aluminium and gallium garnets by similar methods. He found that it is very difficult to buffer solutions in such a way that the rare earth and gallium or aluminium hydroxides co-precipitate, and gallium and aluminium hydroxides tend to re-dissolve in excess alkali. In addition, the precipitates are gelatinous and difficult to filter. He investigated the possibility of co-precipitating rare earth oxalates with gallium or aluminium hydroxides, and found that although the precipitation points are closer, the oxalate precipitates are coarse sand granular, and do not form the necessary intimate mixture with the hydroxides.

He also investigated the possibility of direct reaction between the finely ground oxides. The stability and hardness

of aluminium oxide (corundum) eliminate this method for production of polycrystalline aluminium garnets. Besides the contamination introduced by grinding, the finest powders produced in this way do not react up to about 1500°C. On the other hand, this method works satisfactorily for gallium garnets, and has the advantage that stoichiometry is readily achieved, since there are no doubts about incomplete precipitation. The method does not work well when one component is present in low concentration (e.g. 1% Er in YGaG) since it is very difficult to obtain homogeneous composition.

Experimental Method.

The constituent oxides are calcined at about 1000°C for at least 24 hours to decompose traces of hydroxides, carbonates and oxalates which are usually present in commercial rare earth oxides. The appropriate amounts are weighed, mixed and finely ground by hand in an agate mortar. The mixture is then subjected to the following regimen of alternate heating and grinding: -

Temperature	Time	Subsequent Treatment
950°C	3 days	re-grind
1000°C	24 hours	re-grind
1400°C	15 hours	re-grind
1460°C	15 hours	re-grind, and press into a pill under 11 tons/sq.inch pressure
1400°C	12 hours, slowly rising to	
1550°C	3 hours	

This method was successful in producing compact highly sintered blocks weighing about 20 g each of YGaG and NdGaG, but ErGaG and YbGaG, while becoming garnet, remained porous in texture and unlike NdGaG and YGaG, were rather unsatisfactory specimens in specific heat measurements made by Dr Colin Bailey (unpublished). It would therefore seem that specific conditions are needed for particular garnets, and it would probably be a matter of trial and error to find the experimental conditions appropriate to each case.

We prepared rare earth aluminium garnets in a different way. Standard solutions of rare earth nitrates were made by dissolving weighed amounts of calcined rare earth oxides in nitric acid solution. Standard aluminium nitrate solution was made by dissolving 'Analar' aluminium wire in 50% HNO_3 in the presence of a trace of mercury.

Appropriate volumes of these solutions to give the correct stoichiometry are measured volumetrically, mixed, and evaporated to dryness in a silica evaporating basin. The final stages of evaporation are performed as quickly as possible to prevent preferential crystallisation of either one nitrate. The dry mixture is allowed to cool in a desiccator, and is thoroughly ground by hand in an agate morter. The powder is transferred to a platinum crucible and placed in a furnace, and the temperature slowly raised to about 900°C over a period of some days. The powder is then re-ground, and fired at 1400°C for 24 hours.

A number of attempts were made to produce highly compact blocks of DyAlG, TbAlG, YAlG, HoAlG and ErAlG, all involving different combinations of heat treatment at temperatures up to 1750°C, grinding, and pressing into compact blocks under 11 tons per square inch pressure, but all the specimens remained porous and chalky in texture.

TbAlG was used as an 'indicator' specimen in a series of experiments to observe the various stages of the process.

Stage	Valency of Tb	Appearance
Mixed nitrates	3	white
Mixed oxides	4	chocolate brown
Garnet	3	white

The actual reaction to form garnet proceeds between 1200 and 1400°C.

A number of small samples of DAG with various substituents were prepared by this nitrate technique, following the first two stages of heat treatment only. X-ray powder diffraction measurements indicated that reaction to garnet was complete, and this was confirmed by the comparisons between the susceptibilities of these materials, and that of single crystals of DAG.

Standard solutions of yttrium, dysprosium and aluminium nitrates were made as above. A standard solution of iron was made by dissolving 'Analar' ferrous ammonium sulphate in distilled water acidified with a trace of sulphuric acid, and the following specimens were made: -

3 samples of pure DAG, and DaG specimens containing 1, 2, 3, 4,

5,6,7,8,9 and 10% Fe and 1% Cr replacing the aluminium, and 5 and 10% Y replacing the dysprosium. The chromium was added as a weighed amount of 'Analar' $CrCl_3.6\ H_2O$. A sample of $DyAlO_3$ was prepared from the same standard solutions in a similar way.

The same method was successfully used for producing a sample of praseodymium gallium garnet, starting from praseodymium oxide and high purity gallium metal.

Discussion.

It is not known whether rare earth and aluminium nitrates co-precipitate under the conditions described, but an intimate mixture of nitrates certainly forms (comparison of the weight of the anhydrous nitrate with that expected indicates that the aluminium nitrate dehydrates without decomposition). This is very soft in texture, and an intimate mixture is readily obtained by grinding. When the nitrate mixture is decomposed by heating, gases are evolved on a molecular scale, possibly in two stages, and this gives an exceedingly fine powder. The aluminium oxide is probably present as the metastable χ-form. In these circumstances, the reaction to garnet proceeds without any difficulty.

Key to Figure 3.2

V - Vibrator

D - Copper-Beryllium Diaphragm

P - Powdér Container

H - Heater

F - High Temperature Firebrick

R - Support Rod (Alumina) for Crystal

L - Centring, Lowering and Clamping Device

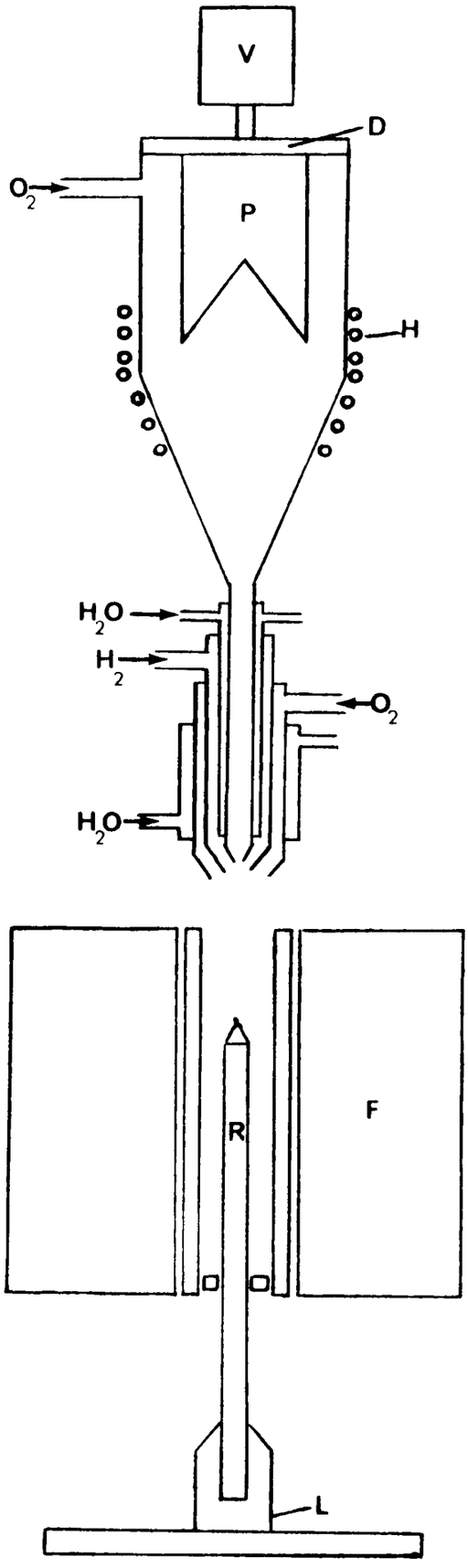

Verneuil Flame Fusion Apparatus.

Figure 3.2

The Verneuil Flame Fusion Technique.

Brief description of the apparatus.

This furnace belongs to Messrs Mullard's Research Laboratories, Redhill, Surrey, and I am indebted to them for being allowed to use it for a period, and for instruction from their staff, particularly Mr Owen Hill, in its working.

A schematic diagram of the furnace is reproduced as Figure 3.2. The powder to be grown as crystal is contained in a canister (P) whose bottom consists of an inverted cone of 60 mesh brass gauze. This canister is suspended from a copper-beryllium diaphragm (D), and may be vibrated by means of an electrically driven vibrator (V). The amplitude of the vibration, and hence the powder feed flow, is varied by altering the current through the vibrator.

The feed powder falls into a conical hopper, and thence via a central feed tube and burner cone to the flame, together with the inner stream of oxygen which enters through a side tube in the hopper. The hopper is highly polished inside, and electrically heated (H) to just above 100°C to ensure smooth powder flow.

The burner consists of three concentric tubes terminating in stainless steel nozzles. The whole assembly is water-cooled. The central jet has an internal diameter of 1/16", and an external end diameter of 5/16"; the next cone through which the hydrogen is introduced has an end diameter of 7/16", and the outer cone which also carries oxygen has an end diameter of 9/16".

The flame burns in an alumina tube i.d. 40 mm, which is surrounded by refractory firebricks (F). The tip of the flame where the crystal grows is observed through dark glass through a window 2 x 1¼ cm cut in the side of the tube, 14 cm below the burner nozzles. Some 8 cm lower, a larger window is cut to allow exhaust gases to escape. The crystal is grown on an alumina rod (R) which passes down the centre of the alumina tube. At the lower end, the rod passes through an asbestos ring which seals off the tube and prevents the hot exhaust gases from playing on the centring and clamping devices in which the rod is mounted. They in turn are attached to a platform (L) which can be raised or lowered by means of a variable speed electric motor.

There are a number of variables in this method, namely the rate of powder flow, the rate of gas flow in each of the nozzles and the rate of lowering of the crystal mount. The gas flow rates primarily affect the size, shape and temperature of the flame, while the powder flow and lowering rate influence the size and quality of the crystal produced. The main problem of growing single crystals by the Verneuil technique is that of finding empirically the correct combination of these variables for the various stages of crystal growth.

The most difficult stage is the initial one, that is, the formation of a suitable seed crystal. One way is to build up a sintered cone of powder on the alumina support rod (Figure 3.3d) by starting with a cool flame and fast powder flow. The

Key to Figure 3.3

(a) Method used for growing ruby crystal

(b),(c),(d) Methods used in attempts to grow DAG crystal

R - Supporting Alumina Rod

C - Refractory Alumina Cement

S - Seed Crystal

L - Contact Angle between Molten and Solid Material

D - DAG Powder

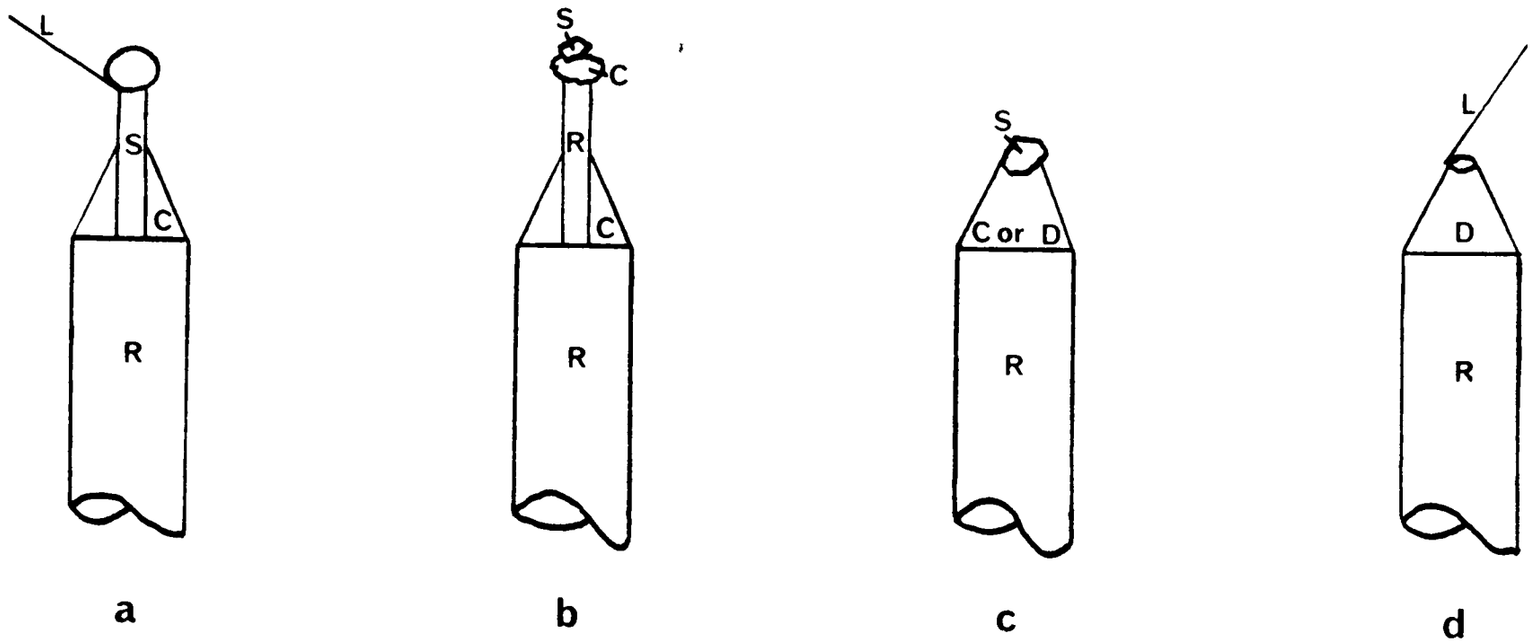

Figure 3.3

temperature of the flame is then increased, and the tip of the cone melted. The rate of lowering is greatly reduced (to about 1cm per hour) and the powder flow adjusted so that the molten surface remains in the same position in the flame. Thus, solidified material is effectively slowly withdrawn from the molten cap, and formation of a single crystal commences.

The next stage is to adjust the conditions ,particularly the powder flow,and temperature, in such a way that the narrow seed crystal gradually increases in diameter. Great care must be taken that all the powder is properly molten, and that the molten liquid does not overflow and run down the outside of the seed crystal, either effect causing polynucleation.

An alternative method is to start from a seed crystal whose tip is carefully melted in the flame, and continue with the widening process from there. This is a much simpler proceedure, and was the one we employed, flux grown DAG crystals being used as seeds.

A single crystal of chromium-doped aluminium oxide was very easily grown starting from a seed crystal rod (see Figure 3.3a). The approximate gas flow rates were 20-30 litres per minute of hydrogen, 3 litres per minute of oxygen through the central nozzle and between 0 and 9 litres per minute through the outer nozzle.

The viscosity and surface tension of molten aluminium oxide are so high that there is no difficulty in widening

the crystal. The molten cap of liquid is very stable, and tends to widen almost automatically on crystallising (Figure 3.3a).

We made a number of attempts to grow a single crystal of dysprosium aluminium garnet by the Verneuil technique. A large batch of powder was prepared by the mixed nitrate method. Various methods of mounting the seed crystals (each weighing about 90 mg) were tried, and these are illustrated in Figure 3.3b and c. Of these, only (c) with the seed crystal mounted in DAG powder was satisfactory. In the other cases, the crystal melted completely, and it was necessary to start again using the sintered cone technique (Figure 3.3d)

The viscosity and surface tension of molten DAG seem to be much lower than molten aluminium oxide, so that only a much smaller liquid cap can be produced without overflowing. The crystal therefore tends to narrow rather than widen (compare Figure 3.3a and d), so that this stage demands very careful and precise control of temperature and powder flow. As a result of overflowing of the molten cap, we were unable to produce a large single crystal of DAG. However, a compact sintered block resulted from one attempt, and an excellent specific heat sample weighing about 21g was prepared from it. (see Chapter 7).

Conclusions.

There seems to be no inherent reason why aluminium garnets should not be produced as good big single crystals

by the Verneuil process. There were substantial areas of single crystals in some of the attempts we made, but much effort would have to be expended in finding the correct crystal growth conditions, and the effort and expense involved in this research, and also in producing sufficient starting materials, probably make the project scarcely worthwhile.

Chapter 4.

The Paramagnetic Susceptibility Apparatus.

Introduction.

The magnetic susceptibility of a substance is defined as the ratio of the magnetic moment induced by a magnetic field to the magnitude of the field as it tends to zero

$$\chi = \left(\frac{\delta M}{\delta H}\right)_{H=0}$$

The direction of the induced moment does not necessarily lie in the direction of the field, so that measurements must be made along the principal directions of a crystal, not more than three measurements being necessary for a complete determination.

The methods for measuring small magnetic moments may be divided into two main classes, namely those in which the force on a sample in a non-uniform field is measured, and those in which magnetic induction is measured. Force methods can be made very sensitive, and can yield absolute susceptibilities, but they are neither convenient methods for low temperature operation, nor suitable for measuring anisotropic crystals (Wolf, 1957).

Magnetic induction methods usually depend on the change in mutual inductance of a coil system caused by the sample. This change may be observed ballistically with a galvanometer, or by balancing an a.c. bridge. In the former method, the galvanometer is connected to the secondary coil, while a d.c. current flows in the primary. Then either the d.c. current

is reversed, or the specimen is quickly pulled out of the coil, and the deflection of the galvanometer measured.

In the a.c. method, an a.c. current flows in the primary, and the secondary is connected to an a.c. bridge, where the continuous signal is measured by a null method. Probably the main disadvantage of an a.c. method is that it cannot be used to measure metals and other electrical conductors, because of the large signal produced in the secondary coil by the eddy currents induced.

The apparatus to be described was designed as an a.c. method, and has in general been used in this way in the work described in this thesis. However, in the case of dysprosium aluminium garnet (Chapter 6) it was adapted for d.c. measurements by passing a steady d.c. current through the primary, and observing the deflection on a ballistic galvanometer connected to the secondaries when the specimen was moved from one secondary to another (in the way described below).

The Hartshorn Bridge Circuit.

A block diagram of the circuit used is reproduced as Figure 4.1. It resembles that described by Benzie and Cooke (1950), the tuned null-detector being of the kind described by Erickson, Roberts and Dabbs (1954).

The primary coil is supllied with an a.c. current of 175 c.p.s. from an oscillator through a power amplifier.

Key to Figure 4.1

O - Oscillator

A - Power Amplifier

P - Potentiometer

I - Mutual Inductance Bridge

T - Tuned Amplifier

c.r.o. Cathode Ray Oscilloscope

S - Specimen

C - Mutual Inductance Coil System

Electrical Circuitry of Susceptibility Apparatus.

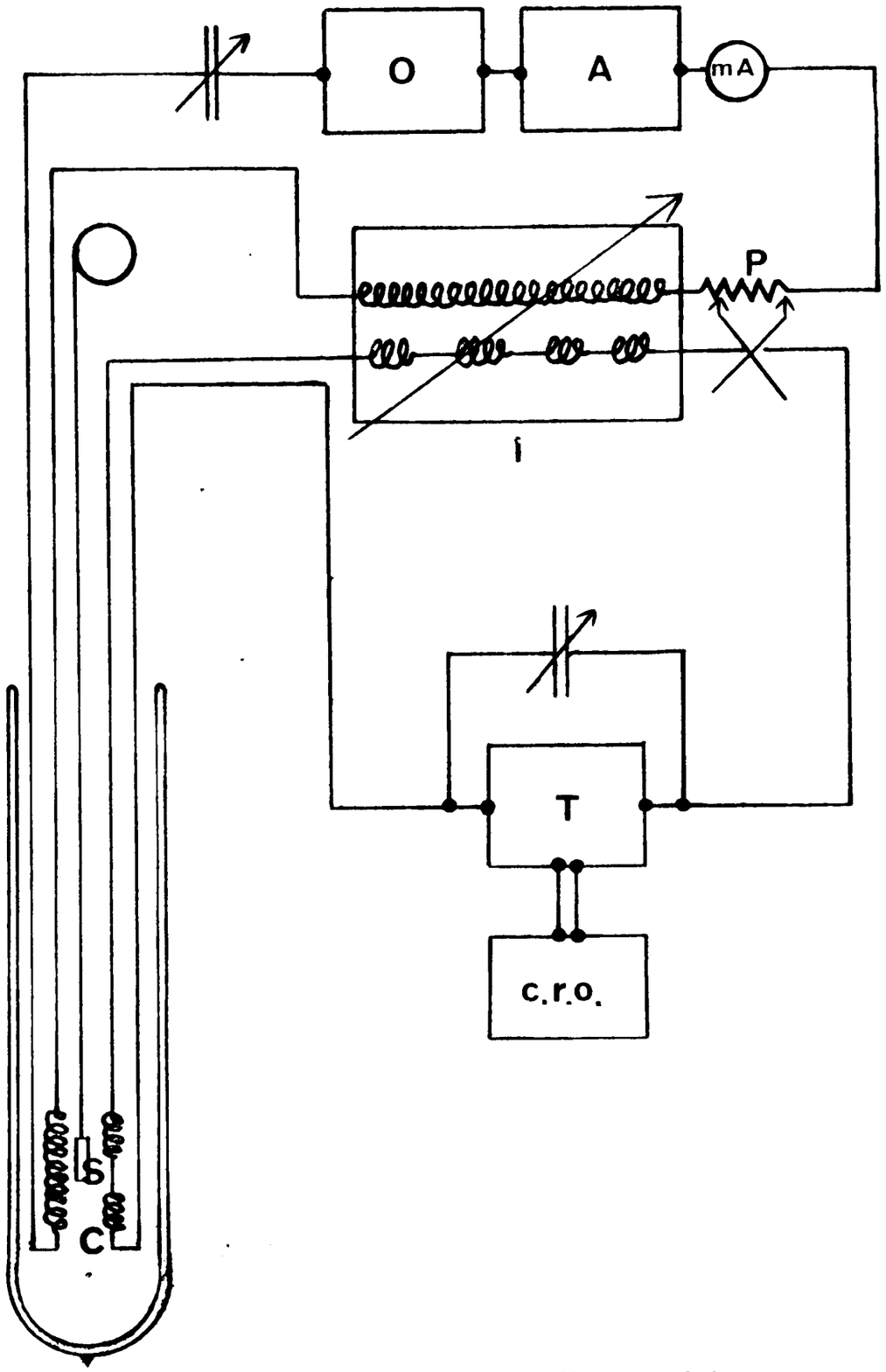

Figure 4.1

This frequency was chosen as a good compromise between reduced sensitivity at lower frequencies, and introduction of spurious higher frequency effects caused by the big self-capacitance of the mutual inductance coil system. 175 c.p.s. is distinguishable from mains pick-up, but beats with it to produce a simple stationary pattern on the cathode ray oscilloscope, which greatly facilitates location of the balance point.

Although ideally susceptibility is independent of frequency in small fields (DAG was an exception, see Chapter 6), the balance point of the coil is slightly frequency-dependent, owing to the self-capacitance of the coils. Since two balance points are needed for each susceptibility reading, care was taken that the frequency did not drift appreciably between any pari of inductance readings.

The bridge is balanced by adjusting the mutual inductance and potentiometer of the bridge. The mutual inductance bridge consists of five switched decades ranging from about 1.5×10^{3} μH to about 1.5×10^{-2} μH. The self-consistency of the decades was often checked during experiments by switching from ten units of one decade to one unit of the next higher decade after the balance point had been found. The position of the balance point never had to be altered. The potentiometer was used to balance out the effect of the self-capacitance of the coils, and of losses within the specimen, by feeding into the secondary circuit a small

out-of-phase voltage from the primary circuit. The change of phase caused by the sample can be regarded as an out-of-phase contribution to the susceptibility, and is usually very small or zero for paramagnetic substances.

To increase the sensitivity of the circuit, and its discrimination against frequencies other than 175 c.p.s., both the primary and secondary circuits are tuned with suitable capacitors. Owing to the push-pull output of the oscillator power amplifier, the second harmonic was negligible, but in spite of the tuning, some third harmonic was present as a result of harmonic distortion in the primary current. So that the bridge could be completely balanced, this distortion is removed by means of a filter in the input of the tuned amplifier.

The Mutual Inductance Coils.

Following the original design of McKim and Wolf (1957), the apparatus consists at heart of a coil system in which the secondary is wound in two sections as nearly identical as possible, and in opposition to each other. Susceptibility is then measured by moving the specimen from the centre of one half of the secondary to the centre of the other half. Before this design was evolved, either the specimen had to be removed completely from the coil at each point, so that the inductance of the empty coil system could be measured, or the specimen had to be kept stationary, and only the change

in mutual inductance with temperature measured.

To achieve sufficient sensitivity within reasonable dimensions, the secondary windings must consist of a large number of turns of very fine gauge wire (about 46 s.w.g.) Owing to the stresses and strains caused by repeated cooling and warming cycles, these windings have a limited life varying from a few cycles to several hundred, according to the detailed construction of the coil.

Leask (1960) and Wyatt (1963) made considerable developments in coil design. Leask lengthened the primary windings to improve the uniformity of the field at the secondaries, and investigated the use of fibreglass resin to bond the turns together, rather than 'Tufnol' varnish as used originally. Wyatt made a coil approximately 20 times more sensitive by winding many more turns on primary and secondaries, but the instability of the coil increased almost as much as the sensitivity, so that the net gain in accuracy was very slight. Wyatt also used 'Araldite X83/11' epoxy resin as a "potting" agent, painting it on the coils during the winding process. He also instituted separate telescopic formers for the primary and secondary windings, a great improvement on the previous system of winding the primary directly on top of the secondaries. Normally, it is the secondary windings which break (more turns and higher gauge wire), and with the old system, it was necessary to destroy a perfectly good primary in order to replace the faulty secondary.

Key to Figure 4.2

H - Adjustable Stops

F - Traverse Mechanism

D - Flexible Coupling

G - Tufnol Rod

Q - Low Pressure Helium

P - Pressure Measuring Tube

N - Pumping Line

I - Thermal Contact Clips

L - Outer Dewar Vessel

M - Inner Dewar Vessel

J - Liquid Refrigerants

E - Mutual Inductance Coil

S - Specimen

R - Heating Resistor

Mutual Inductance Coil for Susceptibility Apparatus.

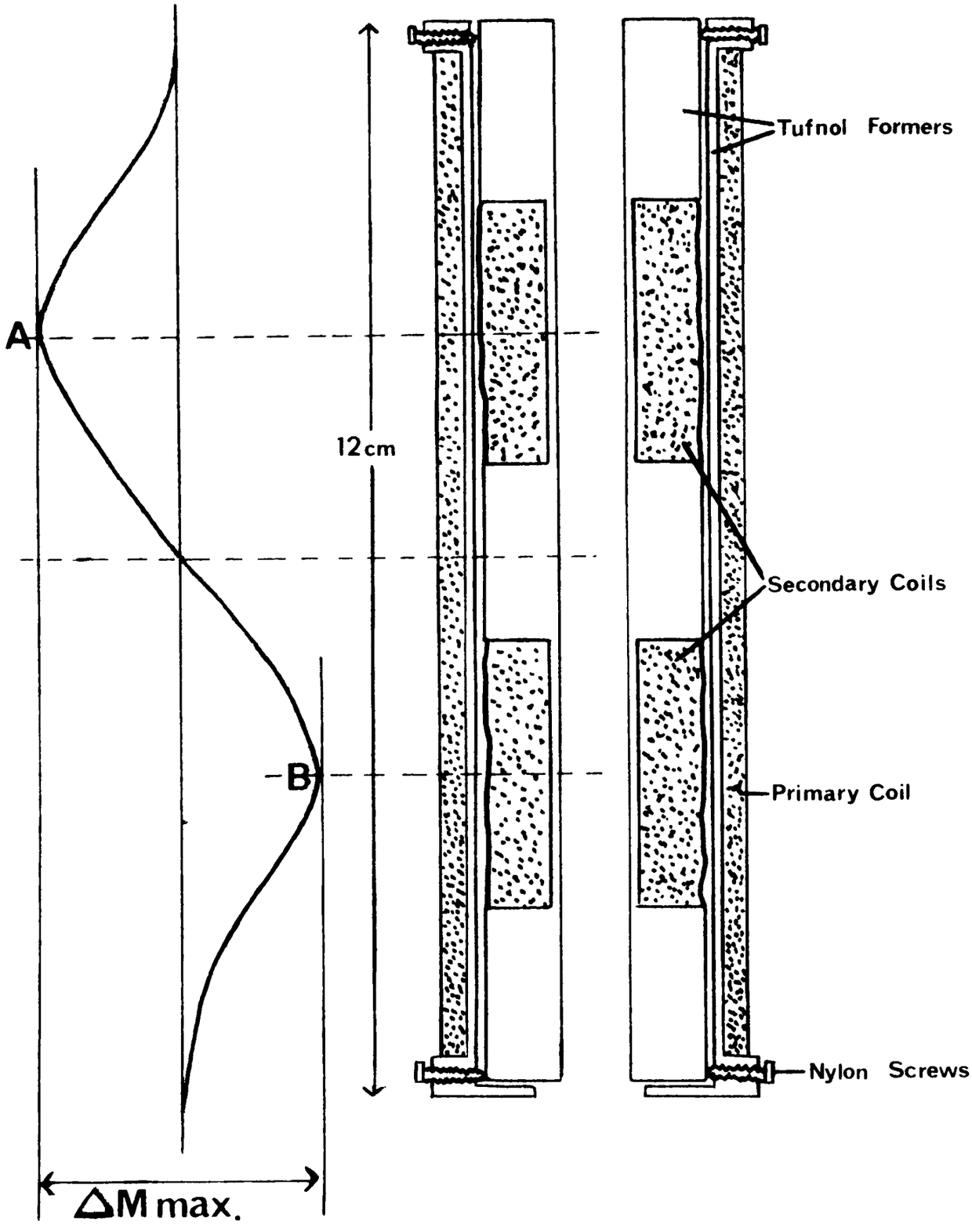

Figure 4.2

Figure 4.2 represents a coil constructed according to the improved design of Wyatt. The two opposing secondaries each consist of 12,100 turns of 46 s.w.g. copper wire with double rayon insulation wound on a 'Tufnol' former. 'Araldite' was painted on continuously during the winding process, and hardened at the end by being baked at 90°C for 2-3 hours. The primary consists of 2,232 turns of 38 s.w.g. single rayon enamelled copper wire on a second 'Tufnol' former, carefully machined to be a tight sliding fit over the secondary coil former. These windings were also potted in 'Araldite' and baked. The coil system was assembled, and the two coils firmly fixed with respect to each other by six nylon screws.

In spite of the care taken to make the coils as alike as possible, the inductance had to be balanced finally by adding more turns to one end of the primary. The coil was connected into the bridge circuit, and cooled to liquid nitrogen temperatures. The mutual inductance decades were set to half of their full reading, and the bridge balanced by inserting a piece of iron a short distance into one end of the coil. The iron was removed, and additional turns wound on the primary at the same end as the iron was inserted, till the bridge was more or less balanced. 'Araldite' was painted on these additional turns and baked, and the coil was then built into the cryostat.

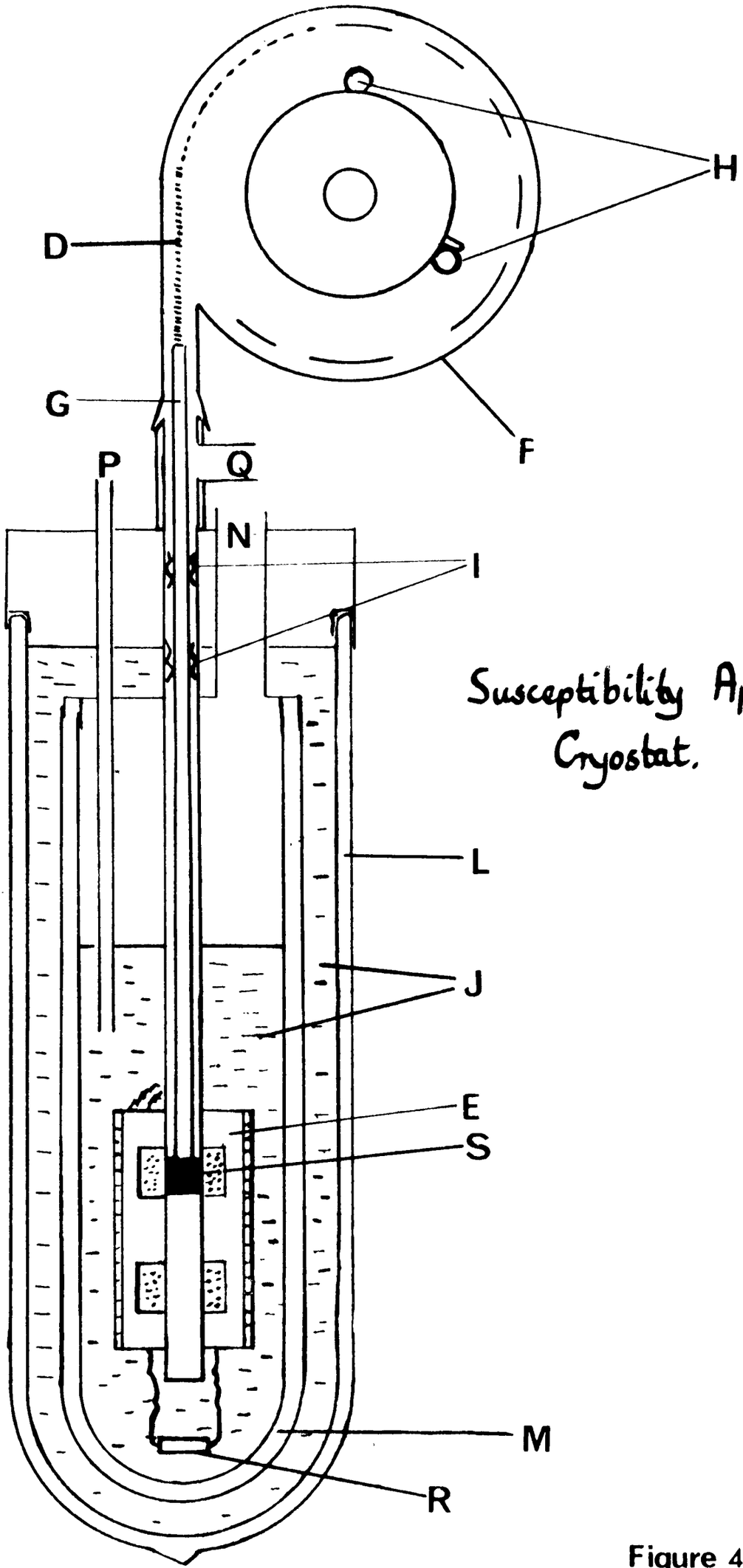

Susceptibility Apparatus
Cryostat.

Figure 4.3

General Description of the Cryostat.

Figure 4.3 is a simplified diagram of the cryostat showing the main features of the apparatus. The specimen (S) in its holder is a sliding fit in the specimen space, a glass tube sealed off at the lower end, and joining an 8 mm german silver tube just below the inner dewar cap. This tube is evacuable, and experiments are carried out with a few mm of helium gas in the tube to maintain thermal contact without introducing serious convection. A glass tube is used to minimise heat leakage and avoid spurious eddy current effects which would be caused by metal tubing in the vicinity of the coil. The specimen is moved on the end of a long 3 mm paper-bonded 'Tufnol' rod (G) by means of the traverse mechanism placed at the top of the apparatus (F). This consists of a grooved brass drum to which is fixed one end of a flexible coupling (D)(a piece of spring curtain rod) which is also joined to the upper end of the 'Tufnol' specimen rod. The brass drum rotates between end-stops (H) arranged so that both the position and length of traverse of the specimen in the coil are adjustable. The drum shaft is sealed with an O-ring.

The casing of the traverse mechanism is attached to the apparatus by means of a greased ground metal cone joint, so that it is possible to remove the specimen rod and insert a new specimen without dismantling the apparatus. Heat flow down the specimen rod is limited by two small

metal spring clips (I) which press against the metal specimen tube, and anchor the rod thermally at liquid hydrogen temperatures.

The coil system is a sliding fit on the specimen tube, and is held in position by a piece of rubber tubing. This also locates a piece of cardboard which fixes the coil with respect to the wall of the inner Dewar (M), and thus prevents vibration and mechanical oscillation of the coil. The electrical leads from the coil are anchored to the specimen tube, and are brought out of the inner dewar via two 2 mm german silver tubes which pass through the liquid hydrogen shield to room temperatures, where they are sealed with black wax. These tubes also carry the leads to the heating resistor (R) which is suspended at the bottom of the dewar (M) and dissipates up to three watts.

The inner dewar, which holds the liquid refrigerant, consists of two similar concentric monax glass envelopes terminating in glass to metal 'Covar' seals. They are sealed to the inner dewar cap with Wood's metal solder. The space between them is sealed off after evacuation with a mercury diffusion pump through a tube extending to the top of the cryostat. The dewar cap also includes a 12 mm pumping line, an 8 mm vapour pressure line and a 10 mm helium syphon line.

The outer dewar (L) is a conventional sealed off vessel which contains the shielding refrigerant, liquid hydrogen or nitrogen.

Figure 4.4

The Specimen Containers.

The normal specimen containers were 'teflon' cylinders 20 mm long, 5 mm internal diameter and 0.5 mm wall thickness. One end was tapped with a 6 B.A. thread by which it was screwed on the specimen rod. The other end was closed by a lid held in place with a nylon pin. A diagram is reproduced as Figure 4.4a. Any space unoccupied by the specimen was filled with cotton wool or 'Kleenex' tissue, both of which were found by experiment to be diamagnetic. In the case of powders, this also prevented loss or movement of the specimen during an experiment. For measurements on more powerfully paramagnetic materials, needing a smaller sample of known shape, box (b) was used, fitting inside box (a). This box had internal dimensions of a 7:1 cylinder. For the most accurate measurements, two 'teflon' inserts were manufactured (c), their internal shape being accurately machined to form halves of a 4:1 oblate spheroid. (d) shows a special holder manufactured from 'tufnol' to hold an oriented single crystal sphere of DAG. 'Tufnol' was chosen chosen since it is diamagnetic, yet unlike 'teflon' bonds with 'Araldite', allowing the crystal to be firmly attached. A 'teflon' sleeve fitted tightly round the 'tufnol' holder to make a tight sliding fit inside the specimen space.

The susceptibilities of all the boxes were found to be negligible for all but the very weakest specimens.

Gas-handling Apparatus.

The usual techniques of low temperature experiments were used in transferring liquid refrigerants, pumping them to reach the desired temperatures, measuring their vapour pressures, and in evacuating dewar and specimen spaces.

Experimental Procedure.

The apparatus was pre-cooled to liquid nitrogen temperatures overnight. A contact rod, copper from the liquid hydrogen level to the coil, and german silver at the top, was inserted in the specimen space, which was then evacuated together with the cryostat with a rotary pump. The outer dewar was then filled with liquid nitrogen and helium gas allowed to enter the specimen space and cryostat very slowly to a pressure of one atmosphere. In this way, the helium is cold from the time of its entry, and there is very little further contraction as a result of cooling. After about 3 hours, or more usually, the following morning, the nitrogen was poured out of the outer dewar, and replaced by hydrogen, the helium gas pressure being maintained at one atmosphere throughout. Cooling to liquid hydrogen temperatures took about 45 minutes from introduction of the liquid. The contact rod was then removed as quickly as possible while a stream of helium gas was allowed to escape from the specimen space to prevent condensation of air. The specimen and rod were then inserted

in similar conditions, and the specimen space evacuated to a few mm pressure. Liquid helium (or hydrogen) was then syphoned into the inner dewar, normally 350-400 cc of liquid helium were boiled off in cooling, and between 400 and 600 cc of liquid remained for the experiment.

The traverse of the specimen in the coil was then adjusted for maximum ΔM.

Specimens were changed by filling the specimen space to atmospheric pressure with helium gas, and rapidly removing the specimen rod. The new specimen was then put in as far as the liquid hydrogen level, and allowed to pre-cool there for about a minute. During this time, the space was sealed with a split rubber bung around the specimen rod, and a slight over-pressure of helium gas maintained. When the specimen was then lowered into the liquid helium level, very little was boiled off.

Measurements were generally made as a function of temperature. This was controlled by adjusting the vapour pressure over the refrigerant by controlling the pumping speed through a needle valve, or a Saunders valve. The pressure was measured on a mercury manometer, and monitored by means of a differential oil manometer.

Calibration of the Apparatus.

Since this method is not capable of giving absolute susceptibility measurements, it is necessary to calibrate

the apparatus against some substance whose behaviour is accurately known. Ideally, this substance would also be chemically inert, and of known shape, and preferably be magnetically isotropic, for instance, a sphere of garnet. Such a standard could then be set up once, and thereafter used whenever re-calibration was necessary. Unfortunately, there does not seem to be any substance with all these desirable properties. The standard chosen was hexahydrated manganous ammonium sulphate, $Mn(NH_4)_2(SO_4)_2.6H_2O$ whose magnetic behaviour is well known, but which must be freshly prepared when needed, since it tends to effloresce. It is fairly readily crystallised by dissolving equimolar amounts of 'Analar' ammonium sulphate and manganous sulphate in warm de-ionised water. The crystals for the measurements are individually selected for freedom from occlusion and other defect, and are carefully dried with tissue before being packed into a specimen container.

In spite of the care taken with purity and good crystal quality, the agreement between different calibration samples was not always good, and it was often necessary to take the average value from a number of different samples. It follows that the overall absolute accuracy of the apparatus cannot be greater than 1% because of this uncertainty in calibration.

The apparatus was also calibrated in the liquid hydrogen

temperature range, and the calibration constant was found to be identical. The susceptibility of manganous ammonium sulphate is too low at liquid nitrogen temperatures for an accurate calibration, but there is some indication from the apparently slightly different Weiss Θs of the same materials between the two temperature ranges that there is a small change (see Chapter 9 and Wyatt,1963). This is not unreasonable, since thermal expansion of the coil would be expected to affect its inductance.

A secondary standard of a single crystal of ytterbium gallium garnet was set up, and this was always found to give the same reading on the bridge to within 0.1%, showing that the characteristics of the coils do not alter with time over long or short periods. It also indicates that the apparatus is capable of much higher absolute accuracy if a suitable calibration constant can be found.

Using a calibration sample, the characteristics of each coil were mapped out by finding the two positions (A and B on Figure 4.2) having the greatest effect on the inductance, and adjusting the length of traverse to correspond with the distance between (A) and (B). The difference in calibration between long and short specimens is not found to be significant.

The Magnetic Properties of the Calibration Standard.

The ground state of Mn^{II} in manganous ammonium sulphate

is $^6S_{5/2}$. The crystalline field splitting is very small (about 0.3 cm^{-1} Bleaney and Ingram,1951) and there are no excited states lower than 10,000 cm^{-1} above the ground state (Condon and Shortley,1935). The susceptibility may therefore be calculated from the ideal 'spin only' expression: -

$$\chi_M = \frac{N g^2 \beta^2 S(S+1)}{3k(T-\theta)} = \frac{4.375}{T-\theta}$$

where N Avogadro's number = 6.0247×10^{23}

Bohr magneton = 0.92733×10^{-20}

k Boltzmann's constant = 1.3805×10^{-16}

g Spectroscopic splitting factor = 1.998

S Spin quantum number = 5/2

Since this salt is magnetically dilute, the interactions between ions are small, and somewhat variable, according to the aggregate state and surface condition of the specimen, but the Weiss θ is of the order of 0.003° (Erickson and Roberts, 1954). A large number of small crystals was taken as the specimen, so that it could be regarded as a powder, and the slight anisotropy of the salt ignored.

Chapter 5.

The Paramagnetic Susceptibilities of Rare Earth Garnets.

Introduction.

In this Chapter we report measurements of the low temperature paramagnetic susceptibilities of most of the known rare earth aluminium and gallium garnets. The only exceptions are the diamagnetic lutecium aluminium and gallium garnets, and samarium and europium gallium garnets. These latter two compounds are potentially interesting, but only weakly paramagnetic, and the traces of very strongly paramagnetic impurities (mainly Gd) present in the commercially available oxides would mask the inherent behaviour of the Sm and Eu.

The two general aims of the work were to obtain data towards an understanding of the ferrimagnetic rare earth iron garnets, and to survey the properties of this class of materials in order to find suitable specimens for more detailed investigation. Although praseodymium and neodymium do not form iron garnets, the gallium compounds have been included here for the sake of completeness.

Some measurements of dilute garnets have also been made for comparison with the paramagnetic resonance results on the same materials, and also for comparison with the concentrated materials.

In almost every instance, the measurements were made on single crystals, selected individually for optical quality and freedom from inclusions. Hence, there are no

TABLE 1

Principal g values for four rare earth ions

in each of four diamagnetic garnet lattices

Ion	Host Lattice	g_x	g_y	g_z
Nd^{3+}	LuGaG	2.083 ± 0.007	1.323 ± 0.007	3.550 ± 0.007
	YGaG	2.027 ± 0.008	1.251 ± 0.008	3.667 ± 0.018
	LuAlG	1.789 ± 0.005	1.237 ± 0.006	3.834 ± 0.005
	YAlG	1.733 ± 0.002	1.179 ± 0.002	3.915 ± 0.026
Dy^{3+}	LuGaG	13.45 ± 0.10	0.57 ± 0.10	3.41 ± 0.03
	YGaG	11.07 ± 0.2	1.07 ± 0.14	7.85 ± 0.10
	LuAlG	2.29 ± 0.03	0.91 ± 0.05	16.6 ± 0.3
	YAlG	0.73 ± 0.15	0.40 ± 0.20	18.2 ± 0.4
Er^{3+}	LuGaG	3.183 ± 0.015	3.183 ± 0.015	12.62 ± 0.05
	YGaG	4.69 ± 0.03	4.03 ± 0.02	10.73 ± 0.05
	LuAlG	6.93 ± 0.02	4.12 ± 0.03	8.43 ± 0.04
	YAlG	7.75 ± 0.09	3.71 ± 0.02	7.35 ± 0.08
Yb^{3+}	LuGaG	3.653 ± 0.013	3.559 ± 0.013	2.994 ± 0.011
	YGaG	3.73 ± 0.02	3.60 ± 0.02	2.85 ± 0.02
	LuAlG	3.842 ± 0.005	3.738 ± 0.007	2.594 ± 0.004
	YAlG*	3.87	3.78	2.47

*Carson and White (1960)

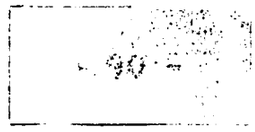

uncertainties concerning composition or phase. In the one exception, praseodymium gallium garnet which was polycrystalline, an x-ray powder photograph of the specimen was carefully compared with a similar photograph of powdered neodymium gallium garnet single crystals, and since there were no unidentified lines, it was assumed that the sample was a substantially pure garnet phase.

Owing to the nature of the specimens, there was usually some uncertainty concerning the demagnetising corrections which should be applied for the shapes of the samples, since neither these, nor the packing fractions were accurately known. This effect is negligible with the weakly paramagnetic thulium and praseodymium materials, but would make a small difference to the values of the Weiss Θs of some of the other garnets. The gadolinium garnet specimens were packed into a known shape of container (a 7:1 cylinder) so that a shape correction has been made for these measurements.

Comparison of Results with Resonance g-values.

It is apparent from Table 1 that the behaviour of most rare earth ions is dependent on the slight changes in crystal field caused by altering the host lattice. Thus, for instance, there are appreciable differences between the g-values of dysprosium in lutecium aluminium garnet, and in yttrium aluminium garnet. It follows that the

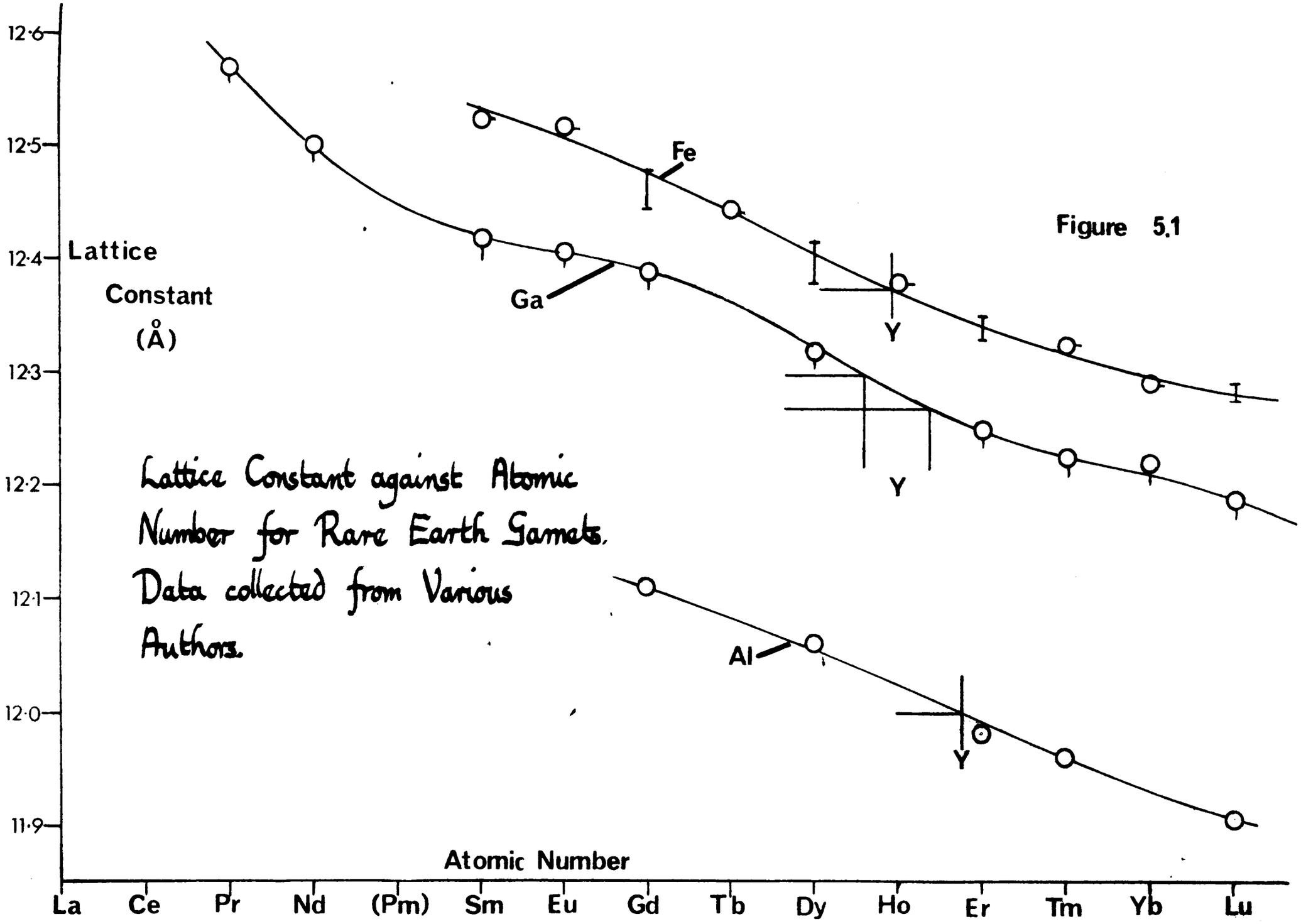

Figure 5.1

Lattice Constant against Atomic Number for Rare Earth Garnets. Data collected from Various Authors.

g-values will be different again in dysprosium aluminium garnet, though they cannot be measured directly by resonance in such a material, since the line-widths are too great.

On the evidence of the lattice constants of the garnets (see, for instance, Bertaut and Forrat,1956 and Euler and Bruce, 1962) yttrium can be regarded as a rare earth with atomic radius approximately intermediate between holmium and erbium, Figure 5.1.* Any comparisons between the magnetic behaviour of a particular rare earth in concentrated and in dilute garnets should be made with minimum lattice constant difference. Thus, for instance, the g-values of Yb in lutecium garnets should be invoked to explain the behaviour of concentrated Yb garnets, rather than the corresponding g-values in yttrium garnets. Conversely,

---

* The factor actually determining the crystal field in detail is not the lattice constant, but rather the values of the oxygen parameters, which must be determined for each individual garnet. Thus, it is quite possible that yttrium is not intermediate between erbium and holmium in this respect. When the g-values of the four ions measured by resonance (Table 1) are arranged in progression of ascending or descending order, the same order of host lattice is reached in each case. This order does not correspond with the order of ascending or descending lattice constants of the host garnets, however.

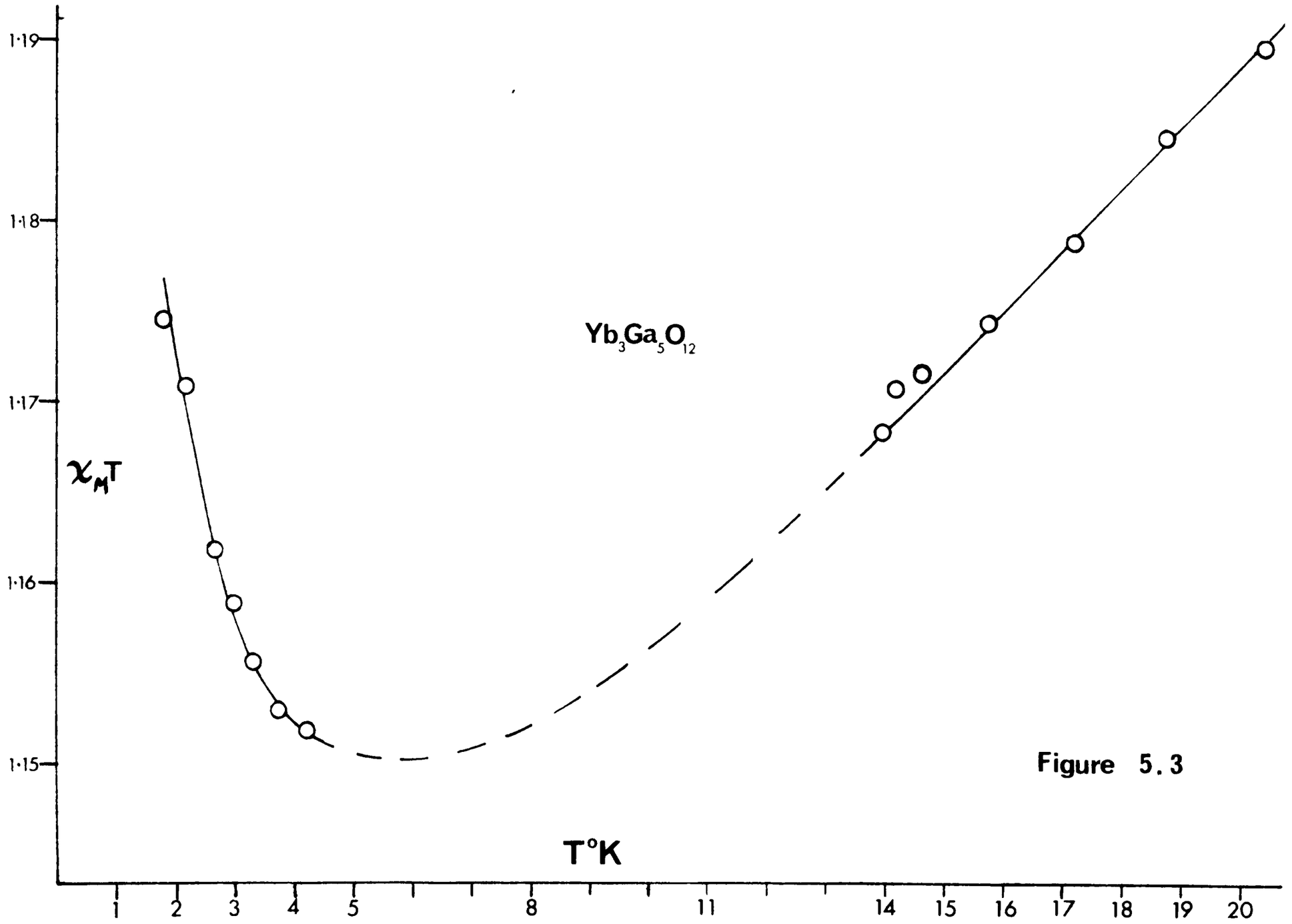
1·19
1·18
1·17
1·16
1·15
$\chi_M T$
$Yb_3Ga_5O_{12}$
T°K
1
2
3
4
5
8
11
14
15
16
17
18
19
20

Figure 5.3

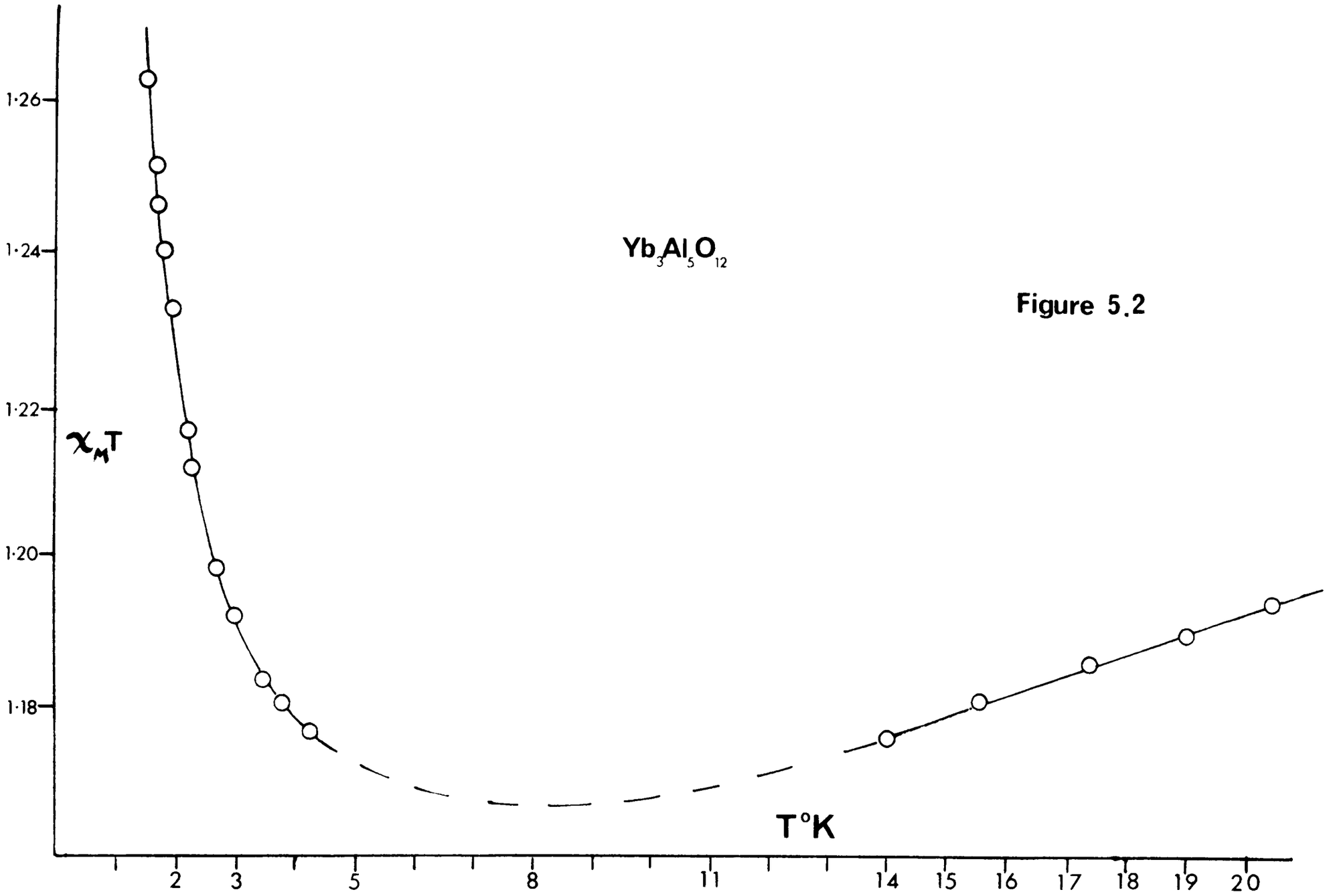
1·26
1·24
1·22
1·20
1·18
$\chi_M T$
$Yb_3Al_5O_{12}$
T°K
2
3
5
8
11
14
15
16
17
18
19
20

Figure 5.2

the behaviour of dysprosium in pure DAG is closer to its behaviour in yttrium than in lutecium aluminium garnet. Extrapolation of the behaviour of an ion such as neodymium from the yttrium garnet to the concentrated garnet is very uncertain. A further difficulty concerning extrapolation is the possibility of added distortion of the local crystal field when a large ion such as Nd (ionic radius 0.995) is accomodated in a lattice comprising mainly yttrium ions (ionic radius approximately 0.89)(Wells,1962).

Ytterbium aluminium and gallium garnets.

The smoothed experimental results for these two compounds (Figures 5.2 and 5.3) were fitted to a law of the form: -

$$\chi_M = C/(T - \theta) + \alpha$$

with the following constants

	YbGaG	YbAlG
θ (corrected to spherical shape)	$-0.048 \pm 0.01^{\circ}K$	$-0.139 \pm 0.01^{\circ}K$
α	0.00358 ± 0.00002 mole^{-1}	0.00359 ± 0.00002 mole^{-1}
C (experimental)	1.116 ± 0.005 mole^{-1}	1.111 ± 0.0005 mole^{-1}
C (calculated from Lu g-values)	1.096 ± 0.003 mole^{-1}	1.111 ± 0.003 mole^{-1}

The agreement between the measured Curie constants and those calculated from the resonance results is very good. There is no immediate detailed explanation of the ferromagnetic Weiss θs observed, though it must be assumed that this is the result of the combined magnetic dipole and

Energy Levels of Yb^{3+}

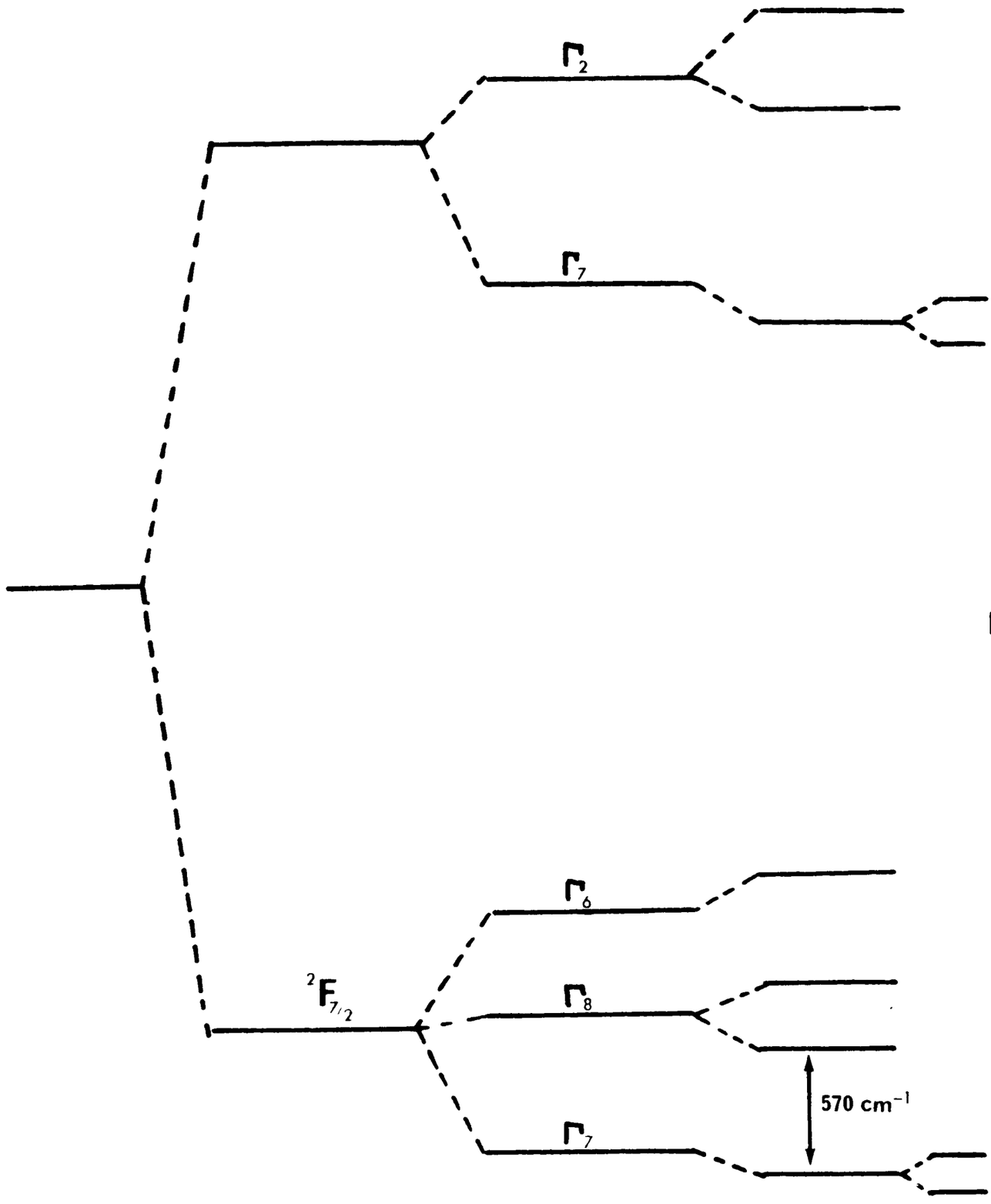

Figure 5.4

exchange interactions between the Yb ions. The stronger interactions in the aluminium garnet are typical of the whole series of compounds, and probably result from the smaller lattice constant which brings the interacting ions closer together. Of all the garnets measured, only the Yb compounds showed a negative Weiss θ, that is, a tendency to ferromagnetic ordering.

The very similar values of the temperature independent susceptibilities indicate that the energy separation between the ground state and the higher state or states giving rise to the temperature independent paramagnetism is much the same in each case. Assuming that the crystal field in the garnet has purely cubic symmetry, the energy separation between the groundstate Γ_7 doublet and the excited state Γ_8 quartet (see Figure 5.4) is approximately 570 cm^{-1}. This is in good agreement with the spectroscopic work of Pappalardo and Wood (1960), but not in good agreement with the specific heat measurements of Bailey (unpublished) who finds a separation between the states less than half of this value.

The general similarity in behaviour between the aluminium and gallium compounds is in agreement with the resonance measurements of Carson and White (1960), Ryan (1960) and Hutchings (1963), Table 1, and also additional results on Yb in EuGaG, TmGaG and TmAlG (Hutchings, 1963). The isotropy of the resonance g-values also suggests that

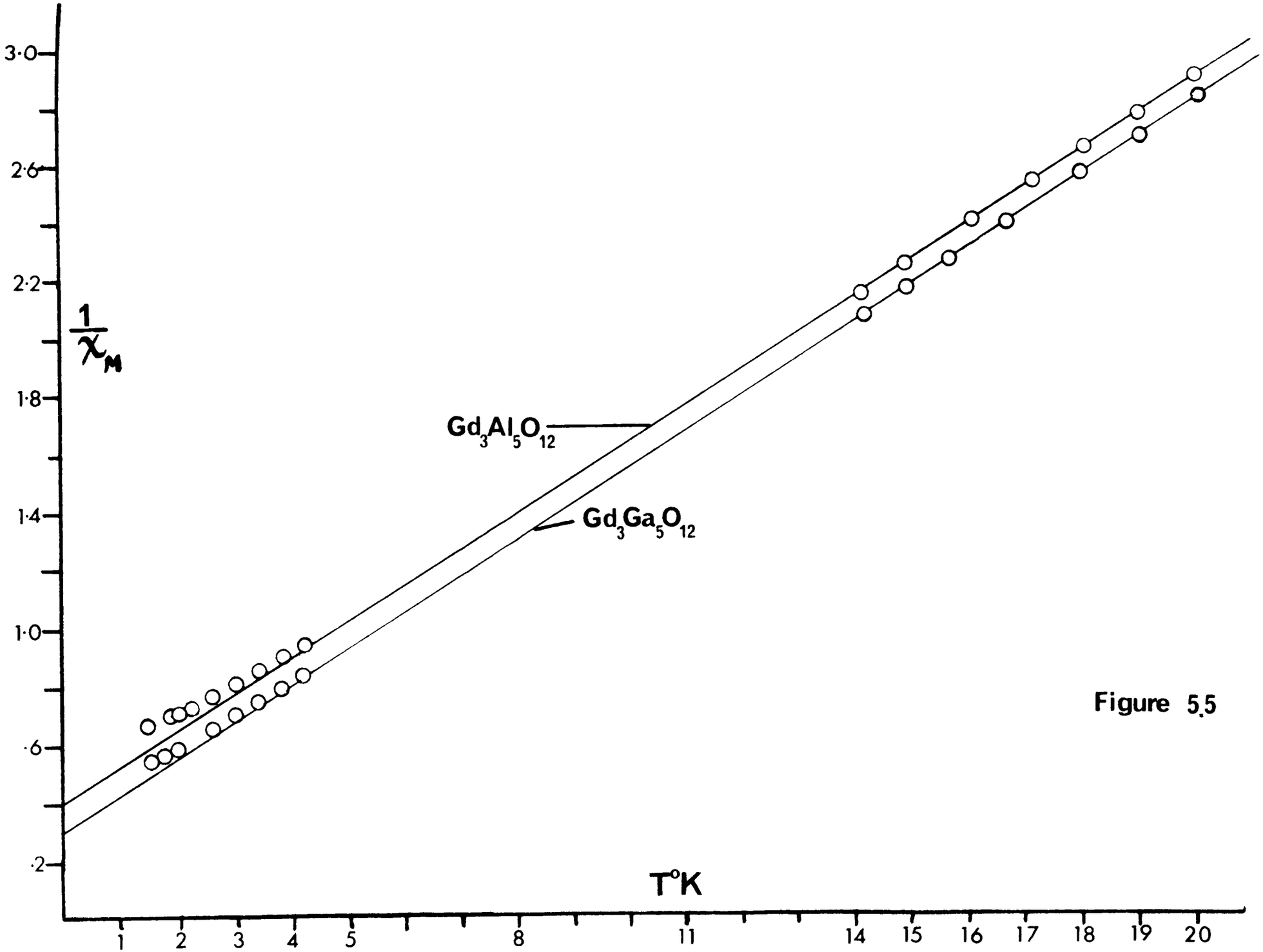
3·0
2·6
2·2
1·8
1·4
1·0
·6
·2
$\frac{1}{\chi_M}$
$Gd_3Al_5O_{12}$
$Gd_3Ga_5O_{12}$
T°K
1
2
3
4
5
8
11
14
15
16
17
18
19
20

Figure 5.5

it is a good approximation to regard the Yb ion as having a Γ_7 doublet lowest, since this would have an isotropic g-value of 3.43 (Hutchings,1963). This is also in agreement with the calculations of Lea,Leask and Wolf (1962).

The behaviour of Yb in YbIG is probably much the same as in the aluminium and gallium garnets, since it seems to be rather insensitive to lattice environment. This is further discussed by Wolf (1959).

Gadolinium aluminium and gallium garnets.

Since Gd is an S-state ion, its crystal field splitting is small (Remai and de Mars,1962), and the g-value is isotropic. It follows that any deviations from a Curie law are caused by exchange interactions, since dipole-dipole interactions for an isotropic ion in a cubic crystal field cancel out.

The experimental points, after shape correction to a sphere, are plotted in Figure 5.5 as reciprocal susceptibility against temperature. In the hydrogen ranges, the susceptibilities obey Curie-Weiss laws with Weiss θs of 2.3° and 3.0°K for the gallium and aluminium compounds respectively. There is slight deviation from these laws in the helium range, presumably caused by local ordering. With antiferromagnetic Weiss θs of this magnitude, ordering transitions might have been expected in the measured helium range.

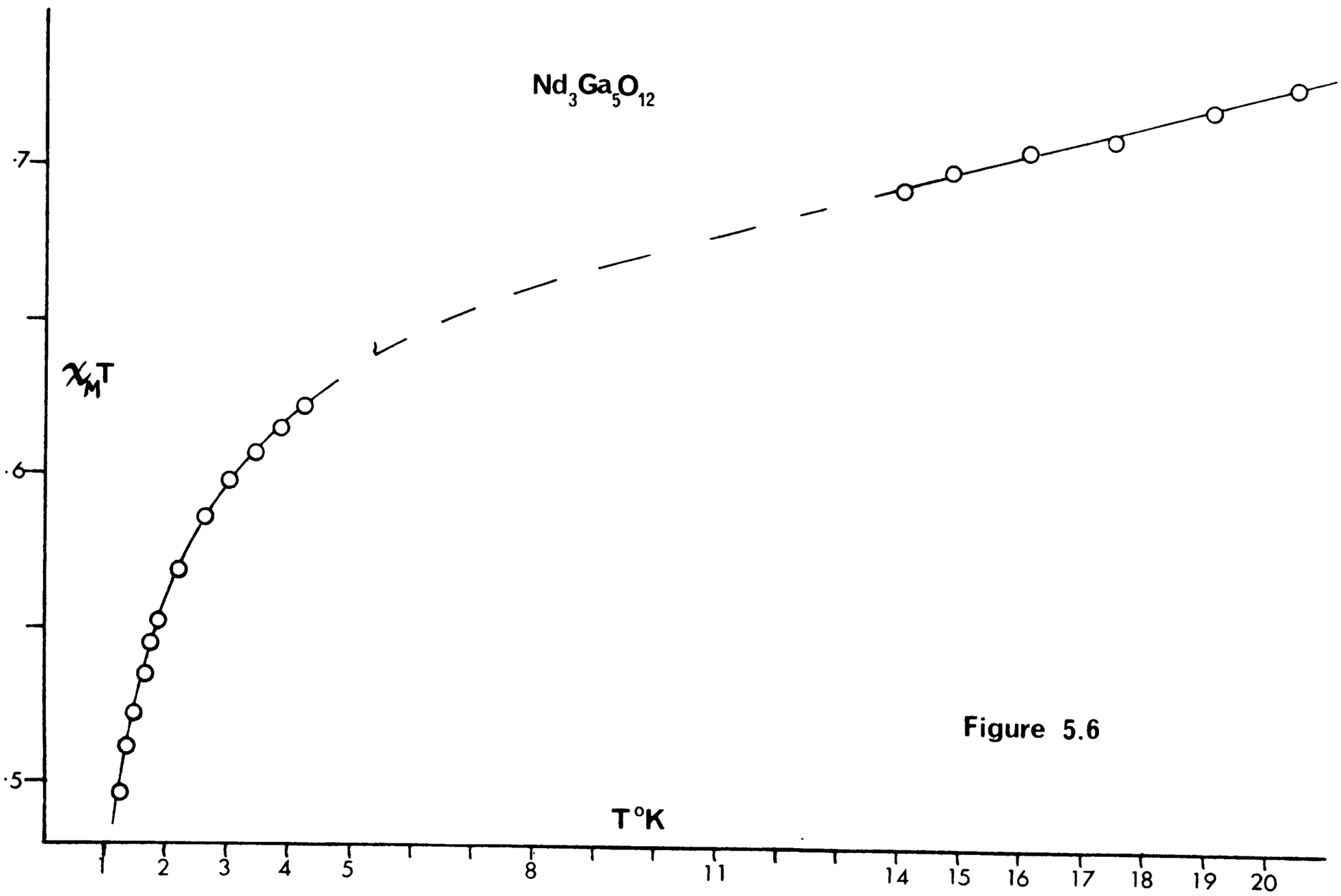

Figure 5.6

The agreement on the gallium compound with the work of Pauthenet (1957) and Leask (1960) who found Weiss θs of 2.3 and 2.19°K respectively on polycrystalline samples is very good.

Neodymium gallium garnet.

The experimental points are represented by a graph of T against T (Figure 5.6), and the susceptibility over the whole range is described fairly well by the law

$$\chi_M = 0.667/(T + 0.42) + 0.0036$$

The linearity of χT in the hydrogen range, and small temperature independent contribution to the susceptibility both suggest that the first excited state is at least 100°K above the ground state.

The free-ion ground multiplet of Nd is $4f^3\ {}^4I_{9/2}$ which is further split by a crystal field (Kynch, 1937). The ground state is a Γ_8 quartet split to two doublets by the crystal field (Lea, Leask and Wolf, 1962). If the ground state measured by resonance were predominantly a simple Γ_6 doublet, the admixtures of higher states would be small, and the g-values would be largely isotropic. That this is not the case (Table 1, c.f. Yb) confirms that the ground doublet forms a part of the Γ_8 quartet.

The agreement with the Curie constant calculated from the g-values of Nd in YGaG (0.599) is as good as can be expected. Specific heat measurements by Bailey (unpublished)

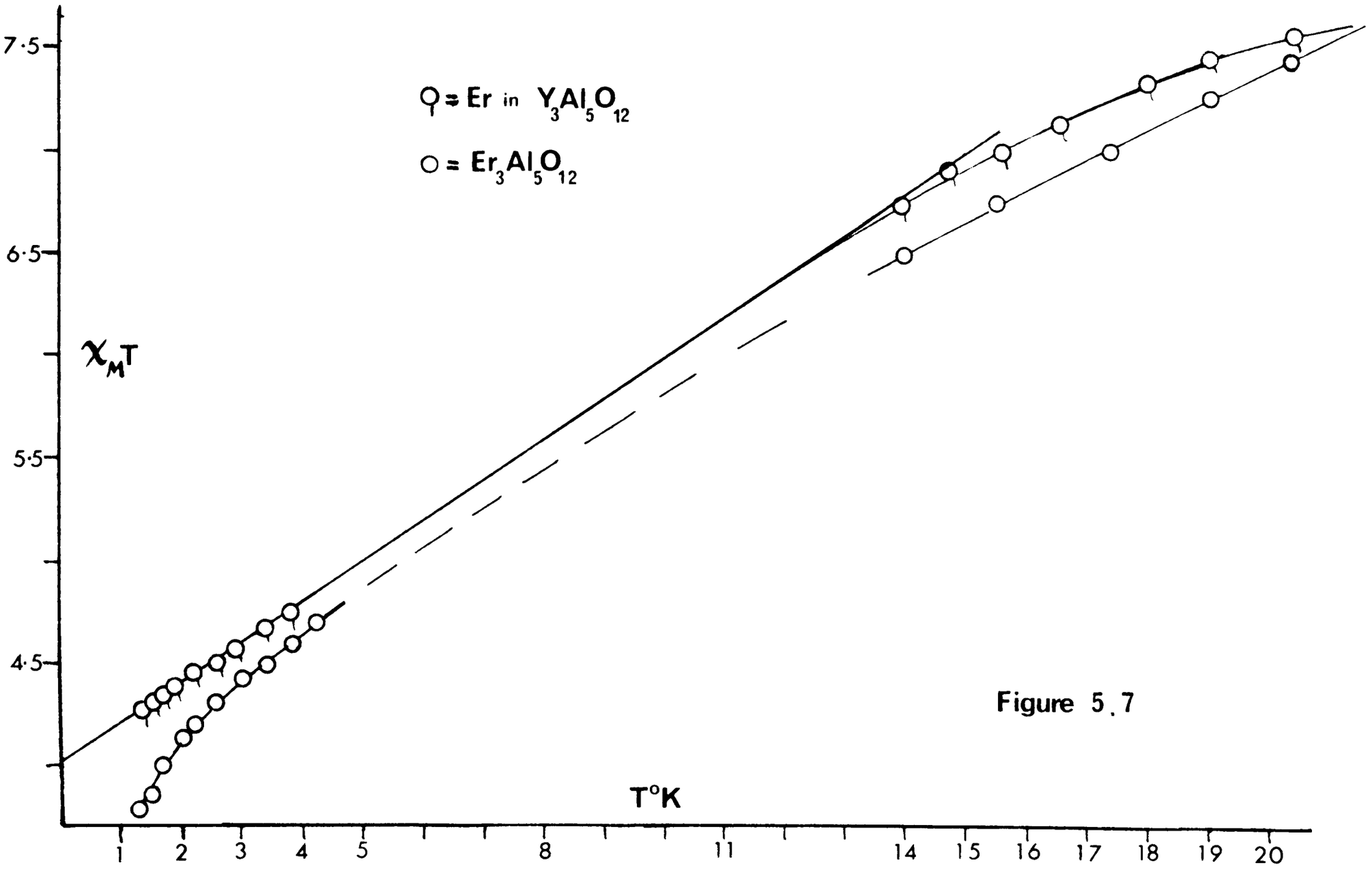
7·5
6·5
5·5
4·5
$\chi_M T$
Q = Er in $Y_3Al_5O_{12}$
○ = $Er_3Al_5O_{12}$
T°K
1
2
3
4
5
8
11
14
15
16
17
18
19
20

Figure 5.7

also indicate a first excited state above 100°, though no precise estimate can be made.

Erbium Aluminium Garnet.

In a cubic crystal field, Er would have a Γ_7 or Γ_6 doublet lowest, with a Γ_8 quartet somewhat higher, probably split by distortions from cubic symmetry to give two doublets of about the same energy. Thus, the actual ground state in any given garnet lattice is likely to be very complicated, and sensitive to slight changes in the crystal field which will even alter which state is lowest.

Both the pure material, and a dilute sample were measured, and the results are reproduced in Figure 5.7 as graphs of χT against T. The dilute measurements were 'normalised' to have the same Curie constant as that calculated from the resonance work. The concentrated material obeys a law

$$\chi_M = 4.3/(T + 0.234) + 0.145$$

while the temperature independent term for the dilute garnet is 0.196. From these large values, it may be deduced that one or more excited states lies not far above the ground state in both garnets.

The Curie constants calculated from the measurements in YAlG and LuAlG respectively are 4.01 and 4.25.

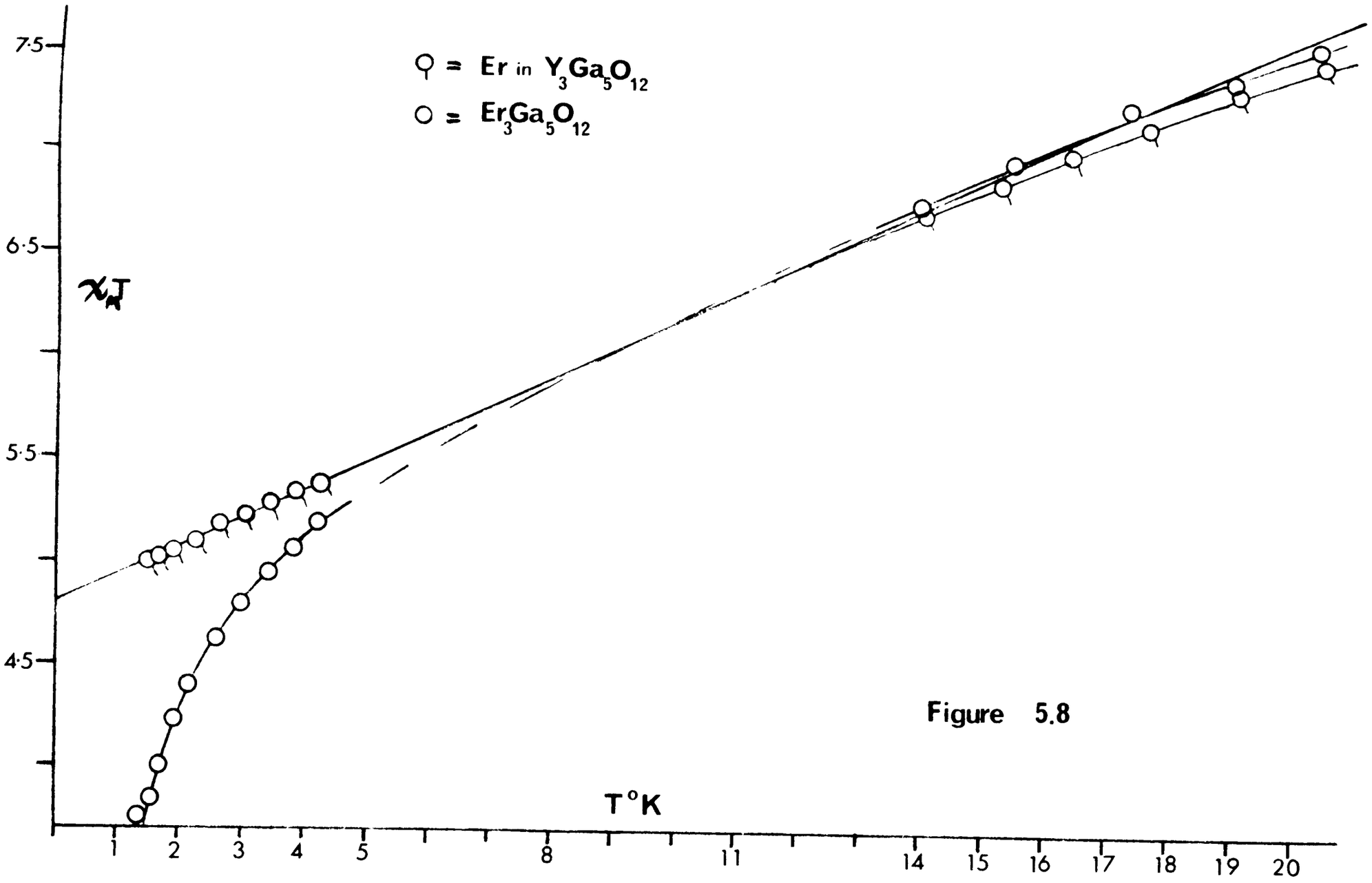
7·5
6·5
5·5
4·5
$\chi_M T$
♀ = Er in $Y_3Ga_5O_{12}$
○ = $Er_3Ga_5O_{12}$
T°K
1
2
3
4
5
8
11
14
15
16
17
18
19
20

Figure 5.8

Erbium Gallium Garnet.

As with the aluminium compound, both the concentrated and a nominally 1% Er material were measured (Figure 5.8). The points in the helium range may be described by a law

$$\chi_M = 6.42/(T + 1.0)$$

but it is very doubtful whether the behaviour of this garnet can adequately be described by a Curie-Weiss law, since a non-zero temperature independent term would be expected.

The Curie constant of the dilute material is 'normalised' to the value calculated from the resonance results, and the curvature exhibited in the hydrogen range probably means exponential population of the first excited state.

The Curie constants calculated from the g-values of Er in YGaG and LuGaG respectively are 4.80 and 5.61. Since these differ by 13% and the law derived for ErGaG is of doubtful significance, the poor agreement between the Curie constants is not surprising.

Dysprosium Aluminium Garnet.

The susceptibility of this material is discussed in detail in Chapter 6.

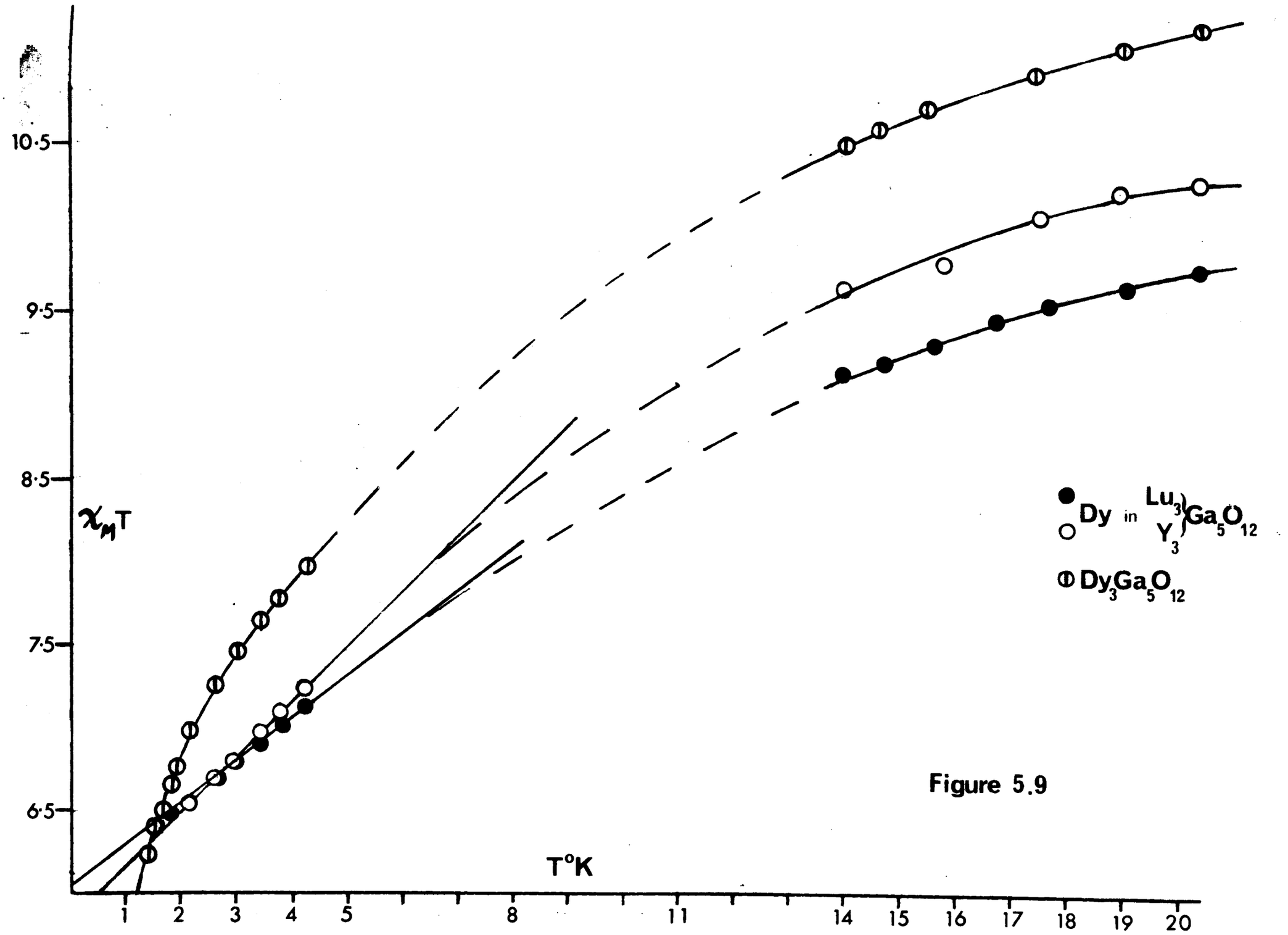
10·5
9·5
8·5
7·5
6·5
$\chi_M T$
T°K
1
2
3
4
5
8
11
14
15
16
17
18
19
20
Dy in Lu_3 Y_3 Ga_5O_{12}
$Dy_3Ga_5O_{12}$

Figure 5.9

Dysprosium Gallium Garnet.

The ground state of Dy in a predominantly cubic crystal field is either a Γ_7 doublet, or a Γ_8 quartet (Lea, Leask and Wolf, 1962) . As with erbium, it is doubtful whether an analysis of the results as a Curie-Weiss law is very meaningful, but the susceptibility in the helium range can be fitted to the following law:-

$$\chi_M = 7.80/(T + 0.436) + 0.212$$

These results, together with the behaviour of nominally 1% samples of Dy in YGaG and LuGaG are plotted as T against T in Figure 5.9. The two dilute samples are 'normalised' in the usual way. The yttrium garnet obeys a law:-

$$\chi_M T = 5.80 + 0.389T$$

while the lutecium garnet obeys the law:-

$$\chi_M T = 6.03 + 0.256T$$

The great differences between the temperature independent terms indicate the sensitivity of the separation of the ground and first excited states to the crystal field. In all three garnets, there is some deviation from the laws in the hydrogen range, owing to population of the first excited state.

The 'Non-Kramers' Ions.

Introduction.

Pr, Tb, Tm and Ho all have an even number of 4f electrons in the trivalent state, so that the crystal field splits the J manifold into Γ_1, Γ_2, and Γ_3 singlet states which

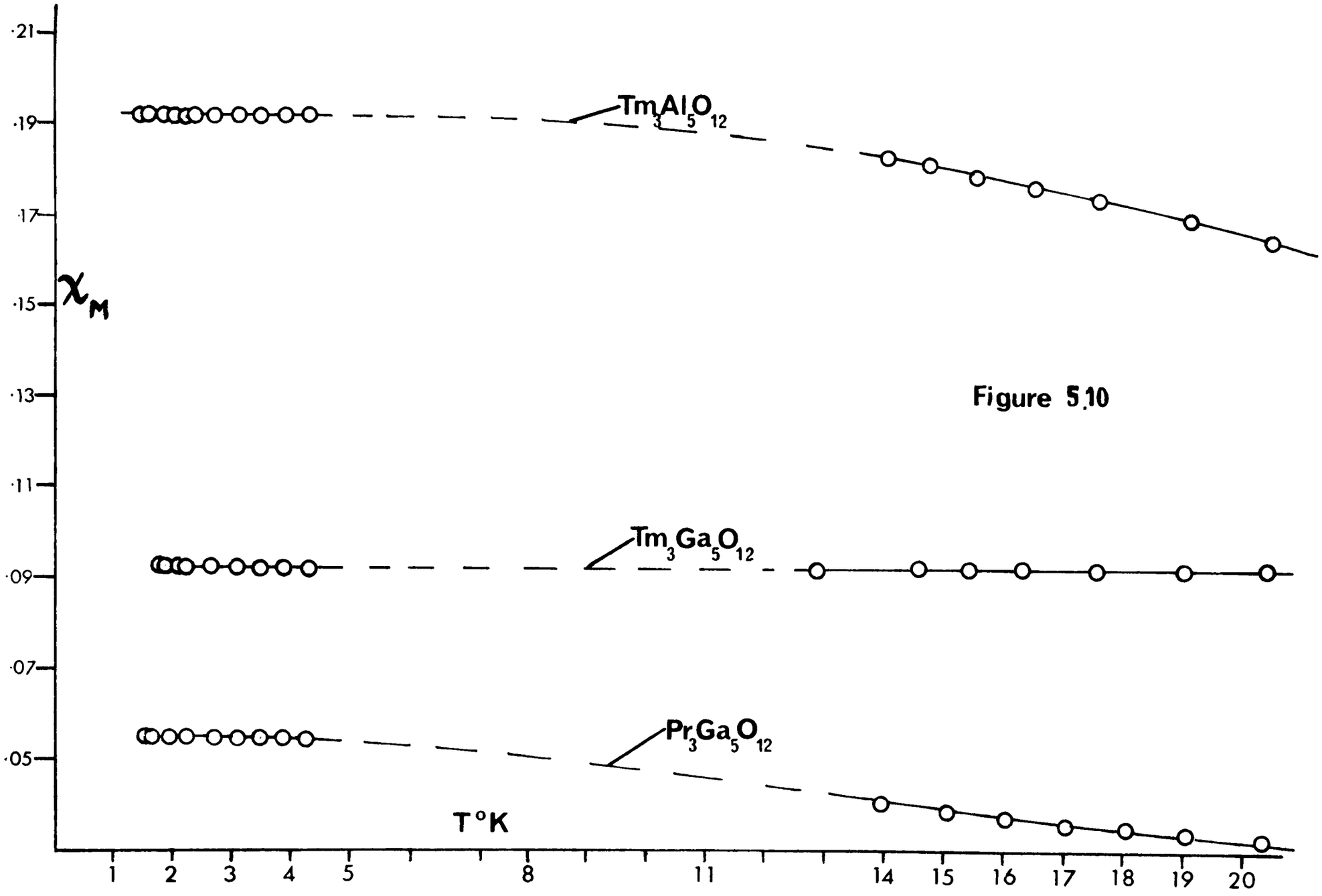
·21
·19
·17
·15
·13
·11
·09
·07
·05
χ_M
$Tm_3Al_5O_{12}$
$Tm_3Ga_5O_{12}$
$Pr_3Ga_5O_{12}$
T°K
1
2
3
4
5
8
11
14
15
16
17
18
19
20

Figure 5.10

are non-magnetic, and Γ_4 and Γ_5 triplet states which split very much like a spin S = 1. Although there is no paramagnetism from individual singlet states, a magnetic field admixes other states, giving rise to a relatively small, temperature-independent susceptibility, inversely proportional to the separation of the energy levels involved. If this separation is large by comparison with kT, then only the ground state will be populated, and the susceptibility will be small and temperature-independent.

On the evidence of the rare earth garnets already discussed, the crystal field seems to have rather low symmetry, so the energy levels in the 'even number' rare earth garnets should be quite widely spaced.

Praseodymium Gallium Garnet.

The ground state of this ion in the garnet will be Γ_1 or Γ_5 (Lea, Leask and Wolf, 1962). Its molar susceptibility is plotted as a function of temperature in Figure 5.10, and in general behaviour, it conforms to the pattern outlined above. It is the most weakly paramagnetic of all the concentrated garnets measured, and shows some curvature in the hydrogen range, indicating a first excited state at about 70°K.

Thulium Aluminium and Gallium Garnets.

This ion has a Γ_2 or Γ_3 ground state, but there is also a Γ_5 triplet with not very different energy (Lea, Leask

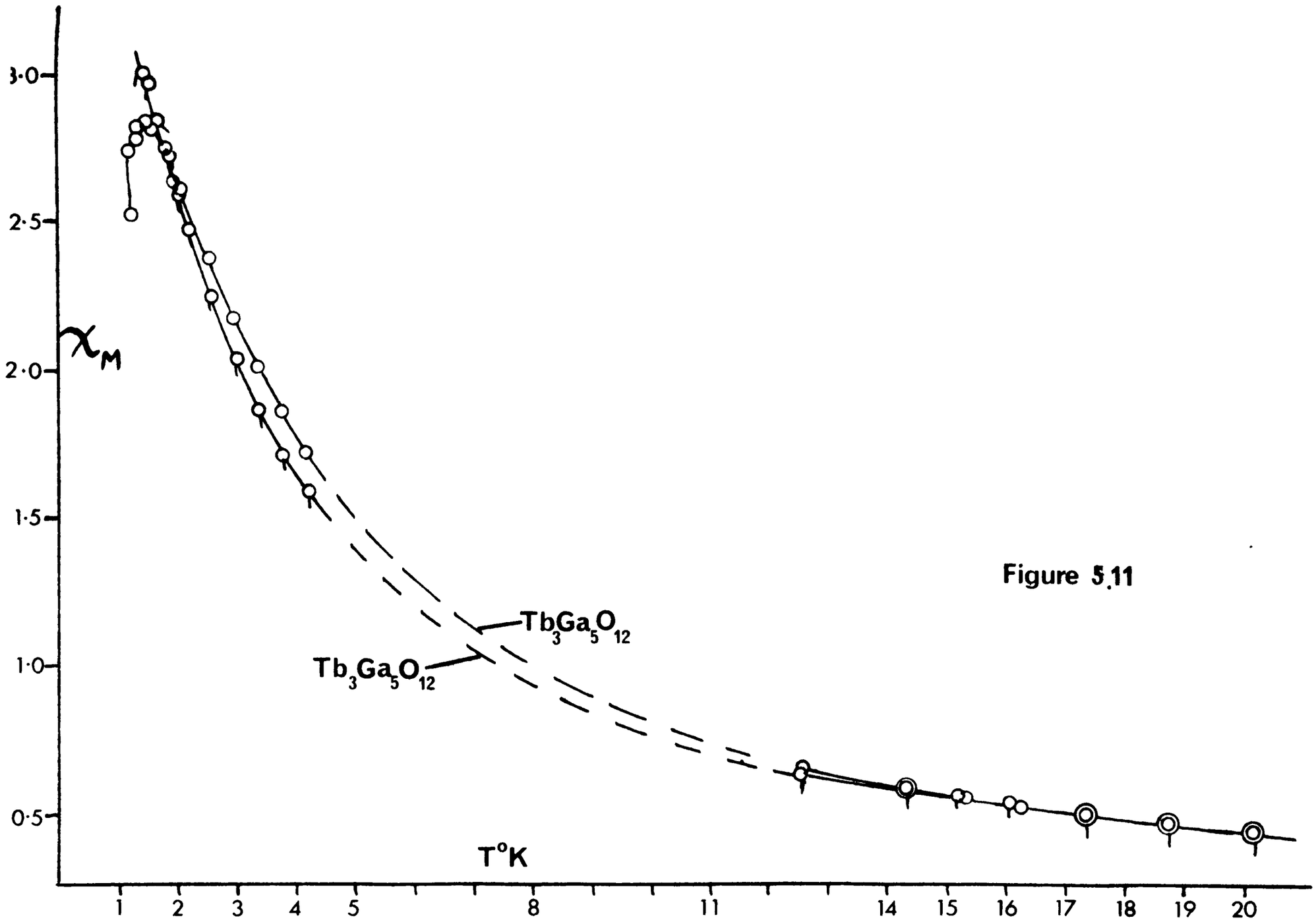
3·0
2·5
2·0
1·5
1·0
0·5
χ_M
$Tb_3Ga_5O_{12}$
$Tb_3Ga_5O_{12}$
T°K
1
2
3
4
5
8
11
14
15
16
17
18
19
20

Figure 5.11

and Wolf, 1962). The molar susceptibilities are plotted against temperature in Figure 5.10. The behaviour of the aluminium garnet is very similar to that of PrGaG, but in this case with an excited state at about 50°K. The first excited state is higher than 150°K for TmGaG.

The rather great difference between the aluminium and gallium compounds accords well with the measurements on Dy and Er garnets, and again indicates considerable differences in the crystal fields.

Terbium Aluminium and Gallium Garnets.

The molar susceptibilities of these two garnets are shown in Figure 5.11. Unexpectedly, the absolute magnitudes of the susceptibilities are very great, and they are strongly temperature-dependent down to the lowest temperatures measured. In addition, the behaviour of the two compounds is virtually the same, in complete contrast with the thulium compounds which have similar ground states and energy level relationships (Lea, Leask and Wolf, 1962).

The magnetic interactions in TbAlG are sufficiently great in the helium range to cause a sudden decrease in the susceptibility at 1.4°K, presumably the result of antiferromagnetic ordering. Susceptibilities as large as these can only result from energy levels whose separation is very small, that is, of the same order of magnitude as the interactions between neighbouring ions as indicated by the ordering of TbAlG. Thus, any quantitative treatment of

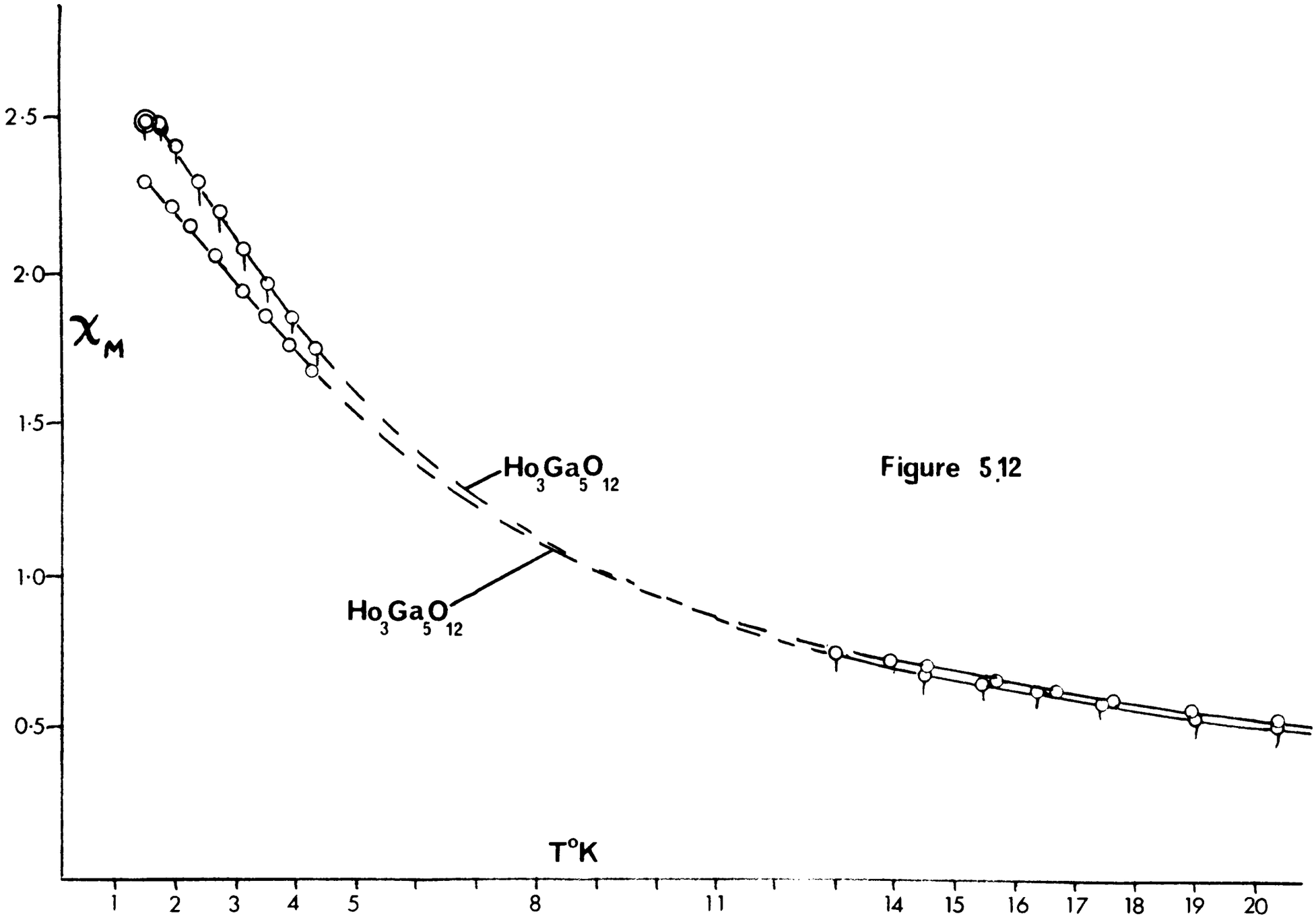
2·5
2·0
1·5
1·0
0·5
χ_M
$Ho_3Ga_5O_{12}$
$Ho_3Ga_5O_{12}$
T°K
1
2
3
4
5
8
11
14
15
16
17
18
19
20

Figure 5.12

these compounds is impossible, especially since there are no data on the behaviour of individual ions.

Holmium Aluminium and Gallium Garnets.

The susceptibilities of these two garnets are very similar to each other (Figure 5.12) and to the terbium garnets (Figure 5.11). The ground state in the garnets is Γ_3 or Γ_5 (Lea, Leask and Wolf, 1962), and for some admixtures of 4th and 6th order crystal field terms, these two states are of identical energy. Thus, the necessary small splitting to give such powerful paramagnetism is reasonable. Neither compound gives any indication of ordering in the measured temperature range.

Conclusions.

Of the garnets measured, the behaviour of GdAlG, GdGaG, YbAlG, YbGaG, PrGaG, TmAlG and TmGaG is fairly well understood, at least qualitatively. The agreement between resonance g-values and Curie constants is only good in the case of Yb, and it is probably significant that this ion seems to have a very large crystal field splitting, and that the g-values were measured in the neighbouring lutecium garnets.

It is possible that the susceptibilities of some of the garnets for which the agreement is very bad cannot be adequately analysed in terms of a Curie-Weiss law, maybe for the reasons suggested by Lea, Leask and Wolf (1962), in particular, that L and S cease to be good quantum numbers.

The differences between Tm and Tb with similar energy level diagrams in crystal fields, and the similarities between Tb and Ho with different diagrams (Lea, Leask and Wolf, 1962) indicate that discretion must be used in predicting the behaviour of the rare earths from these calculations alone.

For Er, Dy and Tm, the differences between the Al and Ga garnets are very considerable, while for Gd, Yb, Tb and Ho there is very little difference. The interactions between the rare earth ions are greater in the Al than in the Ga garnets, which results from the closer spacing in the former materials. These interactions must in general be magnetic dipole and exchange forces.

In general, there does not yet seem to be enough data for satisfactory extrapolation from the aluminium and gallium garnets to the iron garnets. It is clear, however, that the rare earth interactions are very small indeed, especially when compared with the ferrimagnetic iron interactions.

Chapter 6.

The Susceptibility of Dysprosium Aluminium Garnet (DAG).

Introduction.

This very interesting material has been the subject of a considerable amount of work, in view of its unusual magnetic and structural properties. In subsequent chapters, we shall discuss specific heat and magnetic moment measurements, but in order to clarify the motives behind some of the experiments, and to show the overall pattern of the investigations, we preface this chapter with a chronological survey of the experiments performed.

Historical Introduction to DAG.

The susceptibility of DAG was first measured on a single crystal sample as part of the general survey of rare earth garnet susceptibilities (Chapter 5). The most interesting feature of its behaviour was the maximum in the susceptibility at 2.5-2.6^{o}K, presumed to indicate antiferromagnetic ordering (Ball et al.,1961). A parallel survey of the paramagnetic resonance spectra of rare earth ions in YAlG and YGaG was being undertaken at the same time, and the resonance of Dy in YAlG could not be detected, even though various concentrations and temperatures were tried, and the dilute samples appeared to have normal susceptibility (Ball et al.,1961). Carson and White (private communication) working in the U.S.A. also failed to detect this resonance.

The research programme was widened to include the

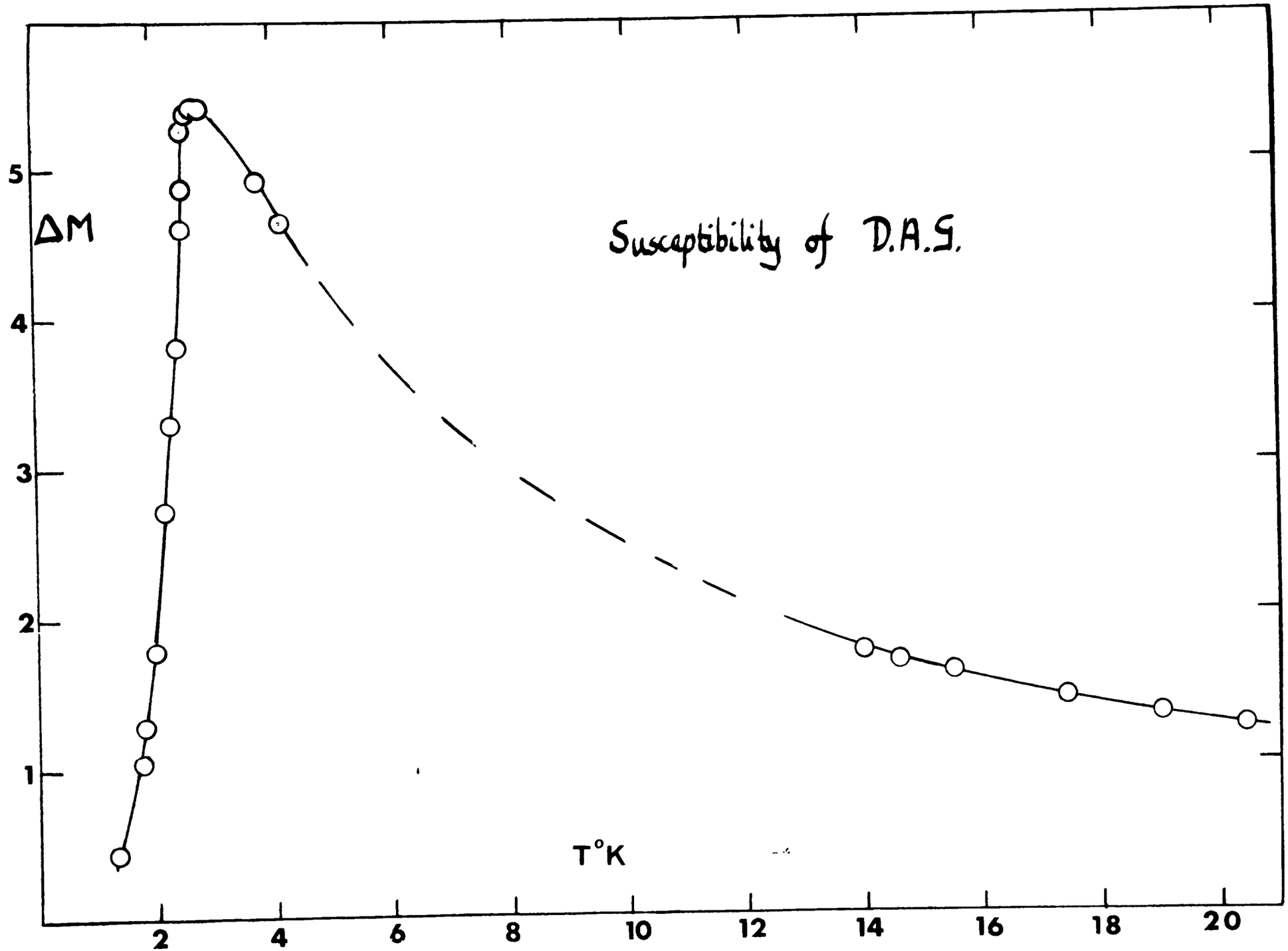

Figure 6.1

resonance of the same rare earths in LuAlG and LuGaG, and the resonance of Dy in DuAlG was observed, with g-values $g_x = 2.29$, $g_y = 0.91$ and $g_z = 16.6$ (Bell et al.,1962. See Table 1) This immediately suggested that the spectrum in YAlG might be even more anisotropic, and careful investigation by Dr M.T.Hutchings revealed lines attributable to Dy. These lines were always very small, at some angles very broad, and their resonance fields varied extremely rapidly with angle, explaining why they had previously been overlooked. The g-values were found to be $g_x = 0.73$, $g_y = 0.40$ and $g_z = 18.3$.

This extreme anisotropy re-awakened interest in DAG, since it seemed likely that Dy could be regarded as a magnetic dipole in DAG too, since the g-values did not seem too sensitive to crystal field changes. It seemed that DAG might well provide a physical example of the 'Ising' model of magnetic interactions, and that a detailed theoretical treatment of the antiferromagnetism of DAG might be possible.

We decided to check these ideas by measuring the specific heat of DAG (Chapter 7,Bell et.al. 1963). In general, the measurement was in excellent agreement with the susceptibility work and the 'magnetic dipole' theory of DAG, except for a difference in the transition temperatures, 2.54°K from susceptibility, 2.49°K from specific heat, a discrepancy outside the combined experimental errors.

It seemed quite possible that impurities had found

their way into one or other sample, from the flux or from the Verneuil flame fusion apparatus (which had also been used for preparing ruby crystals), and that these foreign paramagnetic ions were responsible for the divergence of the results. We therefore investigated the effect of deliberately added impurities on the transition temperature of DAG by measuring the susceptibilities of suitable polycrystalline specimens, and found that Fe, Cr and Y all depress the transition temperature.

In the course of this investigation, we also prepared some pure polycrystalline DAG samples as 'blank' checks on the preparative method. The susceptibilities of these powders showed extraordinary frequency and current dependence, as did their out-of-phase susceptibilities, in the vicinity of the transition temperature. The d.c. susceptibility of these powders was also measured, and they were found to exhibit a small ferrimagnetism with two components, one permanent and one induced, below the transition temperature. Though interesting, these experiments did not at all illuminate the main problem of the transition temperature discrepancy. The susceptibility of a piece of the sintered block from which the specific heat sample was prepared was measured, and was also found to exhibit some of the strange properties of the powders. Finally, the specific heat block itself was destroyed, and the susceptibility transition temperature found to be exactly the same as the specific heat.

Finally, a new batch of single crystals of DAG was prepared, and one of the larger ones worked into a sphere. The susceptibility of this was measured as a definitive experiment, and the transition temperature was found to be in excellent agreement with the specific heat measurements. The magnetic moment properties of this same sphere were also investigated.

As an appendix to this set of experiments, three samples of DAG, a portion of the polycrystalline powder, a single crystal, and a piece of the specific heat block were examined spectroscopically for paramagnetic and other impurities by Dr F.J.Bryant and Mr M.S.W.Webb of the Woolwich Outstation Group of the Analytical Branch,A.E.R.E., Harwell, to whom we acknowledge our indebtedness. They found (all figures quoted as parts per million): -

	Fe	Pb
Single crystal	7	200
Specific heat block	20	5
Polycrystalline powder	35	20

The following elements could not be detected in any of the samples (detection limits given in parenthesis): -
Pt (50), V (30), Cr (5), Mn (2), Co (5),Ni (5), Cu (5), Ti (100).

These measurements confirm our conclusion that there is no major chemical difference between the samples prepared in various ways, and show that the measures taken to avoid chemical contamination during preparation (Chapter 3) were effective.

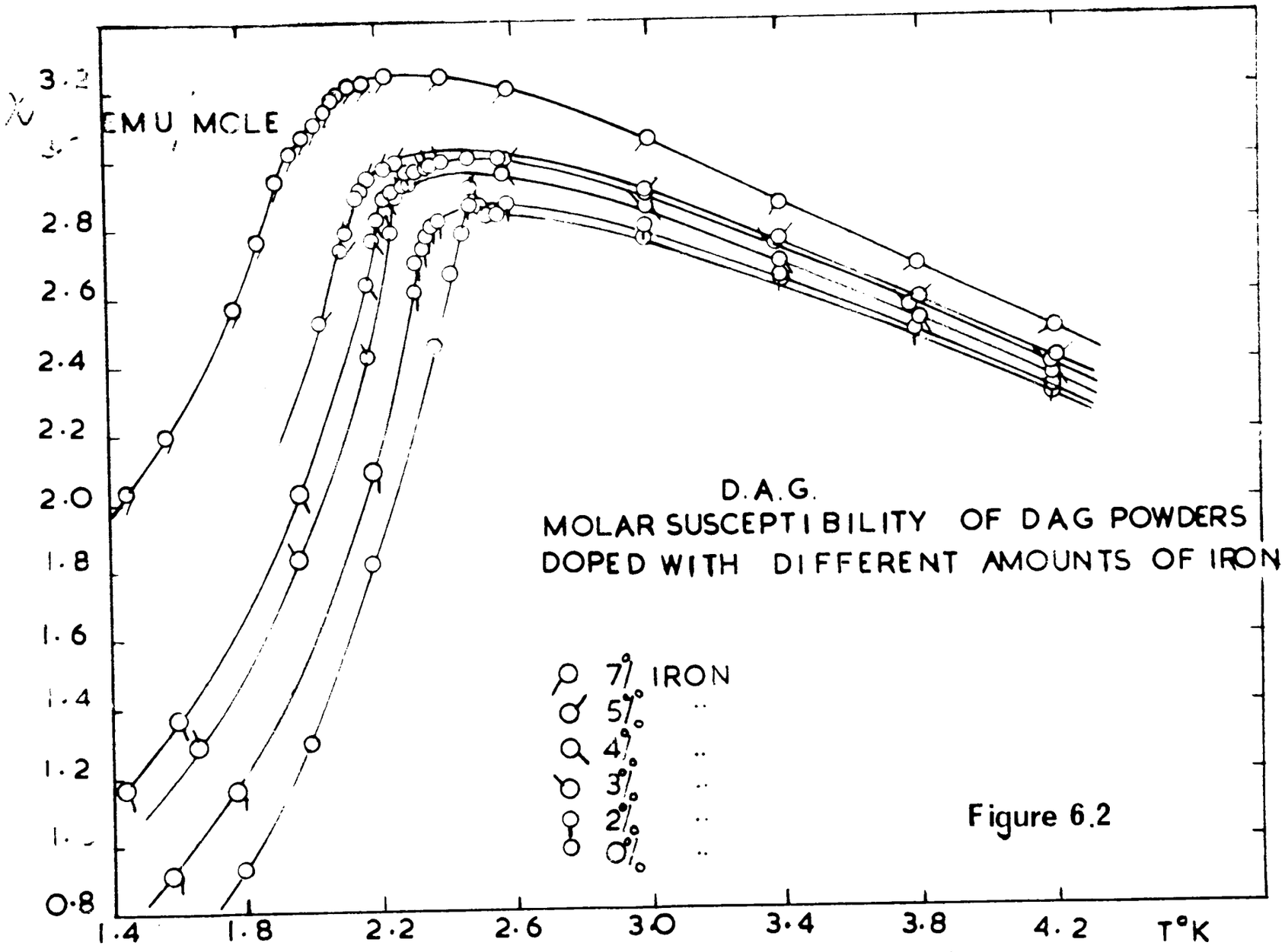
χ
EMU MOLE
3·2
2·8
2·6
2·4
2·2
2·0
1·8
1·6
1·4
1·2
0·8
1·4
1·8
2·2
2·6
3·0
3·4
3·8
4·2
T°K
D.A.G.
MOLAR SUSCEPTIBILITY OF DAG POWDERS
DOPED WITH DIFFERENT AMOUNTS OF IRON
7% IRON
5% ..
4% ..
3% ..
2% ..
0% ..

Figure 6.2

Iron-doped Powder Samples of DAG.

The preparation of these samples is described in Chapter 3. A preliminary investigation showed conclusively that the presence of iron measurably altered the apparent transition temperature of DAG, so a number of different samples were made and measured to establish a concentration dependence.

The results of most of these measurements are shown in Figure 6.2. For the sake of clarity, the results of the 1% material are omitted, and no correction has been made for the shape of the samples, but since all measurements were made in the same container (Figure 4.4b) and on approximately the same weight of material, the measurements can fairly be compared with each other, though they are not absolute determinations.

Two of the effects of iron doping are as expected. Firstly, the magnitudes of the susceptibilities above the Néel temperature are increased, roughly in proportion to the percentage of iron added. Secondly, the anomaly becomes increasingly broad and smeared out with increasing iron impurity. This is reasonable, since the presence of iron transforms DAG from a homogeneous substance to a statistical distribution of slightly different physical situations, according to the local concentration of iron. As a result, the transition temperature becomes a less meaningful concept with the higher iron concentrations,

and nothing would be learned from measurements on samples containing more than about 7% or iron.

The detailed way in which the iron affects the ordering of DAG is almost certainly very complicated, and there is at present no explanation of why the Néel temperature is lowered. However, the effect does seem to be approximately linear with the addition of iron, 1% causing a fall of about 0.08°K.

Thus, the discrepancy between the apparent transition temperatures of the specific heat material and the single crystals could have been caused by about 1% of iron in the former. This hypothesis was rejected on two grounds. Firstly, it is unlikely that such a large amount of impurity could have found its way into the specific heat material in view of the care taken to avoid this, a conclusion vindicated by spectroscopic work (page 6.4) at a later stage. Secondly, the evidence points to a 'smearing' of the transition in the presence of iron, whereas in fact, the specific heat anomaly appeared particularly sharp (Figure 7.5).

An unusual feature of the pure DAG powder is the small peak in the curve, immediately preceeding the sharp fall. This was also observed to a lesser extent in some of the 'doped' samples, particularly the 3% iron, and the chromium and yttrium doped samples (see Figure 6.3), and is further discussed in a subsequent section.

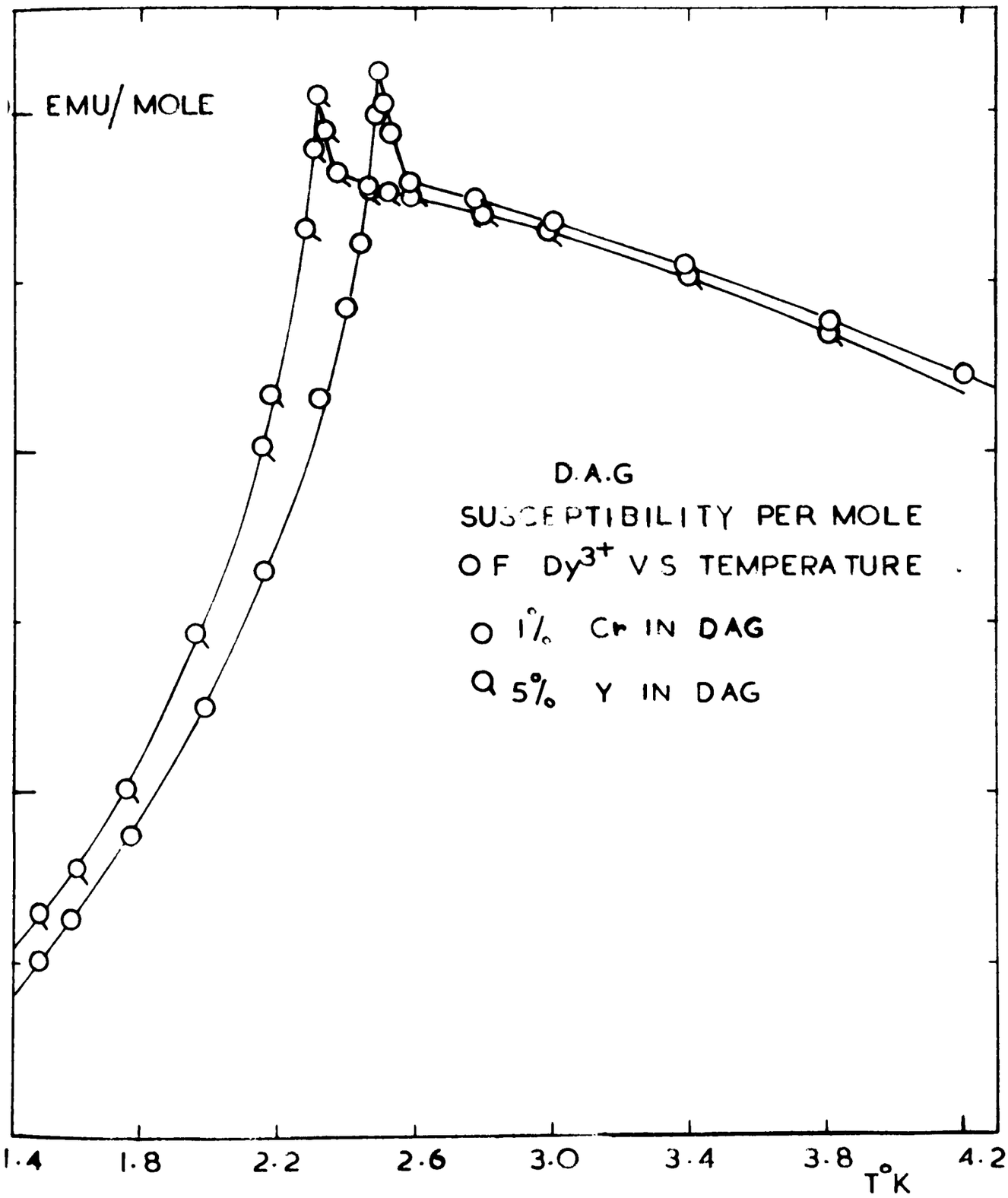
EMU/ MOLE
D.A.G
SUSCEPTIBILITY PER MOLE
OF Dy^{3+} VS TEMPERATURE
O 1% Cr IN DAG
Q 5% Y IN DAG
1.4
1.8
2.2
2.6
3.0
3.4
3.8
4.2
T°K

Figure 6.3

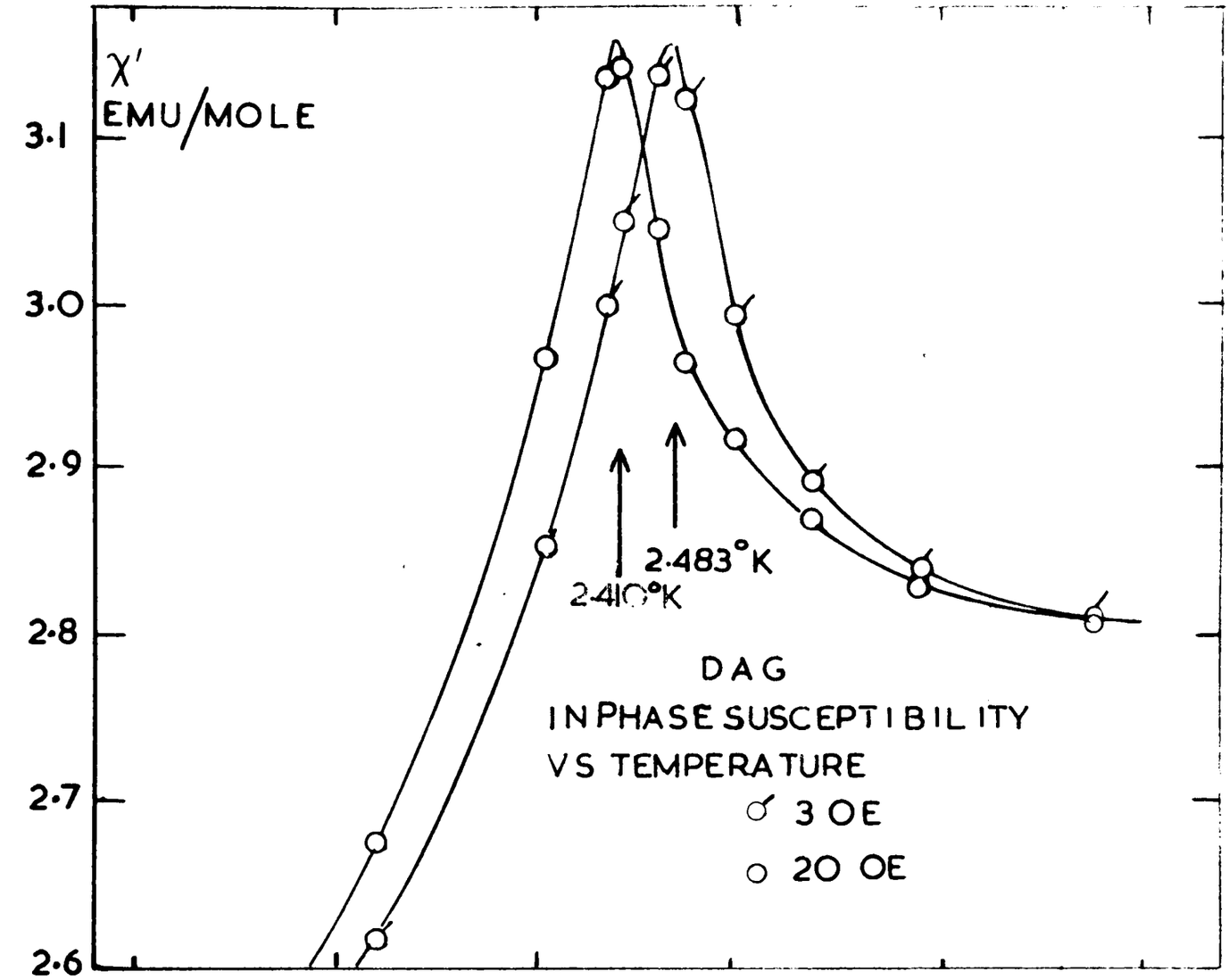
χ'
EMU/MOLE
3·1
3·0
2·9
2·8
2·7
2·6
2·483°K
2·410°K
DAG
IN PHASE SUSCEPTIBILITY
VS TEMPERATURE
3 OE
20 OE

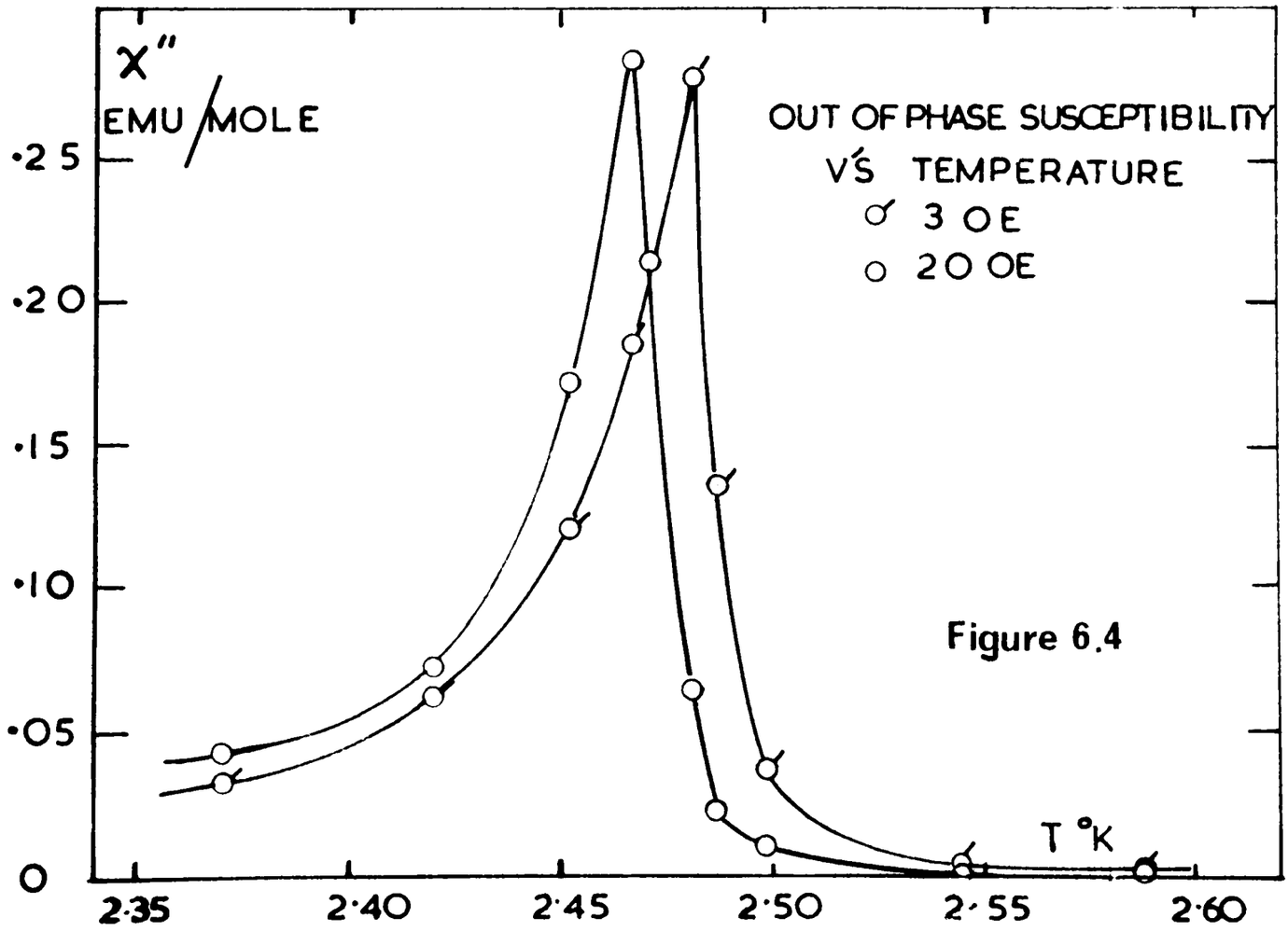
χ"
EMU/MOLE
·25
·20
·15
·10
·05
0
OUT OF PHASE SUSCEPTIBILITY
V'S TEMPERATURE
3 OE
20 OE
T °K
2·35
2·40
2·45
2·50
2·55
2·60

Figure 6.4

Chromium and Yttrium Doped Samples of DAG.

The behaviour of DAG doped with 1% Cr and with 5% Y is shown in Figure 6.3. The effect of both impurities is to lower the transition temperature. In the case of Cr, this is to be expected by analogy with the case of iron doping. The result of replacing 5% of the Dy by Y is the same as that of replacing 1% of Al by Fe. This is reasonable, since the latter case amounts to introducing paramagnetic ions which interact strongly with the Dy sublattices, while the former amounts to making diamagnetic 'holes' in these sublattices, a lesser effect.

The replacement of some of the Dy by Y must weaken the interactions, and the lowered transition temperature is qualitatively what would be expected.

The Anomalous a.c. Susceptibility of pure DAG powder.

The small peak in the susceptibility of DAG samples in the critical region was most pronounced in pure samples, and was exhibited by all such prepared by the 'mixed nitrate' method (Chapter 3). There was also a corresponding peak in the out-of-phase susceptibility (Figure 6.4), and we found that the temperatures at which these peaks occurred were dependent on the size of the measuring field. Thus, Figure 6.4 represents $\sim$20 and $\sim$3 oe.

Both susceptibilities behave in a very similar fashion, and in both cases, the higher-field peak occurs at lower temperature, with a separation of approximately 13 millidegrees.

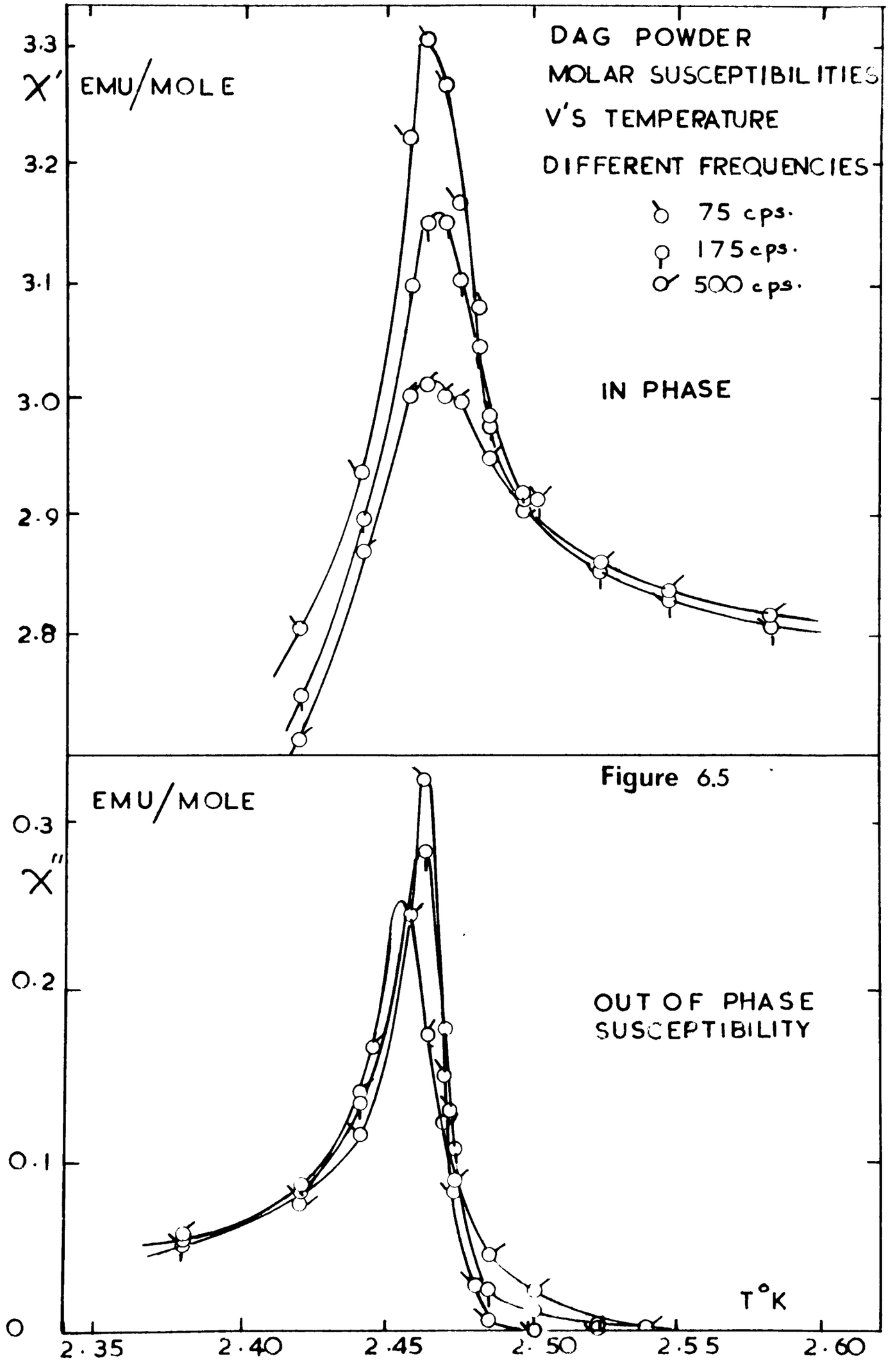
DAG POWDER
MOLAR SUSCEPTIBILITIES
V'S TEMPERATURE
DIFFERENT FREQUENCIES
75 cps.
175 cps.
500 cps.
IN PHASE
χ' EMU/MOLE
3.3
3.2
3.1
3.0
2.9
2.8
EMU/MOLE
χ''
0.3
0.2
0.1
0
OUT OF PHASE
SUSCEPTIBILITY
T°K
2.35
2.40
2.45
2.50
2.55
2.60

Figure 6.5

Since we have found no other paramagnetic material with a field-dependent susceptibility, we conclude that electrical heating of the coil at higher currents cannot be responsible, and that the apparent field dependence results from relaxation heating of the sample, Thus, the higher measuring field causes more heat dissipation in the specimen, and hence a lower coolant bath temperature is needed to produce the same specimen temperature. This conclusion is vindicated by the following experiments.

We measured the in phase and out-of-phase susceptibilities at constant field, but at two frequencies, namely 75 and 500 c.p.s. in addition to the usual 175 c.p.s. The results are shown in Figure 6.5, from which it may be seen that the size of peak is inversely related to the measuring frequency, while the temperatures at which the peaks occur are lower for the higher frequencies.

This frequency dependence suggested that a significant experiment might be to measure the susceptibility in the limiting case of low frequency, namely in a d.c. field.

Ballistic Measurements on Pure DAG Powder.

These measurements were performed on the usual apparatus, but according to the method described on page 4.2. In the first experiment, the susceptibility was measured in a constantly applied field of $\sim$ 20 oe (Curve c in Figure 6.6). However, we found that the sample had become permanently

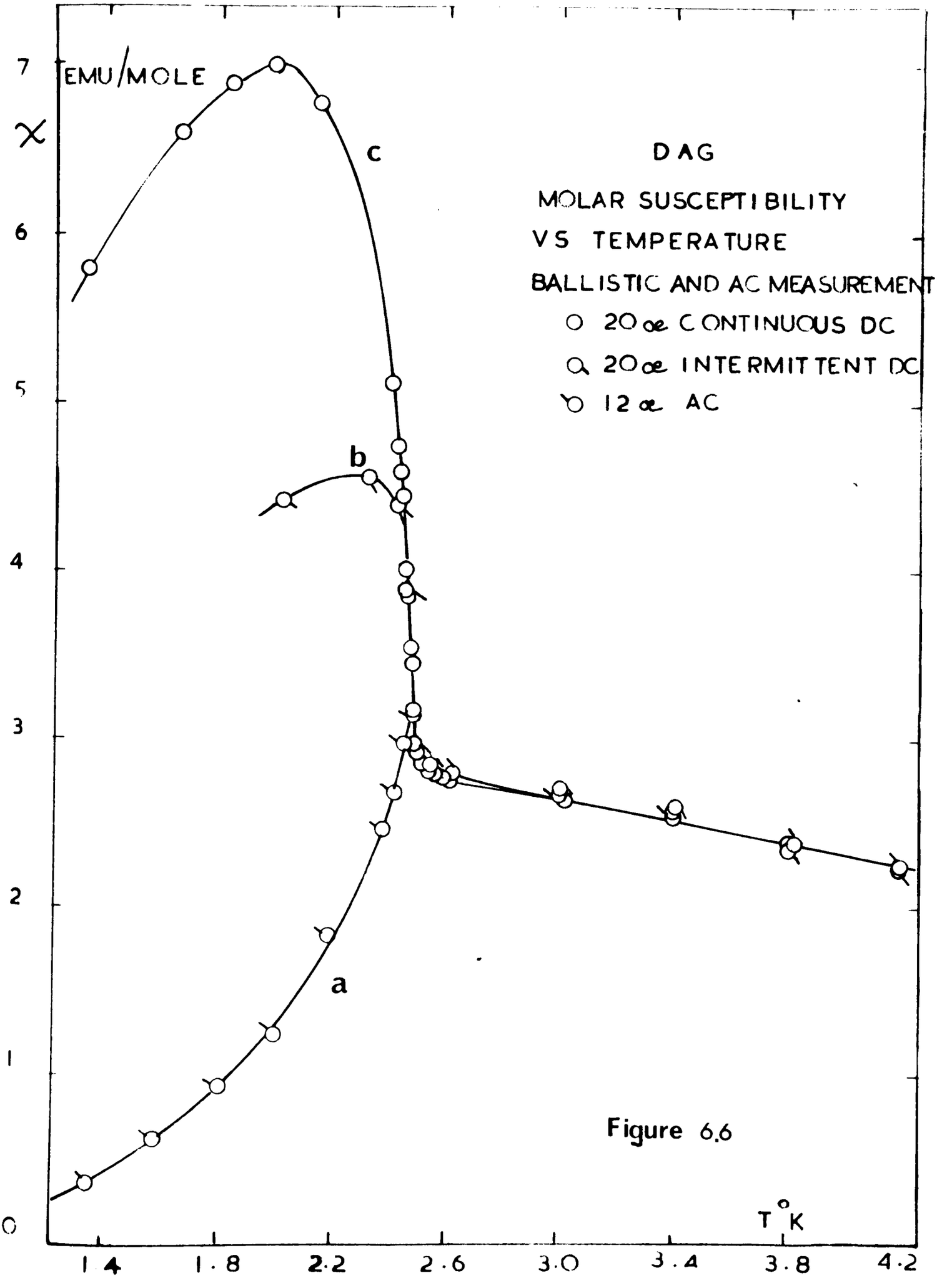
EMU/MOLE
χ
7
6
5
4
3
2
1
0
c
b
a
DAG
MOLAR SUSCEPTIBILITY
VS TEMPERATURE
BALLISTIC AND AC MEASUREMENTS
20 oe CONTINUOUS DC
20 oe INTERMITTENT DC
12 oe AC
T °K
1.4
1.8
2.2
2.6
3.0
3.4
3.8
4.2

Figure 6.6

magnetised below the Néel temperature, and that the moment could not be destroyed, even by reversing the applied field for some minutes. We performed a second experiment, therefore, in which the field was only switched on for the duration of each ballistic point, so that any cooling of the specimen was in the earth's magnetic field only. These results are plotted in Figure 6.6, curve b, and in this case there is no permanent moment induced. Curve a represents the a.c. susceptibility for comparison.

It is apparent that polycrystalline DAG has a much larger susceptibility in d.c. fields than in a.c., in agreement with the frequency dependence of the a.c. measurements. The anomalous d.c. moment seems to comprise two parts, one which is permanently locked into the material below the Néel temperature, and a second of roughly the same magnitude which is induced by an applied field and decays rapidly after its removal.

The frequency dependence and d.c. measurements can be explained on the assumption that there are a few (about 1 in 30,000) dysprosium ions which behave ferromagnetically when the remainder become antiferromagnetic. The permanent magnetisation shows that below the transition temperature, the relaxation time of these ions is infinitely slow (the other part of the moment was also slow to reach its highest value: a period of several minutes had to be allowed between applying the field and measuring the susceptibility). Above the transition temperature, these

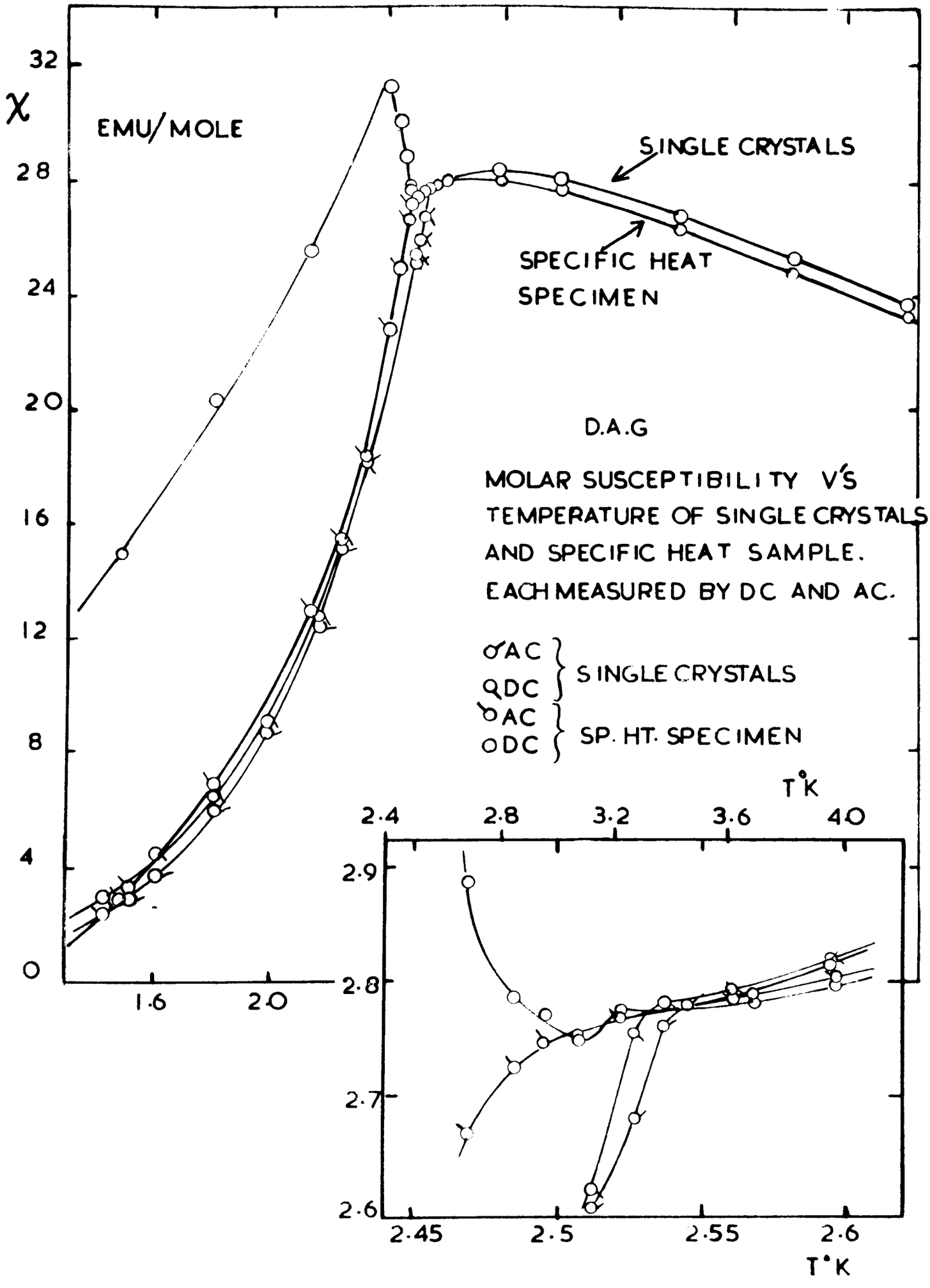
χ
EMU/MOLE
32
28
24
20
16
12
8
4
0
1.6
2.0
SINGLE CRYSTALS
SPECIFIC HEAT
SPECIMEN
D.A.G
MOLAR SUSCEPTIBILITY V'S
TEMPERATURE OF SINGLE CRYSTALS
AND SPECIFIC HEAT SAMPLE.
EACH MEASURED BY DC AND AC.
AC
DC
SINGLE CRYSTALS
AC
DC
SP. HT. SPECIMEN
T°K
2.4
2.8
3.2
3.6
4.0
2.9
2.8
2.7
2.6
2.45
2.5
2.55
2.6
T°K

Figure 6.7

6.10

ions relax at much the same rate as the bulk of the dysprosium ions. Thus, as the ferromagnetic complement pass through the transition, their relaxation time lengthens, and becomes comparable with the frequency of the a.c. measuring field at one stage. In this region, these ions make a contribution to the a.c. susceptibilities, giving rise to the observed frequency-dependent peaks.

Ballistic Measurements on Single Crystals and S.H.Block.

To prove that these d.c. effects result from the physical state of the powder, and are not an inherent property of DAG or the result of chemical impurity, we measured the d.c. susceptibilities of single crystal and specific heat samples. In each case, the d.c. field was removed during every cooling stage, and a.c. measurements taken at each temperature for comparison (Figure 6.7).

The behaviour of the specific heat sample closely resembled that of the powder samples, while for the single crystals, the a.c. and d.c. susceptibilities were virtually indistinguishable. However, the discrepancy between the apparent transition temperatures remained unresolved.

The temperature dependence of the ferromagnetic moment was computed by subtracting the a.c. curve of the specific heat sample from the d.c. curve, the resulting graph being shown in Figure 6.8. Although the absolute value of the ferromagnetic moment was field dependent (in low fields only;

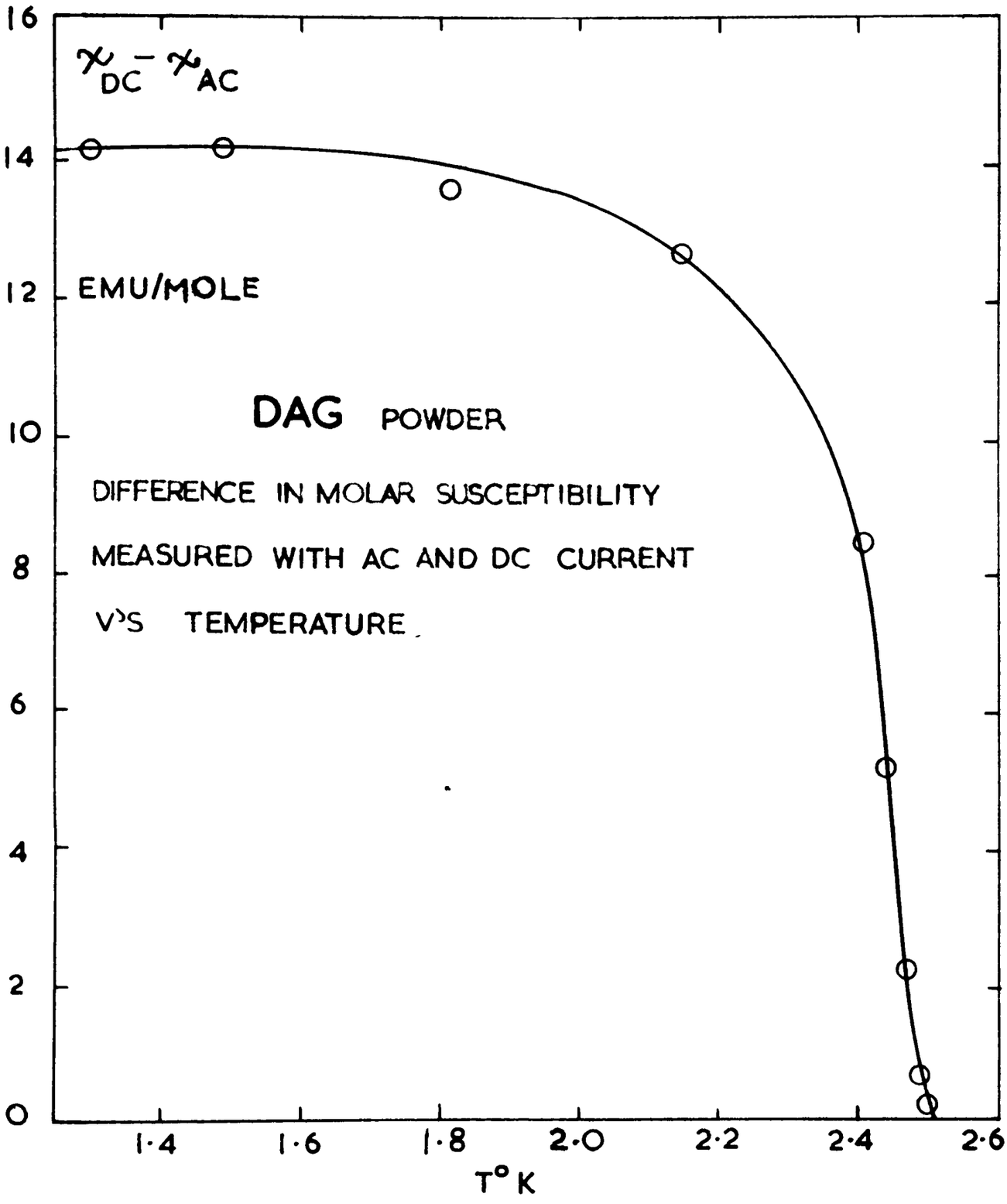
16
14
12
10
8
6
4
2
0
$\chi_{DC} - \chi_{AC}$
EMU/MOLE
DAG POWDER
DIFFERENCE IN MOLAR SUSCEPTIBILITY
MEASURED WITH AC AND DC CURRENT
V'S TEMPERATURE
1·4
1·6
1·8
2·0
2·2
2·4
2·6
T° K

Figure 6.8

an experiment in the magnetic moment apparatus at high fields indicated that the ferromagnetic moment was negligible) the curve looks like a typical saturation curve for a ferromagnet.

Very finely powdered single crystals of DAG did not exhibit any anomalous d.c. susceptibility behaviour.

The Susceptibility of a Spherical Single Crystal of DAG.

A new batch of single crystals was prepared, and one of the larger ones worked into a sphere, and oriented (see Chapter 8). The susceptibility of this specimen was investigated with the utmost care, and since its shape was accurately known, the results (Figure 6.9. The inset represents the critical region on a larger scale) can be regarded as definitive.

The measurements were carried out as usual, except that the temperatures were measured by means of a vapour pressure bulb. By this method, the vapour pressure above liquid helium in a bulb positioned next to the coil in the main refrigerant liquid, and opposite the mid-point of the specimen traverse, defines the temperature, rather than the vapour pressure above the bulk refrigerant. In this way, the thermal gradients, hydrostatic head effects, and other factors introducing inaccuracy in the normal method for measuring temperatures are by-passed.

There is no hint of any anomalous peak, and the point of steepest slope (which corresponds with the Néel

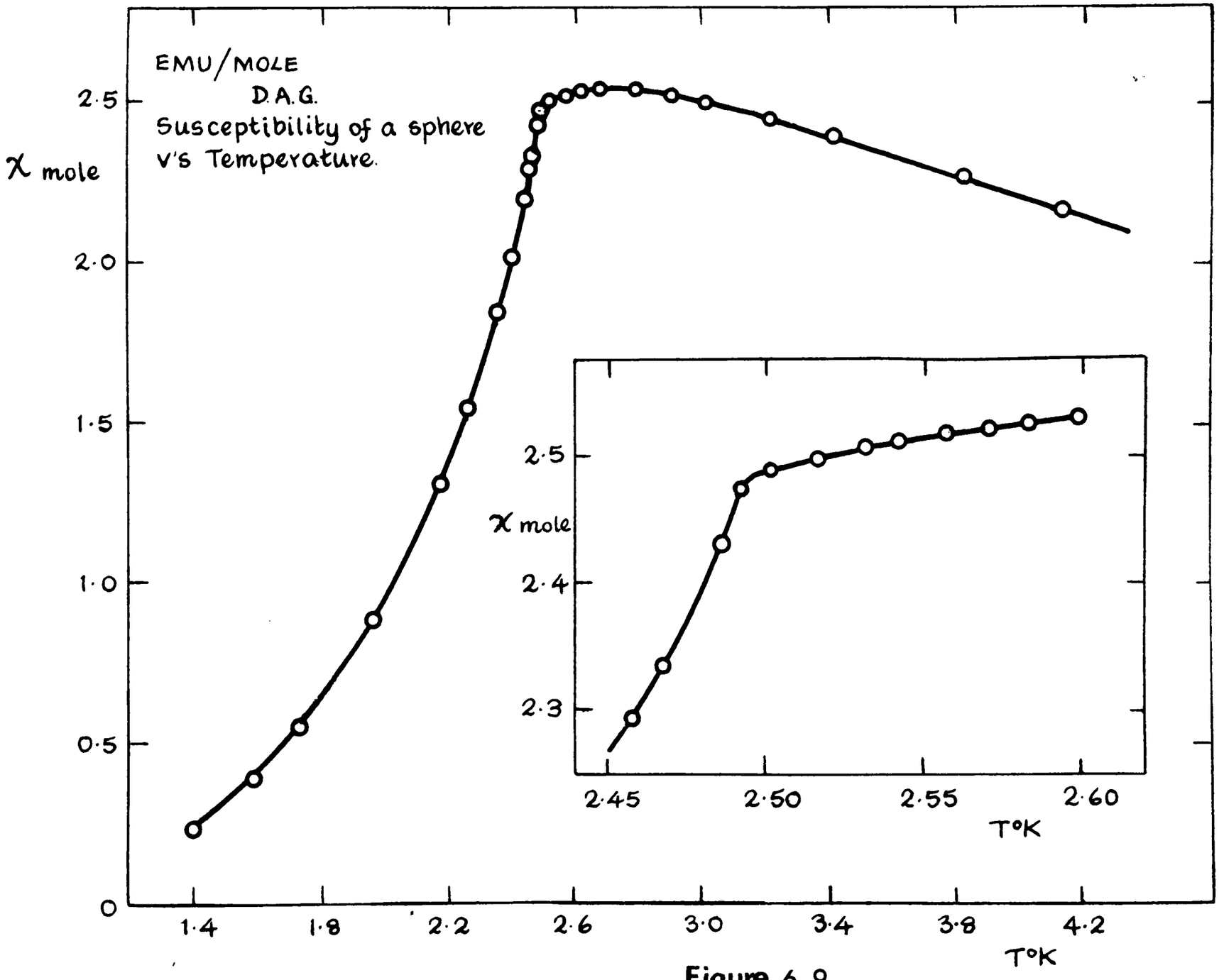
EMU/MOLE
D.A.G.
Susceptibility of a sphere
v's Temperature.
χ mole
2·5
2·0
1·5
1·0
0·5
0
1·4
1·8
2·2
2·6
3·0
3·4
3·8
4·2
T°K
2·5
χ mole
2·4
2·3
2·45
2·50
2·55
2·60
T°K

Figure 6.9

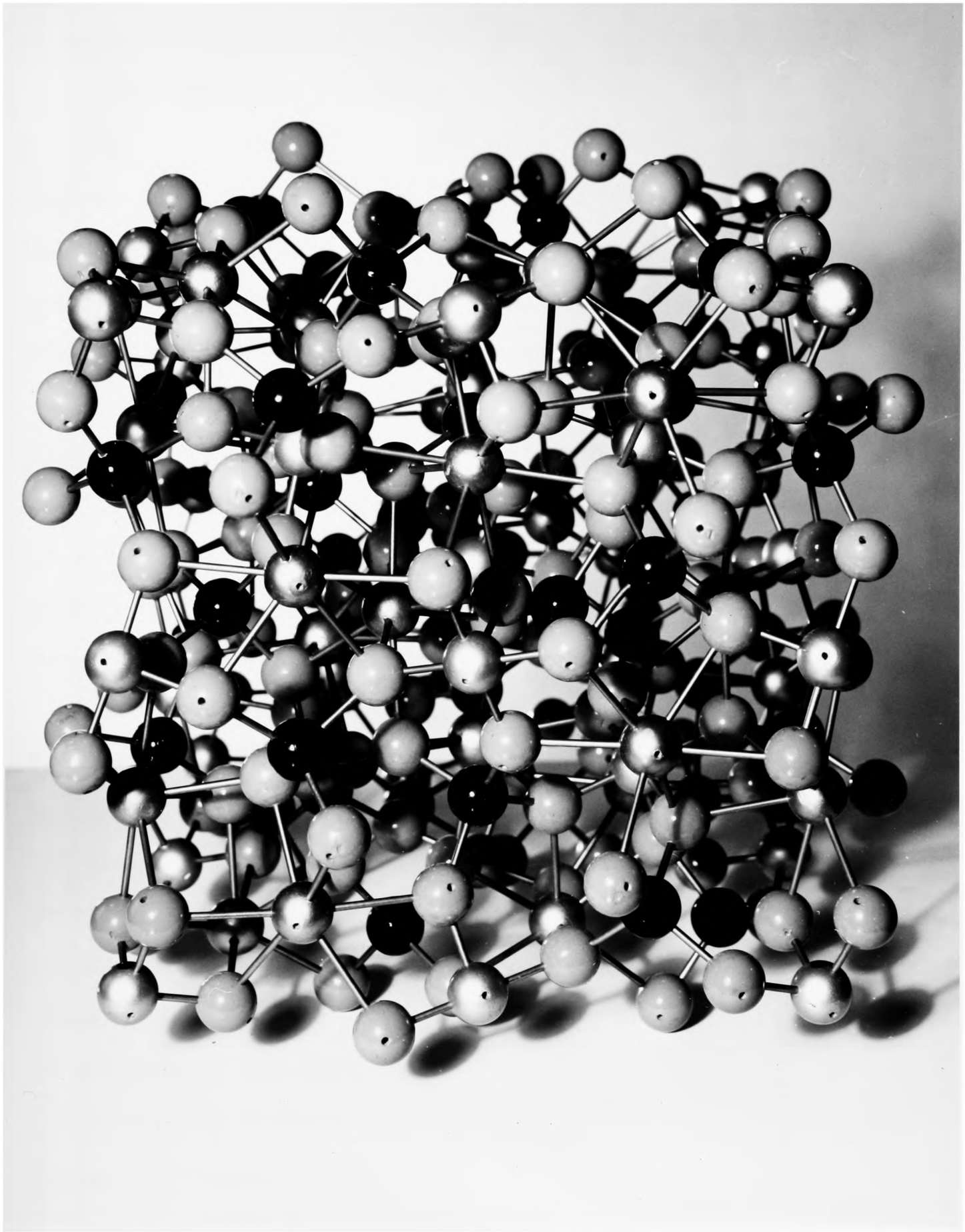

Figure 6.10

point, Sykes and Fisher,1958) is at 2.493 ± 0.005°K, in excellent agreement with the specific heat value.

The susceptibility tends to a very low value at T = 0°K, in contrast with the behaviour of most antiferromagnets (see, for instance Figure 7.6,9.10 and 10.4; Nagamiya,Yoshida and Kubo,1955 .Since DAG is cubic, the susceptibility is isotropic, and a measurement on a single crystal is equivalent to a powder measurement).

Discussion.

Before any detailed discussion of the antiferromagnetism of DAG can be undertaken, its crystal structure must be clarified, since this has a very important bearing on the magnetic properties.

The space group of the garnets is O_{10}^{h} - Ia3d, number 230, and the unit cell contains 8 formula units of $P_3Q_2(RO_4)_3$, making a total of 160 ions. The positions of all the metal ions are defined by the symmetry, but the oxygen ions, arranged to provide approximately cubic, octahedral and tetrahedral coordination around P,Q and R respectively, are in non-parameter positions which must be determined for each garnet by neutron diffraction (Prince,1957) or sophisticated x-ray diffraction techniques (Euler and Bruce,1962).

Figure 6.10 is a photograph of one unit cell of garnet, giving an indication of the complexity of the

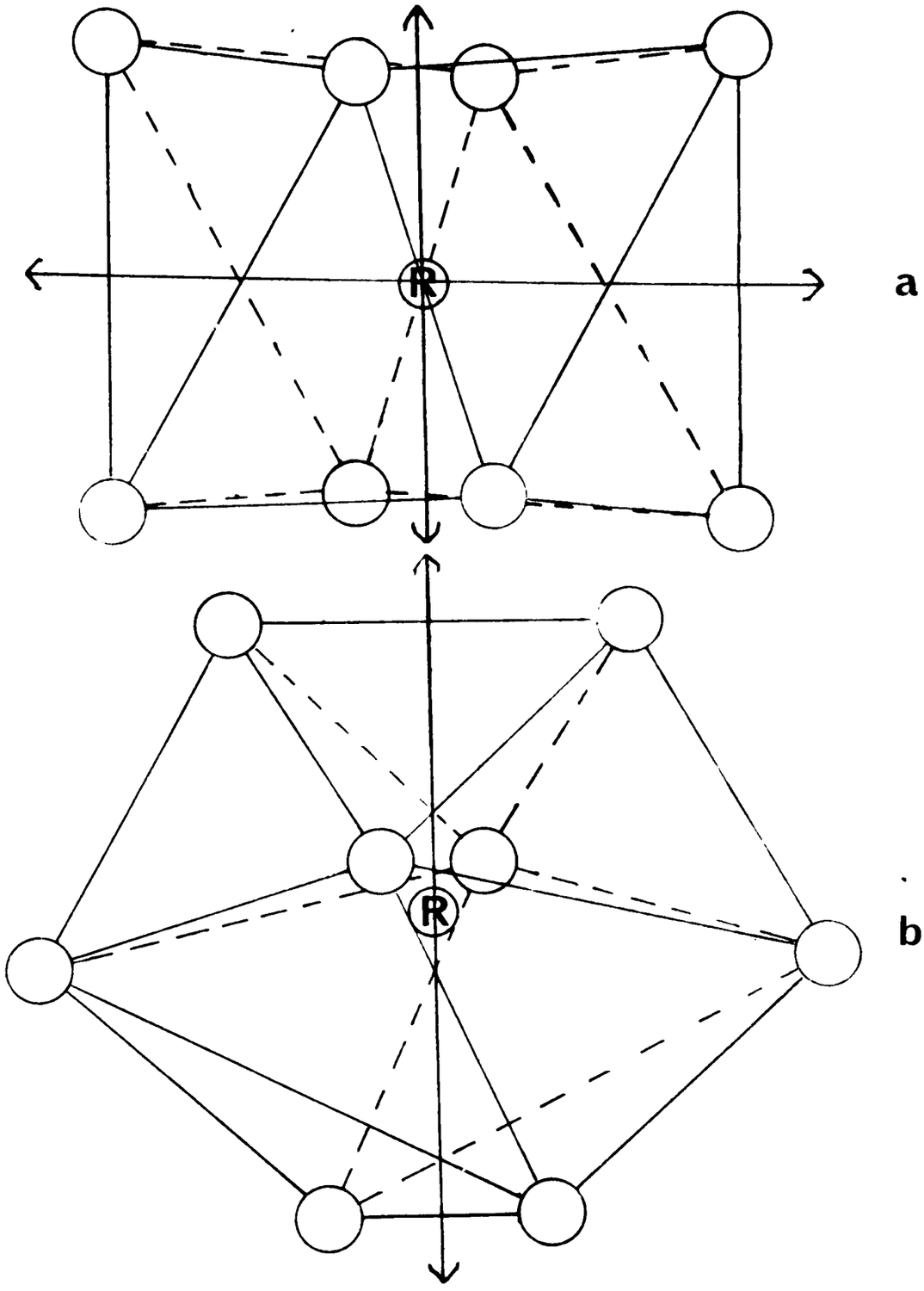

Figure 6.11

structure. Since the aluminium ions do not contribute to the magnetic properties of DAG, they can be neglected in the present considerations. Thus, the relevant parts of the unit cell are the 24 rare earth ions, each with a partial share in the eight oxygen ions comprising its local crystal field. Two projections of these 8 ions and associated rare earth ion are illustrated in Figure 6.11. This distorted cube has a "[110]" axis vertical in Figure 6.11a, and a "[111]" axis vertical in Figure 6.11b.

The local symmetry of the rare earth sites is 2,2,2; that is, three mutually perpendicular twofold axes. These are so oriented that for each rare earth site, one of the two-fold axes is parallel with one of the major unit cell axes, while the other two are at 45° to the remaining two cell axes. There are thus six different rare earth sites per unit cell, with axes parallel with $\pm X$, $\pm Y$ and $\pm Z$, a total of four ions of each type. Since the splitting of the J-manifold in rare earth ions is a direct result of the crystal field, the resulting g-tensor has the same symmetry properties as the crystal field. By convention, the g_z value corresponds with the two-fold axis parallel with the unit cell principal axis (Boakes et al., 1959).

The symmetry elements of the local oxygen ion arrangement are not obvious from the full structure, and attempts to consider the relative orientations of all the rare earths in the unit cell by consulting the complete model (Figure 6.10) were confusing and difficult. We therefore

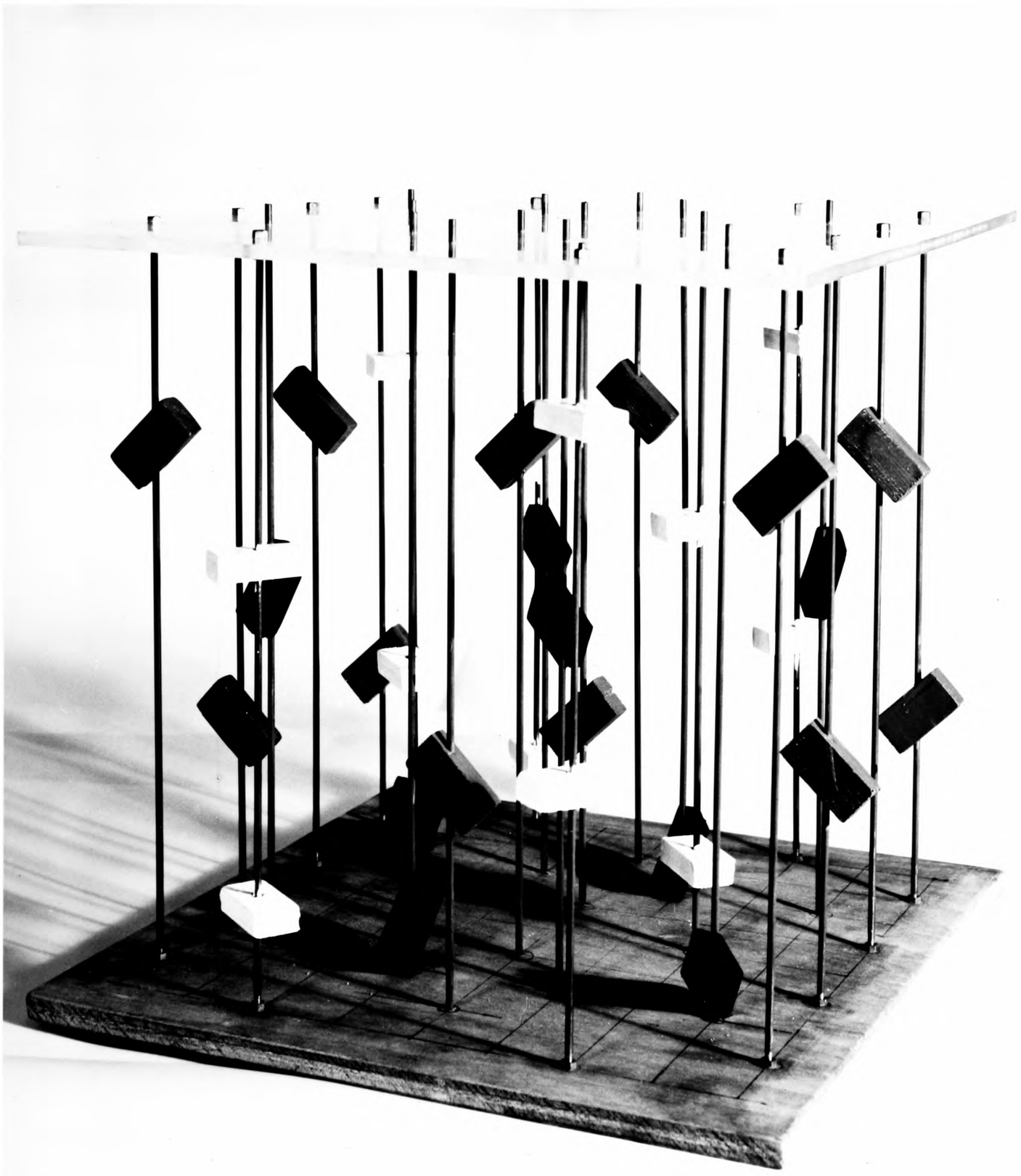

Figure 6.12

constructed a 'g-value' model of the unit cell to the same scale as the full model for ease of comparison. A photograph appears as Figure 6.12. The aluminium ions are omitted completely, and each rare earth and its crystal field of oxygen ions is replaced by a small parallelopiped whose axes correspond with the three two-fold axes of the point symmetry, and with the three principal g-values. $g_z \equiv$ the shortest axis of each parallelopiped. The parallelopipeds were painted black, white or grey according to whether g_z is parallel with the X,Y or Z axis of the unit cell.

In the case of DAG, the g-values are $g_x \approx g_y \approx 0$, $g_z = 18$; that is, in the model (Figure 6.12), the parallelopipeds can be replaced by dipoles which point parallel with the cube axes (i.e., with the shortest edge of the parallelopipeds). Since the splitting of the magnetic moment tensor is the same whether the field is applied in a positive, or negative sense, the number of types of magnetically inequivalent ions reduces to three, that is, in DAG, to dipoles pointing along the three cube axes. To give an overall moment of zero at $0^{\circ}K$, equal numbers of ions must point in a positive and negative sense along each crystal axis.

Because of the symmetry properties, all the Dy ions in DAG are identical apart from orientation, and a visual inspection of the model (Figure 6.12) reveals that each ion has four identical nearest neighbours. The magnetic dipolar

ENERGY OF TWO POSSIBLE SUBLATTICE ARRANGEMENTS FOR DAG

ORIGIN ION IN DIRECTION + Z.

		Arrangement 1		Arrangement 2	
Neighbour	Distance from origin	Moment direction	Energy /pair(μ^2/a^3)	Moment direction	Energy (μ^2/a^3)
1st nearest (4)	3.67 A	+ X	- 17.4	+ X	- 17.4
		+ Y	- 17.4	+ Y	- 17.4
		- X	- 17.4	- X	- 17.4
		- Y	- 17.4	- Y	- 17.4
		Total	- 69.6	Total	- 69.6
2nd nearest (8)	5.61 A	+ X(2)	- 6.3	- X(2)	+ 6.3
		- X(2)	- 6.3	+ X(2)	+ 6.3
		+ Y(2)	- 6.3	- Y(2)	+ 6.3
		- Y(2)	- 6.3	+ Y(2)	+ 6.3
		Total	- 50.4	Total	+ 50.4
3rd nearest (2)	6.00 A	- Z(2)	+ 16.00	+ Z(2)	- 16.00
		Total	+ 32.00	Total	- 32.00
4th nearest (4)	7.30 A	+ X	- 6.1	+ X	- 6.1
		+ Y	- 6.1	+ Y	- 6.1
		- X	- 6.1	- X	- 6.1
		- Y	- 6.1	- Y	- 6.1
		Total	- 24.4	Total	- 24.4
Energy of 18 nearest neighbours			- 112.2		- 75.6
Energy of 172 nearest neighbours			- 97.8		- 72.7

Figure 6.13

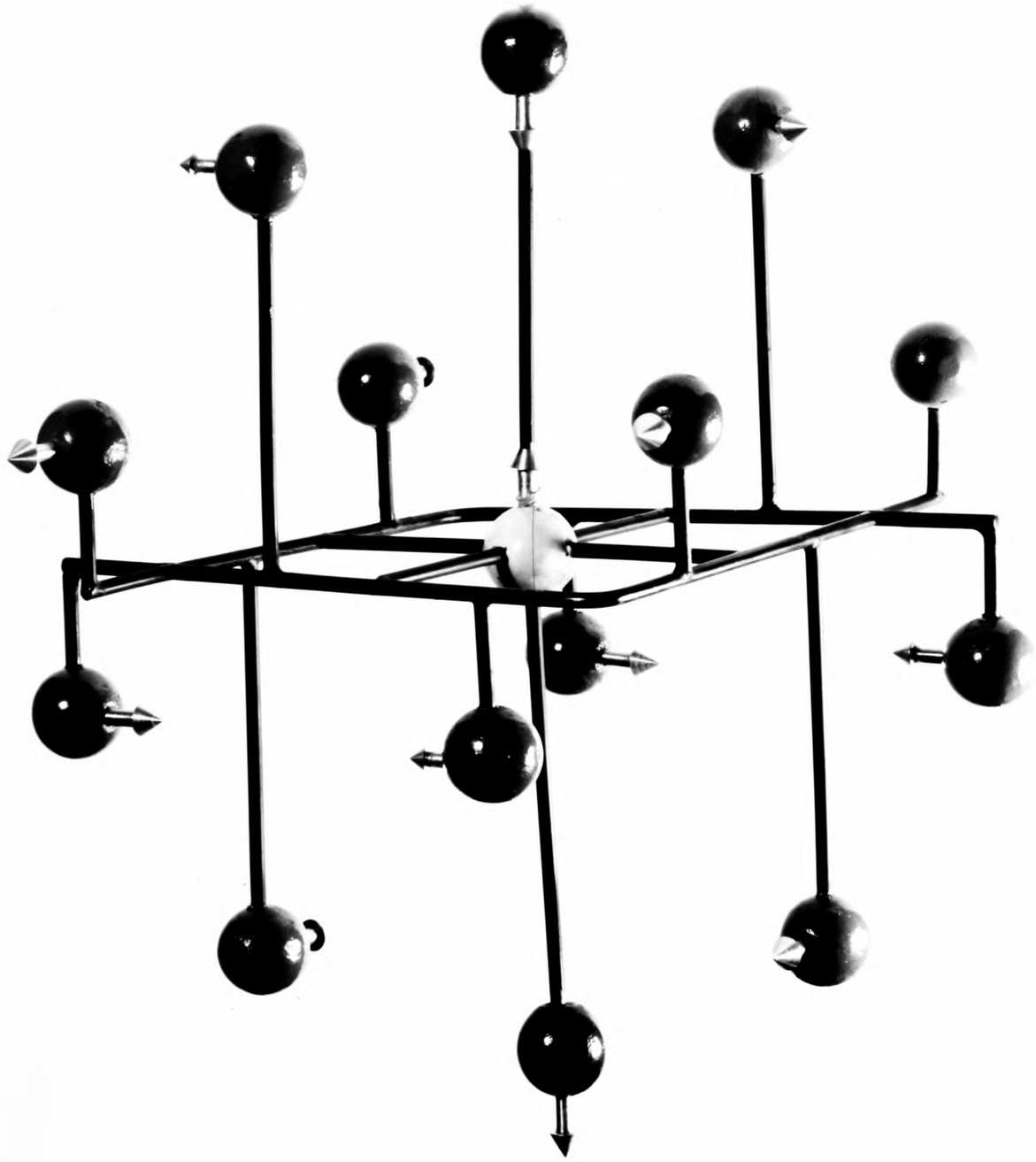

Figure 6.14

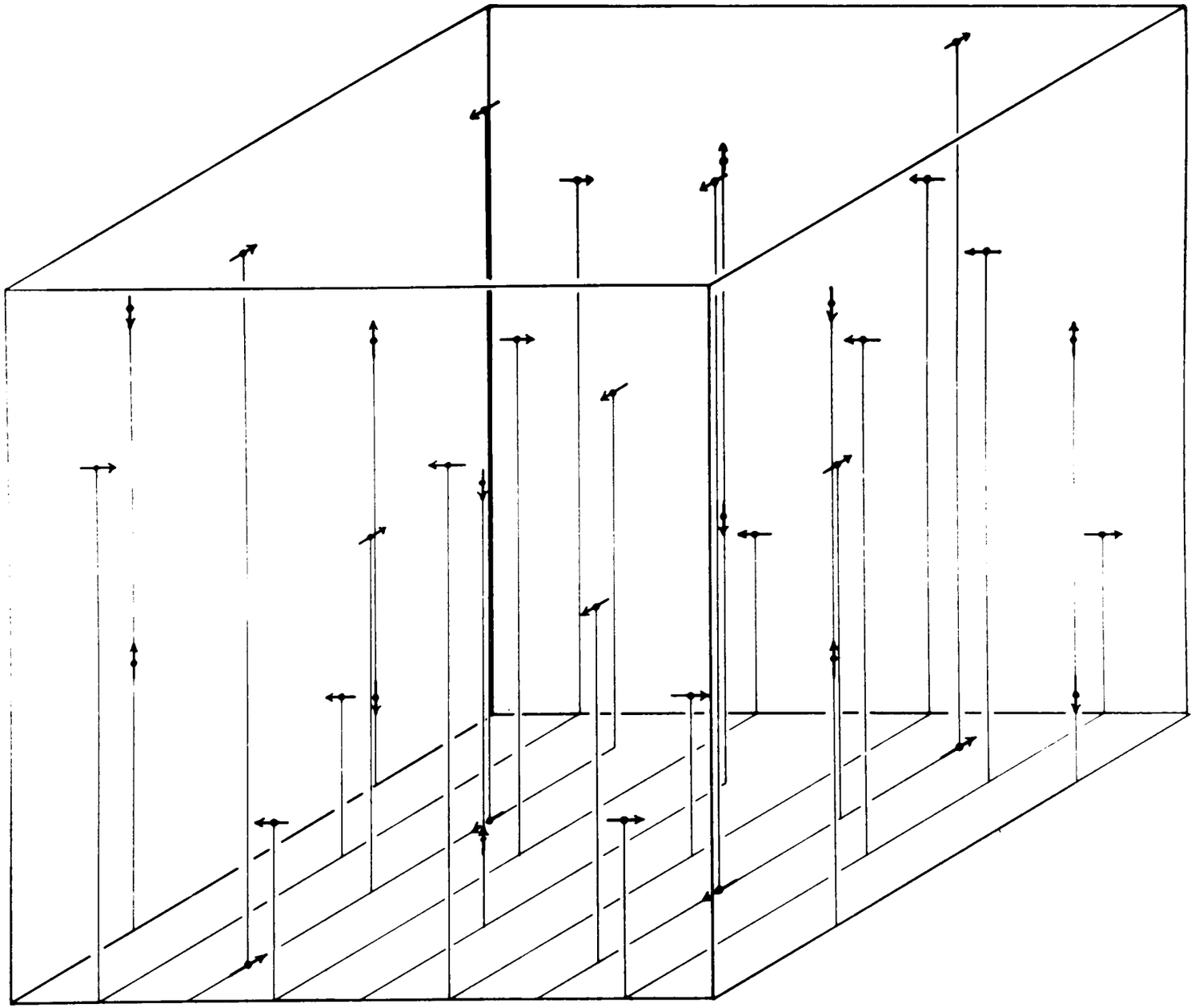

Figure 6.15

POSSIBLE SUB-LATTICE STRUCTURE FOR DYSPROSIUM ALUMINIUM GARNET.

interaction energy of these ions is so great, that any spin arrangement prevailing in DAG below the Néel point must almost certainly have these ions oriented for minimum energy (see Figures 6.13 and 14). To preserve this nearest neighbour condition throughout the lattice, there are certain limitations on the arrangements of second and third nearest neighbours, namely, the signs of the energies must be opposite. The dipolar energies for the two possible spin arrangements are tabulated in Figure 6.13.

Arrangement 1 can be described as antiferromagnetic chains of ions in the $\pm X$, $\pm Y$ and $\pm Z$ directions, while arrangement 2 consists of ferromagnetic chains in these directions.

The dipole sum was made by Dr M.J.M.Leask (private communication) using the Oxford University Computer. It seems clear that the first arrangement (illustrated in Figure 6.15) is the one energetically most favoured, and it is the arrangement assumed by Leask and Wolf (Ball et al., 1962) in calculating the low temperature susceptibility according to a molecular field approximation.

The agreement at low temperatures is very bad, the theory systematically predicting a susceptibility higher than observed. Wyatt (1963) has estimated that the molecular field constants need to be increased by about 35% to give good agreement at low temperatures. It follows that magnetic dipolar forces alone cannot account for the behaviour of

DAG, a conclusion confirmed by the behaviour of the gadolinium garnets (page 5.6) which show that there are some exchange forces. It follows that the ordering arrangement deduced on a consideration of dipolar forces alone is no longer necessarily correct, though its probability remains very high.

Conclusions.

Impurities have been shown to depress the transition temperature of DAG, but these cannot be invoked to explain the discrepancy between the first batch of DAG crystals, and all other samples, in transition temperatures.

Some samples of DAG exhibit a weak ferromagnetism, and this seems to be related to the aggregate state of the sample. The single crystals reveal no anomalous effects, while the polycrystalline powders show a two-component ferromagnetism. The sintered specific heat block has intermediate properties. The various methods of preparation would suggest a grain size diminishing in the order single crystals/sintered block/polycrystalline powder, and since no significant chemical differences were detectable between these samples, it seems that a physical difference is responsible, and there does not seem to be a more likely candidate than grain size.

The polycrystalline powder was examined optically at a magnification of x500, and the particles appeared to be amorphous.

It is possible that this effect is superparamagnetism (Néel,1961) arising from uncompensated spins at the edges of particles in the antiferromagnetic state. However, for an effect as large as that we observed, the powder would have to be exceedingly fine, and it is rather unlikely that the grains in the sintered specific heat block would be sufficiently small to give a high enough proportion of surface ions.

Chapter 7.

The Specific Heat of DAG.

Introduction.

In view of the interesting susceptibility measurements made on DAG, we decided to extend the investigation to include specific heat. If it had proved possible to obtain a sufficiently large crystal, we should have measured its specific heat in applied magnetic fields (c.f. the magnetic moment results of Chapter 8) as well as in zero field, since the λ-anomaly could almost certainly have been broadened, displaced in temperature, or even dissociated into smaller peaks according to the direction and strength of the applied field. However, the experiment on a polycrystalline block enabled us to make a precise measurement of the ordering temperature, and to estimate the internal energy and entropy for comparison with theoretical values.

Description of Apparatus.

The apparatus was kindly loaned by Dr A.J.Croft, and is described in Croft et al (1953) and Croft and Exell (1961). The specimen (K) is suspended in a brass calorimeter from cotton threads (I). The calorimeter is surrounded by liquid helium, and thermal contact is maintained with the specimen by helium exchange gas in the calorimeter until the specimen reaches the lowest temperature to be measured. The helium gas is then pumped away, and the specimen is

Key to Figure 7.1

A - Pumping Tube

B - Liquid Hydrogen

C - 'Covar' metal-glass Seal

D - Outer Dewar Vessel

E - Inner Dewar Vessel

F - Liquid Helium

G - Specimen Space Evacuation Tube

H - Specimen Space

I - Cotton Specimen Suspension

J - Copper Wire Specimen Cage

K - Specimen

L - Ground Brass Cone Cap, sealed with Glycerol-Soap

Specific Heat Apparatus Cryostat.

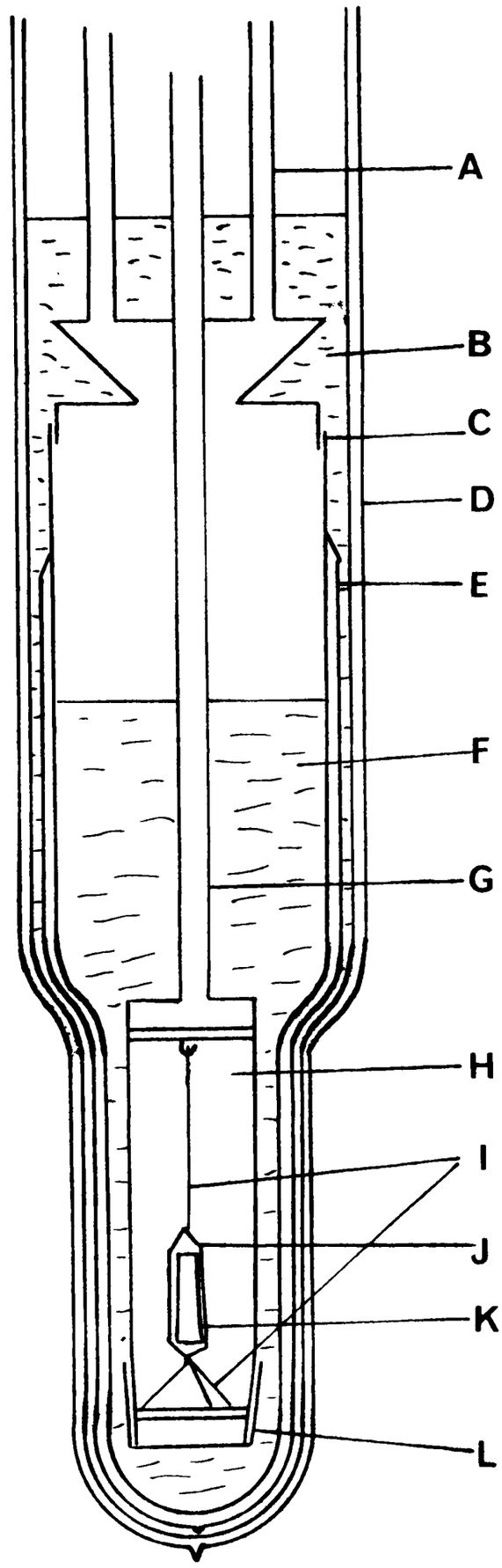

Figure 7.1

electrically heated in small steps while the corresponding temperature rises are measured by means of a carbon resistance thermometer.

The cryostat is shown schematically in Figure 7.1. The monax glass helium dewar (E) is permanently evacuated, and terminates in a 'Covar' seal (C) by which it is attached to the upper part of the helium space. The liquid helium is cooled by pumping through 2 1cm diameter german silver tubes (A) with a powerful rotary pump, giving a minimum temperature of 1.15°K. The temperature is measured by reading the helium vapour pressure on mercury and oil manometers with a cathetometer.

The specimen is mounted inside an open brass cage with cotton threads, which are tensioned by means of a screw. The cage is a sliding fit inside the calorimeter. The bottom of the calorimeter is sealed to gas and helium liquid by means of a brass cone joint (L) coated with glycerol-soap solution. The electrical leads from the specimen emerge through platinum-glass seals in the bottom of the calorimeter.

The resistance used as a heating element was in the form of a loosely woven tape, in which a continuous fine constantan wire ~~wires~~ formed the warp, and insulating fibres the weft. This readily assumed the shape of the specimen, and when stuck on with G.E.Varnish No. 7031, made excellent thermal contact with the specimen. A length of tape having a resistance of about 1000 ohms was used, and the heating

Key to Figure 7.2

P - Potentiometer

R_s - Standard Resistance

D - Dummy Load

H - Heater

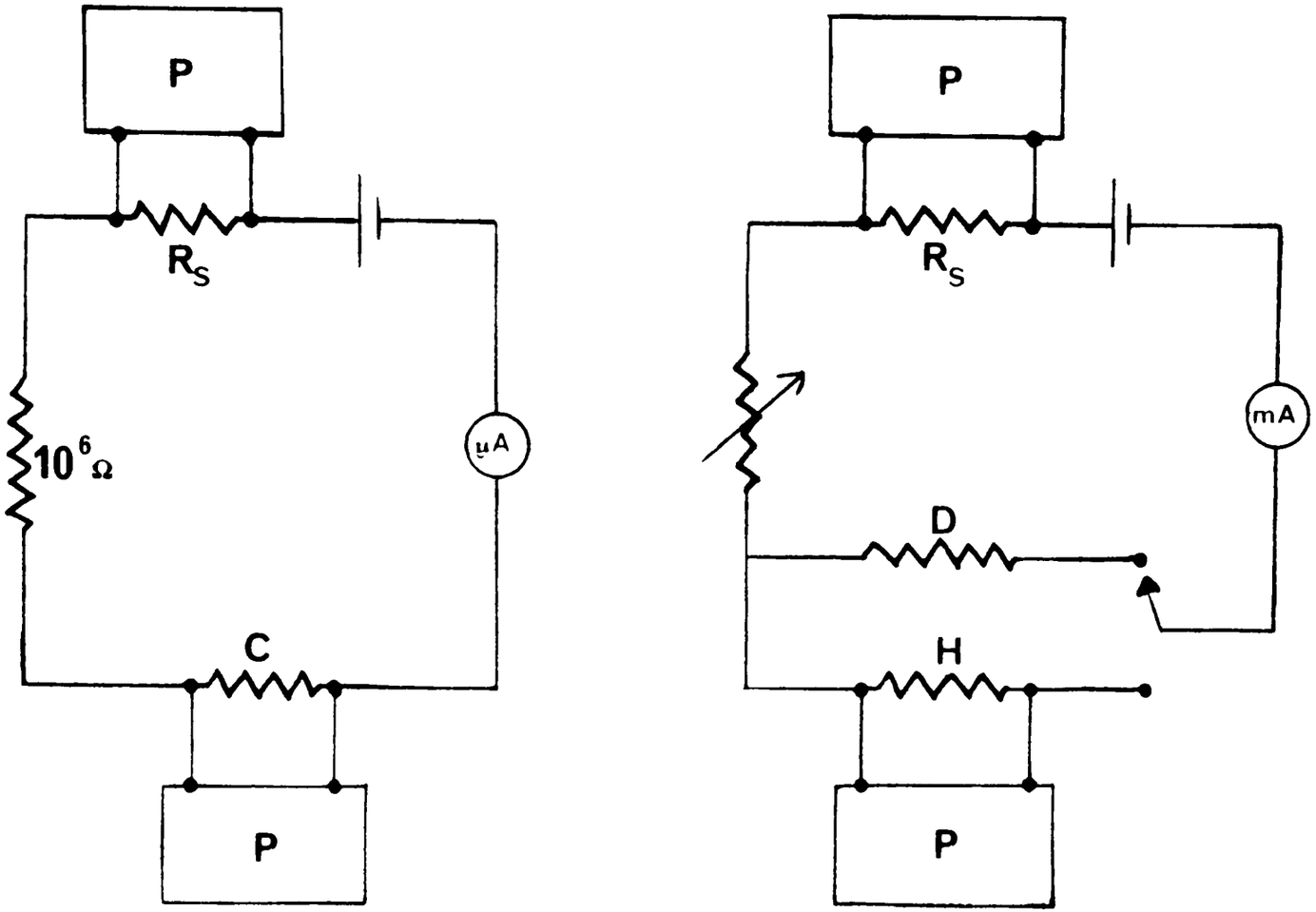

Figure 7.2

Specific Heat Electrical Circuitry.

current varied during the experiment to give a temperature rise of the order of 50 millidegrees in the course of about 45 seconds.

A circuit dia ram is reproduced as Figure 7.2. The heating current was measured by finding the voltage across a standard 1000 ohm resistance in series with the heater. The potential across the heater was measured from the half-way point of the leads joining the heater to the platinum-glass seals. This compensates for heat generated in the leads, presuming that half flows into the specimen, and half into the calorimeter, but since the leads have a small resistance compared with the heater (about 2%), the possible source of error from imbalance is small.

The carbon resistance chosen for use as a thermometer had a wide variation of resistance in the liquid helium region (from 650 ohms at 4.2°K to 15,000 at 1.15°K). In order to mount it on the specimen in good thermal contact, a piece of silver foil was hard soldered at one side to a thin-walled copper tube of slightly greater diameter than the resistor. The resistor was insulated by wrapping in a single layer of cigarette paper coated in Araldite, which also glued it inside the copper tube, with good thermal contact. The silver foil readily assumed the shape of the specimen, and when stuck on with G.E. varnish, excellent thermal contact between specimen and thermometer was achieved.

The Specific Heat Sintered Block of DAG with Thermometer and Heating Element Mounted.

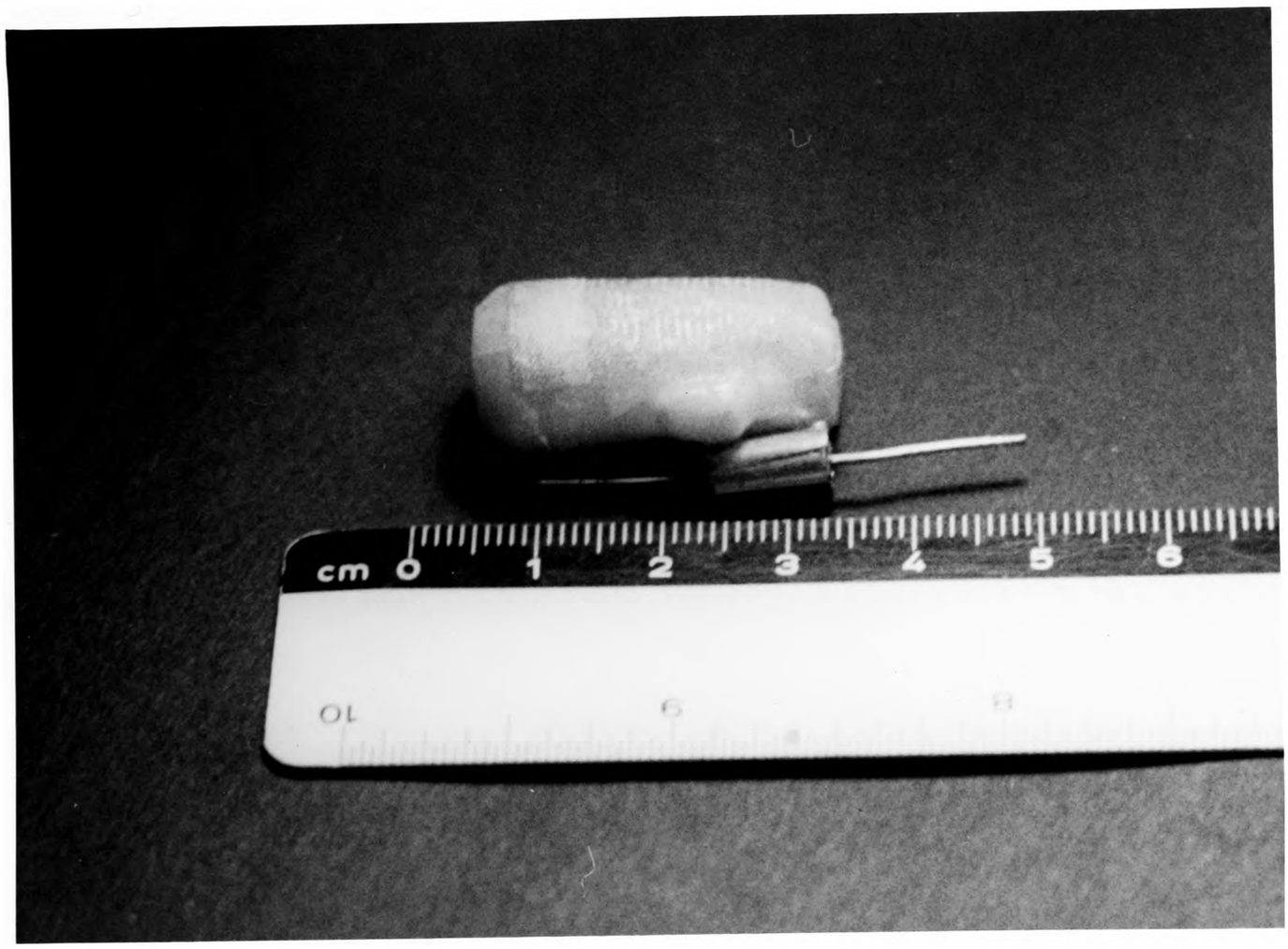

Figure 7.3

Because of slight variations in its characteristics, the resistance thermometer had to be calibrated before each experiment. The cooling was interrupted at various stages, and the resistance of the thermometer and the temperature measured. The results were expressed as a law: -

$$T = \frac{A \log R}{(\log R - B)^2}$$

where A and B are constants, whose average values were 1.60 ± 0.02 and 1.775 ± 0.005 respectively during these experiments. All the experimental points except those just above the liquid helium λ-point fitted this law to within $\pm$ 4 millidegrees. It was assumed that the characteristics of the resistance thermometer changed only as the result of complete cooling and warming cycles to room temperature.

The thermometer resistance was measured with a very low d.c. current (about 5 μamps) to avoid incidental heating of the specimen. This current was kept virtually independent of the thermometer resistance by having a one megohm resistance in series. The potential across the thermometer was of the order of 5 millivolts, and was measured with a potentiometer using a sensitive galvanometer. The current and potential were measured after each heating interval, though the current scarcely changed, and was assumed to remain constant during the establishment of drift-rates.

Experimental Procedure.

The fused block of DAG (see page 3.27) was carefully cleansed of adhering areas of sintered spongy material, and the surface smoothed to simplify fixing the thermometer and heating element using emery cloth and a carborundum block. The final weight was 21 g, and Figure 7.3 shows the specimen after the thermometer and heating element had been fixed. To simplify its mounting in the calorimeter, an inner cage of copper wire (J) was constructed round the specimen, which was carefully painted with several layers of G.E.varnish to restrict helium absorption.

With the specimen in position, the cryostat was cooled to liquid nitrogen temperatures with an atmosphere of helium gas in the inner dewar and calorimeter. The specimen space was then pumped with a mercury diffusion pump while the cryostat was cooled to liquid hydrogen and then helium temperatures. About 0.5 mm of exchange helium gas was then admitted to the specimen space, and the liquid helium pumped and thermometer calibrated.

At the lowest temperatures, the specimen was isolated by pumping away the exchange gas, a slow process taking about 2 hours. The pumping was continued throughout the measurements to remove any gas desorbed on warming, and for the purpose of preventing desorption, the helium bath was maintained at 1.15°K throughout.

The temperature was measured at 30 second intervals

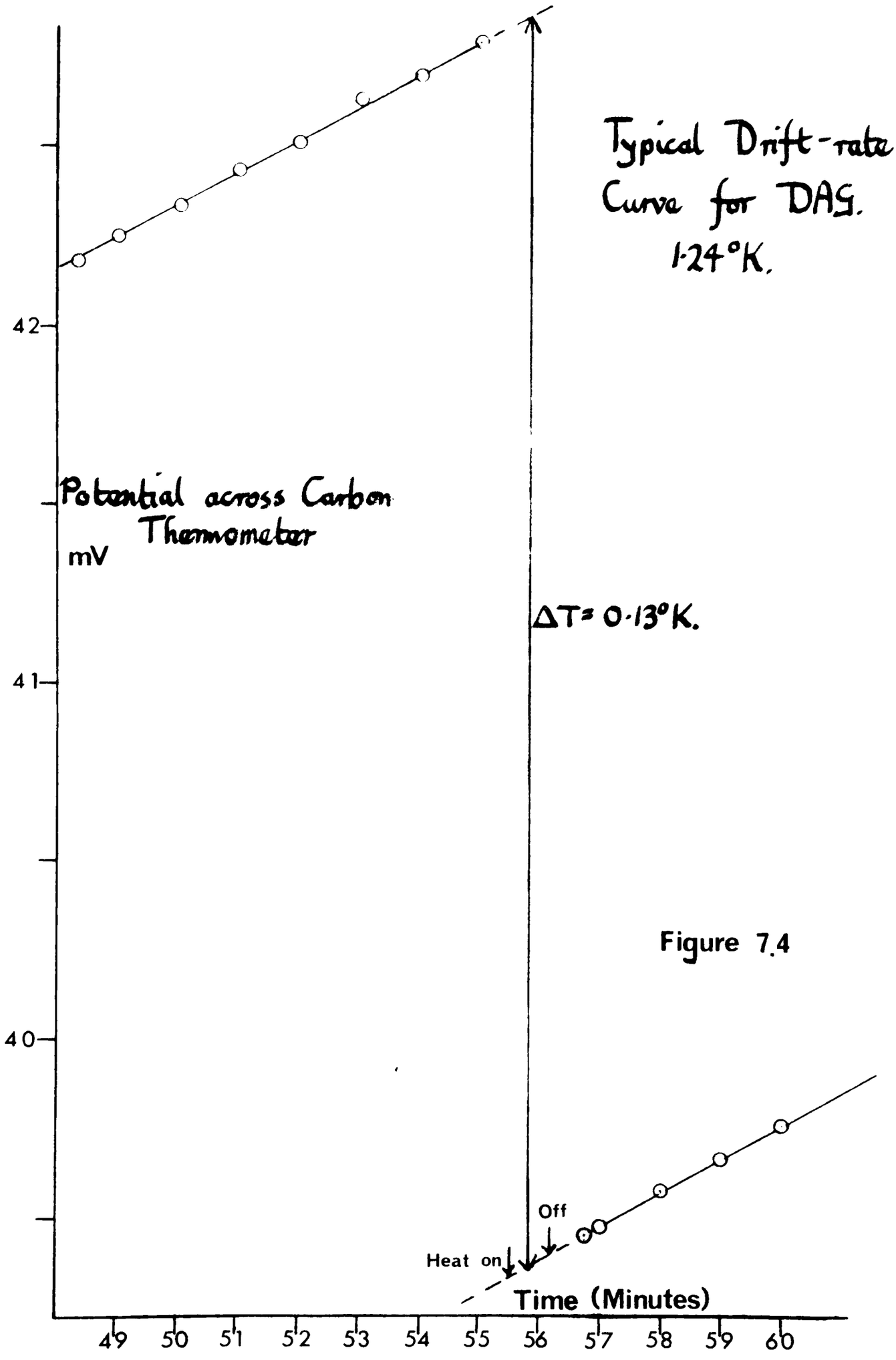
Typical Drift-rate Curve for DAS. 1·24°K.
42
Potential across Carbon Thermometer
mV
ΔT= 0·13°K.
41
40
Off
Heat on
Time (Minutes)
49
50
51
52
53
54
55
56
57
58
59
60

Figure 7.4

before and after each specific heat point to establish a drift-rate. This was plotted continuously, and measurements continued until steady behaviour was obtained. The experimental process was continuous, the upper drift rate for one point serving as the lower rate for the subsequent one. The electrical heating was switched on at a known time and timed with a stop-watch. The two drift-rates were extrapolated to the mid-point of the heating period, and the temperature rise there taken as that caused by the electrical heating. A typical point is shown as Figure 7.4.

This procedure was varied only in order to measure the entropy in the neighbourhood of the peak of the anomaly. The specimen was heated from just below the critical temperature to just above it, the temperature being continuously monitored and the heating stopped immediately upon any change. Thus, the internal magnetic energy was measured directly.

Impurity and Other Corrections to the Data.

The results of four experiments are plotted as specific heat against temperature in Figure 7.5. In general, the features are according to expectation, except for the slight bump on the curve at about 3.4°K. It seemed unlikely that this was a genuine property of DAG - an impurity undergoing a magnetic ordering seemed a more reasonable explanation. Assuming that the impurity is not completely foreign, the two possible magnetic impurities in a sample of DAG prepared

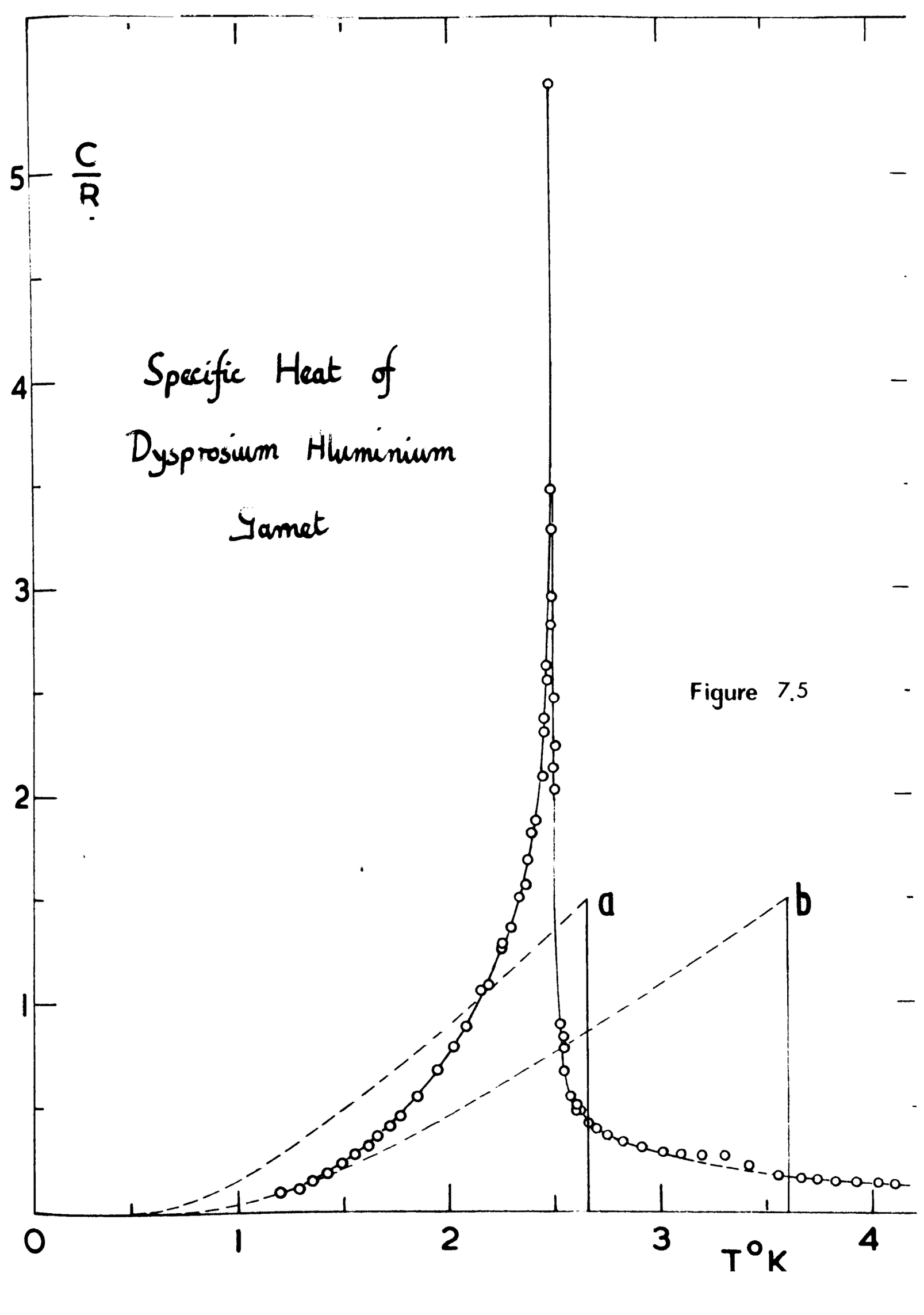
C/R
5
4
3
2
1
0
1
2
3
4
T°K
a
b
Specific Heat of
Dysprosium Aluminium
Garnet

Figure 7.5

in this way are dysprosium oxide, and more likely, the perovskite phase $DyAlO_3$ both resulting from a slight excess of dysprosium oxide.

We measured the susceptibilities of the polycrystalline $DyAlO_3$ (page 3.23) and of some calcined commercial Dy_2O_3. The results of these experiments are shown in Figure 7.6. The susceptibility of the simple oxide increases steadily with decrease in temperature throughout the measured range, while the perovskite manifests a peak in the susceptibility at about 3.5°K, after which it falls away rapidly in the way typical of antiferromagnets.

It seems that a small amount of the perovskite phase in the DAG sample accounts for the bump in the specific heat curve, and a comparison of the estimated entropy associated with this bump with that of the whole sample indicates that about 1% perovskite was present. Even if this did not arise from local inhomogeneity (compensated by excess aluminium oxide elsewhere), the amount of excess Dy_2O_3 necessary to convert 1% of the garnet to perovskite

$$Dy_3Al_5O_{12} + Dy_2O_3 \rightarrow 5\ DyAlO_3$$

is rather small, and could hardly be avoided in the processing of such a large batch of starting material (more than 300 g). Subsequent analysis (page 6.4) and susceptibility experiments (Chapter 6) imply that the bump could not have been caused by 'foreign' impurities.

The specific heat of this impurity can be neglected at all temperatures except those near 3.4°K.

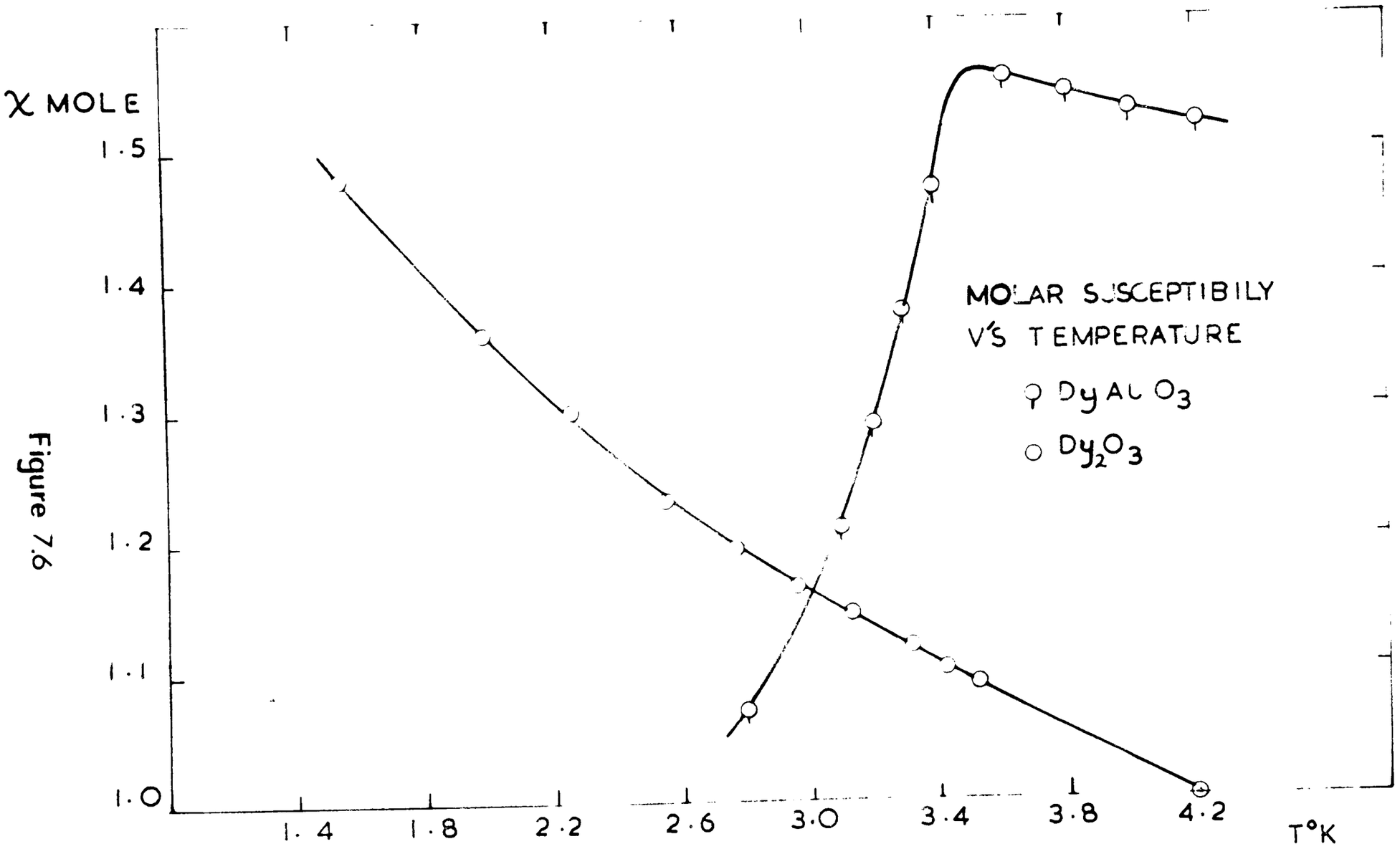
χ MOLE
1·5
1·4
1·3
1·2
1·1
1·0
1·4
1·8
2·2
2·6
3·0
3·4
3·8
4·2
T°K
MOLAR SUSCEPTIBILY
V'S TEMPERATURE
♀ DyAlO3
○ Dy2O3

Figure 7.6

From the point of view of the present work, the interesting part of the measured specific heat is that caused by the interactions of the magnetic ions, but there are three other possible contributions which must be considered.

1) The inner copper cage, thermometer, heating element and G.E.varnish. These are in fact negligible within the experimental accuracy.

2) Nuclear hyperfine splitting. Wyatt (1963) has estimated this contribution from data on Dy in the ethyl sulphate lattice, and the resonance g-values of Dy in YAlG, and concludes that the necessary correction lies within the experimental error throughout the whole measured temperature range.

3) Lattice contributions. The lattice specific heat can be estimated from specific heat measurements on YGaG, which has a similar structure to DAG, and whose molecular weight is virtually identical (807.4 and 814.4 respectively). Bailey (unpublished) finds that the specific heat in the helium range of YGaG obeys a Debye T^3 law: -

$$C/R = 1.15 \times 10^{-4}\ T^3 \text{ joules/mole/}^{\circ}K.$$

or according to the units adopted in this thesis: -

$$C/R = 3.83 \times 10^{-5}\ T^3 \text{ joules/g.ion of Dy/}^{\circ}K$$

The greatest contribution will be at the higher temperatures, and at $4^{\circ}K$ will amount to 0.00243 joules/g.ion/$^{\circ}K$, compared with a total specific heat of 0.133 that is, just within

the experimental error of 3% at these temperatures.

Harris and Meyer (1962) find an expression for the lattice contribution to the specific heat of YIG: -

$$C/R = 1.3 \times 10^{-6} T^3 \text{ joules/g ion of Y/}^{\circ}K.$$

Since this was only an estimated expression, whereas Bailey's result was a direct measurement, it is probable that his expression provides a better indication of the likely lattice contribution in DAG, but in any event, the lattice contribution is small. In view of the somewhat conflicting data, and the small correction involved, the lattice contribution has been ignored throughout the measured temperature range.

Discussion of Results.

The peak of the specific heat anomaly at $2.49 \pm 0.1_5{}^{\circ}K$ (Figure 7.5) is in good agreement with the susceptibility measurements on the same sample, and on later single crystal samples.

Interesting features of the anomaly are its sharpness (It has already been pointed out on page 6.6. that this may almost certainly be taken as an indication of the chemical purity of the specimen), the very rapid fall of specific heat below the transition temperature, and the lack of symmetry of the anomaly, which is very much steeper on the high than on the low temperature side. This second feature is also in good agreement with the susceptibility behaviour

of this material, which rapidly tends to zero below the transition temperature (Figure 6.9).

As with the susceptibility, the molecular field approximation should give the specific heat accurately at low temperatures. Curve (a) in Figure 7.5 represents the molecular field behaviour of DAG, assuming that the interactions are only magnetic dipolar between ions with effective $S = \frac{1}{2}$, $g_z = 18.3$, $g_x = g_y = 0$. The agreement found is very bad, even at the lowest temperatures where the approximation is most valid. Curve (b) represents a molecular field approximation in which the interactions are increased empirically to give good agreement at low temperatures. Thus it is again found (c.f. page 6.15) that simple magnetic dipolar interactions can account for not more than 65% of the total interactions in DAG.

The asymmetry of the anomaly about the transition temperature is in accordance with general predictions made on the basis of the Ising model of cooperative phenomena. This model considers the interactions between the z components of nearest neighbour spins only. Although the garnet lattice has not been treated theoretically, Wakefield (1951) has considered ferromagnetic interactions in a simple cubic lattice, and Domb and Sykes (1957) and (1962) have considered ferromagnetic interactions in a body-centred cubic lattice, and in each case, an infinite discontinuity which is asymmetrical about the transition

temperature is predicted. The latter authors suggest that the results would be very similar for antiferromagnets.

Although DAG is not strictly an Ising substance, since there are long-range interactions, and although none of these theoretical treatments corresponds exactly with the particular case of DAG, the theoretical conclusions are generally supported by the specific heat measurements.

The internal energy and entropy changes associated with the transition have been determined by numerical integration of the area under the specific heat curve, since

$$-\frac{\Delta U}{R} = \int_{T_1}^{T_2} \left(\frac{C}{R}\right) dT$$

where ΔU is the internal energy between T_1 and $T_2^{\circ}K$ and assuming that $C = C_p = C_v$, i.e., the lattice does not contribute to the internal energy below $4^{\circ}K$. The area in the vicinity of the anomaly was measured physically (page 7.6). The contribution to the internal energy from the range $0 - 1.2^{\circ}K$ was estimated from the fitted molecular field curve (b), but only amounted to about 1% of the total. The contribution from the range $4.0 - \infty\ ^{\circ}K$ was estimated by a $1/T^2$ extrapolation.

According to this integration, the total internal energy at $0^{\circ}K$ ($-U^{(0)}/R$) is 1.94 ± 0.25. Now according to molecular field theory: -

$$-U^{(0)}/R = H_i^{(0)} \cdot M^{(0)}/2k$$

where $M^{(0)} = \frac{1}{2} g_{\parallel} \mu_B$, i.e. the moment per spin

$H_i^{(0)}$ = the internal field at 0°K.

But $H_i^{(0)}$ is related to the Néel temperature

$$T_N = H_i^{(0)} . M^{(0)} / k$$

whence it follows that

$$2 U^{(0)}/R = T_N = 3.9 \pm 0.5^{\circ}K.$$

This value is in good agreement with that obtained by fitting the molecular field to the low-temperature specific curve (b in Figure 7.5), and also to that deduced from the susceptibility measurements.

The total entropy: -

$$\frac{S}{R} = \int_{T=0}^{T=\infty} \left(\frac{C}{T R} \right) dT$$

was also obtained by numerical integration, and gave the value 0.69 ± 0.4. This is in excellent agreement with the entropy expected for an alignment transition of a spin $S = \frac{1}{2}$, namely ln 2 = 0.693. The assumption that Dy in DAG behaves as a Kramer's spin is thus validated.

MFisher (1962) has shown that there is a mathematical relationship between the susceptibility and specific heat of a simple two-lattice antiferromagnet

$$\chi T = 1 - A|U|P$$

where P is a slowly varying function of temperature and A is a constant. Fisher's approach neglects dipole interactions completely, hence there is no rigorous reason why the theory should apply to DAG. However, a comparison

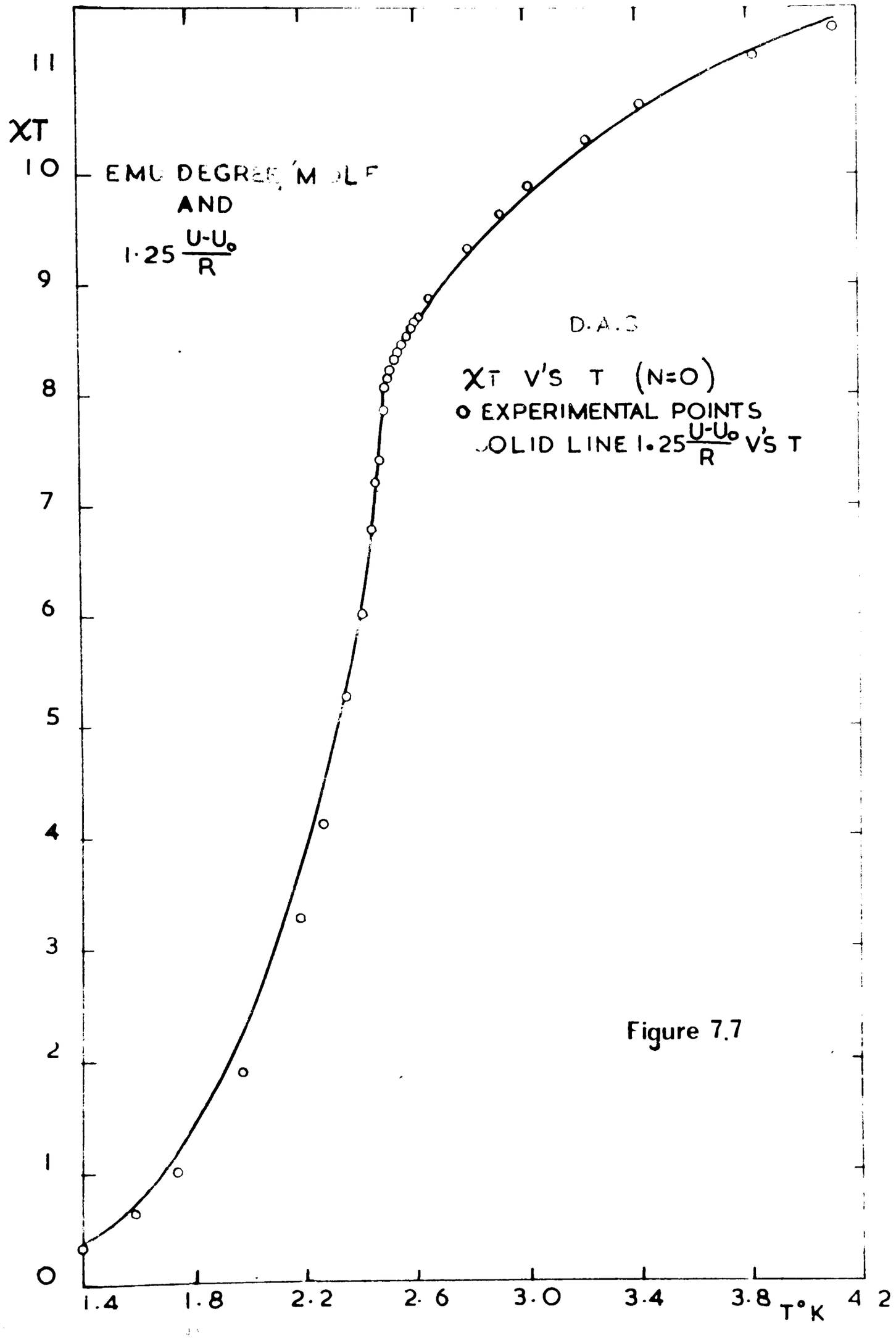
χT
EMU DEGREE MOLE
AND
1·25 (U-U₀)/R
D.A.C
χT V'S T (N=0)
o EXPERIMENTAL POINTS
SOLID LINE 1·25 (U-U₀)/R V'S T
11
10
9
8
7
6
5
4
3
2
1
0
1.4
1.8
2.2
2.6
3.0
3.4
3.8
4 2
T°K

Figure 7.7

of the functions χT and $U - U^{(0)}/R$ (Figure 7.7) reveals a close similarity of behaviour. In the graph, the susceptibility is corrected for demagnetisation to a shape $N = 0$, and the thermodynamic function is multiplied by an arbitrary factor of 1.25 to normalise the two graphs at the transition temperatures.

Conclusions.

The specific heat measurements are in good agreement with the susceptibility results, and the molecular field treatment of the specific heat gives approximately the same error as the treatment of susceptibility.

The entropy indicates that Dy can be regarded as an effective spin $S = \frac{1}{2}$ in DAG, while qualitative comparisons between the properties of DAG and various theoretical models are sufficiently worth while to indicate that further useful theoretical work might be carried out on this substance.

Chapter 8.

Magnetic Transitions in Dyspresium Aluminium Garnet.

Introduction.

On the evidence of the low ordering temperature of DAG, the internal forces responsible are relatively small, and comparable with the forces experienced by the ions as a result of applied magnetic fields of reasonable magnitude. The rare earth ions in garnets are strongly coupled to the crystal field, so that for Dy in DAG, only two orientations are permitted for each ion -'spin up' and'spin down'. Thus, depending on orientation, an applied field sufficiently big should cause the spins in one or more of the DAG sublattices to 'flip' - i.e. become ferro- instead of antiferromagnetic. We have investigated this effect by measuring the magnetisation of a single crystal of DAG as a function of applied field at various temperatures, and with the applied field parallel with several symmetry axes of the crystal.

Description of the Apparatus.

The apparatus used was a vibrating sample magnetometer of the type first described by Foner (1959), built by Drs A.F.G.Wyatt and W.P.Wolf (Wyatt,1963). The main modification to the original design was that the magnet was rotated rather than the specimen.

A schematic diagram of the apparatus is shown in Figure 8.1. The specimen is vibrated between the poles of an electromagnet at a low audio frequency (75 c.p.s.) on

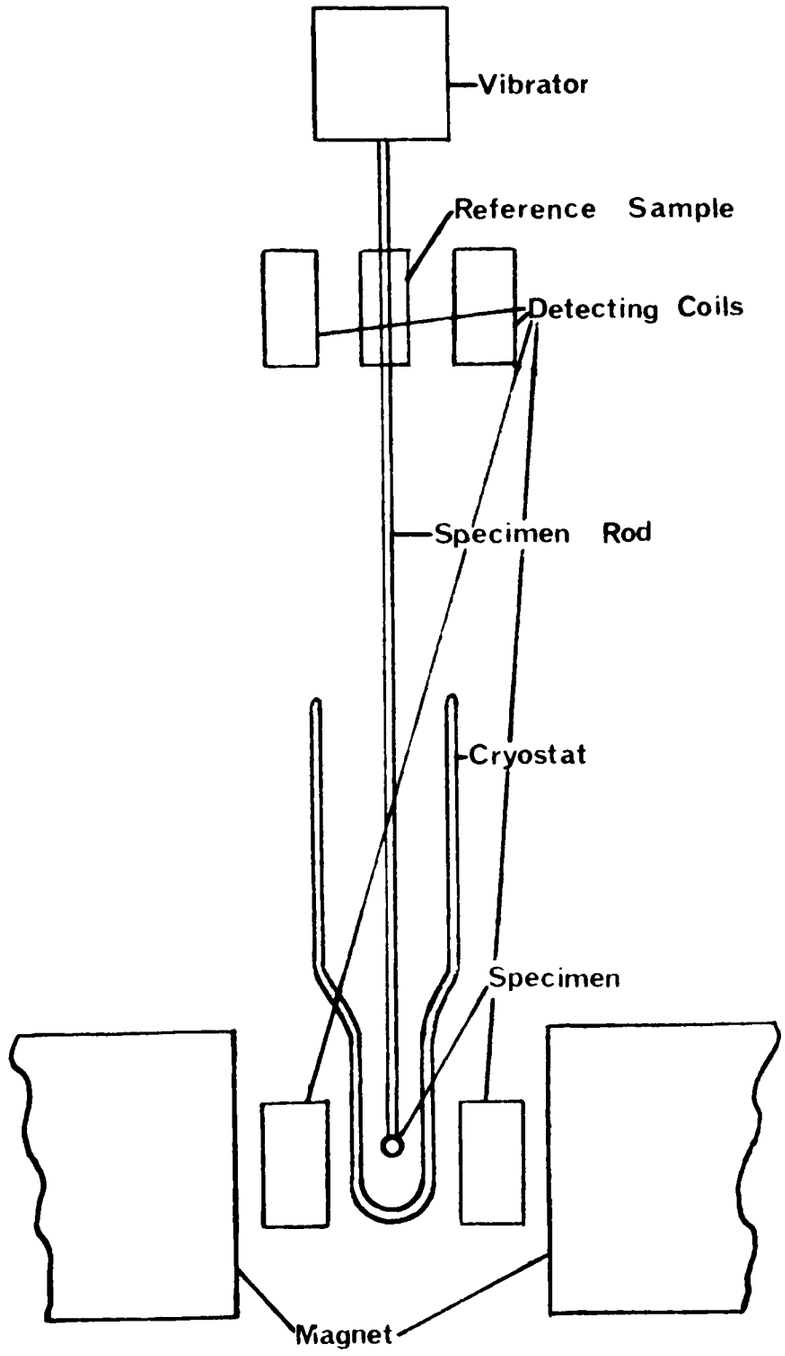

Block Diagram of Magnetometer

Figure 8.1

the end of a rigid rod, Surrounding the specimen, and also between the magnet's poles, is a coil system which produces an a.c. signal from the motion of the specimen. The size of this signal is proportional to the magnetisation of the specimen, and also to the amplitude and frequency of the vibration. The two latter effects are nullified by comparing the signal from the specimen coils with the signal from a reference system comprising a d.c.coil attached to the vibrating specimen rod, and also moving within a similar pick-up coil system. The current to the d.c. coil is adjusted by variable resistors to balance the signal from the specimen, as observed by a null point on the cathode ray oscilloscope (Figure 8.2). The magnitude of this d.c. current is measured across a standard resistance by means of a potentiometer.

A current-field relationship derived by Dr M.T.Hutchings for the magnet using a nuclear resonance probe was used in estimating the magnetic field from the current flowing in the magnet, which was measured by means of a potentiometer across a standard resistance. Great care was exercised in always making the measurements on the same section of the magnet's hysteresis loop.

The apparatus was calibrated by measuring the moment of the specimen as a function of field, and extrapolating the curves of M/H against H to zero field, where moment is equivalent to susceptibility.The results were then compared

Key to Figure 8.2

V	-	Vibrator
O	-	Power Oscillator
P	-	Potentiometer
R_s	-	Standard Resistance
R_v	-	Variable Resistance
S	-	Specimen
A	-	Pre-Amplifier
T	-	Tuned Amplifier
c.r.o.		Cathode Ray Oscilloscope

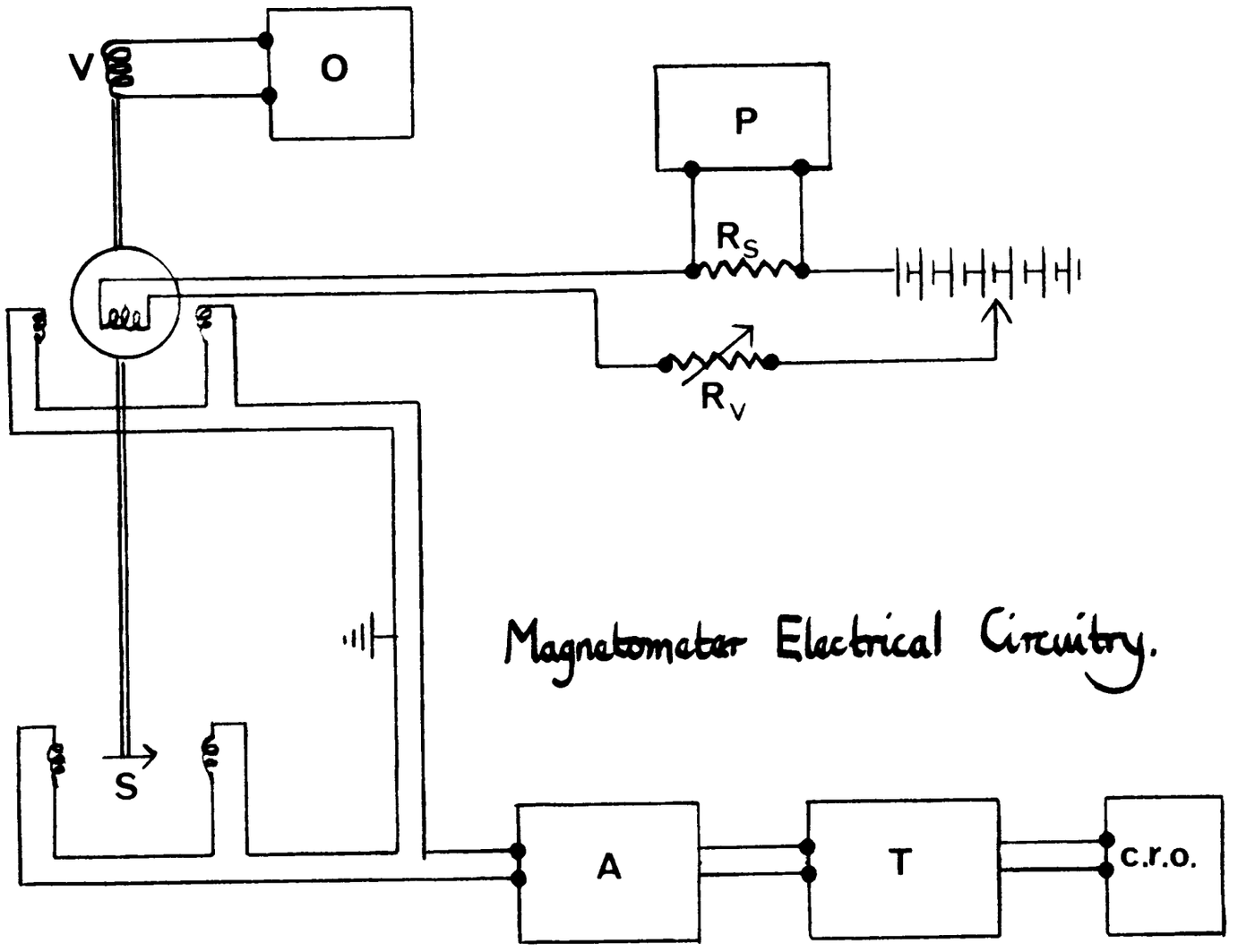

Magnetometer Electrical Circuitry.

Figure 8.2

with the susceptibility of the same specimen as measured directly on the susceptibility apparatus (Chapter 4), with an overall accuracy of 1.5%.

Preparation of DAG Sample.

The simplest shape to prepare for which an accurate demagnetisation correction can be made is a sphere, which for the sake of accuracy in the present experiments, had to be as large as possible. Since the angular variation of moment was to be measured, the specimen also had to be a single crystal.

The largest available perfect single crystal of DAG weighed 107 mg. It was found by trial and error, that unworked garnet crystals can be very effectively made into rough spheres by rapid shaking in a 'Wig-L-Bug' micro grinding and mixing mill (Glen Creston Limited) in an agate tube. This machine moves the agate tube in a complicated 'figure 8' motion combined with rocking, at very high speed. The presence in the tube with the crystal of abrasive powders, other crystals, and steel ball bearings of various sizes were all found to be detrimental. About an hour's shaking was needed, and the shaping process appeared to be rather the result of repeated slight chipping of the protruding areas than any kind of grinding process.

The rough sphere was then lapped between two Dural tubes of diameter only slightly less than the largest

diameter of the crystal (otherwise the crystal 'stuck' and became less rather than more spherical). A slurry of lubricating oil and carborundum powder was used as the grinding agent, progressively finer grades of powder being substituted as the shape approached that of a sphere. The shape was checked from time to time by placing the crystal in a conical recess in a metal block, and measuring various diameters with a travelling microscope until these were the same to within $\sim 2\%$. In this respect, it was necessary to compromise between accuracy of shape, and decrease in mass (and hence in accuracy of measurement) by continued working of the specimen. The final weight of the sphere was 44 mg.

Orientation of Specimen.

The crystal was oriented by a two-stage process. It was mounted initially in plasticine on an x-ray back reflection camera in a random orientation. The symmetry points on the photograph were identified by comparison with the known symmetry axes of the garnets, and the crystal adjusted by hand to have a $[110]$ axis vertical. The crystal was then transferred to a goniometer head with minimum loss of orientation, and fixed in position with black wax.

The crystal was then accurately oriented by finding $[110]$, $[100]$, and $[111]$ axes,,all of which lie in a (110) plane, and relating the measured angles between them to the theoretical values, and checking that their symmetries

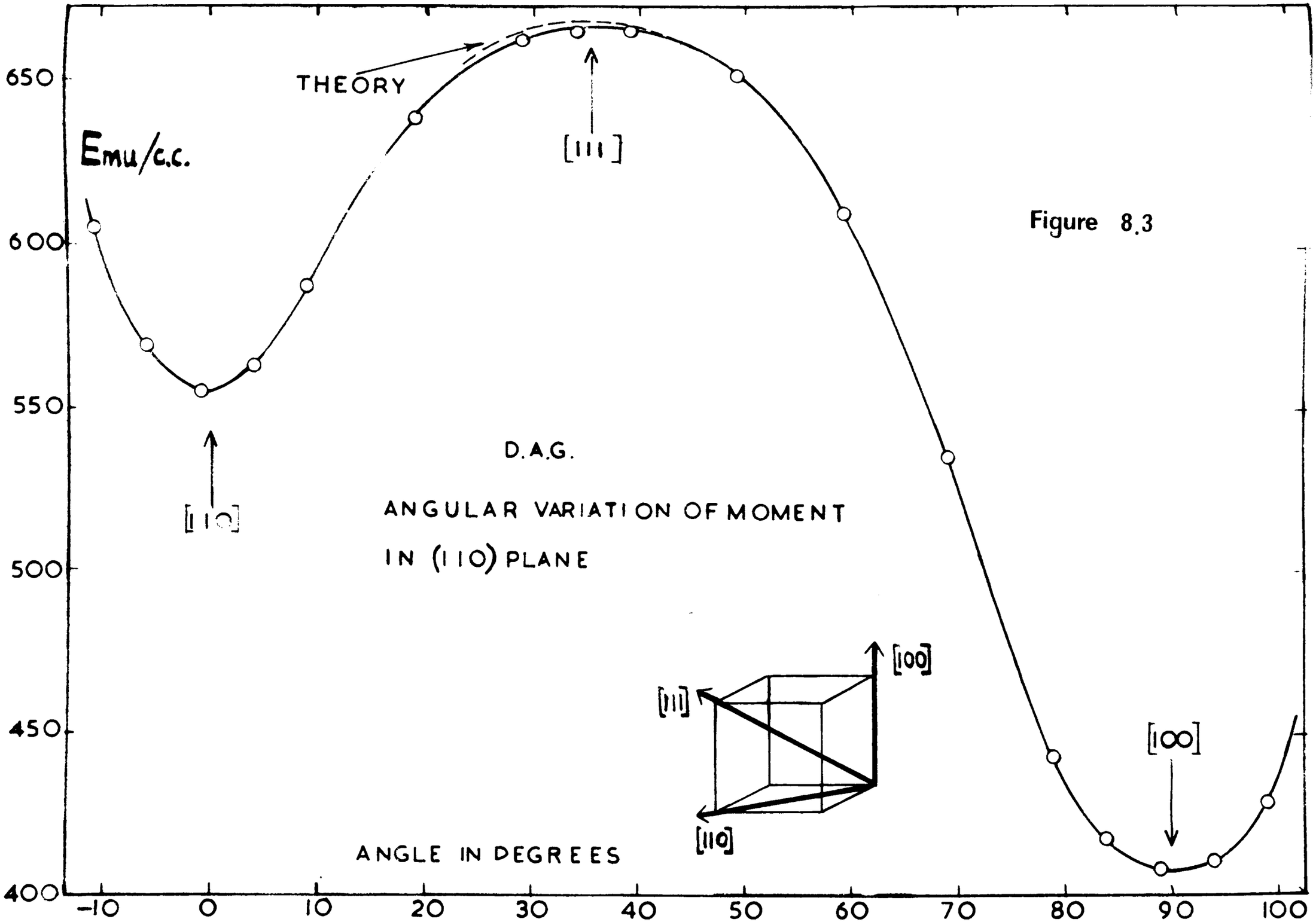
650
600
550
500
450
400
Emu/c.c.
THEORY
[111]
[110]
D.A.G.
ANGULAR VARIATION OF MOMENT
IN (110) PLANE
[100]
[111]
[110]
[100]
ANGLE IN DEGREES
-10
0
10
20
30
40
50
60
70
80
90
100

Figure 8.3

corresponded with a vertical [110] axis.

When the crystal was aligned to within about 1°, it was transferred to a special sample holder (Figure 4.4d, page 4.9), the orientation being preserved by using a lathe to mount the goniometer and sample holder. 'Araldite' was the adhesive. The orientation was then finally checked by mounting the crystal on the x-ray camera once again so that its supposed [110] axis was parallel with the x-ray beam. The resulting photograph was found to display the correct symmetry.

The orientation was confirmed after the specimen had been transferred to the magnetic moment machine. The variation of moment with angle of applied field at 1.1°K and a field of 10 k.oe. was measured (Figure 8.3). The symmetry of this graph corresponds exactly with that of the paramagnetic resonance spectra of rare earths in garnets when the field is also applied in a (110) plane (see, for instance, Ball et al.,1960). The angles between the maxima and minima correspond exactly with the angles between the [111], [110] and [100] axes in a (110) plane (see inset in Figure 8.3).

The Experiments.

The measurements were made along the [111], [110] and [100] axes of the crystal. Since the sublattices of DAG are oriented along the major crystal axes (page 6.14), fields

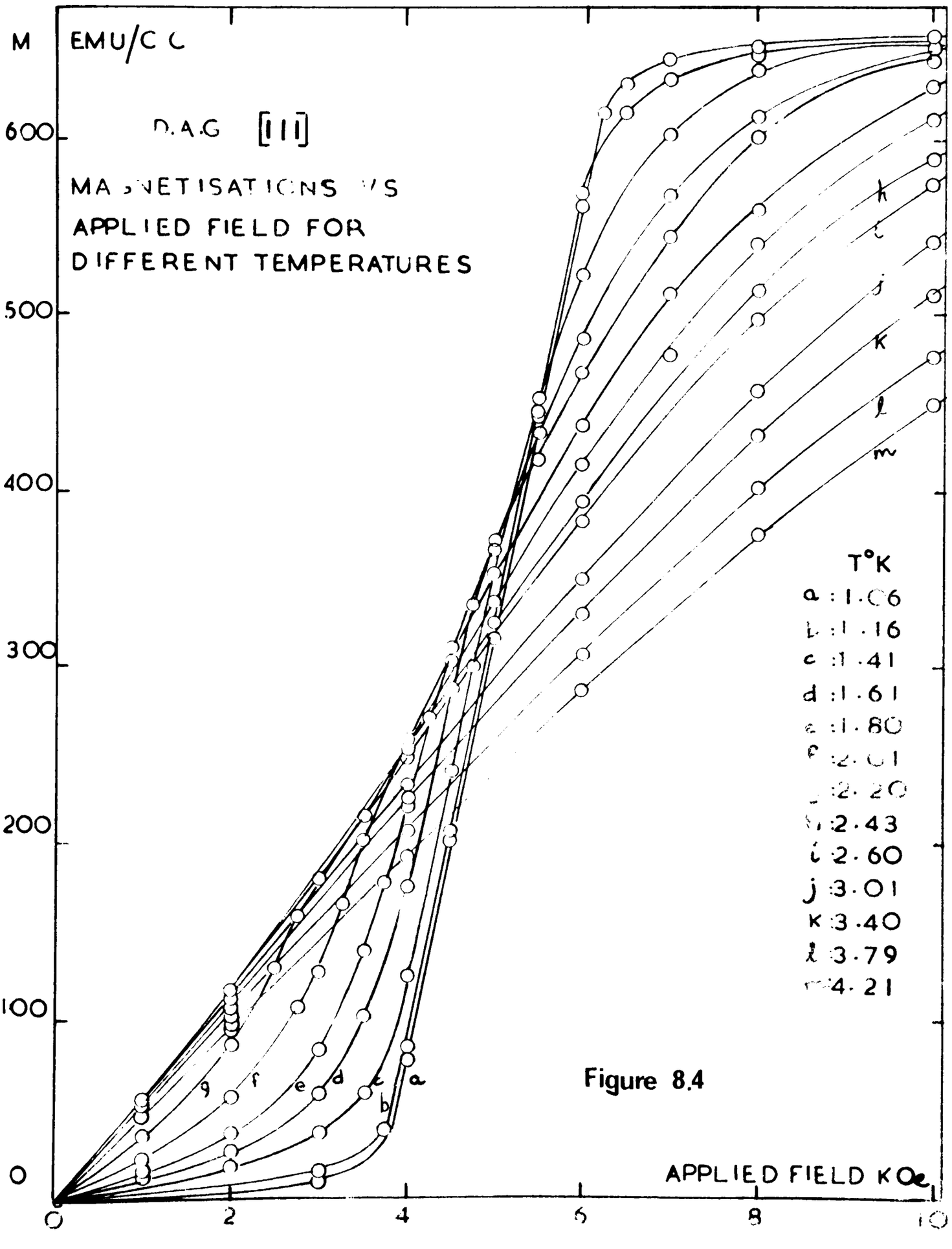
M EMU/C C
D.A.G [11]
MAGNETISATIONS V/S
APPLIED FIELD FOR
DIFFERENT TEMPERATURES
600
500
400
300
200
100
0
0
2
4
6
8
10
APPLIED FIELD KOe
T°K
a : 1.06
b : 1.16
c : 1.41
d : 1.61
e : 1.80
f : 2.01
g : 2.20
h : 2.43
i : 2.60
j : 3.01
K : 3.40
l : 3.79
m : 4.21

Figure 8.4

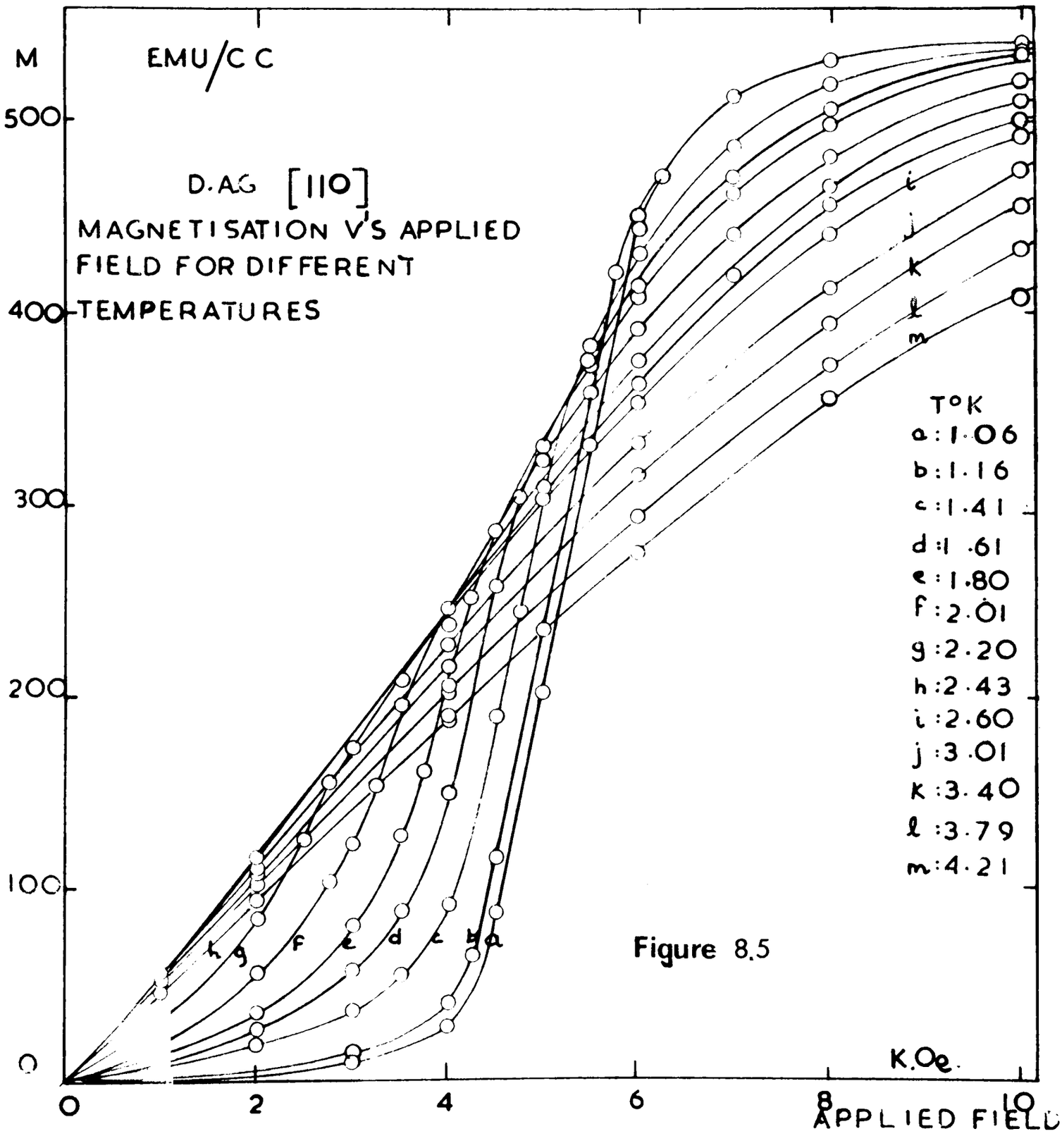
M
EMU/C C
500
400
300
200
100
0
D.AG [110]
MAGNETISATION V'S APPLIED FIELD FOR DIFFERENT TEMPERATURES
T°K
a: 1·06
b: 1·16
c: 1·41
d: 1·61
e: 1·80
f: 2·01
g: 2·20
h: 2·43
i: 2·60
j: 3·01
k: 3·40
l: 3·79
m: 4·21
0
2
4
6
8
10
K.Oe.
APPLIED FIELD

Figure 8.5

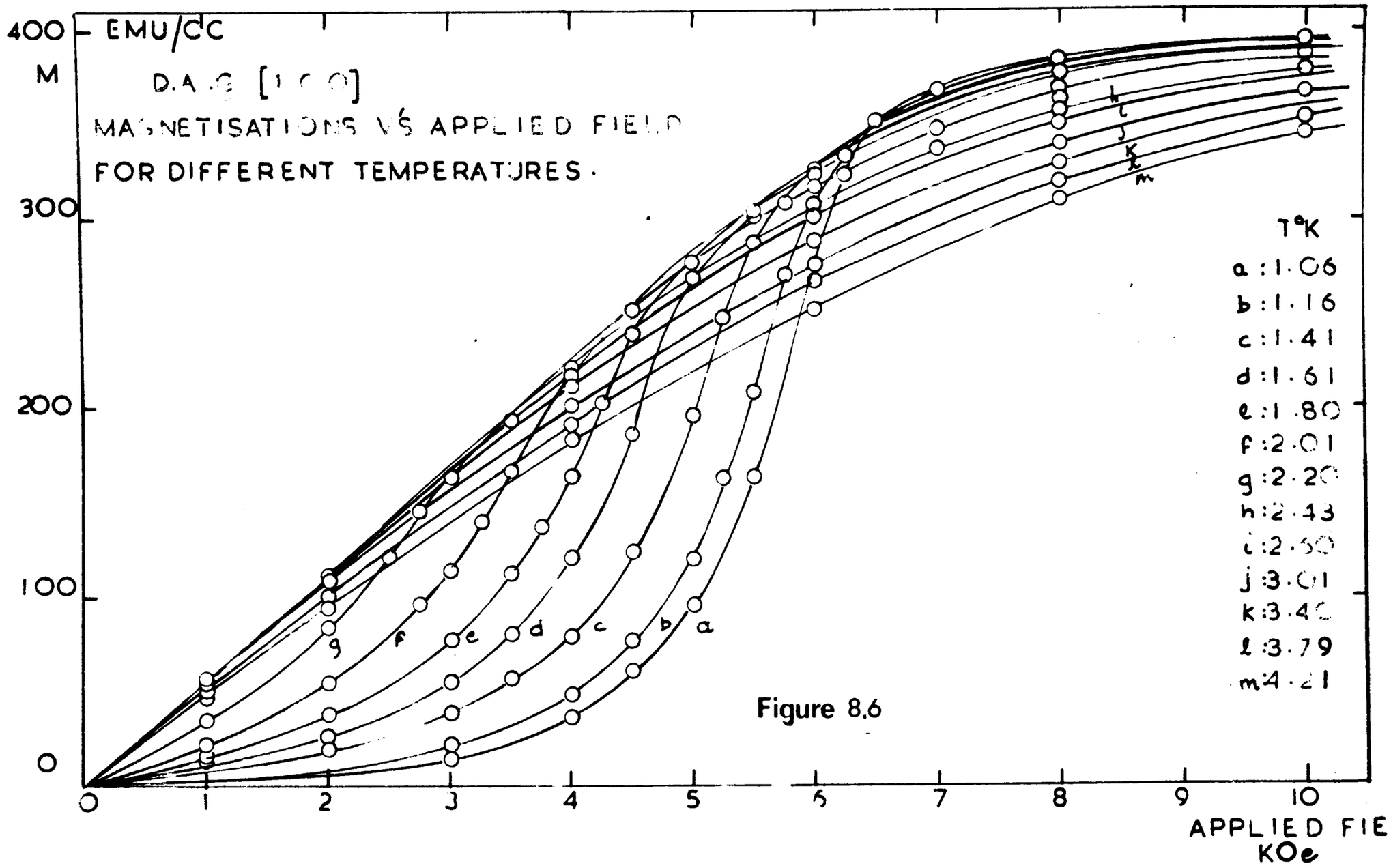
400
M
EMU/CC
D.A.C [1 C C]
MAGNETISATIONS VS APPLIED FIELD
FOR DIFFERENT TEMPERATURES.
300
200
100
0
T°K
a : 1·06
b : 1·16
c : 1·41
d : 1·61
e : 1·80
f : 2·01
g : 2·20
h : 2·43
i : 2·60
j : 3·01
k : 3·4
l : 3·79
m : 4·21
0 1 2 3 4 5 6 7 8 9 10
APPLIED FIELD
KOe

Figure 8.6

applied along these axes affect three, two and one sublattice respectively (since if the Dy ions are true magnetic dipoles, as we assume, fields applied perpendicular to them are without effect upon them. Inasmuch as the Dy ions are known to have finite moments in the x and y directions, as well as the z, this is not strictly true. However, since the force is proportional to g^2, $g_x{}^2$ and $g_y{}^2$ are negligible by comparison with $g_z{}^2$.).

At each temperature, measured with a mercury manometer or Macleod gauge, and monitored on a differential oil manometer, the magnet was carefully cycled and the moment measured at various fields, starting with the highest. This procedure was repeated for each orientation of the field. The results were plotted continuously as graphs of induced magnetisation against applied field strength, and regions in which the variation was fast were mapped out in more detail. The resulting curves are shown in Figures 8.4, 8.5 and 8.6.

Discussion.

If $g_z = 18.3$, $g_x = g_y = 0$, and the atomic moments are saturated at low temperatures and high applied field, some of the anisotropy properties of DAG should be calculable from simple geometric considerations, since individual spins must lie along one of the principal cube axes of the crystal.

Thus, for instance, a cubic crystal is symmetrical in the (110) plane about the [100] and [110] axes, and

asymmetrical about the [111] axis. Inspection of Figure 8.3 reveals that the magnetic moment is symmetrical about the [100] and [110] axes, and asymmetrical about the [111] .

The values of the moments should also be related by simple geometrical ratios. Thus, with an applied field in the 100 direction, only two of the six sublattices are parallel with the field. Thus, the moment in this direction should be one third of the moment which would be produced by aligning all ions in the same direction (M). With the applied field along the [111] axis, all the sublattices are equivalent, and the components of their moments along the [111] axis should total $1/\sqrt{3}$ M. Similarly, a field in the [110] direction is perpendicular to two sublattices, and makes an angle of 45° with the other four, so that the total moment should be $2/3\sqrt{2}$ M. Thus, the ratio of the moments in the [111] , [110] and [100] directions should be $\sqrt{3}:\sqrt{2}:1$, or 1.73:1.41:1. The actual experimental values (Figure 8.3) were 1.63:1.41:1 - very reasonable agreement considering the assumptions.

Assuming that the sublattices all remain ferromagnetic, and that the components of the applied field parallel with the sublattice magnetisation directions remain big enough to saturate the atomic moments, it is possible to calculate the variation of moment with angle in the vicinity of the [111] axis. If the field makes an angle θ with the [100] direction, the component from the sublattice magnetised in this direction is 1/3 M cos θ, and from each of the other

two sublattices 1/3 M(1/$\sqrt{2}$ sin θ), making a total moment in the direction of the field of 1/3 M(cos θ + $\sqrt{2}$ sin θ). This relationship is plotted for g_z = 18.3 in Figure 8.3. The agreement is quite good, indicating the validity of the assumptions.

Remarkable features of the curves, particularly those for the [111] and [110] axes (Figures 8.4 and 8.6) are the linear variation of moment with field at the lowest temperatures. This effect becomes yet more striking if the curves are corrected to toroidal shape (Figures 8.8, 8.8, 8.9) when especially in the [111] direction, critical fields appear at which the moment reaches saturation very rapidly. At the lowest temperatures, the value of this critical field becomes independent of temperature. Thus,we have the remarkable effect that the transition is first order only for certain shapes of specimen. This has not been predicted in any theoretical consideration of the magnetisation of an antiferromagnet, but Wyatt (1963) has tentatively explained the phenomenon by postulating filamentary ferromagnetic domains within the material. The same author also interpolates curves of constant magnetisation against temperature, and demonstrates the qualitative resemblances between them and similar curves calculated by Fisher (1960) for a two-dimensional Ising antiferromagnet.

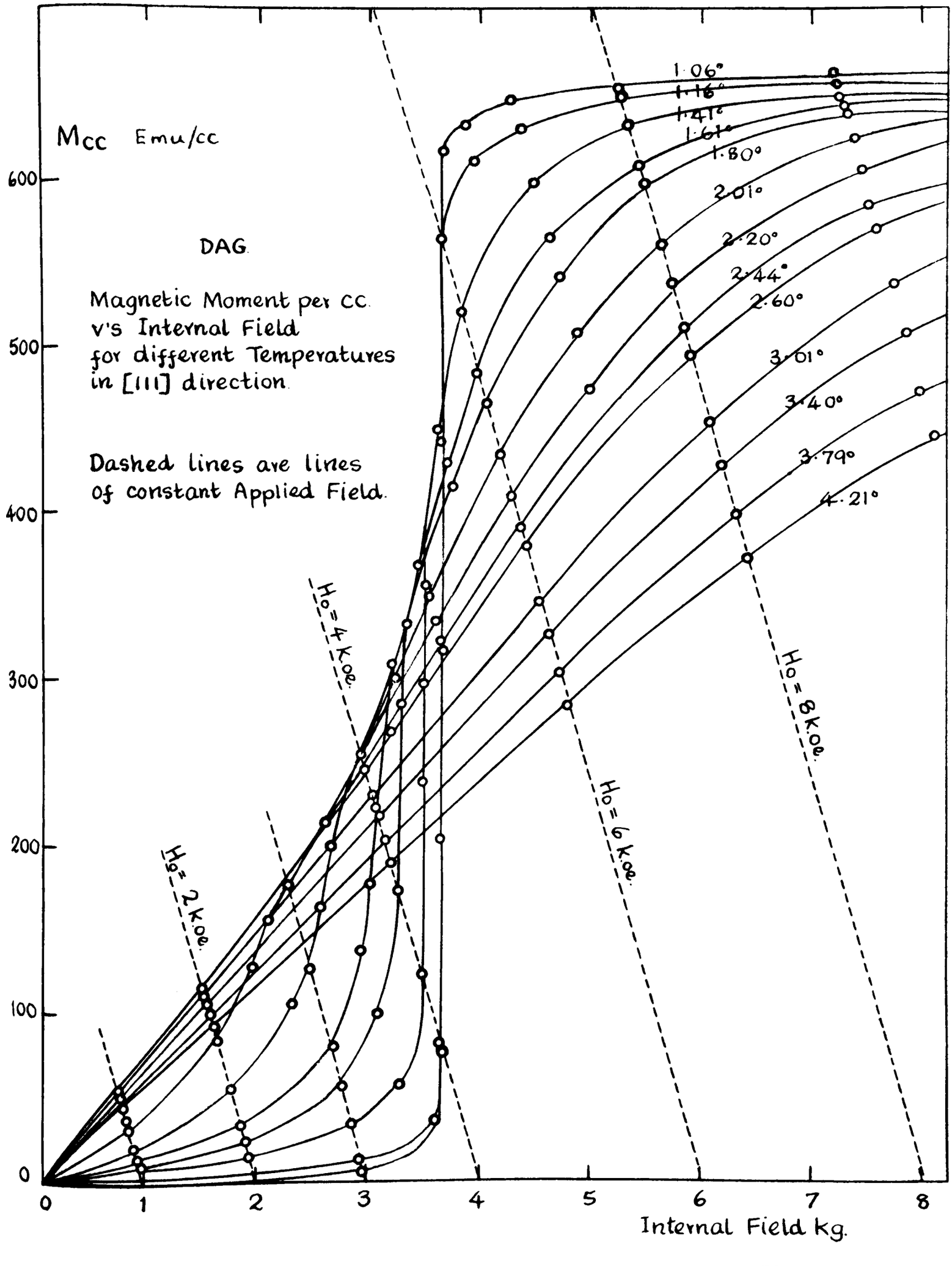
Mcc Emu/cc
DAG
Magnetic Moment per cc.
v's Internal Field
for different Temperatures
in [111] direction.
Dashed lines are lines
of constant Applied Field.
1.06°
1.16°
1.41°
1.61°
1.80°
2.01°
2.20°
2.44°
2.60°
3.01°
3.40°
3.79°
4.21°
Ho = 2 K.oe.
Ho = 4 K.oe.
Ho = 6 K.oe.
Ho = 8 K.oe.
0
100
200
300
400
500
600
0
1
2
3
4
5
6
7
8
Internal Field kg.

Figure 8.7

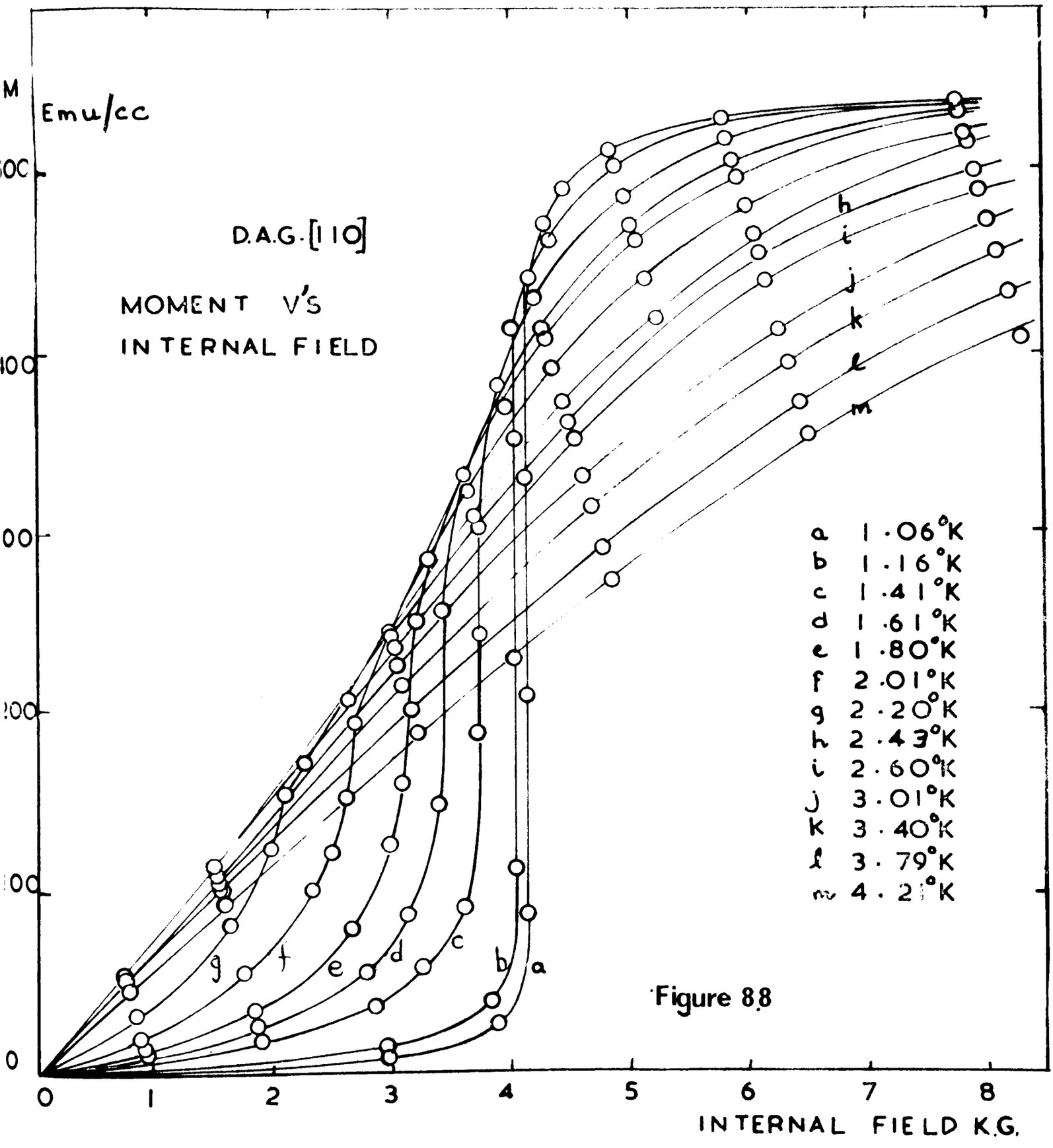
M
Emu/cc
D.A.G.[110]
MOMENT V'S
INTERNAL FIELD
a 1·06°K
b 1·16°K
c 1·41°K
d 1·61°K
e 1·80°K
f 2·01°K
g 2·20°K
h 2·43°K
i 2·60°K
j 3·01°K
k 3·40°K
l 3·79°K
m 4·21°K
0
1
2
3
4
5
6
7
8
INTERNAL FIELD K.G.

Figure 8.8

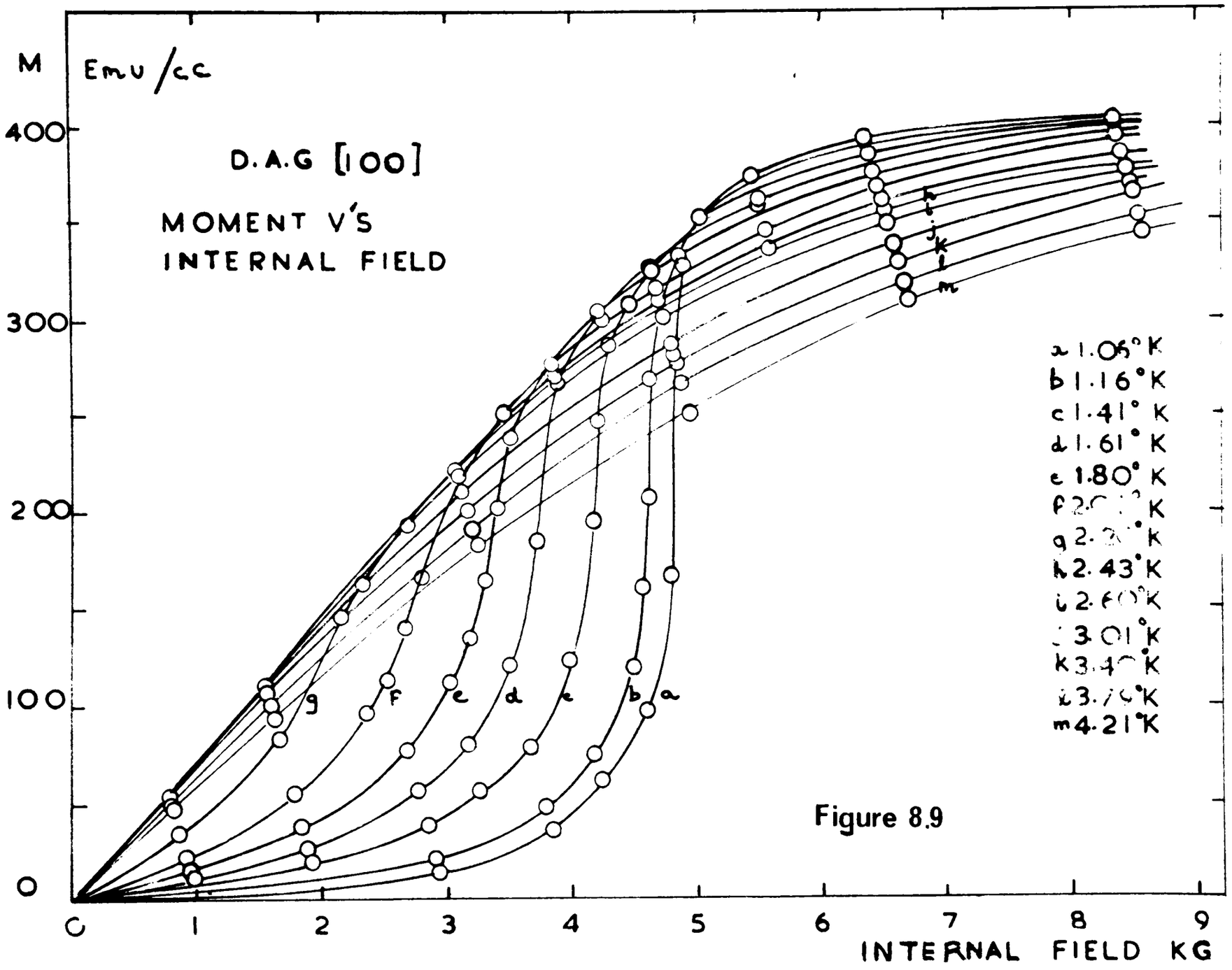
M Emu/cc
D.A.G [100]
MOMENT V'S
INTERNAL FIELD
400
300
200
100
0
0
1
2
3
4
5
6
7
8
9
INTERNAL FIELD KG
a 1.05° K
b 1.16° K
c 1.41° K
d 1.61° K
e 1.80° K
m 4.21° K

Figure 8.9

Conclusions.

The magnetic moment measurements on DAG are in accordance with the theories elaborated from the susceptibility, specific heat and paramagnetic resonance results on the same material and ion, and confirm that it may be regarded as a 6-sublattice Ising-type antiferromagnet with a transition temperature of 2.49°K.

They further show that it is possible to cause one, two or three of the pairs of antiferromagnetic lattices to become ferromagnetic, according to the direction of the applied field. The existence of critical fields at low temperatures for a toroidal specimen has been demonstrated.

Chapter 9

The Oxides of Europium

Introduction.

Until quite recently, only two oxides of europium were known, namely, the divalent oxide EuO (despite the doubts of Sidgwick, 1950) with NaCl structure (Eick, Baenziger and Eyring, 1956), and the trivalent oxide Eu_2O_3 which exists in two modifications, a low-temperature cubic form common to the heavier rare earth sesquioxides (Warshaw and Roy, 1961) which transforms irreversibly into the high-temperature monoclinic form (Curtis and Tharp, 1959) at temperatures over 1050°C.

The divalent oxide is particularly interesting magnetically, since it is one of the very few known electrically insulating ferromagnets, and orders at quite a high temperature. Matthias, Bozorth and Van Vleck (1961) measured the magnetic moment of this material as a function of temperature in fields of 8 and 12 k.oe., and extrapolated a Curie temperature of 77°K from their results.

In the last few years, a number of workers have investigated intermediate oxides. A compound claimed to have the composition $EuO.Eu_2O_3$ has been prepared in a number of ways. Bärninghausen and Brauer (1962) obtained it by heating together equimolar amounts of Eu_2O_3 and EuO at 900°C in an inert atmosphere. Achard (1960) formed an impure oxide by heating stoichiometric amounts of Eu_2O_3 and pure carbon. Rau (1963) was unable to obtain single

phase Eu_3O_4 in this way, since even when the mixture was heated for two hours at 1300°C and then for five minutes at 1700°C in argon, the product contained unreacted carbon, and presumably other europium phases. Rau (1963) claims to have produced consistently single phase Eu_3O_4 by reducing Eu_2O_3 or $Eu(OH)_3$ in hydrogen at 1650°C, and by melting Eu_2O_3 in hydrogen. His product takes the form of black chunks, which give a red-brown powder when finely divided, and which contain small dark red crystals on which he carried out single crystal x-ray studies. He reports that Eu_3O_4 crystallises in the orthorhombic system, and is isomorphous with Eu_2SrO_4, a compound in which Sr replaces Eu^{II} (Bärninghausen and Brauer, 1962).

Garton and Hukin (1963) also claim to have prepared Eu_3O_4 by controlled oxidation of EuO, as a bright yellow powder. This they analysed by ignition in air, and by low temperature susceptibility and magnetic moment measurements, all compatible with the formula Eu_3O_4. They also made x-ray powder diffraction measurements, but were not able to determine the structure.

Rau (1963) also prepared another orthorhombic intermediate valency europium oxide which he called 'Ortho I', a terminology we shall also adopt. This was first obtained as yellow or red crystalline deposits on Eu_2O_3 during measurements of the compatibility of Eu_2O_3 and noble metals

in hydrogen at 1425°C. He subsequently prepared well-formed orange-yellow crystals of ortho I by heating Eu_2O_3 powder in a stream of dry hydrogen for 60 - 120 hours at 1425 - 1650°C. He analysed this material by ignition in air, and found an approximate oxygen to europium ratio of 1:1.

It seems from x-ray crystallographic work, that ortho I has a very unusual structure. Initial examination of the rotation photograph indicated approximate lattice parameters of a = 9.71 Å, b = 7.07 Å and c = 5.63 Å. However, a closer examination revealed weak layer lines which could only be indexed if the true repeat distance along the b-axis were seven times 7.07, i.e. b = 49.5 Å. From these x-ray measurements and a density determination, Rau concludes that the unit cell contains ~64 Eu atoms, and tentatively suggests (private communication) that the unit cell might comprise four formula units of $Eu_{16}O_{21}$.

The similarity in appearance between Garton and Hukin's 'Eu_3O_4' and Rau's 'Ortho I' suggests that they might be the same substance, and a direct comparison of the x-ray powder photographs confirms this. There thus remain four well-defined oxides of europium. The magnetic properties of the two new oxides were unknown, so we measured the paramagnetic susceptibilities both for the inherent interest of these measurements, and also in the hope that information concerning the chemical composition of these oxides might

be obtained.

Conventional chemical techniques are not very effective in analysis of a substance such as ortho I because of the high atomic weight of Eu, and small difference in oxygen content between Eu^{II} and Eu^{III} compounds. The large unit cell would make a complete structural determination by x-ray techniques a major research project. However, the magnetic properties of the two valency states of europium are very different. Eu^{III} ($4f^6$) as in Eu_2O_3 is virtually diamagnetic, especially at low temperatures, while Eu^{II} ($4f^7$) is strongly paramagnetic. In addition, for the electronic configuration $4f^7$, J = S = 7/2, which is not split appreciably by the crystal field. Hence, the apparent molecular weight containing 1 g.ion of Eu^{II} may readily be calculated from the observed and calculated susceptibilities, and weight of specimen. If it is assumed that Eu^{III} is completely diamagnetic, and that the compound contains only Eu and O, then the empirical formulae can be computed.

Europium Sesquioxide (Eu_2O_3).

We measured a large sample of commercial (i.e. 99.9% pure in terms of other rare earths, largely Gd and Nd) Eu_2O_3 and found a susceptibility of 0.8×10^{-2} e.m.u. per g.ion of europium which was virtually temperature-independent. This is in agreement with expectation (Van Vleck, 1937),

Figure 9.1

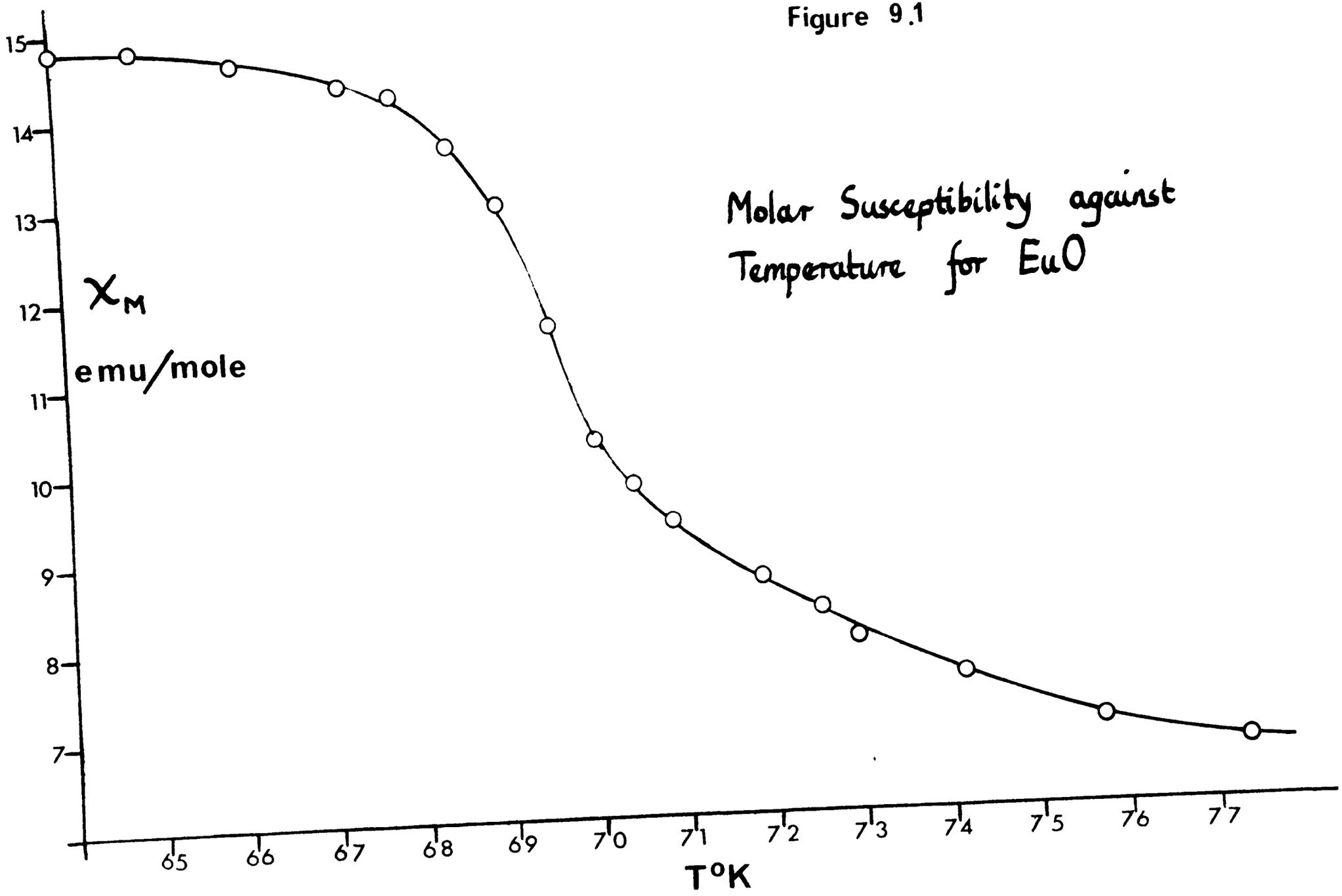
Molar Susceptibility against Temperature for EuO
χ_M
emu/mole
15
14
13
12
11
10
9
8
7
6.5
6.6
6.7
6.8
6.9
7.0
7.1
7.2
7.3
7.4
7.5
7.6
7.7
T°K

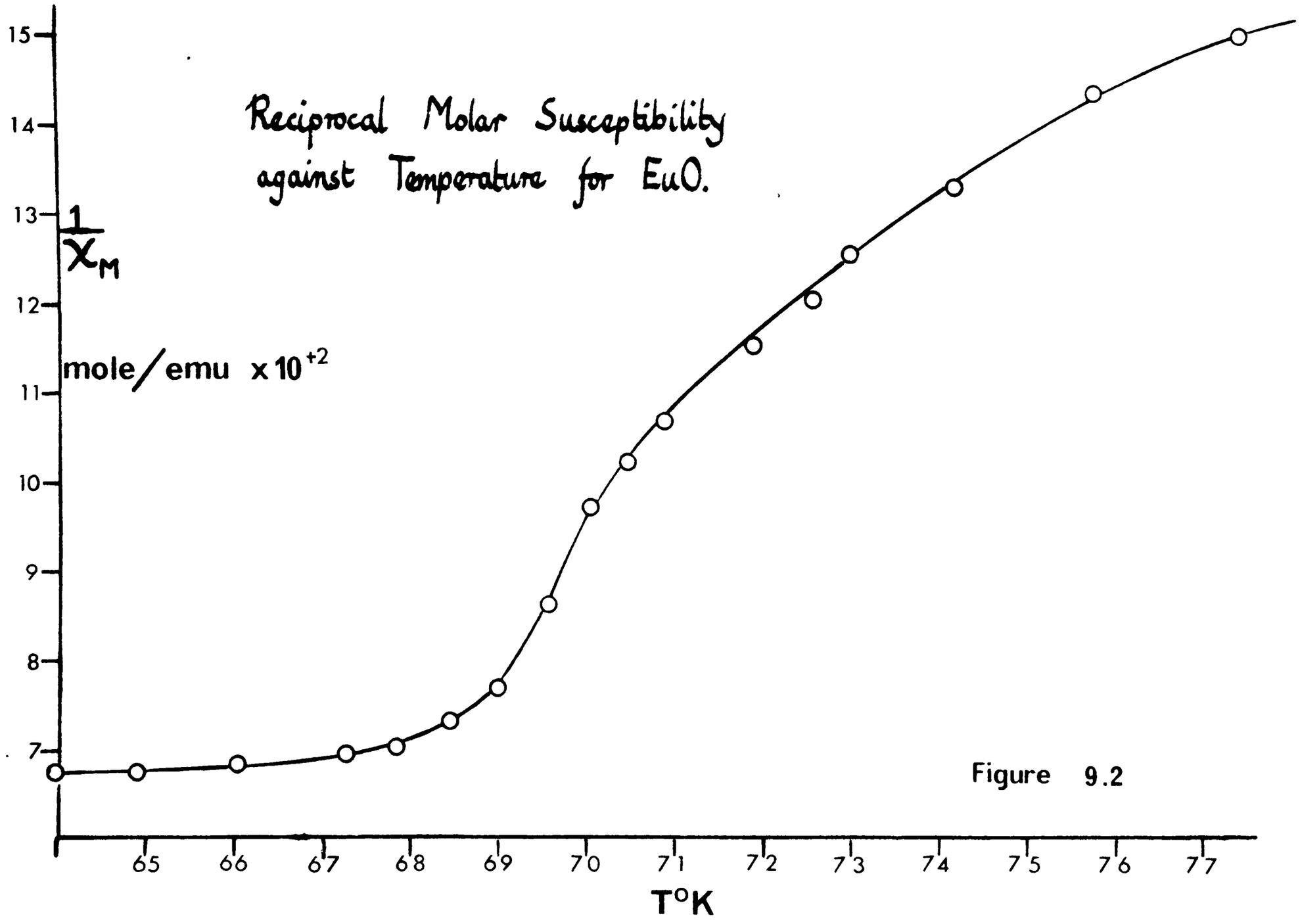
Reciprocal Molar Susceptibility
against Temperature for EuO.
$\frac{1}{X_M}$
mole/emu x 10^{+2}
15
14
13
12
11
10
9
8
7
65
66
67
68
69
70
71
72
73
74
75
76
77
T°K

Figure 9.2

and for the remainder of the chapter, we shall assume that the paramagnetism of Eu^{III} is negligible compared with Eu^{II}.

Europous Oxide (EuO).

Bozorth et al. (1959) measured the alloy $EuIr_2$, in which x-ray studies indicate trivalency for the europium, and found that this compound appears to become ferromagnetic at about 70°K, but with a very small saturation moment, extremely contradictory behaviour. Matthias, Bozorth and Van Vleck (1961) suspected that this might be an impurity effect, and unaware of the existence of intermediate oxides, concluded that EuO was probably responsible for the anomaly.

They prepared a sample of EuO by heating stoichiometric amounts of Eu and Eu_2O_3 in a silica tube at 1220°C, and measured its magnetic moment. By applying a Weiss-Forrer extrapolation to their results, they obtained a value of the Curie temperature of 77°K, only fair agreement with the temperature of the anomaly in $EuIr_2$.

We have checked this work by measuring the susceptibility of a sample of EuO in the liquid nitrogen range. This was prepared by controlled oxidation of Eu foil, followed by removal of excess europium metal by volatilisation in vacuo. I am indebted to D.A.Hukin and Dr G.Garton for preparing this specimen.

Figure 9.3

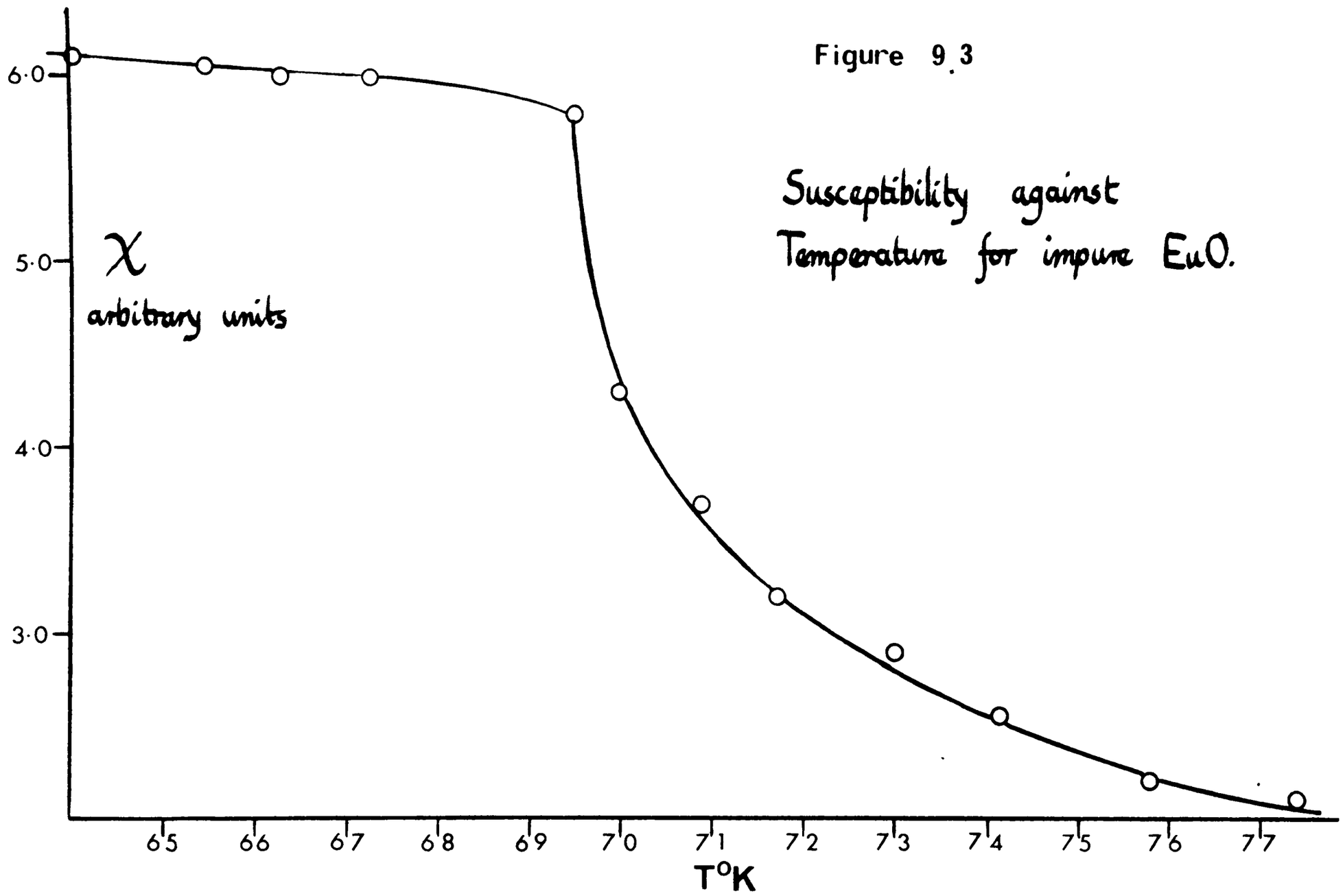
Susceptibility against
Temperature for impure EuO.
χ
arbitrary units
6·0
5·0
4·0
3·0
6'5
6'6
6'7
6'8
6'9
7'0
7'1
7'2
7'3
7'4
7'5
7'6
7'7
T°K

The results are presented as a plot of molar susceptibility against temperature in Figure 9.1. Only a very small sample was used ($\sim$20 mg) since EuO is very strongly paramagnetic, so it was not possible to estimate the shape of the sample and apply a demagnetising correction. All the measurements were made in the critical region where a Curie-Weiss law is not obeyed, but the apparent saturation value of the susceptibility is of the right order of magnitude for EuO.

The discontinuity appears slightly more marked in Figure 9.2, which represents the behaviour of the reciprocal susceptibility. The Curie temperature is most probably at 69°K, $\pm$ ½°K.

The measurements were very difficult to perform, since the signal from the coil was very distorted, and there were large ($>$ 7 units) ΔR effects indicating a big out-of-phase susceptibility. No peak was observed in ΔR, and the susceptibility was not dependent on the size of measuring field.

Additional evidence for a Curie temperature of 69°K is provided by measurements on other samples which contained EuO as an impurity. One of these (Figure 9.3) resulted from an attempted preparation of EuO which was accidentally over-oxidised. The general form of the graph is the same as Figure 9.1, but in this case, the measurements were made with much less difficulty. A

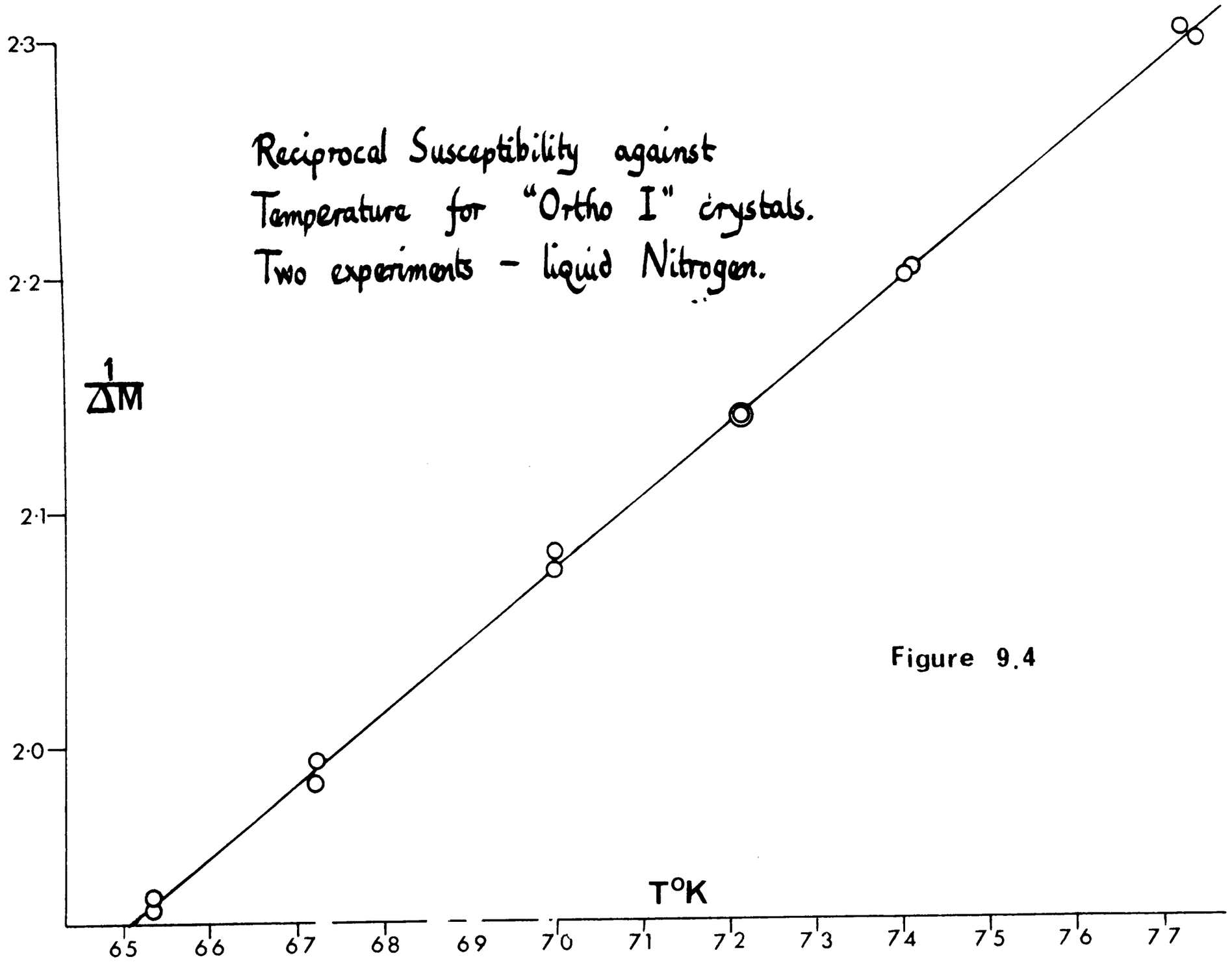
Reciprocal Susceptibility against
Temperature for "Ortho I" crystals.
Two experiments - liquid Nitrogen.
2·3
2·2
2·1
2·0
1/ΔM
T°K
65
66
67
68
69
70
71
72
73
74
75
76
77

Figure 9.4

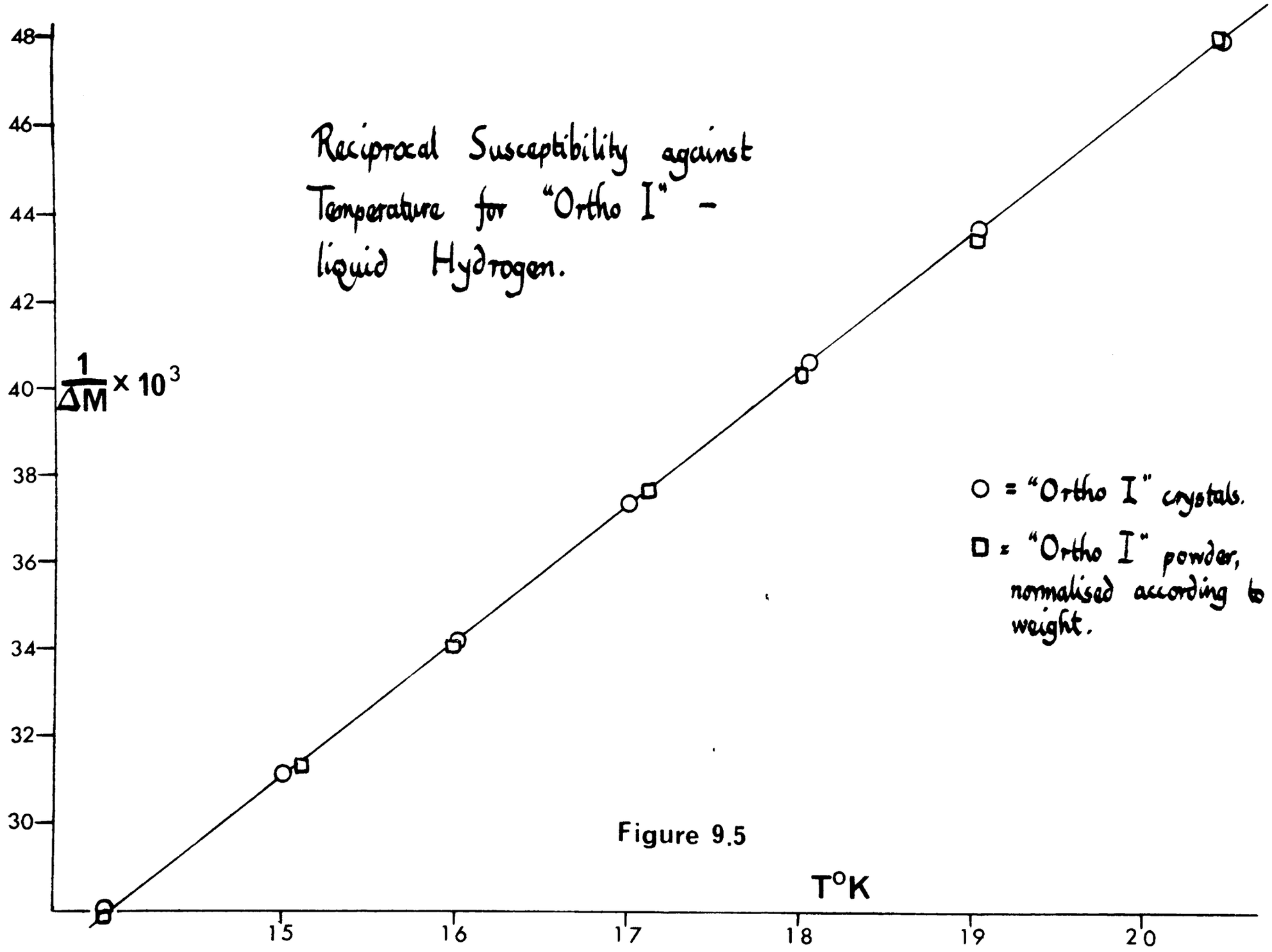
Reciprocal Susceptibility against Temperature for "Ortho I" - liquid Hydrogen.
48
46
44
42
40
38
36
34
32
30
$\frac{1}{\Delta M} \times 10^3$
○ = "Ortho I" crystals.
□ = "Ortho I" powder, normalised according to weight.
15
16
17
18
19
20
T°K

Figure 9.5

similar discontinuity was also observed in an incompletely reacted powder specimen of $EuO.Gd_2O_3$ prepared by solid phase reaction from EuO and Gd_2O_3.

'Ortho I'

Three different samples of this material were measured, two of which behaved identically within the experimental accuracy, and a third which seemed to be contaminated with Eu_2O_3 or some other diamagnetic impurity. The two samples with identical behaviour were one of bright yellow powder, and the other of small orange-red crystals, both kindly supplied by Dr R.Rau. The third sample was of the yellow powder originally identified as 'Eu_3O_4' and supplied by Dr G.Garton and Mr D.A.Hukin.

Figure 9.4 shows the results of two measurements of the variation of susceptibility in the nitrogen range for a sample of the red crystals, expressed as a plot of reciprocal χ_M against T. Figure 9.5 shows the results in the hydrogen range of the same sample of red crystals and for a sample of Rau's yellow powder, the results being normalised according to the weights taken. The yellow 'Eu_3O_4' sample was also measured at hydrogen temperatures, and was found to have the same Weiss constant, but a Curie constant much lower than the other samples. Hence, it was concluded that this sample was identical with the others, apart from containing some diamagnetic impurity,

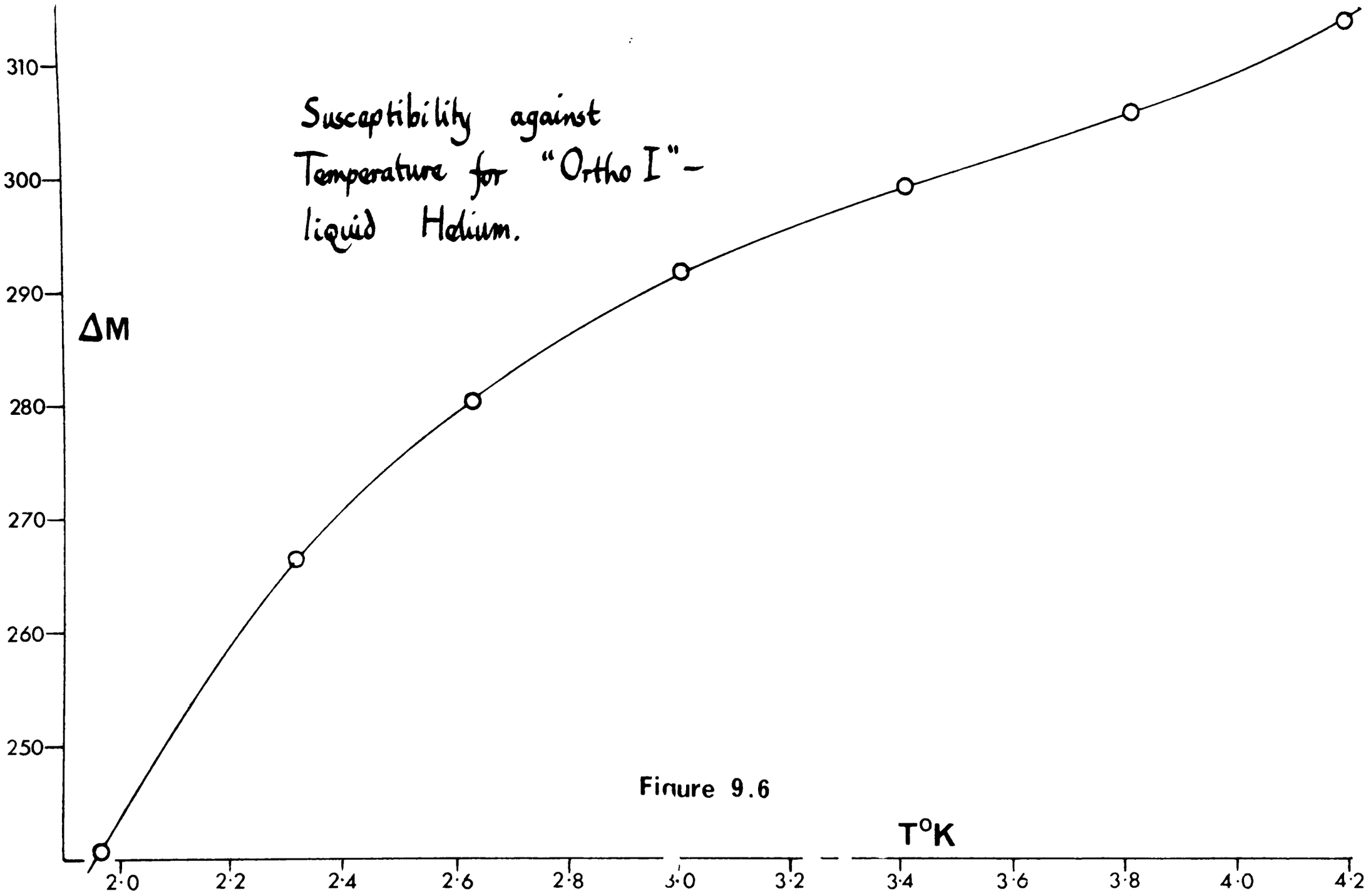
Susceptibility against
Temperature for "Ortho I"-
liquid Helium.
ΔM
310
300
290
280
270
260
250
T°K
2·0
2·2
2·4
2·6
2·8
3·0
3·2
3·4
3·6
3·8
4·0
4·2

Finure 9.6

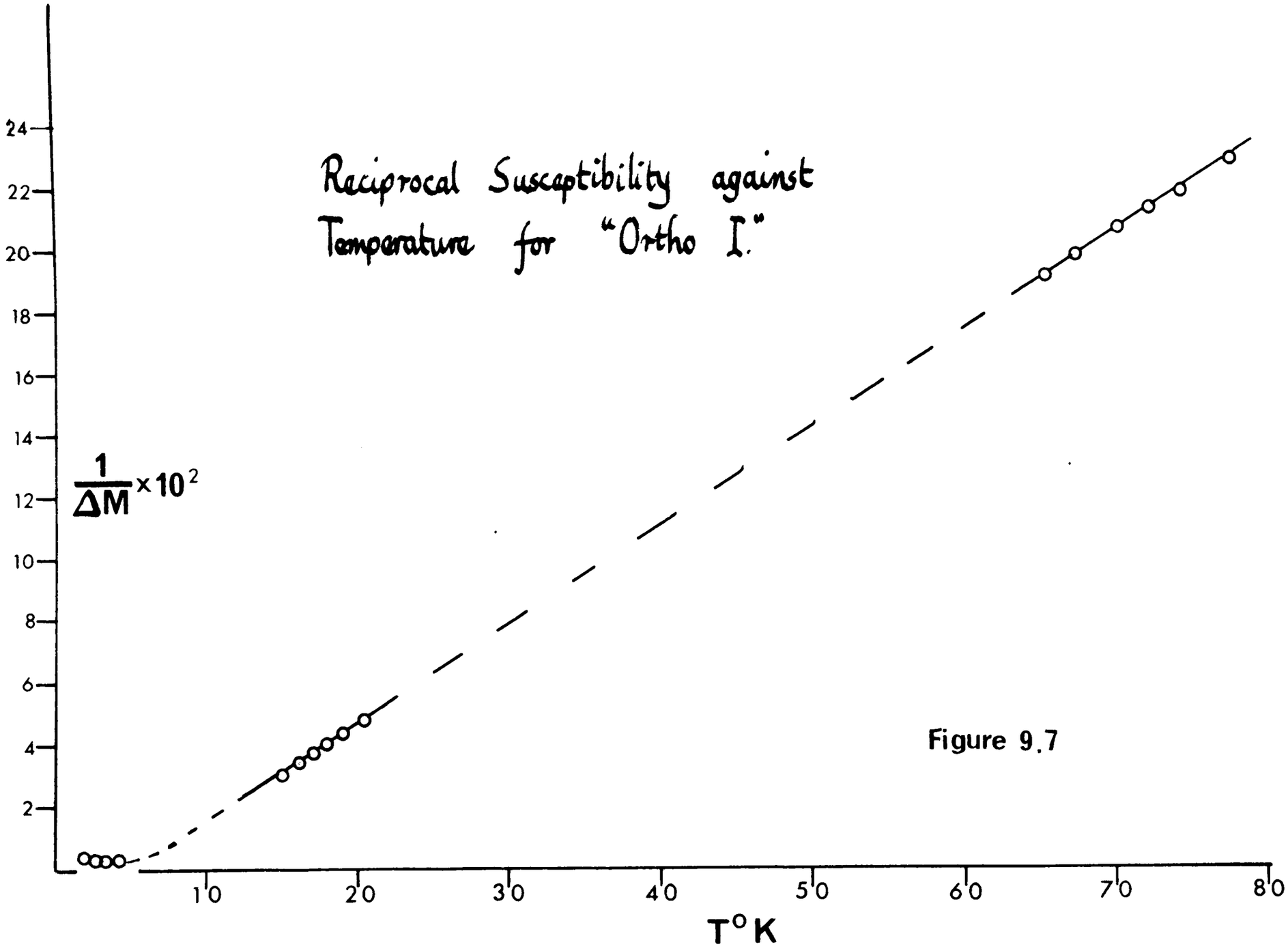
Reciprocal Susceptibility against Temperature for "Ortho I."
$\frac{1}{\Delta M} \times 10^2$
24
22
20
18
16
14
12
10
8
6
4
2
10
20
30
40
50
60
70
80
T°K

Figure 9.7

so no further measurements were made.

The susceptibility of the red crystals in the helium range was high, and there were large $\triangle R$ effects, though the susceptibility was independent of measuring field. The results are shown in Figure 9.6, while Figure 9.7 shows the behaviour of the red crystals throughout the temperature range. All susceptibilities are in arbitrary units, since the molecular weight of this substance was unknown.

Results and Discussion.

Ortho I obeys a Curie-Weiss law in the nitrogen and hydrogen temperature ranges. In the nitrogen range, the law (determined by a 'least squares' fit) is:-

$$\triangle M = \frac{31.82}{T - 4.0}$$

though the Weiss constant is not thus accurately determined, owing to the insensitivity of the expression to it.

In the hydrogen range, both powder and crystalline samples obeyed the expression: -

$$\triangle M = \frac{31.82}{T - 5.1}$$

It is slightly surprising that the susceptibility in the hydrogen range obeys a Curie-Weiss law, since with a Weiss Θ of 4-5°K, there should be appreciable departures at the lower temperatures caused by local ordering.

The results are uncorrected for shape, but the two samples were of comparable mass and shape.

The difference between the Weiss θs of the two expressions is almost within the limits of experimental error, but it is probably significant. A change of less than 2% in the calibration constant of the coil owing to expansion between the two temperature ranges would account for the discrepancy. It has already been pointed out (page 4.13) that this cannot be checked since the susceptibility of the calibration standard is too low at nitrogen temperatures. It is also conceivable that this is a genuine physical effect. The Weiss θ, representing the interactions between the ions, appears to be smaller at the higher temperatures. This could result from anisotropic lattice expansion (in an orthorhombic substance) increasing the interatomic distances, and altering the interatomic angles. However, it is not possible to make even a rough estimate of the order of magnitude of such an effect, though it is consistent with the lower Weiss θ at higher temperatures. A similar difference between the Weiss θs in the two temperature ranges has been observed by Wyatt (1963) in $GdCl_3$.

The Curie constant of an ion with configuration $4f^7$ can be calculated from the expression quoted on page 4.14, substituting S ($= (L+S) = J$, since $L = 0$) $= 7/2$, and a value C = 7.819 e.m.u. per g.ion of Gd^{III}, Tb^{IV} or Eu^{II} is obtained.

Using this value, the gradients of the graphs of

reciprocal ΔM against T (Figures 9.4 and 9.5), the calibration constant of the apparatus and the weight of the sample taken, the effective molecular weight of ortho I containing 1 g.ion of Eu^{II} can be calculated, and the value obtained is 198. Thus, after allowing for experimental error, the molecular weight lies between 196 and 200.

Assuming that this material contains only europium and oxygen, the empirical formula lies between $EuO_{1.069}$ and $EuO_{1.077}$.

From Rau's (1963) x-ray and density measurements, it is possible to calculate an empirical formula, very crudely, using the expression

$$r = \frac{1.6604\ M.n}{V}$$

where r is the density in g/cc

M is the molecular weight

n is the number of formula-units per unit cell

V is the volume of the unit cell in $Å^3$.

Therefore, for ortho I,

$$M.n = 10,980$$

No. of Eu atoms per unit cell	Empirical formula
65	$EuO_{1.076} - EuO_{1.039}$
64	$EuO_{1.227} - EuO_{1.184}$
63	$EuO_{1.417} - EuO_{1.377}$

Since Rau does not quote any errors for his x-ray

and density measurements, so that it is not possible to estimate the error in the molecular weight calculation made above, but unless it is very gross, a comparison of the empirical formulae calculated by x-ray and magnetic methods indicates that there are 65 Eu atoms in the unit cell. This does not accord well with Rau's observations of a 7-fold layer structure, for which 63 ions would seem more reasonable.

The data accumulated on ortho I can almost all be explained if this substance contains silicon as well as oxygen and europium. The effective molecular weight of Eu_2SiO_4 per g.ion of Eu^{II} is 198, and the molecular weight of 28 formula units (a suitable number for 7-fold layers) is 11,090, not very different from the molecular weight calculated from Rau's work. Garton and Hukin analysed their material (now shown to have been a mixture) for silicon, with negative results, but it seems significant that formation of ortho I in their apparatus was always associated with formation of glassy silicon monoxide, indicating some silicon present in the vapour phase. Rau gives no details of the material of his apparatus, but it seems likely that it was made of silica, or some silicate such as mullite, and the actual weight of silica needed to convert a small amount of EuO to $\frac{1}{2}(Eu_2SiO_4)$ is very small.

A sample of Rau's powder ortho I gave a positive ammonium molybdate/stannous chloride test, for silicates,

but this test is extremely sensitive (Vogel, 1945), and insufficient material was available for a quantitative measurement. The question must at present be left open, pending more definite chemical analyses of the relevant materials, or alternatively, magnetic studies of genuine Eu_2SiO_4.

Perhaps a final clue is provided by the colour of this material. If it were genuinely an oxygen-rich EuO phase, a very dark colour might be expected as a result of charge transfer (c.f. Tb_4O_7, Pr_6O_{11}) while the typical colour of divalent europium (Garton and Hukin, 1963) is yellow, as in the carbonate, formate, hydroxide etc. Thus, the balance of evidence seems to indicate that this substance is a silicate, rather than an oxide.

The results in the liquid helium range seem to suggest that ortho I undergoes a ferromagnetic transition between 4.2 and 14°K, and is ferromagnetic throughout the liquid helium range. The apparent fall in the susceptibility is probably spurious, since the out-of-phase component was very large, and increased with decreasing temperature. Because of this fall, and the unknown shape, it was not possible to estimate the saturation value of the moment.

Mr K.A.Gehring and Dr A.H.Cooke of this laboratory have measured the magnetic moment of ortho I by a d.c. method, and confirm that it is indeed ferro- (or ferri-) magnetic in the liquid helium range, and that the true susceptibility is virtually temperature-independent. They

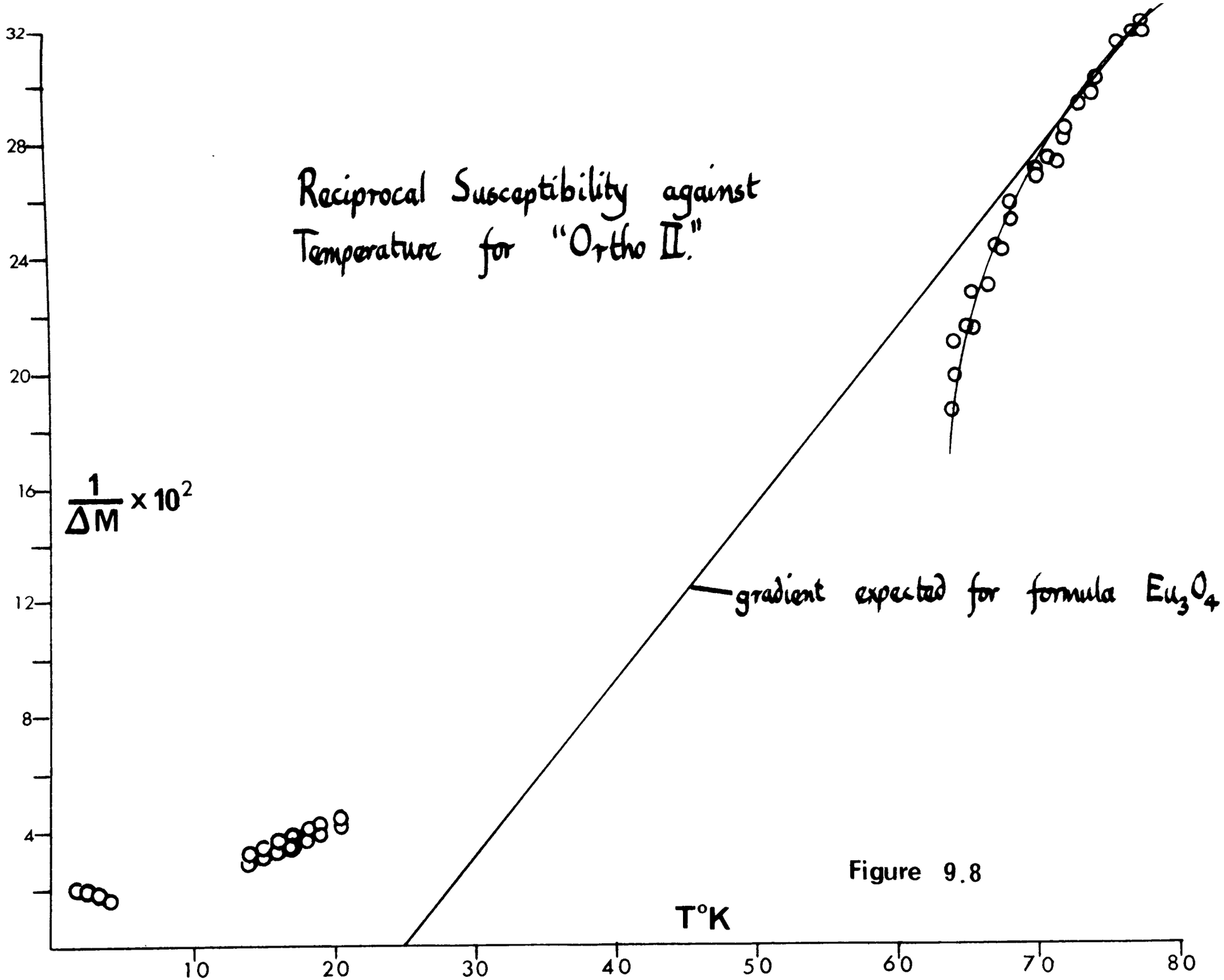
Reciprocal Susceptibility against Temperature for "Ortho II."
$\frac{1}{\Delta M} \times 10^2$
32
28
24
20
16
12
8
4
10
20
30
40
50
60
70
80
T°K
gradient expected for formula Eu_3O_4

Figure 9.8

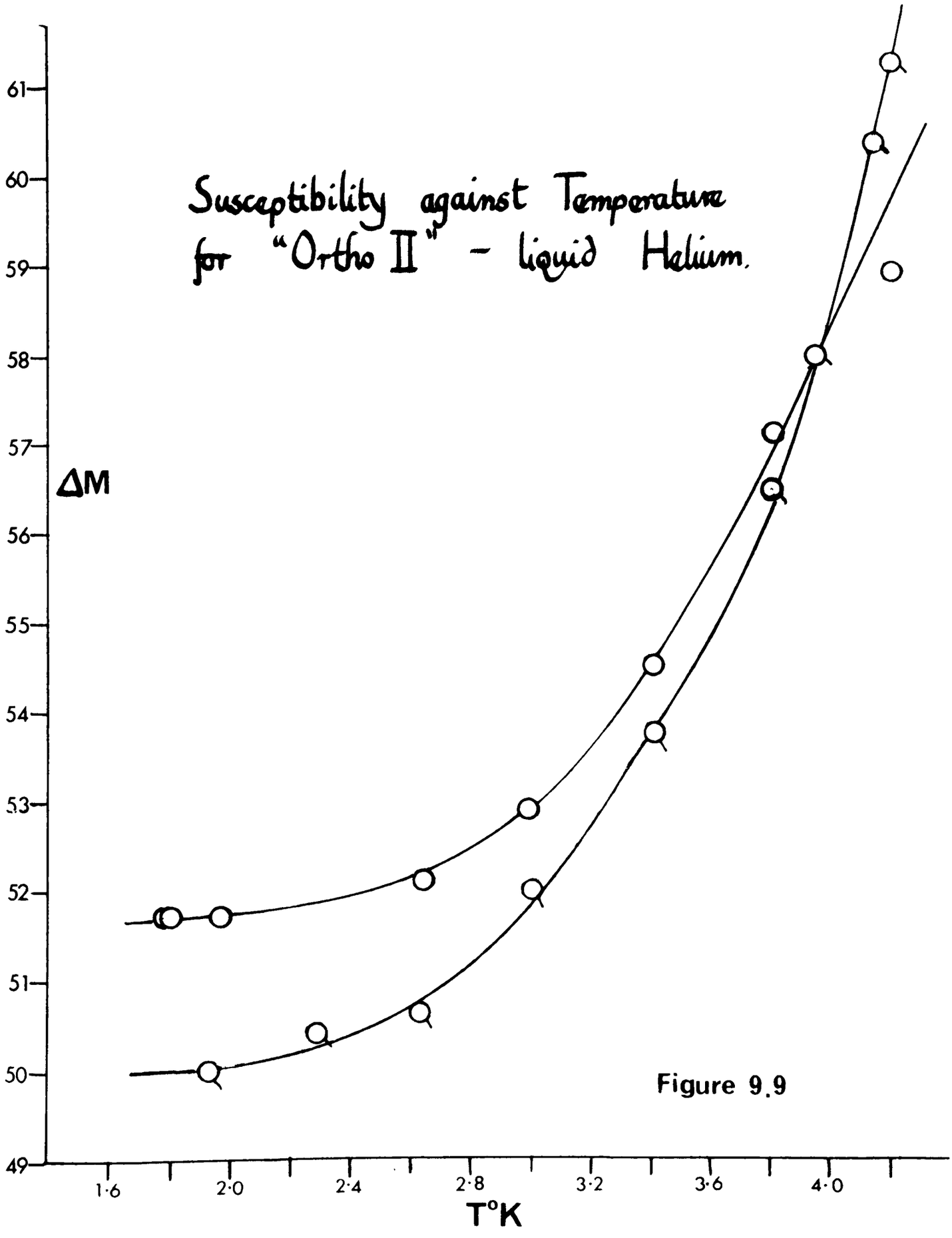
Susceptibility against Temperature
for "Ortho II" - liquid Helium.
ΔM
61
60
59
58
57
56
55
54
53
52
51
50
49
1·6
2·0
2·4
2·8
3·2
3·6
4·0
T°K

Figure 9.9

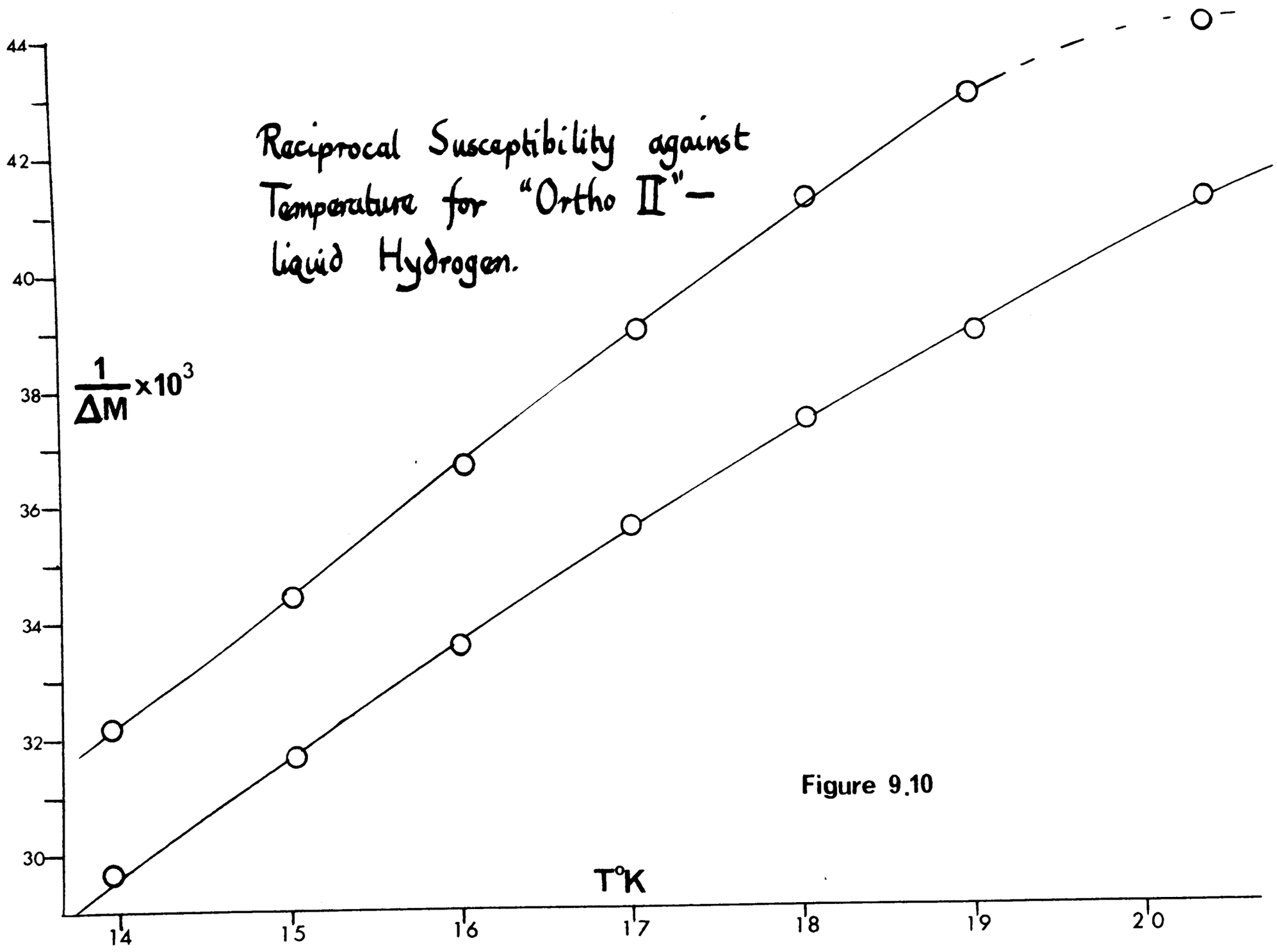
Reciprocal Susceptibility against Temperature for "Ortho II"- liquid Hydrogen.
$\frac{1}{\Delta M} \times 10^3$
44
42
40
38
36
34
32
30
T°K
14
15
16
17
18
19
20

Figure 9.10

find a transition temperature of $4.6^{\circ}K \pm 0.3^{\circ}$ (private communication). This is consistent with the observed ferromagnetic Weiss constant in the hydrogen and nitrogen ranges.

'Eu_3O_4'

The material measured was supplied by Dr R.Rau, and consisted of shiny black chunks, claimed by him to be substantially single phase Eu_3O_4. The material seemed to be homogeneous under microscopic examination. Two separate samples were measured in the liquid nitrogen, hydrogen and helium temperature ranges, and a third sample was measured more carefully in the liquid nitrogen range. The results of all these experiments seem to be consistent, within the combined experimental errors, and differences caused by varying (uncorrected) demagnetising corrections. The results are given as ΔM, and the measurements are normalised according to the different weights of the samples.

Figure 9.8 represents the behaviour of all three samples measured throughout the temperature range, expressed as reciprocal susceptibility against temperature. Figure 9.9 represents the variation of susceptibility with temperature in the helium range, and Figure 9.10 the behaviour in the hydrogen range as reciprocal susceptibility against temperature. Figure 11 shows the variation of susceptibility throughout the temperature range.

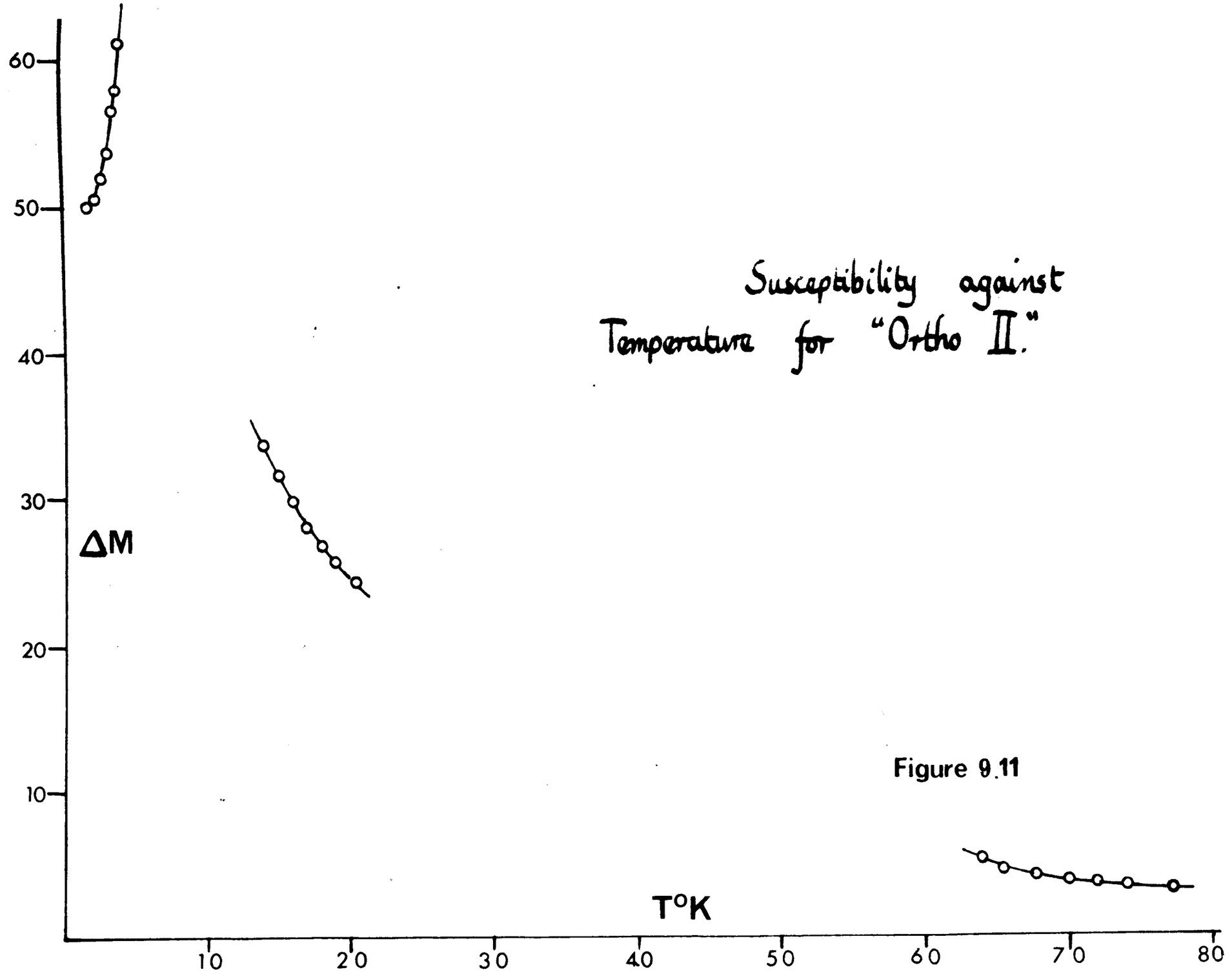
Susceptibility against
Temperature for "Ortho II."
ΔM
T°K
60
50
40
30
20
10
10
20
30
40
50
60
70
80

Figure 9.11

Results and Discussion.

It is immediately apparent from Figures 9.8 and 9.11 that this substance does not obey a Curie-Weiss law in any part of the temperature range investigated, so that if it is indeed a single phase, then its behaviour is very unusual indeed.

From Figure 9.9 it seems that this substance undergoes an ordering transition just above 4.2°K. Although the susceptibility appears to fall with temperature, there were large R effects which increased with decreasing temperature, so that, as with ortho I, it is not clear whether the ordering is ferro- or anti-ferromagnetic.

The solid line on Figure 9.8 shows the gradient to be expected of a phase with composition Eu_3O_4 obeying a Curie-Weiss law, and neither the hydrogen nor the nitrogen points obey a law even approximating to this.

The nitrogen range points seem to indicate an ordering transition to a ferromagnetic state, and the most likely candidate in an oxygen-europium phase is EuO, though the shape of the curve does not show a discontinuity at 70°K (see Figures 9.1,2 and 3, and pages 9.6-7).

If a small amount of EuO ($\sim$1%) is present in the Eu_3O_4, the moment of the EuO will be saturated by liquid hydrogen temperatures, and it should be possible to analyse the measured susceptibility to a Curie-Weiss law with temperature-independent term: -

$$\chi = \frac{\Delta M}{T - \theta} + \alpha$$

where M and θ relate to the paramagnetic phase, and

α relates to the ferromagnetic phase.

The better set of results (lower curve in Figure 9.10) were analysed in this way, and obeyed an expression

$$\chi = \frac{238}{T - 6.0} + 17.15$$

The value of the molecular weight per g.ion of Eu^{II} calculated from this Curie constant lies within 5% of the expected value for Eu_3O_4, while the Weiss θ is fully compatible with the observed ordering of the specimen in the helium range. The temperature independent term could be caused by the presence of about 1% of EuO, based on the measurements reported earlier in this chapter.

The second set of measurements were made on a much smaller specimen, and are correspondingly less accurate, but within the experimental accuracy, fit a similar law with a somewhat higher Curie constant and temperature independent term, indicating that the specimen was not completely homogeneous, a result also indicated by the difference between the two specimens in the helium range.

Conclusions.

The oxygen-europium system seems to be very interesting. While the Curie temperature of EuO is somewhat lower than suggested by earlier work, it is still very high - especially

when compared with the ordering temperatures of other compounds containing the $4f^7$ configuration ion (see Figures 5.5,10.3 and pages 10.1-3; and Wyatt,1963).

A single phase discovered independently in this country and the U.S.A., and claimed to be an intermediate europium oxide, has been tentatively identified as the silicate of Eu^{II}, Eu_2SiO_4, a formula which accords well with the magnetic and x-ray structural evidence. It is just possible that the compound is a very slightly oxygen-rich modification of EuO with empirical formula approximately $EuO_{1.073}$. The compound becomes ferromagnetic at about $4.6^{\circ}K$.

Another phase identified as Eu_3O_4 on the basis of its x-ray diffraction properties has been investigated magnetically, and shown to undergo an ordering transition at a temperature somewhat higher than $4.2^{\circ}K$. It is not possible to determine whether this is to ferro- or antiferromagnetic state, since the a.c. method does not give unambiguous results. Its behaviour in the liquid hydrogen and nitrogen temperature ranges is not explicable in terms of a single phase. Since the material is not visibly inhomogeneous, the impurity must be widely dispersed in the sample, and approximately 1% of EuO, its detailed behaviour slightly modified by its finely divided state, or partial solid solution in Eu_3O_4, would cause the strange effects observed. An accurate analysis of the results in these terms is not possible,

since impurity amounts of EuO swamp the true behaviour of Eu_3O_4 in the liquid nitrogen range, and in the liquid hydrogen range, the susceptibility of Eu_3O_4 should be asymptotic to a Curie-Weiss law with a Weiss θ of several degrees. However, qualitatively, the results are compatible with those to be expected from a sample of Eu_3O_4 containing about 1% of EuO. It is not easy to see how Eu_3O_4 can be prepared free from EuO, or how the presence and concentration of EuO in a sample can be demonstrated in any other way.

Postscript.

Since this Chapter was written, a paper has appeared in Phys.Rev.Letters, 15th.,September,1963,Volume 11,p.251 on the magnetic properties of Eu_2SiO_4. M.W.Shafer, T.R.McGuire and J.C.Smith prepared this compound as bright lemon yellow crystals by solid state reaction between EuO and SiO_2. This was found by direct comparison with Rau's 'Ortho I' to be identical, and to have the same unit cell dimensions quoted on page 9.3, with 28 formula units per unit cell. The magnetic moment measurements indicated a Curie temperature of $7 \pm 1^{\circ}K$, and the substance was in fact ferromagnetic in the liquid helium temperature range.

Thus, the conclusion that we had reached independently, that 'Ortho I' is a silicate rather than oxide phase is vindicated, and the deduced formula and measured magnetic properties confirmed.

Chapter 10.

The Paramagnetic Susceptibilities of Various Materials.

A) Terbium Tetrafluoride and Gadolinium Tri-iodide.

Extensive investigations have recently shown that anhydrous $GdCl_3$ is a very interesting compound magnetically (Wolf et al.,1961;Garton et al.,1962;Leask,Wolf and Wyatt, 1962; Wyatt,1963). It undergoes a ferromagnetic transition at a temperature convenient for accurate physical measurements (2.2°K) and is therefore one of the few known ionic non-conducting ferromagnets. In addition, its structure is well known, and it is conveniently grown into single crystals (Shore,1963).

The susceptibilities of some other rare earth anhydrous halides have been surveyed in order to select materials likely to repay further detailed investigation (Wyatt,1963). Since the $4f^7$ ions present less theoretical difficulties than most of the other rare earth ions, Wyatt has measured $EuCl_2$, GdF_3, $GdBr_3$ in addition to $GdCl_3$. $GdBr_3$ appears to become ferromagnetic at 1.8°K, while $EuCl_2$ and GdF_3 obey Curie-Weiss laws with ferromagnetic Weiss θs of 1.2 and 0.1° respectively. We add to the series with measurements on TbF_4 and GdI_3.

Figure 10.1 shows the susceptibility of TbF_4 in the liquid helium and hydrogen ranges as a plot of reciprocal susceptibility against temperature. In the hydrogen range, the behaviour may be represented by a law: -

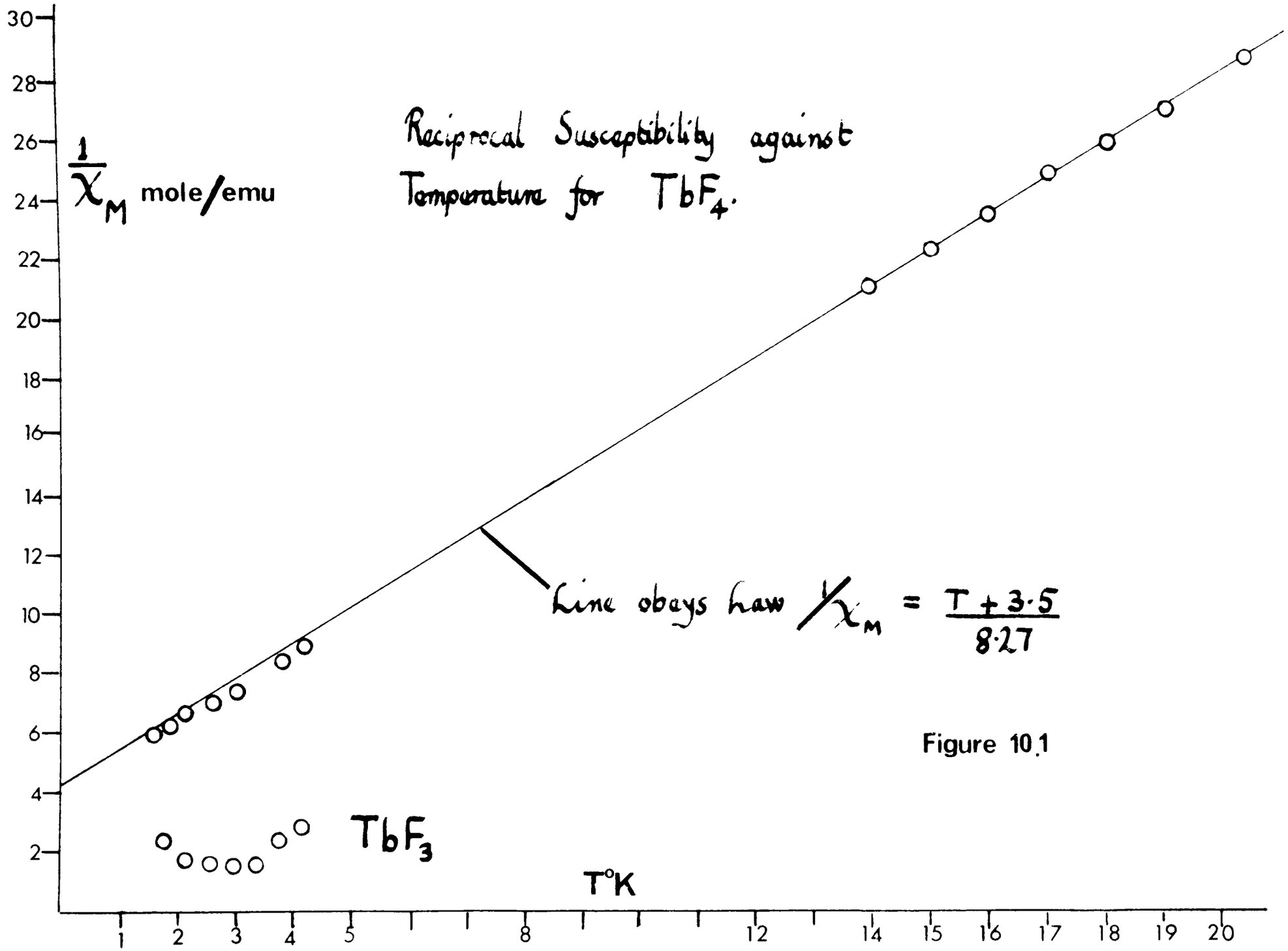
Reciprocal Susceptibility against Temperature for TbF_4.
$\frac{1}{\chi_M}$ mole/emu
30
28
26
24
22
20
18
16
14
12
10
8
6
4
2
Line obeys law $1/\chi_M = \frac{T + 3.5}{8.27}$
TbF_3
T°K
1
2
3
4
5
8
12
14
15
16
17
18
19
20

Figure 10.1

$$\chi_M = 8.27/(T + 3.5)$$

In spite of the large Weiss θ, there is no indication of ordering in the helium range, though there are departures from linearity. Plotted on the same graph to the same scale is the reciprocal molar susceptibility of TbF_3 (after Wyatt, 1963), and the dip in the TbF_4 curve is seen to correspond with a minimum at 3.2°K in the TbF_3 curve. Since the apparent Curie constant is also too high (8.27 instead of 7.82), it is probable that this sample of TbF_4 contains about 5% of TbF_3, which would account satisfactorily for both discrepancies.

The specimen was prepared by Mr R.Shore, by heating anhydrous finely powdered TbF_3 in a stream of fluorine gas at about 300°C for 15 minutes. The product was a pale pink powder, smelling strongly of fluorine. All the lines on an x-ray powder photograph were indexed in terms of the expected monoclinic unit cell of TbF_4 (Cunningham, Fesy and Rollier, 1954). An attempt to analyse the product by estimating the active fluorine as iodine liberated from KI solution indicated that the material was only 84% TbF_4, but bubbles of gas were noted when the compound was added to the solution, probably resulting from oxidation of the water by the fluorine.

Gadolinium Tri-iodide.

This compound is very difficult to produce in the pure state, since it is very readily oxidised and hydrolysed by

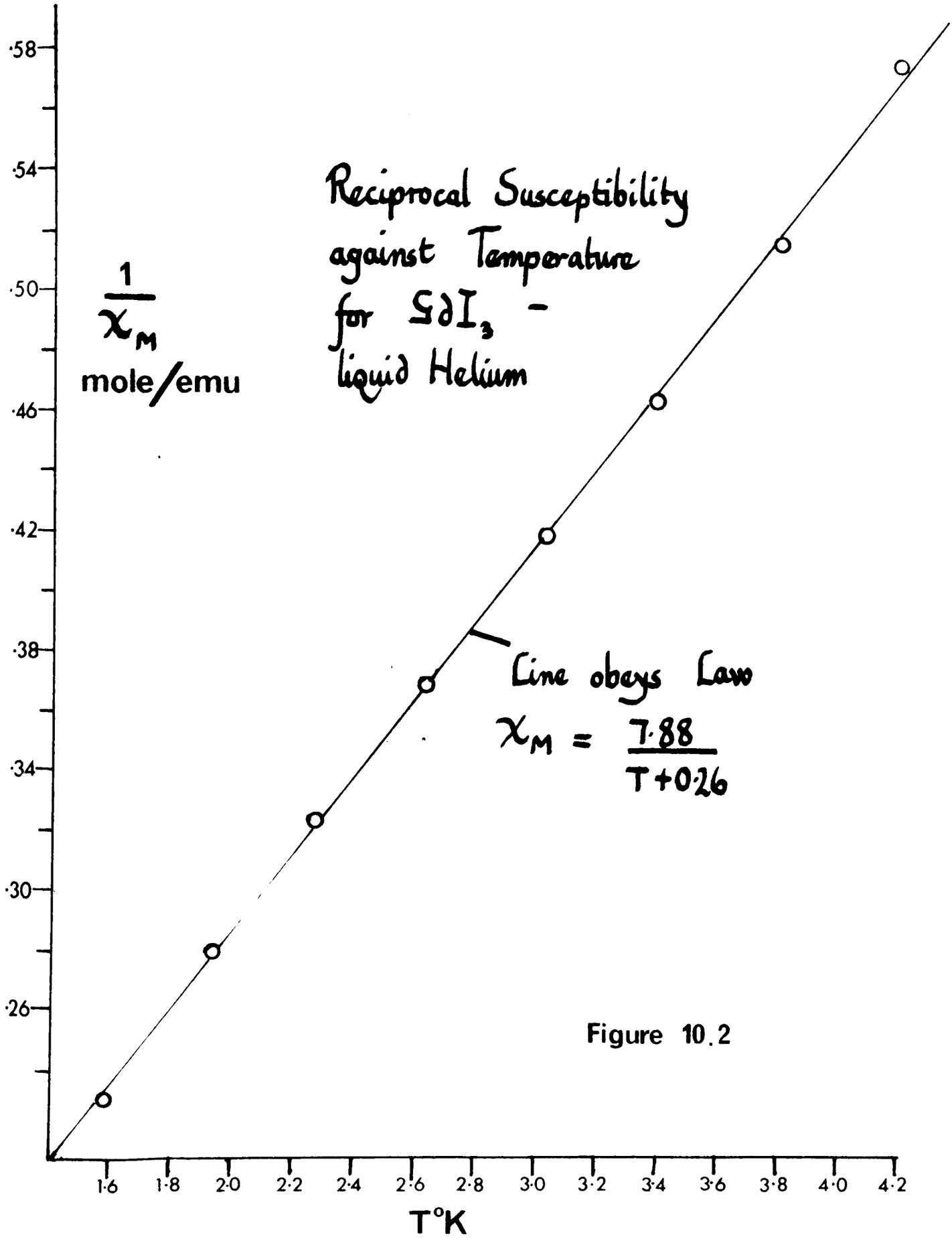
Reciprocal Susceptibility against Temperature for SmI_3 - liquid Helium
$\frac{1}{\chi_M}$ mole/emu
·58
·54
·50
·46
·42
·38
·34
·30
·26
Line obeys Law
$\chi_M = \frac{7.88}{T+0.26}$
1·6
1·8
2·0
2·2
2·4
2·6
2·8
3·0
3·2
3·4
3·6
3·8
4·0
4·2
T°K

Figure 10.2

air and water, and decomposes to the elements on sublimation. However, a small amount of pure material was collected, and stored in liquid nitrogen until its susceptibility could be measured. The results in the liquid helium range are shown in Figure 10.2 as a plot of reciprocal molar susceptibility against temperature, and obey a Curie-Weiss law: -

$$\chi_M = 7.88/(T + 0.26)$$

The agreement with the theoretical Curie constant is very good, and shows that the material was substantially pure. Since iodine has such a high atomic weight, any substitution of oxygen for iodine would have a gross effect upon the molecular weight, and hence upon the apparent molar susceptibility. Owing to its unstable chemical properties, this compound would be extremely difficult to obtain as a single crystal. It is therefore quite convenient that the Weiss Θ is very low, since no further investigations on this material are worth while.

B) <u>The Rare Earth Oxyfluorides.</u>

Introduction.

The rare earth oxyfluorides, general formula ROF, are a series of simple compounds of known stoichiometry and structure which might prove suitable for investigating the behaviour of rare earth ions. Like the garnets, they are chemically inert, and contain only one type of lattice site for the rare earth ions. There are three diamagnetic host

lattices, YOF, LaOF and LuOF for investigating the individual properties of the rare earth ions. Nielsen (1960) claimed to have produced fairly large single crystals of YOF as a by-product of YIG growth in the presence of a high concentration of F^-, so that it appeared that these compounds might be fairly readily available as sizeable single crystals after a certain amount of development work.

Their crystal structure is closely related to the fluorite structure, but attempts to prepare cubic modifications of the oxyfluorides with random distribution of the fluorine and oxygen ions have been unsuccessful (Zachariasen, 1951). Two modifications of the fluorite structure are known in the rare earth oxyfluorides, a metastable tetragonal form and a rhombohedral form. In a number of cases (CeOF, for instance) the deviation of the tetragonal form from cubic is too small to be detected. The deviation increases as a function of increasing atomic number.

The local crystal field about each rare earth consists of four fluorine and four oxygen ions at the corners of a more or less distorted cube, with the rare earth at the body centre. The anions are so disposed that each body diagonal of the cube has an oxygen ion at one end, and a fluorine at the other. Alternatively, the crystal field may be described as overlapping tetrahedra, one of F^-, and the other of O^{--}. Thus, the local crystal field symmetry

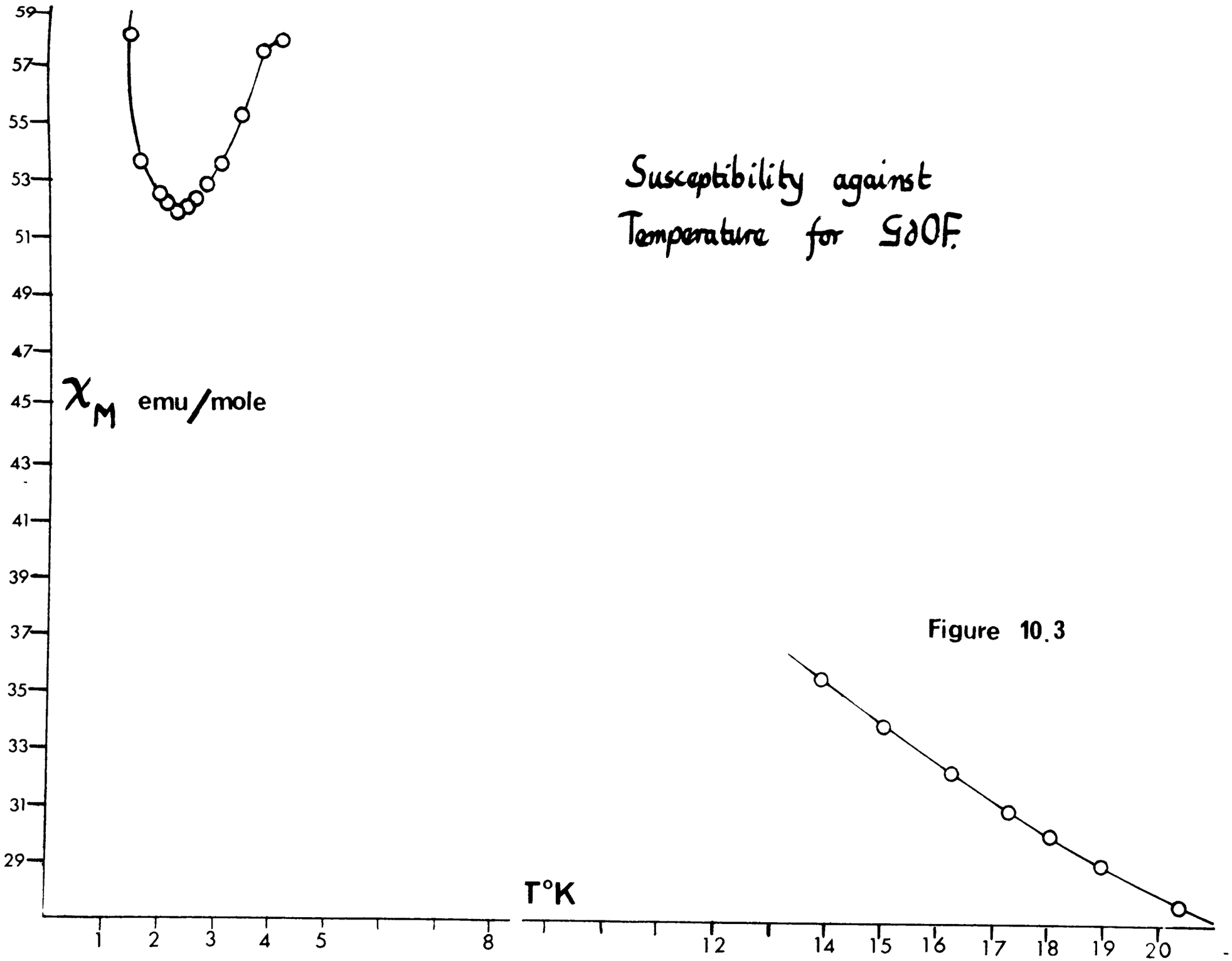

Susceptibility against Temperature for SdOF.

Figure 10.3

at the rare earth ions is cubic, the slight departures being expressed as a small axial contribution. This is qualitatively the same situation as the rare earth ions in garnets, and basically similar magnetic behaviour might be expected.

The susceptibilities of micro-crystalline samples of some of the rhombohedral rare earth oxyfluorides have been measured, as a preliminary survey. The samples were prepared by Mr E.S.Albone (1963) in attempts to produce large single crystals, and were identified by indexing their x-ray powder photographs on the basis of the known structure parameters. Under the microscope, they were seen to be homogeneous crystalline phases.

Gadolinium Oxyfluoride.

The results for the liquid hydrogen and helium temperature ranges are shown in Figure 10.3 as molar susceptibility against temperature. In the hydrogen range, the points obey a law: -

$$\chi_M = 7.92/(T + 8.2)$$

but in view of the large Weiss Θ, the points in the hydrogen range must lie on a curve asymptotic to the true Curie-Weiss law, so not too much reliance can be placed on the exact figures. The higher temperature points in the liquid helium range are fully compatible with an antiferromagnetic ordering transition between 4.2 and 14°K.

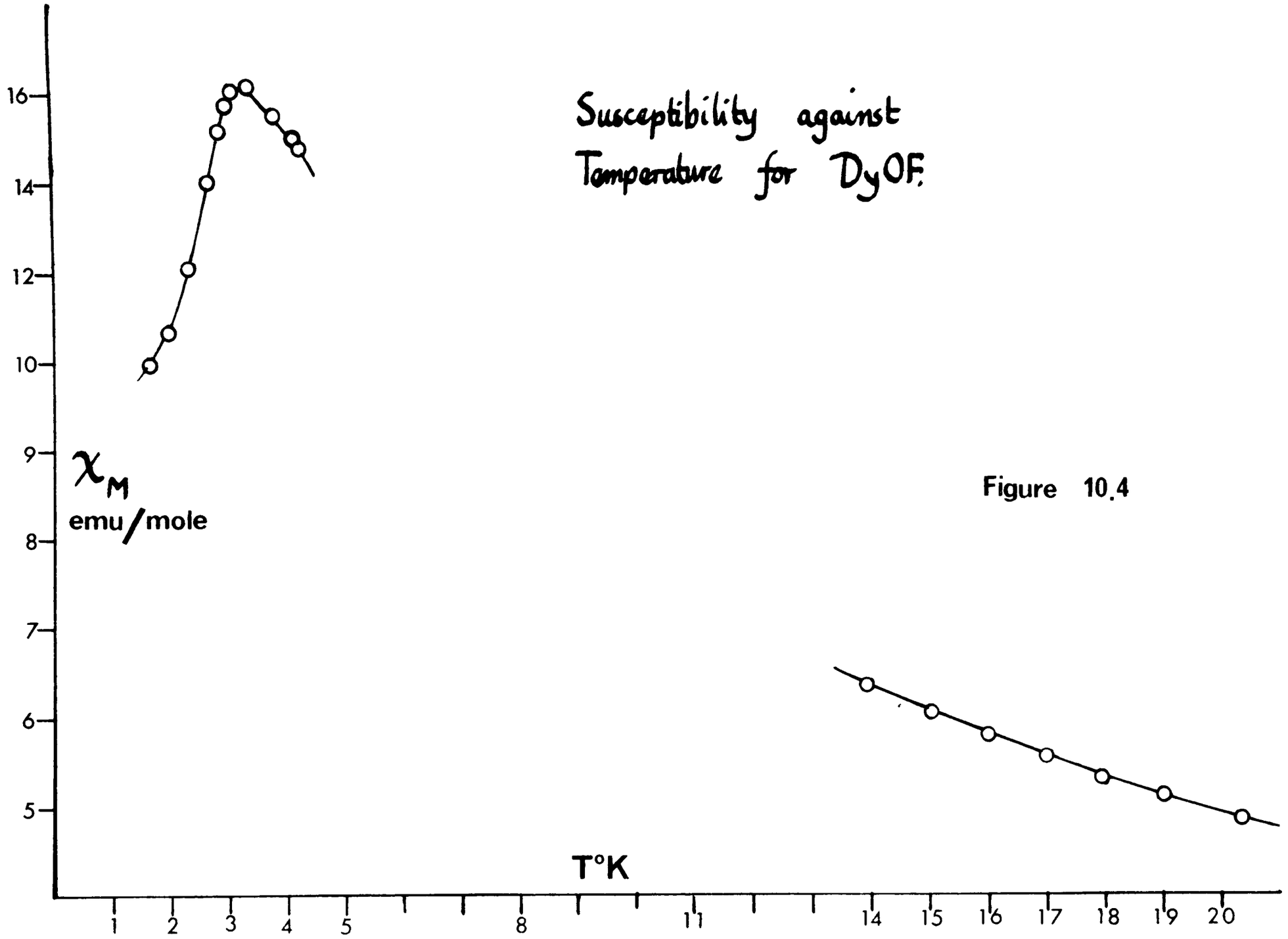
Susceptibility against Temperature for DyOF
16
14
12
10
9
8
7
6
5
χ_M
emu/mole
T°K
1
2
3
4
5
8
11
14
15
16
17
18
19
20

Figure 10.4

The minimum in the susceptibility is rather mysterious, and there is at present no detailed explanation, but experience has shown that spurious and misleading effects are observed in the vicinity of magnetic ordering phenomena using an aa.c method. When a large single crystal becomes available, further work on this material would be worth while.

Dysprosium Oxyfluoride.

Figure 10.4 represents the temperature variation of χ_M for this substance, and like GdOF above, and DAG, the susceptibility reaches a maximum, and then falls away sharply. The point of steepest slope seems to be $3.0^\circ \pm 0.1$ Unlike DAG, the susceptibility does not tend to zero at $0^\circ K$, but seems to be approaching a value approximately 2/3 the maximum value, as is usual for powder samples of antiferromagnets (Nagamiya, Yoshida and Kubo, 1955). In the absence of out-of-phase susceptibility effects, it can reasonably be assumed that this material undergoes an antiferromagnetic transition.

In the hydrogen range, the points obey a law: -

$$\chi_M = 13.32/(T + 7.01)$$

but as with GdOF, the points must be asymptotic to the true Curie-Weiss law, and the possibility of a temperature independent contribution to the susceptibility from an excited state cannot be eliminated.

The general similarity of behaviour between this

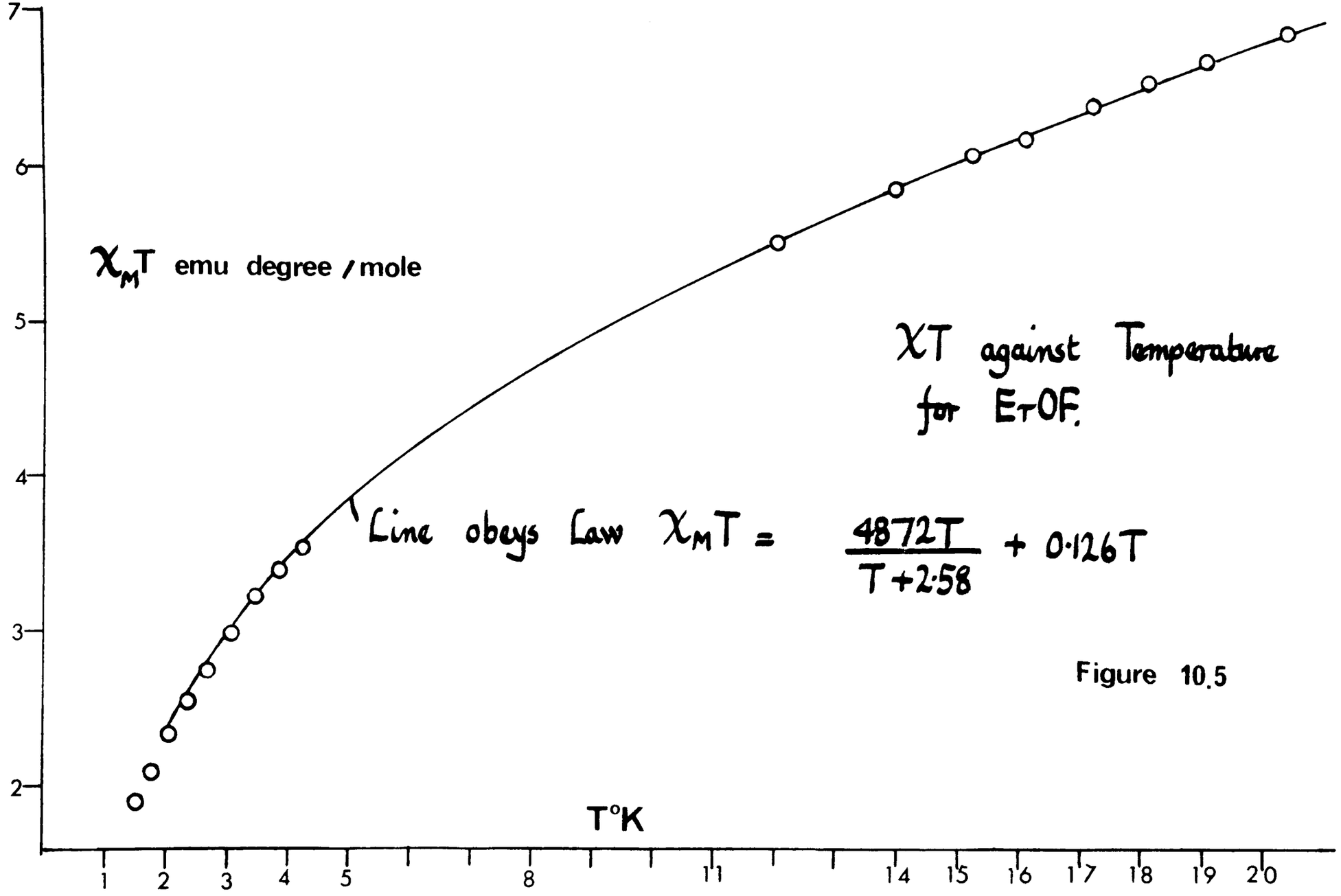
7
6
5
4
3
2
$\chi_M T$ emu degree / mole
χT against Temperature for E-OF.
Line obeys Law $\chi_M T = \frac{4872T}{T+2.58} + 0.126T$
T°K
1
2
3
4
5
8
11
14
15
16
17
18
19
20

Figure 10.5

compound and DAG must be remarked. The Curie constants in the hydrogen range are approximately the same, both materials become antiferromagnetic at about 3°K. In the non-cubic oxyfluoride, the sublattice arrangements in the ordered state are not likely to be as simple as in DAG, but this material would probably repay further study.

Erbium Oxyfluoride.

The susceptibility of ErOF over the measured temperature range is shown as a plot of $\chi_M T$ against T in Figure 10.5. The solid line is computed from the expression: -

$$\chi_M T = 4.872T/(T + 2.583) + 0.126T.$$

As with DyOF, the behaviour is strikingly similar to that of the same ion in the aluminium garnet lattice (Figure 5.7), both the Curie constant and temperature independent terms being of approximately similar size. There is no indication of ordering, even at the lowest temperatures measured.

Neodymium Oxyfluoride.

The results for this compound are shown in Figure 10.6 as a plot of reciprocal susceptibility against temperature. The results cannot be satisfactorily fitted to a Curie-Weiss law with temperature independent term. The hydrogen range points deviate from linearity, probably as a result of population of the first excited state, while the helium range points seem to indicate some local ferromagnetic

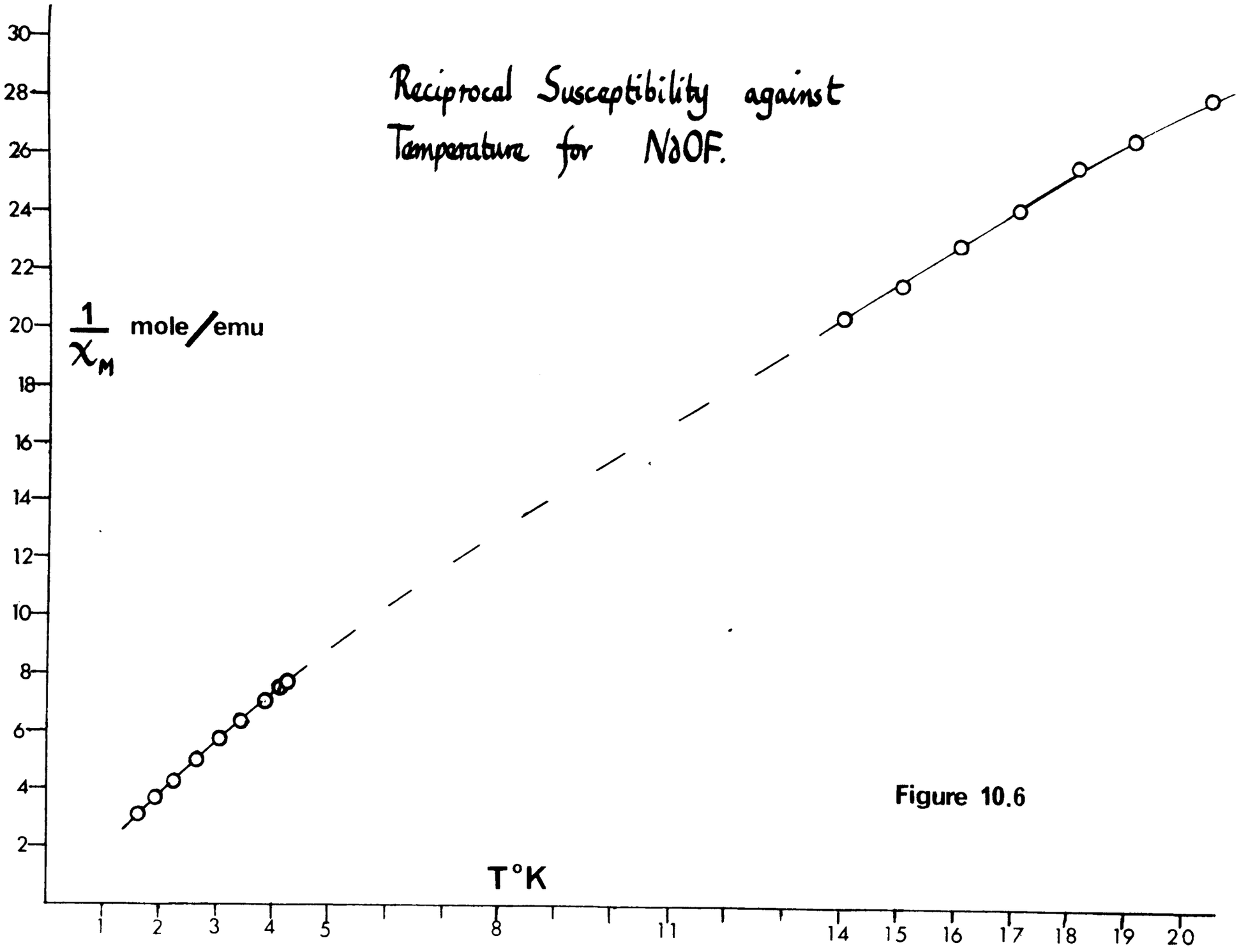
Reciprocal Susceptibility against Temperature for NdOF.
1/χM mole/emu
30
28
26
24
22
20
18
16
14
12
10
8
6
4
2
T°K
1
2
3
4
5
8
11
14
15
16
17
18
19
20

Figure 10.6

ordering.

Discussion.

In a general way, the behaviour of the oxyfluorides of gadolinium, dysprosium and erbium seems to resemble that of the corresponding aluminium garnets, with the main difference that the interactions are stronger in the oxyfluorides. Since the oxyfluorides are more concentrated magnetically than the garnets, and the crystal fields are qualitatively similar in the two lattices, this is in accordance with expectation.

The gadolinium and dysprosium compounds both undergo ordering transitions in the measured temperature range, both almost certainly to antiferromagnetic states. If large enough single crystals can be prepared, these substances will probably repay further detailed investigation, provided that spectroscopic or resonance measurements are made on dilute specimens as well.

C The Rare Earth-Transition Metal Double Nitrates.

The existence of a series of double nitrates of the general formula $R^{III}_2M^{II}_3(NO_3)_{12}.24\ H_2O$, where R^{III} can be Bi, La or one of the lighter rare earths, and M^{II} can be Mg, Zn, Mn, Co, Ni, Fe, Cu has long been known (e.g. Groth, 1908). It is relatively easy to obtain large single crystals of most of these substances from aqueous solution, and since

they are able to incorporate so many different paramagnetic ions, they have been the subjects of many experiments in magnetism. For instance, they have been used as host lattices in many paramagnetic resonance experiments (Bowers and Owen, 1955). Cerium magnesium nitrate has been used in adiabatic demagnetisation (Ambler et al., 1958; Daniels and Robinson, 1953) and there have also been paramagnetic susceptibility, spin-lattice relaxation, nuclear orientation and specific heat measurements.

Recently, Berman, Brock and Huntley (1963) in this laboratory have started to investigate the thermal conductivities of these materials in magnetic fields. The detailed theory of their measurements is complicated, but essentially, thermal conduction at low temperatures is effected by spin phonons of a Boltzmann distribution of energies. Under certain conditions, the spin phonons of a particular energy can be absorbed by paramagnetic ions, which advance to an excited state as a result. In the critical conditions where the phonons are absorbed by the paramagnetic ions, they are no longer available for thermal conductivity, and there is an anomalous fall in this property. The temperature at which this occurs is related to the interactions between the paramagnetic ions.

These compounds were chosen for the investigation because of their availability as sufficiently large, high quality single crystals. Susceptibility measurements are

important, as providing a totally independent measure of the magnetic interactions.

Experimental.

Pure lanthanum nitrate was dissolved in hot distilled water, together with the correct mole proportion of divalent metal nitrate. A few ccs of concentrated nitric acid was added to lower the solubility of the mixed nitrate, and prevent hydrolysis. After the solution had cooled, the saturated liquor was decanted to a Petri dish, and seeded with a few good small crystals from the remaining mass of solid, and the solution set aside to evaporate slowly in a desiccator over concentrated sulphuric acid. The crystals grew as flat hexagonal plates up to 2" in diameter, and ¼" thick.

The susceptibilities are completely defined by measurements parallel with and perpendicular to the crystallographic c axis, whose direction lies perpendicular to the hexagonal plates.

For the direction perpendicular to the c axis, long strips were cut from a single crystal with a fine hacksaw blade, and were shaped by hand, using a razor blade and fine glass paper to make oblate spheroids about 2 cm long, and 0.5 cm in diameter. These specimens were a tight sliding fit in the normal susceptibility specimen boxes.

For the direction parallel with the c axis, compound

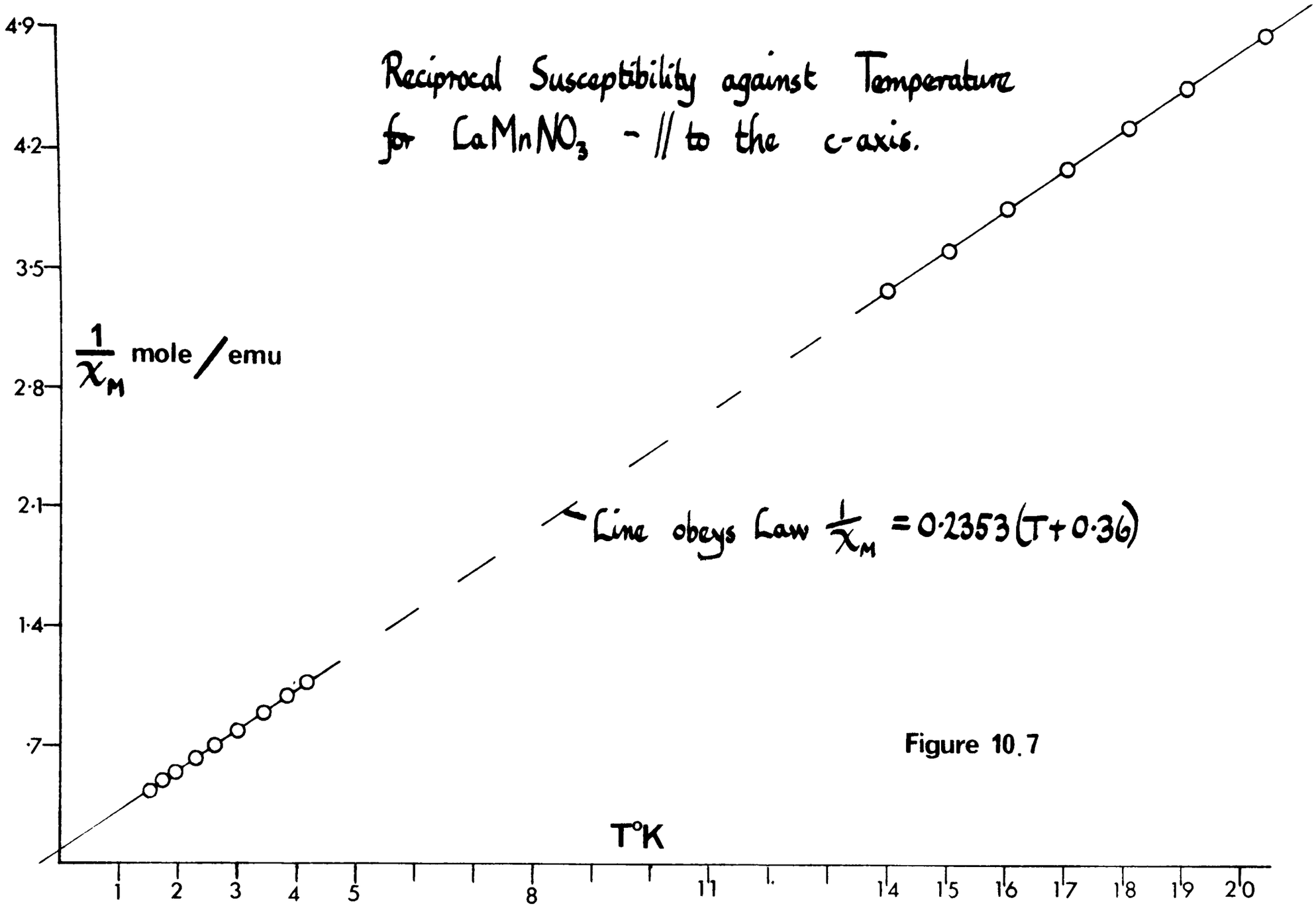
Reciprocal Susceptibility against Temperature for $LaMnNO_3$ - // to the c-axis.
4·9
4·2
3·5
2·8
2·1
1·4
·7
$\frac{1}{\chi_M}$ mole / emu
Line obeys Law $\frac{1}{\chi_M} = 0.2353(T + 0.36)$
T°K
1
2
3
4
5
8
11
14
15
16
17
18
19
20

Figure 10.7

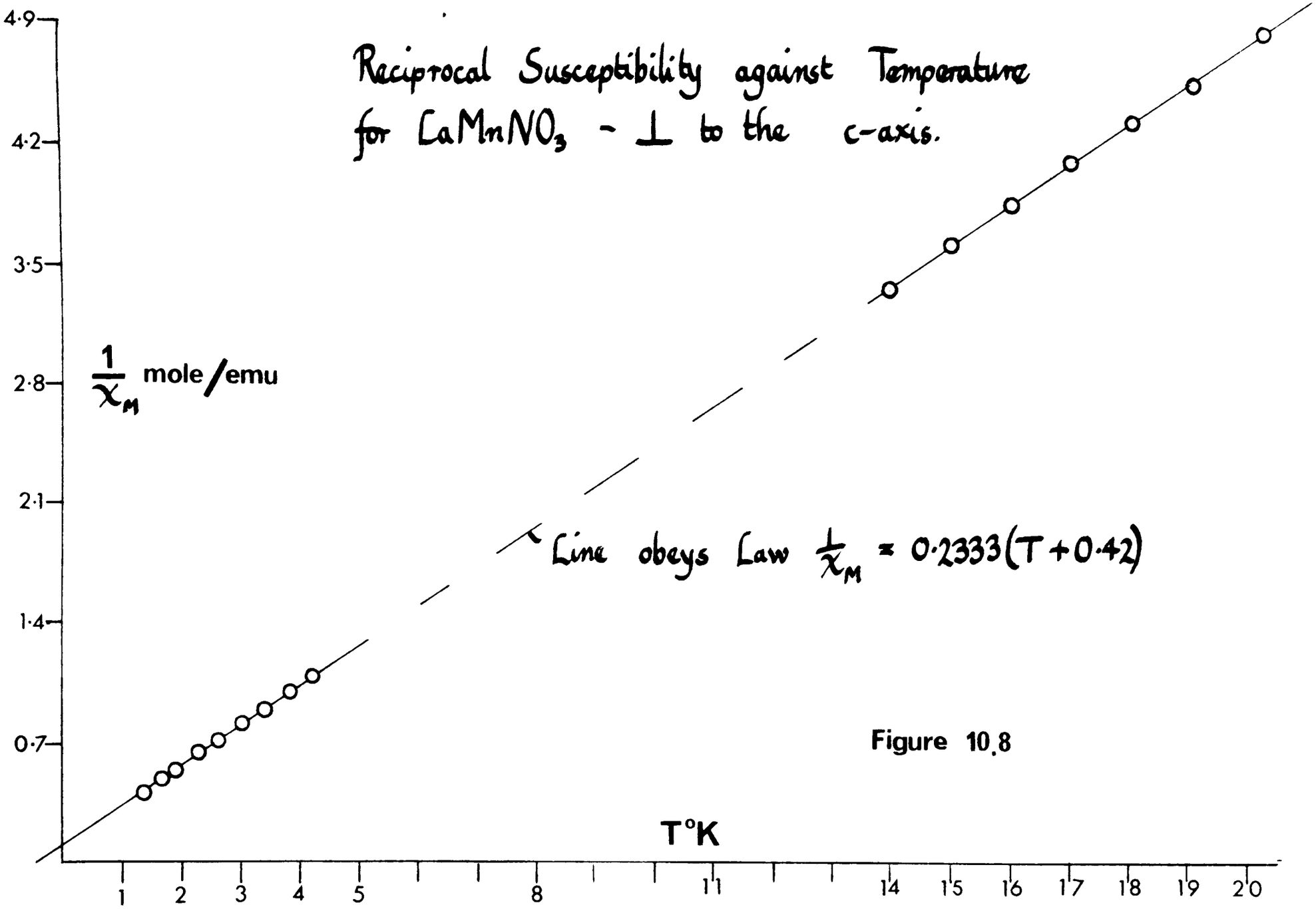
Reciprocal Susceptibility against Temperature
for LaMnNO3 - ⊥ to the c-axis.
4·9
4·2
3·5
2·8
2·1
1·4
0·7
1/χM mole/emu
Line obeys Law 1/χM = 0·2333(T+0·42)
T°K
1
2
3
4
5
8
11
14
15
16
17
18
19
20

Figure 10.8

specimens were prepared from four or five separate discs cut from a crystal, and mounted above each other. The two end pieces were tapered to approximately elipsoidal shape. In order to minimise alignment errors, the faces of the crystals which had grown in contact with the solution were used as standard, rather than those which had been in contact with the Petri dish.

The samples were carefully weighed, and the susceptibilities measured in the liquid hydrogen and helium temperature ranges, in the normal way. The results as shown in Figures 10.7,8,9 and 10 as plots of reciprocal susceptibility against temperature have been corrected for shape.

Results and Discussion.

The g-values of Mn^{II} and Ni^{II} in bismuth magnesium nitrate (quoted by Bowers and Owen, 1955) which is isomorphous with the two salts measured, are 1.998 and 2.54 respectively at liquid nitrogen temperatures. Unlike lanthanum cobalt nitrate (Leask and Wolf, 1962) the ions in the two different types of lattice sites both have the same isotropic g-values. Thus, the expected Curie constants calculated from these g-values (assuming effective spins 5/2 for Mn^{II} and 1 for Ni^{II}) are 4.370 and 1.255 respectively.

Parallel to the c-axis (Figure 10.7), the susceptibility of lanthanum manganese nitrate obeys a law: -

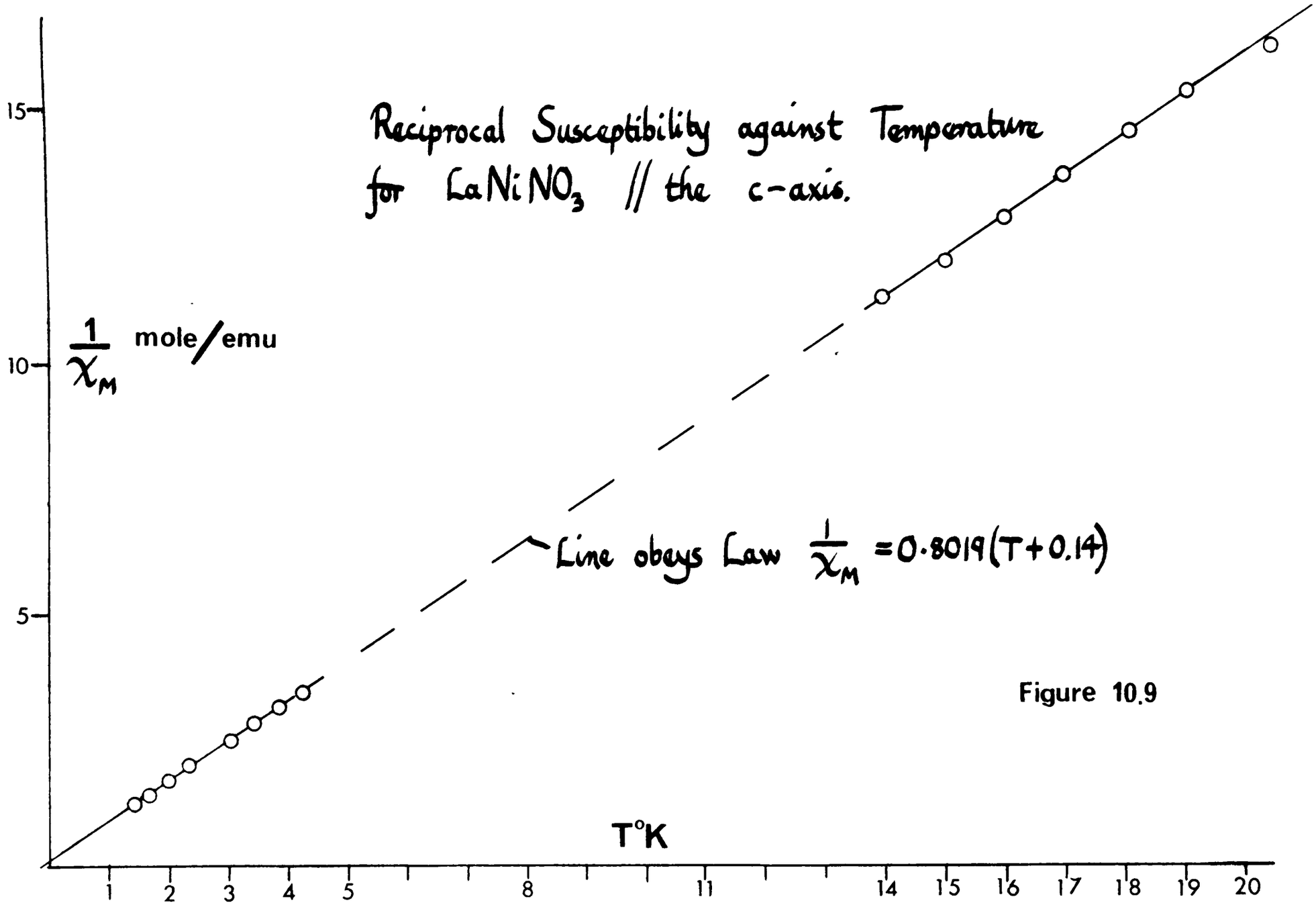
Reciprocal Susceptibility against Temperature
for LaNiNO3 // the c-axis.
1/χM mole/emu
15
10
5
Line obeys Law 1/χM = 0·8019(T+0.14)
T°K
1
2
3
4
5
8
11
14
15
16
17
18
19
20

Figure 10.9

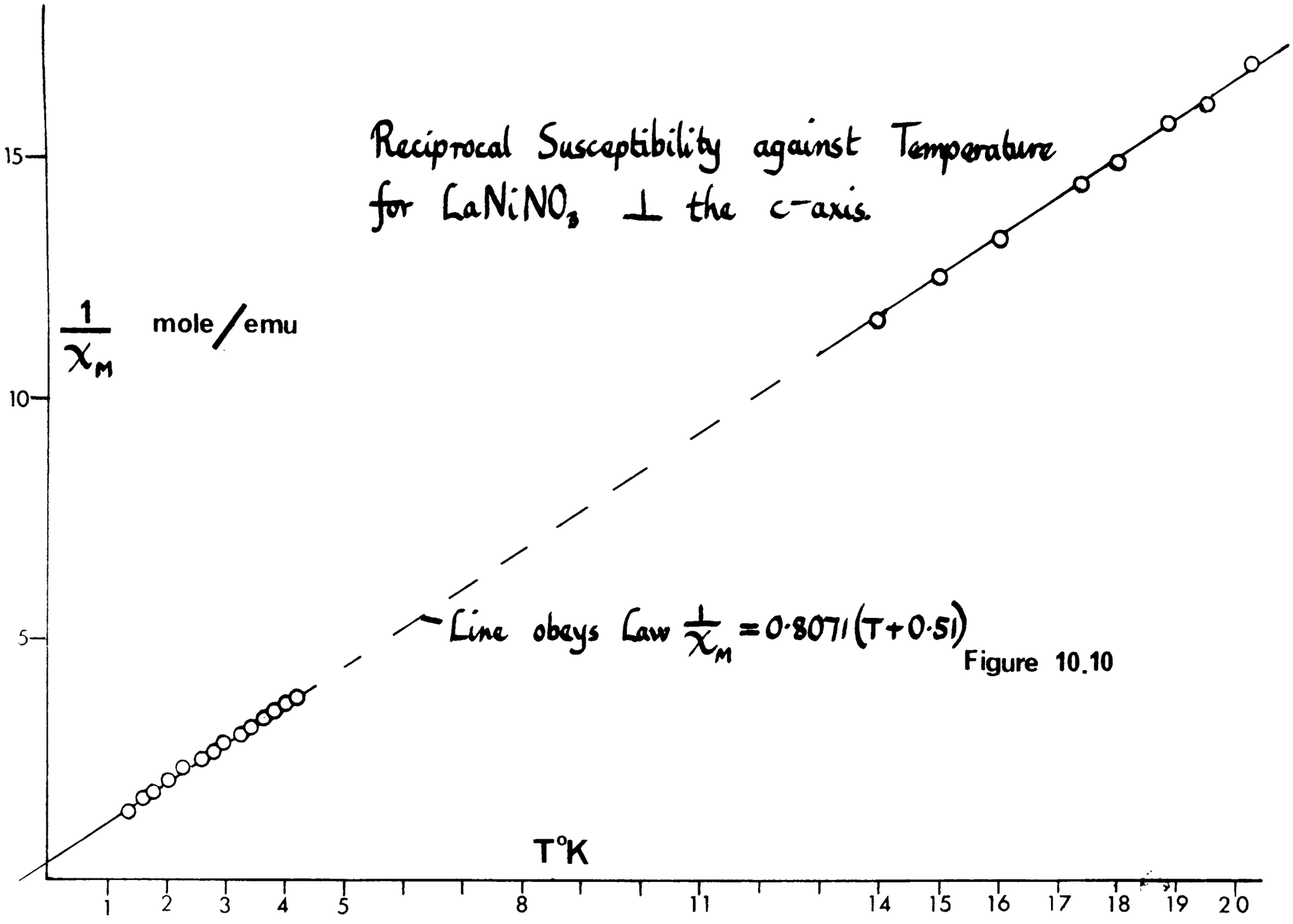
Reciprocal Susceptibility against Temperature
for LaNiNO2 ⊥ the c-axis.
1/χM mole/emu
15
10
5
Line obeys Law 1/χM = 0·8071(T+0·51)
T°K
1
2
3
4
5
8
11
14
15
16
17
18
19
20

Figure 10.10

$$\chi_M = 4.280/(T + 0.36)$$

in both liquid hydrogen and liquid helium temperature ranges. As in the other cases, the law was obtained by applying a 'least squares' statistical method to the experimental data. Perpendicular to the c axis, the law is: -

$$\chi_M = 4.286/T + 0.42).$$

In contrast with lanthanum cobalt nitrate (Leask and Wolf, 1962) the Weiss constants of this material are relatively isotropic, as well as the Curie constants. They are also small, as expected for a dilute magnetic material, and antiferromagnetic in sign.

Parallel with the c axis (Figure 10.9), the susceptibility of lanthanum nickel nitrate obeys a law: -

$$\chi_M = 1.247/(T + 0.14)$$

while perpendicular to the c axis (Figure 10.10), the relationship is: -

$$\chi_M = 1.239/(T + 0.51)$$

Thus, for all four measurements, the measured Curie constant is lower than the calculated value, but the discrepancy is not serious. The Curie constant is related to the square of the *g*-value, so that the error is approximately doubled from the g-value to the Curie constant. In view of the difference in host lattice and temperature of measurement, as well as the unspecified error in the g-value measurement, the agreement is very good.

Any temperature independent contributions to the susceptibility were negligible by comparison with the experimental accuracy. Thus, to a very good approximation, only the ground states of Mn^{II} and Ni^{II} are populated in these compounds.

As in lanthanum cobalt nitrate, the interactions are all small, and antiferromagnetic, and arise from the combined effect of dipole-dipole and exchange interactions.

List of References.

J.C.Achard, Comptes Rendues,250,3025 (1960)

E.S.Albone, Unpublished

E.Ambler,M.A.Grace,H.Halban,N.Kurti,H.Durand,C.E.Johnson and H.R.Lemmer, Phil.Mag.,44,216 (1953)

C.A.Bailey, Unpublished.

M.Ball,G.Garton,M.J.M.Leask,D.Ryan and W.P.Wolf, J.Appl. Phys.,32,267S (1961)

M.Ball,G.Garton,M.J.M.Leask and W.P.Wolf, Proc. 7th International Conference on Low Temperature Physics, Toronto, Canada p.128 (1960)

M.Ball,M.J.M.Leask,W.P.Wolf and A.F.G.Wyatt, J.Appl.Phys., 34,1104, (1963)

M.Ball,M.T.Hutchings,M.J.M.Leask and W.P.Wolf, Proc. 8th International Congress on Low Temperature Physics (to be published)

H.Bärninghausen and G.Brauer, Acta Cryst.,15,1095 (1962)

R.J.Benzie and A.H.Cooke, Proc.Phys.Soc.,A63,201 (1950)

F.Bertaut and F.Forrat, Comptes Rendues,242,382 (1956)

B.Bleaney and D.J.E.Ingram, Proc.Phys.Soc.,A205,336 (1951)

D.Boakes, Unpublished.

D.Boakes,G.Garton,D.Ryan and W.P.Wolf, Proc.Phys.Soc., 74,663 (1959)

D.Bowers,and J.Owen, Rep.Progr.Phys.,18,304,1955

R.M.Bozorth,B.T.Matthias,H.Suhl,E.Corenzwit and D.D.Davis, Phys.Rev.,115,1595 (1959)

J.C.F.Brock,R.Berman and D.J.Huntley, Phys.Letters,3,310 (1963).

E.U.Condon and G.H.Shortley, 'Theory of Atomic Spectra', C.U.P.,London, (1935)

A.J.Croft and R.H.B.Exell, Proc.Roy.Soc.,A262,110 (1961)

A.J.Croft,E.A.Faulkner.J.Hatton and E.F.W.Seymour, Phil. Mag.,44,289 (1953)

B.B.Cunningham,D.C.Feay and M.A.Rollier, J.Amer.Chem. Soc., 76,361 (1954)

C.E.Curtis and A.G.Tharp, J.Amer.Chem.Soc.,42,151 (1959)

J.M.Daniels and F.N.H.Robinson, Phil.Mag.,44,630 (1953)

C.Domb and M.F.Sykes, Phys.Rev.,108,1415 (1957)

C.Domb and M.F.Sykes, Phys.Rev.,128,168 (1962)

H.A.Eick,N.C.Beezinger,L.Eyring, J.Amer.Chem.Soc.,78,5147 (1956)

R.A.Erickson and L.D.Roberts, Phys.Rev.,93,957 (1954)

R.A.Erickson,L.D.Roberts and J.W.T.Dabbs, Rev.Sci.Instr., 25,1178 (1954)

F.Euler and J.Bruce, Proc.20th Pittsburgh Diffraction Conference,(1962)

M.E.Fisher, Proc.Roy.Soc.,A254,66 (1960)

M.E.Fisher,Phil.Mag.,7,1731 (1962)

S.Foner, Rev.Sci.Intstr.,30,548 (1959)

G.Garton and D.A.Hukin, 3rd Rare Earth Conference,Clearwater, Florida, (1963)

G.Garton,M.J.M.Leask,W.P.Wolf and A.F.G.Wyatt, 8th Conference on Magnetism and Magnetic Materials,Pittsburgh(1962). To be published.

K.A.Gehring and A.H.Cooke Private Communication

S.Geller and M.A.Gilleo, Acta Cryst.,10,239 and 787 (1957)

S. Geller, J. Appl. Phys., 31, 30S (1960)

P.Groth, Chemische Krystallographie, 2, 156 (1908)

F.W.Harrison, Research, 12, 395 (1959)

M.T.Hutchings, D.Phil.Thesis, Oxford University (1963)

A.B.Harris and H.Meyer, Phys.Rev., 127, 101 (1962)

J.Kynch, Trans.Faraday Soc., 33, 1402 (1937)

K.R.Lea, M.J.M.Leask and W.P.Wolf, J.Phys.Chem.Solids, 23, 1381 (1962)

M.J.M.Leask, D.Phil.Thesis, Oxford University, (1960)

M.J.M.Leask and W.P.Wolf, Proc.Phys.Soc., 81, 252 (1963)

M.J.M.Leask, W.P.Wolf and A.F.G.Wyatt, 8th International Conference on Low Temperatures, London (1962). To be published

R.A.Lefever, J.W.Torpy and A.B.Chase, J.Appl.Phys., 32, 962 (1961)

B.T.Matthias, R.M.Bozorth and J.H.Van Vleck, Phys.Rev.Letters, 7, 160 (1961)

F.R.McKim and W.P.Wolf, J.Sci.Instr., 34, 64 (1957)

T.Nagamiya, K.Yoshida, R.Kubo, Advances in Phys., 4, 1, (1955)

L.Néel, Comptes Rendues, 252, 4075 (1961)

J.Nielsen, J.Appl.Phys., 31, 51S (1960)

J.Nielsen and E.F.Dearborn, J.Phys.Chem.Solids, 5, 202 (1958)

R.Pappalardo and D.L.Wood, J.Chem.Phys., 33, 1733 (1960)

R.Pauthenet, Comptes Rendues, 243, 1499 (1957)

E.Prince, Acta Cryst., 10, 787 (1957)

L.Remai and G.A.de Mars, J.Appl.Phys., 33, 1254 (1962)

J.P.Remeika, J.Amer.Chem.Soc., 78, 4259 (1956)

J.Roberts Unpublished.

R.C.Rudness and R.W.Kebler, J.Amer.Ceramic Soc., 43, 17 (1960)

R.Shore Unpublished

N.V.Sidgwick Inorganic Chemistry O.U.P. (1950)

M.F.Sykes and M.E.Fisher, Phys.Rev.Letters,1,321 (1958)

A.I.Vogel Qualitative Analysis Longman's London (1954)

A.J.Wakefield,Cam.Phil.Soc.,47,419 and 799 (1951)

I.Warshaw and R.Roy, J.Phys.Chem.,65,2048 (1961)

A.F.Wells, 'Structural Inorganic Chemistry',3rd Edition, Oxford (1962)

R.L.White and J.W.Carson, J.Appl.Phys.,31,53S (1960)

K.A.Wickersheim and R.L.White, Phys.Rev.Letters,4,123 (1960)

W.P.Wolf, J.Appl.Phys.,28,780 (1957)

W.P.Wolf, Proc.Phys.Soc.,74,665 (1959)

W.P.Wolf, J.Appl.Phys.,32,742 (1961)

W.P.Wolf, Rep.Progr.Phys.,24,220 (1961)

W.P.Wolf and R.M.Bozorth, Phys.Rev.,124,449 (1961)

W.P.Wolf,M.J.M.Leask,B.Mangum and A.F.G.Wyatt, J.Phys.Soc. of Japan,17,B-1,487 (1961)

W.P.Wolf and G.P.Rodrigue, Scientific Report No.9, Gordon McKay Laboratory, Harvard, (1957)

W.P.Wolf and J.H.Van Vleck, Phys.Rev.,118,1490 (1960)

A.F.G.Wyatt, D.Phil.Thesis, Oxford University, (1963)

H.S.Yoder and M.L.Keith, Amer.Mineralogist,36,519 (1951)

W.H.Zachariasen, Acta Cryst.,4,231 (1951)

Abstract.

Detailed techniques and suitable apparatus for producing single crystals of rare earth and yttrium gallium and iron garnets, according to the flux technique of Nielsen, are described. A similar method has been shown to be successful in producing single crystals of rare earth and yttrium aluminium garnets, and an improved melt composition has been discovered. A number of crystals of yttrium and lutecium gallium and aluminium garnets doped with various concentrations of other rare earth and paramagnetic ions have been prepared for resonance and spectroscopic work. In addition, the pure rare earth gallium garnets from gadolinium to ytterbium inclusive, as well as neodymium, and the aluminium garnets from gadolinium to ytterbium inclusive have been obtained as single crystals.

Methods for producing polycrystalline garnet samples are reviewed, and a satisfactory and convenient way of preparing pure and doped polycrystalline aluminium garnet samples developed. In particular, a number of small samples of dysprosium aluminium garnet (DAG) doped with various impurities was made.

Large polycrystalline blocks of yttrium, neodymium, erbium and ytterbium gallium, and yttrium, dysprosium, terbium holmium and erbium aluminium garnets were prepared for specific heat samples, but the conditions necessary for sintering to a highly compact form were not discovered in every case.

Samples of praseodymium gallium garnet and dysprosium

aluminate ($DyAlO_3$) were prepared in a similar way.

The possibility of using the Verneuil flame fusion technique for preparing single crystals of dysprosium aluminium garnet is discussed, and various attempts described.

The paramagnetic susceptibilities of all the pure rare earth garnets mentioned, and of some of the dilute samples, were measured in the liquid hydrogen and helium temperature ranges, and the experimental method is discussed in some detail. The results are considered with respect to the paramagnetic resonance measurements made on the 'doped' crystals, and with respect to the effects of crystal field splittings upon the rare earth ions.

A historical survey of the experiments performed upon DAG is given, together with the theories and motives inspiring them. The effects of impurities on the susceptibility of DAG, and the anomalous a.c. and d.c. susceptibility effects observed in DAG samples in different physical states are described and discussed, and tentatively regarded as 'super-paramagnetism'. The susceptibility of a sphere of single crystal DAG was very carefully measured, and shown to undergo an antiferromagnetic transition at 2.49°K.

Using crystallographic data on the garnets, and resonance results on Dy in aluminium garnets, the sublattice ordering below the transition is deduced.

Specific heat measurements on DAG are reported, and the results after correction confirm the sublattice ordering and transition temperature deduced from the susceptibility

measurements.

The magnetic moment of an oriented spherical single crystal of DAG has been measured as a function of strength and angle of applied magnetic field, and these results are shown to accord with the deduced sublattice ordering arrangement. Depending upon the direction of the applied field, one, two or three of the antiferromagnetic sublattices are forced to become ferromagnetic in a sufficiently high field below the transition temperature. The observed magnetisations are compared with expected values deduced from crystallographic and resonance work. A method for working single crystals of garnet into a sphere is described, together with an orientation procedure using x-ray back reflection photographs, and the anisotropy of the magnetisation with angle.

The magnetic properties of various oxygen-europium phases have been investigated at liquid nitrogen, hydrogen and helium temperatures. The reported ferromagnetism of EuO has been confirmed, but the published Curie temperature, extrapolated from magnetic moment measurements, has been corrected from 77 to 69°K by direct observation. A phase previously thought to be $Eu_{16}O_{21}$ or Eu_3O_4 has been tentatively identified as Eu_2SiO_4, and shown to undergo a ferromagnetic transition between 4.2 and 14°K, conclusions very recently vindicated by magnetic moment and other measurements on Eu_2SiO_4. The compound Eu_3O_4 has a magnetic transition between 4.2 and 14°K but the susceptibility measurements do not show unambiguously

whether this is to ferro- or antiferromagnetism. The magnetic properties at higher temperatures are very unusual, and are probably to be explained by the presence of 1% of EuO as impurity in the sample. Eu_2O_3, in accordance with expectation seems to be almost diamagnetic.

$DyAlO_3$ has been shown to undergo an antiferromagnetic ordering transition at 3.4°K, while Dy_2O_3 remains paramagnetic to the lowest temperatures measured.

The susceptibilities of GdI_3 and TbF_4 have been measured at liquid helium and hydrogen temperatures, and their chemical purities deduced from the results. The susceptibilities of GdOF, DyOF, NdOF and ErOF are reported, and the expected general similarities of their behaviour with the corresponding garnets discussed. GdOF and DyOF both appear to undergo antiferromagnetic ordering, though the results for GdOF are not unembiguous.

The susceptibilities parallel with, and perpendicular to the crystallographic c-axis of lanthanum nickel and lanthanum manganese nitrates have been carefully measured.